QATAR UNIVERSITY

COLLEGE OF ENGINEERING

CONCENTRATED SOLAR POWER PLANT FOR KEY LOCATIONS IN DOHA QATAR

BY

MUTAZ BARGAS ELBEH

A Thesis Submitted to the Faculty of

the College of Engineering

in Partial Fulfillment

of the Requirements

for the Degree of

Masters of Science in Mechanical Engineering

June 2017

COMMITTEE PAGE

The members of the Committee approve the Thesis of Mutaz Bargas Elbeh defended on 18/05/2017.

_____

Dr. Ahmad Khalaf Sleiti
Thesis/Dissertation Supervisor

Approved:

_____

Khalifa Al-Khalifa, Dean, College of Engineering

ABSTRACT

ELBEH, MUTAZ,BARGAS, Masters: June: 2017,

Masters of Science in Mechanical Engineering

Title: Concentrated Solar Power Plant for Key Locations in Doha Qatar

Supervisor of Thesis: Dr. Ahmad Sleiti.

One of the pillars of the Qatar National Vision 2030 is the protection and preservation of the environment by decreasing the dependency on hydrocarbon resources and promoting the use and development of renewable energy sources. Moreover, Qatar is located within the sun belt region of the world which receives abundant solar radiation. Thus, solar renewable energy technologies and concentrating solar power (CSP) has a good potential for producing green energy in Qatar. In this thesis, a CSP power tower plant located in Al-Safliya island is designed to power Al-Jasra and Msheireb down town Doha city zones. These two key locations in Doha are with high electricity demand potential. One of the most famous Souqs in Qatar, Souq Waqif, is in Al-Jasra zone. The suggested location of the CSP plant offers a site that is less than 10 km in distance from the targeted zones which means less transmission losses and transmission route cost. Moreover, the location is very near from Hamad International Airport and it can be easily seen during the departures and arrivals flights. The study is based on an actual electrical consumption of more than 600 shops of the Souq measured on year 2014 and 2015. In the CSP

technology side, the four main technologies are studied with more focus on the solar tower technology. The main components of this technology are reviewed as well. As a part of the literature review, a data base for all the CSP projects around the world is made and a Microsoft Excel model for calculating the available solar irradiance in any location of the world is prepared. Two softwares are used in this project, SolarPILOT and System Advisor Model (SAM). Both softwares are validated with a recent power tower project. The result of the study is a CSP project with more than 0.45 km^2 of a solar field area with 2736 heliostats that produces 8 MWe with 10 hours of thermal storage with hybrid steam condensing system. The water that is required for the plant operation is extracted and desalinated from the surrounded sea using a water treatment system based on a reverse osmosis system. The total electrical production of the plant is found to be 37,904,830 kWh with excess of electrical energy of 28,845,986 kWh, after subtracting the consumption of Souq Waqif. The total system installed cost is found to be $ 84,069,896. It is broken down as total direct capital cost of $ 73,395,696 and total indirect cost of $ 10,674,192. The estimated total installed cost per net capacity is found to be $11,120/kW. Finally, one of the main future recommendations is to build an immediate solar and weather station in the state to measures the actual three solar components of the available solar irradiance on both horizontal and dual axes tracking surface.

DEDICATION

I dedicate this work to my father and to my mother who have given me valuable and precious time and effort and were the cause of what I am now.

ACKNOWLEDGMENTS

I would like to first thank Allah and my parents. Then, I would like to record my thanks to our college for giving me the opportunity to submit my thesis and to my supervisor, Dr. Ahmad Sleiti, who lead me throughout this thesis. After that, I would like to thank KAHRAMAA for the information I got about the electrical consumption of Souq Waqif. Finally, I would like to thank my friends for their continuous support and specially Eng. Sami Iyad Hasiba and Eng. Mohamed Ahmed Taha for their assistance.

TABLE OF CONTENTS

LIST OF TABLES

LIST OF FIGURES

1 INTRODUCTION

In this chapter, the introduction and motivation points for this thesis are described along with Qatar's energy status including the renewable energy plans. An introduction about the smart grid technology is given along with Qatar's status and plans. The objectives of the thesis are highlighted and finally the thesis scope of work.

1.1 Introduction and Motivation

Energy provision has been throughout all times a main topic which has a vital impact on the human life and economic growth. Till today, most of global energy is produced from fossil fuel and coal and only 9.8% is produced from utilizing renewables resources [1]. Consequently, a strong evidence is already recognized that global warming and thus the climate changes are anthropogenic and related to the globally excessive fossil fuel consumption and extreme emission of carbon dioxide into the atmosphere. Thus, renewable energy utilization in providing the current and future demand of electricity should be the followed trend globally.

The Gulf Cooperation Council (GCC) region, including Qatar, consists of countries that are considered the world's largest hydrocarbon producing countries that hold virtually a third of proven crude oil reserves, and approximately a fifth of global gas reserves [2]. Because oil in these countries is relatively accessible and inexpensive, the proper

attention was not given to the projects that utilize alternative types of energy. Up till the last decade, there were only scant incentives from the government side to utilize any alternative forms of energy.

Currently, these countries in total has less than 200 MW energy produced by utilizing renewables resources [3]. As the fossil fuel is not everlasting, in the following hundred years it will be depleted and the only continuous reserves will be the renewables resources and the solar energy. In addition, utilizing renewable resources is considered a valid solution to reduce the CO_2 emission from the various sources of fossil fuels. An introduction about the smart grid technology and Qatar's smart grid status and plans are shown in Appendix A.

1.2 Qatar's energy status

Qatar is located approximately within latitude of 25 degrees North and longitude of 51 degrees East. This location is included within the sun belt region of the world which receives abundant solar radiation. Qatar possess relatively huge amount of oil and natural gas reserves. In 2014, Qatar's population was 2.17 million with CO_2 emissions of 35.73 (tonne CO_2/capita) and electrical consumption of 16,736 kWh/capita. The CO_2 emission that year was almost 8 times the world average CO_2 emissions that was 4.47 tonne CO_2/capita only [4].

From energy production point of view, Qatar is considered one of the largest exporter of natural gas, with almost 12% of global exports in 2013 [2]. In 2015, Qatar produced 1898 thousands of oil barrels per day which accounts for 1.8% of the total world production of oil. At the same time, it produced 181.4 billion cubic meters of natural gas which accounts for 5.1% of the total world production. From energy consumption point of view, Qatar consumed in 2015 an equivalent of 51.5 million tonnes of oil [1].

In renewables side, Qatar possess in 2015 a total renewable energy installation of 28 MW [3]. Moreover, in December 2012, the Sahara Forest Project (SFP) Pilot Facility in Qatar was commissioned and started its operation. See Figure 1-1. SFP entered cooperation with the Qatari company Qafco, the world's largest single site producer of urea and ammonia and Yara ASA, the world's largest supplier of fertilizer. This facility includes photovoltaic solar power panels and concentrated solar power (CSP) collector and receivers. The SFP Pilot Facility is home to the first fully operational CSP unit in Qatar [5]

Figure 1-1: SFP Pilot Facility in Qatar [5]

Being in the top list of countries that has the highest CO_2 emission per capita, Qatar has concentrated its research facilities in the utilization of renewable energy as a gradual replacement of the fossil fuels and to increase its energy security. One of the pillars of the Qatar National Vision 2030 is the protection and preservation of the environment by decreasing the dependency on hydrocarbon resources and promoting the use and development of renewable energy sources [6].

With these goals in mind, the renewable energy production target of Qatar by 2030 is 1800 MW that accounts for 20% of the total consumption. Moreover, the energy efficiency target in 2017 is 20% per capita electricity conservation and 35% per capita

water conservation [2]. In addition to that, Qatar plans to build around 1,000 megawatts of solar power generating capacity in line with the QNV2030. This project will be implemented by a solar power company that will be formed as a joint venture between Qatar Electricity and Water Company (QEWC) and Qatar Petroleum (QP) [7].

1.3 Objectives

The main goal of this thesis is to design a CSP system to supply electricity to Al-Jasra and Msheireb down town Doha city zones. These two key locations in Doha are with high electricity demand potential. The CSP system is based on a power tower technology with thermal storage. The specific objectives to achieve this goal are as follows:

1- Verify the yearly electrical consumption of Souq Waqif to determine the CSP plant capacity that is required to be designed.
2- Determine the hourly available solar energy per square meter on a horizontal, sloped, and tracked surface at Qatar land.
3- Use advanced software package that can design a solar power plant including the plant solar field, power block and thermal storage system. The software should have the facility to take into consideration the location of the plant, the solar available data on the location of the plant, utilize the up to date solar and thermal storage technology. Moreover, the software should produce a performance and financial analysis of the project.

4- Select the CSP plant location. The selected plant location should reflect the interest of the government in utilizing the renewable resources in providing electricity to the state.

1.4 Thesis overview and scope of work

The solar power plant facility selected in this thesis is based on CSP power tower technology with thermal storage. The net power output of the plant is to be determined based on the electric consumption data to be collected for Souq Waqif. The solar data for Qatar will be simulated based on a prepared model using theoretical calculation. The CSP power tower technology will consist of heliostats (tracked mirrors) and a receiver that collects the redirected sun rays. The heat transfer fluid (i.e. molten salt) will be routed to the receiver when solar energy is required to be collected. The molten salt will pass through the receiver where it is heated by the reflected concentrated solar energy. After that, the molten salt will be routed to a large insulated tank called the hot tank where it can be stored with minimal energy loss.

Once the electricity is to be generated, the hot molten salt will be pumped and circulated through a series of heat exchangers to generate a high pressure superheated steam. This steam is then used to power a conventional Rankine cycle steam turbine with generator that produces electricity. At the end of the cycle, the turbine's exhaust steam will be condensed and returned through feedwater pumps to the heat exchangers where the high

pressure superheated steam is generated again. After the steam generation, the available energy in the molten salt will be depleted and then it is routed to a tank called the cold tank where it is to be recycled again. The project main components include:

- A solar field consisting of a large area of heliostats that reflect the sun's solar energy into a tower.
- A conventional steam turbine with generator to generate electricity.
- Two thermal storage tanks to store the hot and cold molten salt.
- A hybrid cooling system consists of an air-cooled condenser and a wet cooling augmentation system (for high electricity demand).
- A desalination water treatment system based on a reverse osmosis technology to provide desalinated water for the plant use.
- Electrical transmission system is not included.

2 INTRODUCTION TO CONCENTRAED SOLAR POWER

In this chapter, a general overview about CSP technologies is described. Then, the four CSP technologies that are parabolic trough, linear fresnel, power tower and parabolic dish are explained in details. After that, the main components of any CSP system that are the solar collector, solar receiver, heat transfer fluid, thermal energy storage and power cycle are shown and explained in details.

2.1 General

CSP systems are a booming field worldwide. Many gigawatts of such systems are currently being built. As of December 2016, Solar Power and Chemical Energy Systems (Solar Paces) has released that CSP market has a total capacity of 8,784 MWe worldwide, among which 4815 MWe is operational, 1260 MWe is under construction and 2709 MWe is under development. Spain is the world's leading country in this technology followed by USA.

This technology produces electricity by utilizing the high temperature heat gathered from concentrating solar radiation onto small area receiver using solar collectors, where a heat transfer fluid (usually steam) is heated up and directed to a conventional power cycle with a steam turbine. Electricity is then generated by an electric generator that is driven

by the steam turbine with the efficiency limited by the Carnot cycle. In another words, any current power plant using a heat transfer fluid such as steam as a driving fluid can be transferred to solar power plant by replacing the external heat source, such as boiler in the case of steam that uses fossil fuels, by a concentrating solar field. Unlike solar photovoltaics (PV), only the direct radiation portion of the available solar radiation is used. This is due to the reason that the direct radiation is the only component that can be concentrated in optical systems.

It is worth to mention that technical potential of generating electricity based on CSP in most of these regions is typically several times greater than their electricity demand, resulting in opportunities for electricity export [8].

In this technology, mirrors or reflectors are used to concentrate the direct component of the sunlight onto a receiver or absorber that is basically a heat exchanger that gathers and transfers the concentrated solar energy to a heat transfer fluid. After that, this fluid transfers the collected energy to an application that utilize the energy directly in the power cycle (gas/steam) or circulate it in an intermediate secondary cycle (e.g. as molten salt or thermal oil) that is connected to another cycle that is used to generate electricity through conventional steam turbines [9].

2.2 CSP Technologies types

CSP technology has four main arrangements that are used currently. These arrangements are distinguished by two main criteria, the focus type of the concentrator and the receiver mobility. In the first criterion, the solar collector type concentrates the sun rays into focal line absorbers or single focal point absorbers. In Parabolic Trough plants and Linear Fresnel Reflector plants as mentioned in Figure 2-1, the sun rays are concentrated into a focal line absorber, where the sun ray's concentration in Power Tower plants and Solar Dish plants, as mentioned in Figure 2-2, are directed into a focal point absorber. In the second criterion, the receiver mobility is either fixed, as in the case of Linear Fresnel Reflector plants and Solar Tower plants, or has the ability to track or align with the sun, as in the case of Parabolic Trough plants and Solar Dish plants.

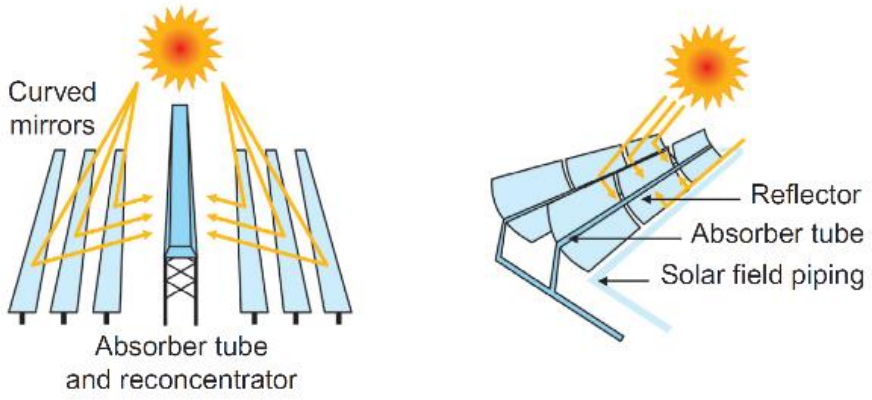

Figure 2-1:Parabolic Trough and Linear Fresnel Reflector - Focal Line Absorber Technologies [8].

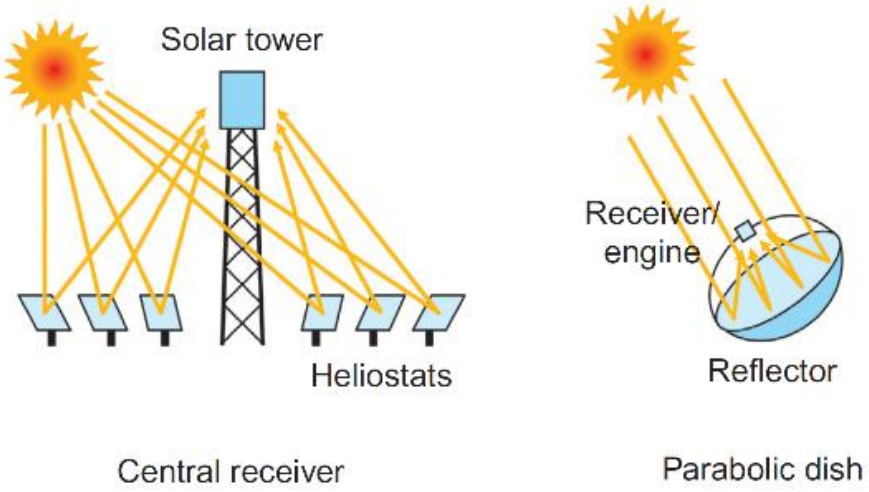

Figure 2-2: Power Tower and Solar Dish - Focal Point Absorber Technologies [8].

2.2.1 Parabolic trough

Parabolic troughs are the most mature CSP technology and it is used by many existing commercial power plants. This technology consists of long rows of parabolic reflectors that focus the solar irradiance received onto receiver tubes that are positioned along the focal line of each parabolic mirror as shown in Figure 2-1. In most of the designs, the receiver tubes are composed of two tubes, steel inner pipe and glass outer tube. Between the both tubes, an evacuated space is made between them to reduce the heat transfer losses from the inner tube that has the heat transfer fluid to the outer glass tube.

In general, parabolic trough technology, has good optical efficiency relative to other technologies with the possibility of having a storage system. However, relative to other technologies, parabolic troughs use higher land space and water for cooling if wet cooling is used.

The concentration of the solar irradiance on the receiver can reach up to an order to 70 to 100 times the originally received solar irradiance on the reflector [10] with annual solar to electricity conversion efficiency of 15-16 % [11]. Regarding the heat transfer fluid, most of the current plants that run with parabolic trough technology are using synthetic oil as the heat transfer fluid and molten salt storage (if there is storage). Superheated steam and molten salt are also used as a heat transfer fluid.

2.2.2 Linear fresnel

Linear Fresnel reflector is a system where one downward-facing receiver tube is fixed above long rows of flat or slightly curved mirrors that have a good mobility in tracking the sun as shown in Figure 2-1. In comparison to parabolic trough system, the receiver in both systems has the sun rays focused into a line not a point. However, the linear Fresnel reflectors are cheaper and at the same time less efficient when the sun position is low in the sky. This lower optical efficiency is due to the greater cosines losses accompanied with this design. As a result of this, the annual solar to electricity conversion efficiency is the lowest of this technology with values of 8-10 % [11]. Unlike the parabolic trough, the

receiver is positioned high enough allowing for a reduced land use and a closer arrangement of collectors.

One of the main advantages of having the receiver fixed is that it can sustain higher pressures of the process fluid and the direct heating (direct steam generation) by using the water instead of having the heat transfer fluid become possible. This eliminates the need for and the cost of a heat transfer fluid and exchanger and reduce the maintenance and operating costs. As result of this and as it is more difficult to store the latent heat of steam than sensible heat, incorporating storage capacity into their design is challenging.

2.2.3 Central receiver or solar tower

A solar tower system uses a large field of flat mirrors that track the sun from a stationary point known as heliostats. These mirrors focus and concentrate the received sunlight onto a receiver on the top of a tower. This arrangement is shown in Figure 2-2. Heliostats can diverge greatly in size, from about $1m^2$ to 160 m^2. With the current maturity of the technology, the maximum thermal power produced is limited to about 600 MW with heliostats that are located about 1.5 km from a tower of about 160 m height [10].
The selection of heliostat size makes a significant trade-off in benefits: large heliostats have a comparatively high power output, however require strong and more stiff structures; on the other hand, small heliostats are light in weight and requires smaller motors, however in order generate the same amount of electricity like the larger

heliostats, more of them are required. Based on many other factors the size will be selected accordingly from either options.

Due to the huge solar field and the relatively small receiver of this technology, high concentration factors up to 1000 can be achieved [12]. High temperatures that matches the operating temperatures of a conventional power plant is attained and this makes this technology suitable replacement of the boiler section or the heat provider section of a conventional power plant. Due to the high concentration factors, medium annual solar to electricity conversion efficiency of 15-17 % can be achieved [11].

Three Heat Transfer Fluid technologies are being used and still under development: steam that can be saturated or superheated, which is difficult to store; molten salts, which induce more challenging to control the flow-ability of the fluid and can be stored; and air that can be at ambient pressure or pressurized, the simplest process technology.

2.2.4 Parabolic dish

Parabolic dishes use a mirrored dish composed of many smaller flat mirrors formed into a dish shape that directs and concentrates sunlight onto a thermal receiver located above the center of the dish. This arrangement is shown in Figure 2-2. The entire apparatus, dish and receiver, tracks the sun with the need of only one fixation point. Thus, a very limited land use is required in comparison to other technologies. This receiver absorbs and

collects the sunlight and transfers it to the engine generator, which is in the most cases a Stirling engine, without the need for a heat transfer fluid and cooling water.

In comparison to other technologies, dish systems have the highest annual solar to electricity conversion efficiency of 20-25 % [11]. However, dish systems are more expensive than other systems and suitable only on a small scale power generation (typically tens of kW or smaller). Most of the dish systems, except very large reflectors that are used in solar farms, are not suited for thermal storage [10].

2.3 Main Components

For any CSP system to be operable, four major components have to be constructed on the site of the CSP plant. These components are, the solar collector or reflector, the solar receiver, the heat transfer medium and the energy storage and finally the power block. Each component will be described separately below.

2.3.1 Solar collector/ reflector

The solar collector or sometimes called solar reflector is the component of a typical CSP system that receive the sun rays and direct it toward the absorber part of the system. It should be very reflective, strong and resisting demanding outdoor environment. There are many types of solar collector that are used currently in CSP systems and they can be of the flat plate or concentrating plate type. In the latter and in most cases, the curvature of

the plate is based on a parabolic concentrator. This means that the collector can be a trough with a 2-diemensional parabolic shape, a 3-diementional dish and two axis tracking heliostats or arrays of mirrors with one axis tracking [13]. The last two collectors resemble Fresnel reflectors. This reflector type is derived from the fresnel lens which is basically a parabola that is divided into smaller flat plates that acts together as a one reflector. The range of solar collectors of the main CSP technologies, parabolic trough, linear Fresnel, power tower and solar dish are depicted in Figure 2-3 along with the concentration ratio and the temperature obtained of each type.

The solar collector/ reflector has optical losses that should be avoided a much as possible to get the maximum radiation into the absorber and reduced its overall efficiency. The resultant optical losses are composed of different factors related to optics and heat losses. The range of these losses depends on the quality finish of the manufacturer and the reflectivity of the collector/ reflector used.

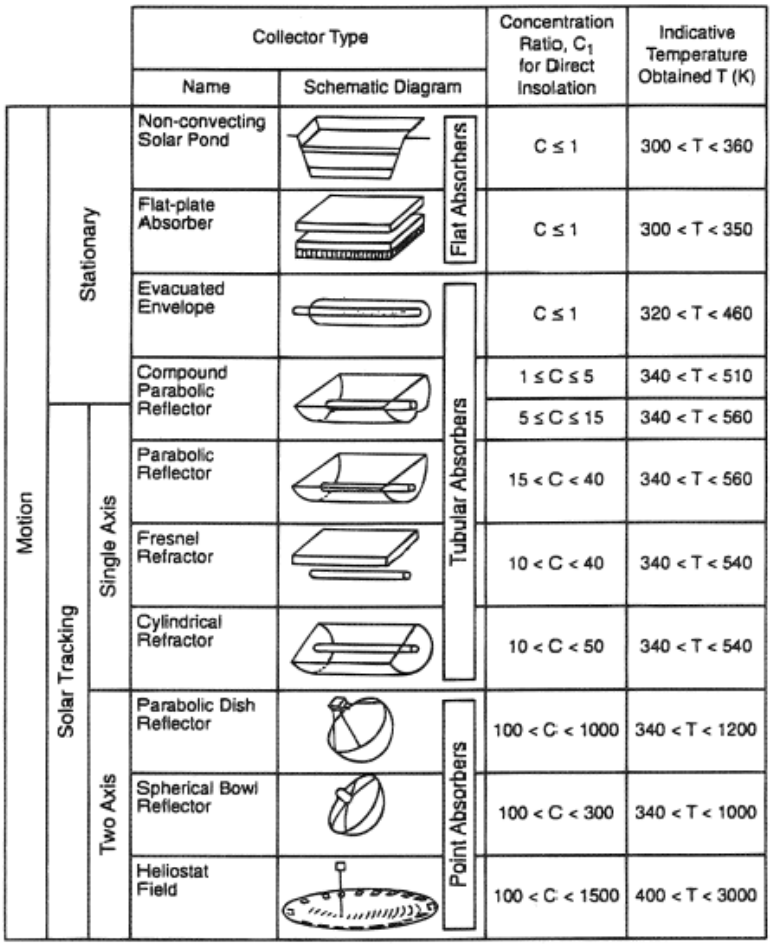

Figure 2-3: *Solar collector types* [14]

To collect the highest amount of coming sun radiations, the solar collector should follow the sun instead of being stationary. For that reason, tracking mechanisms are used to enable the solar collector to follow the sun. These tracking mechanisms can be categorized based on their mode of motion, either single axis tracking or two axes tracking. As shown in Figure 2-4, a flat collector is demonstrated with four mode of

tracking. In the case of the two axes tracking, the collector follows the sun in all direction (Figure 2-4 (a)). On the other hand, in the case of a single axis mechanism, the collector is partially fixed and it follows the sun only by tilting. This motion can be in various ways, it can be east–west (Figure 2-4 (d)), north–south (Figure 2-4 (c)), or parallel to the earth's axis (Figure 2-4 (b)).

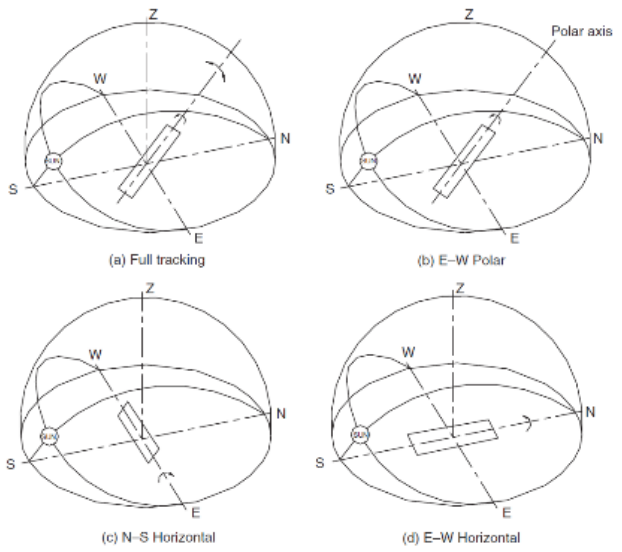

Figure 2-4: Solar collector geometry for various modes of tracking [15]

The selected mode of tracking determines the amount of incident radiation on the collector surface in direct relation with the cosine of the incidence angle. For comparison purposes only, an analysis was performed by Cyprus University of Technology [15]

using the same radiation model to plot the radiation flux for the different types of tracking modes. This analysis includes the full tracking mode as the role model with 100% amount of solar energy collected. In Table 2-1, the amount of energy that is collected on the collector's surface for the different modes at the summer and winter solstices and the equinoxes.

Table 2-1: Comparison of energy received for various modes of tracking [15]

	Solar energy received (kWh m^{-2})			**Percentage to full tracking**		
Tracking mode	E	SS	WS	E	SS	WS
Full tracking	8.43	10.6	5.7	100	100	100
E–W polar	8.43	9.73	5.23	100	91.7	91.7
N–S horizontal	7.51	10.36	4.47	89.1	97.7	60.9
E–W horizontal	6.22	7.85	4.91	73.8	74	86.2

Notes: E, equinoxes; SS, summer solstice; WS, winter solstice.

The performance of the tracking modes in Figure 2-4 are compared to the full tracking mode that has the maximum amount of solar energy collected and indicated by 100%. It can be concluded that the E-W polar tracking mode is the closest mode to the full tracking performance. Thus, it is recommended as a one axis tracking mode.

The more the solar energy is collected by choosing the most appropriate tracking mode, the higher the light concentration that leads to a higher thermal transfer medium temperature. This means that the power-cycle efficiency also increases. However, the sun tracking collectors need to be constructed in a way that enough space is available for rotating/ tilting freely and to avoid shadowing each other. This reduces the ground utilization and a larger area would be required to collect the required solar energy.

2.3.2 Solar receiver

The receiver of a CSP system has the function of receiving the concentrated light from the collector/ reflector and converting it to heat and then into a heat transfer fluid medium.

In one-axis tracking reflector the light would be concentrated in the shape of a line on the receiver however in a two-axis tracking reflector a spot focus is gained.
In the initial days of receiver research and development, the main attention was on tubular designs and currently the attention is given to the development of volumetric receiver designs [16].

2.3.2.1 Tubular receiver designs

The basic principle of the tubular design is that concentrated solar radiation is absorbed by a bundle of tubes and then the energy is transferred to the heat transfer fluid flowing

within the tube. See Figure 2-5.

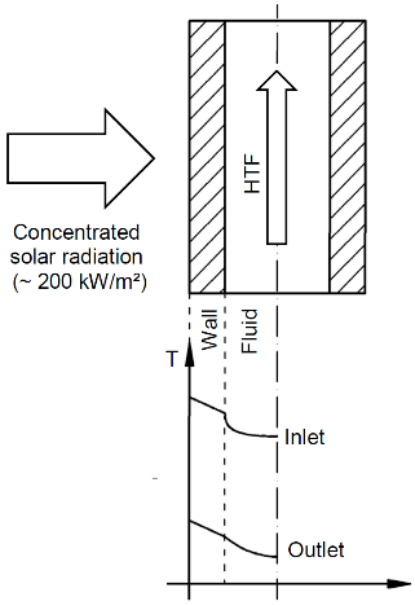

Figure 2-5: Absorption and heat transfer of tubular receivers [17]

It can be noticed that temperature of the tube body is always higher than the heat transfer fluid temperature. This limits the maximum operating temperature and can be considered as a disadvantage. However, the heat transfer fluid in the tube can be easily pressurized and the yield strength of the tube's material is the limiting factor.

Moreover, another disadvantage of a tubular receiver design is the heat loss to the ambient environment. This loss is due to thermal radiation, convection, and reflection losses. In order to reduce the losses in general, the tubular receiver can be placed within a cavity with other receivers. Another way to reduce the reflection losses is by covering the receiver with a selected solar coating to aid the solar absorbance.

The tubular receiver was one of the first receivers utilized in power towers. In Solar One project, the first central receivers ever were an external tubular receiver. It is presented in Figure. It was operated between 1982 and 1988 in USA, Nevada with nominal power output of 10 MWe. The water was directly evaporating within the receiver and the power generation was done using the conventional Rankine cycle [18].

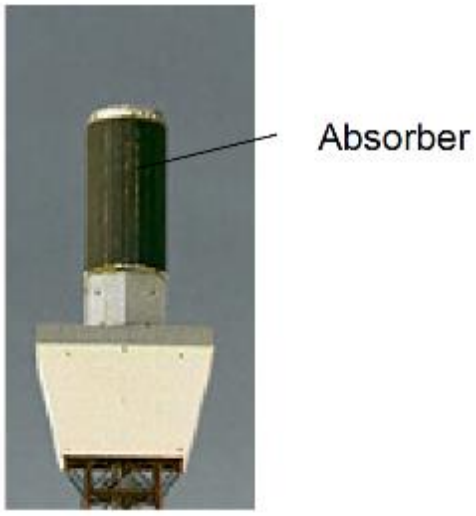

Figure 2-6: Existing Solar One tubular receiver [19]

Another existing tubular receiver is shown in Figure and it is the SOLOGATE low temperature receiver. It can handle fluids up to outlet temperature of below than 550°C as per the SOLOGATE report [20].

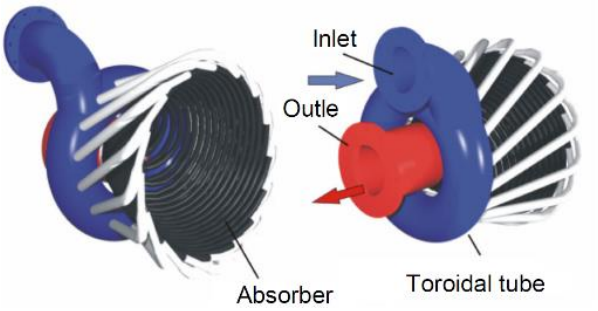

Figure 2-7: Existing SOLGATE low temp. tubular receiver [20]

In the side of developed and recent tubular designs, in Figure 2-8 the SOLar Hybrid power and COgeneration plants (SOLHYCO) tubular cavity design is shown. This system is established on a 100 kW micro turbine with a fluid outlet temperature of around 800°C [21].

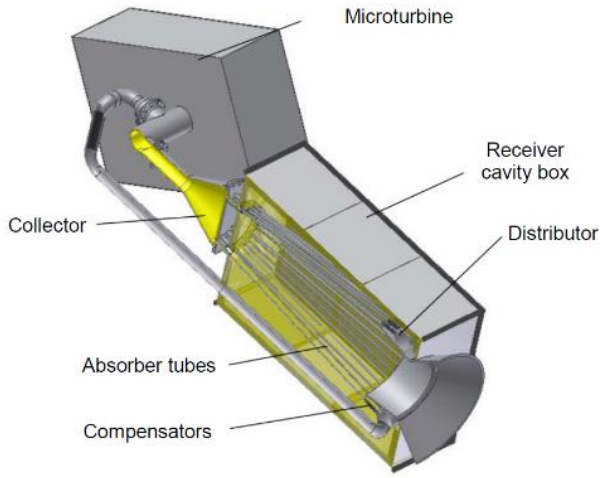

Figure 2-8: Recent SOLHYCO tubular cavity receiver [21]

The main development of this receiver is the absorber tube design that is based on profiled multi-layer (PML) tubes. It is manufactured using three metallic layers: a high temperature nickel-based alloy at the outer side to provide the structural strength, a copper layer as intermediate layer to conduct the heat to the opposite side and another high temperature nickel-based alloy at the inner side of the tube to protects the copper from oxidation and corrosion at elevated temperatures [22].

The second recent and developed tubular receiver is shown in Figure 2-9 and it the Solar Up-scale GAS Turbine System (SOLUGAS) tubular cavity design. It is based on a solar pre-heated Brayton topping cycle and a subsequent Rankine bottoming cycle [23]. The receiver contains several tubular receiver panels and is used to pre-heat the pressurized heat transfer fluid that is air up to 650°C before it enters the combustion chamber of a

commercial 4.6MWe gas turbine. Conventional material can be used here for the absorber tubes due to the relatively low temperatures.

Figure 2-9: Recent SOLUGAS tubular cavity receiver [23]

2.3.2.2 Volumetric receiver designs

Volumetric or direct absorption receiver is a receiver design where the concentrated solar radiation is absorbed directly when it is in contact with the working fluid. The receiver cavity is occupied with the absorber material. Most designs are based on using absorber materials that are comprised of porous meshing shapes such as knit-wire packs, honeycomb structures, foam, packed beds and others with a specific porosity [24]. Once the absorber material is exposed to the incident concentrated radiation, it heats up in depth resulting in one of the main advantages of the volumetric solar receivers that is the heat transfer area is increased unlike the fixed heat transfer area of the tubular receivers. In another words, the volumetric receiver design has the ability to absorb relatively

higher solar flux and be compact even at high temperatures [25].

Moreover, the increase in temperature will occur along with reduction of the local flux density at the absorber surface. This will cause the temperature of the irradiated surface to be lower than the outlet temperature causing decrease re-radiation losses [16]. This is shown in Figure 2-10. The heat transfer fluid, which is usually air, goes through the volume at the same period the solar energy is conveyed through forced convection from the absorber material to the heat transfer fluid.

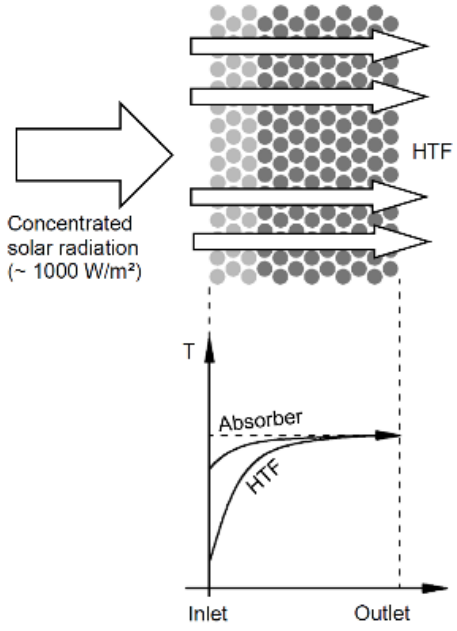

Figure 2-10: Absorption and heat transfer of volumetric receivers [17]

The main heat transfer mechanism that rules the transfer of the heat from the absorber material to the heat transfer fluid is the convective heat transfer. The radiative heating of heat transfer fluid due to the effects of scattering and absorption of the incident concentrated solar radiation are relatively very little compared to the convective heat transfer and usually it is negligible [26],

Regarding the absorber material that can used to withstand the relatively high temperatures, ceramics and metals are the most appropriate choice. The usage of metallic absorber in volumetric receivers makes it possible to produce fluid outlet temperatures from 800°C to 1000°C. Moreover, receivers with siliconized silicon carbide (SiSiC) ceramic are able to absorber temperatures of 1200°C, and receivers with silicon carbide (SiC) absorbers temperatures of 1500°C [16].

Volumetric receivers are able to work either at ambient pressure or at elevated pressure or pressurized. The receiver that operates at ambient pressure is usually called open volumetric receiver and the one that operate at elevated pressure level is called closed volumetric receivers.

2.3.2.2.1 Open volumetric receiver

The working principle of an open volumetric receiver is based on the High Temperature Receiver (HiTRec I) as shown in Figure 2-11. The concentrated solar radiation is

absorbed by a ceramic honeycomb absorber that heats the assembly up. After that, ambient air is drawn into the receivers acting as the heat transfer fluid. One of the methods that are used to increase the efficiency of the open volumetric receiver is to apply the air return system. The system works in a way that cold air that leaves the system is used to cool the receiver structure and after that used as the heat transfer fluid. This is to reuse the absorbed heat during cooling. Some initial receivers like HiTRec I was not equipped with such an air return system however the later developed projects such as HiTRec II, SOLAIR 200, and SOLAIR 3000 were [16].

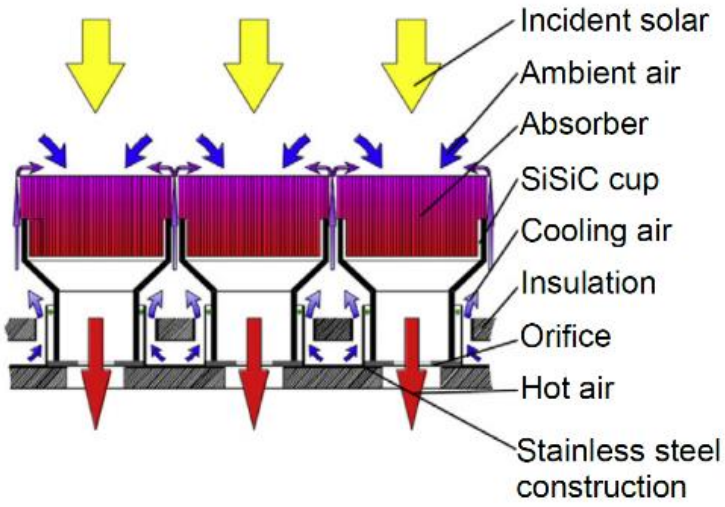

Figure 2-11: Open volumetric receivers HiTRec II [16]

In Figure 2-12, the assembly of multiple open volumetric receivers on top of a solar power tower is shown. It can be seen that the receiver is composed of many individual absorbers that each is around 0.02 square meters area.

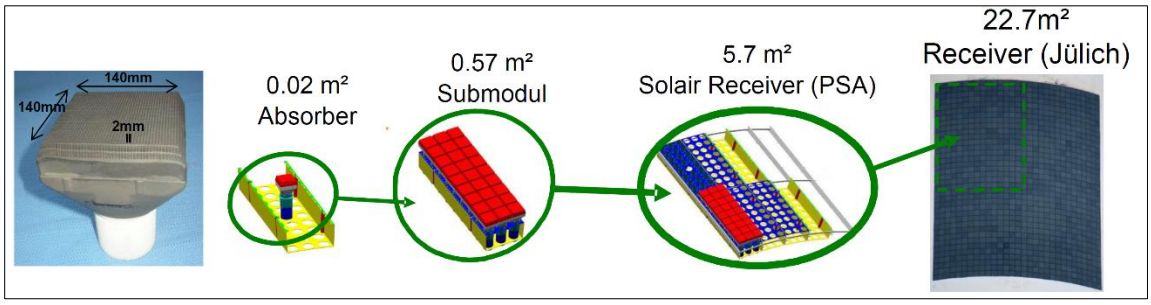

Figure 2-12: Assembly of open air volumetric receivers on top of a solar tower [27]

Usually, the outlet hot air from the open air volumetric receivers is used to produce superheated steam and then generate electricity in a conventional Rankine cycle. In Jülich power plant in Germany, the power tower open air volumetric receiver is drawing air at 120°C and add het to it up to 680°C at an ambient pressure [27].

2.3.2.2.2 Closed volumetric receiver

The second type of volumetric receivers is the pressurized closed volumetric receiver. One major difference between the open and the closed volumetric receiver is that the latter relies on a transparent window to enable high-pressure process and to minimize

reflection, re-radiation and convection losses [24]. Another difference is the usage of secondary concentrators in order to concentrate the solar radiation on the absorber and cover the surrounding receiver structure.

There are two main types of the closed volumetric receiver. The first one is the Directly-Irradiated Annular Pressurized Receiver (DIAPR) that is based on porcupine absorbers made of high temperature ceramics as shown in Figure 2-13.

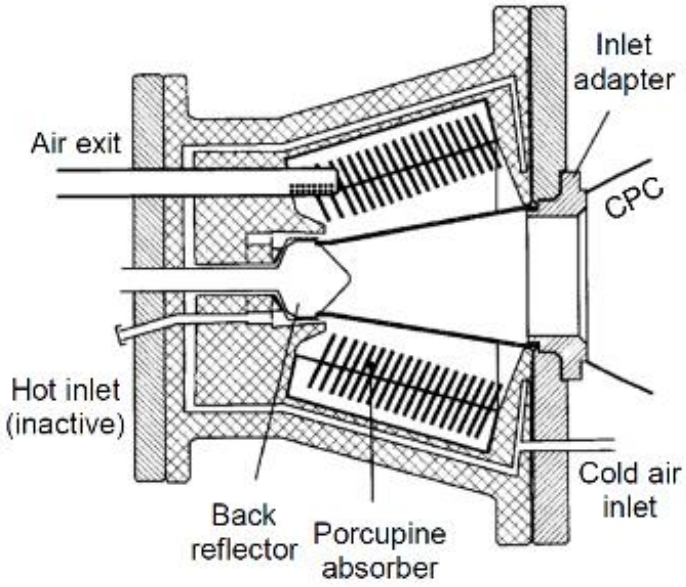

Figure 2-13: Directly-Irradiated Annular Pressurized Receiver (DIAPR) [28]

The second one is the Receiver for Solar-Hybrid Gas turbine and CC Systems (REFOS) with a metallic or ceramic absorber as shown in Figure 2-14. In the case of air as the heat transfer fluid, it is not ambient air but pressurized air entering the receiver and then heated up by the hot absorber and leaves the receiver. The air then can be used in a conventional gas turbine or in a hybrid cycle as preheated air entering the combustion chamber of a gas turbine cycle [24].

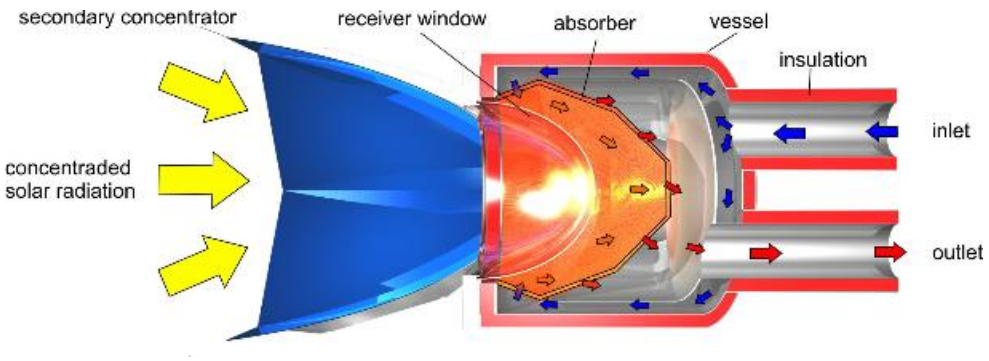

Figure 2-14: Receiver for Solar-Hybrid Gas turbine and CC Systems (REFOS) [27]

In the past a lot of research has been done to overcome the difficulties in the designing of the transparent windows. These difficulties were associated to limitations in size, high variable working temperature, mechanical strength, stress-free installation and cooling capability [16].

Experiments have already showed that project DIAPR was able to work at pressures of 10 to 30 bar and solar radiation flux of up to 10 MW/m², while generating HTF outlet temperature of up to 1300°C [25]. The receiver efficiency was estimated to be between 70 and 90 percent during the tests. Moreover, the reflectivity losses of the glass window were found to be less than one percent. Recently, a company called Aora built a solar tower power plant using the above mentioned DIAPR technology in the Arava desert. The plant was based on a single receiver module and generates 100 kWe and additionally 170 kWth [29].

In the case of the second close volumetric receiver, the REFOS receiver, it was modified in the REFOS project starting in 1996 and was also used within the SOLGATE project starting 2001 [24].

In the REFOS project the receiver was tested and absorbed 350 kWth of concentrated solar radiation at a solar flux of around 1000 kW/m² per module producing air outlet temperatures of 815°C at a pressure of 15 bar [30]. In the same test. the efficiency was not as high as predicted because of the poor secondary concentrator performance.

2.3.2.3 Heat Pipe design

Heat pipe solar receivers was initially used in the aerospace applications and later in the 1970s it they were used for CSP plant emerged [24]. Heat pipe receiver design can

incorporate heat absorption, heat transfer and thermal storage as a one device [31]. It is a container that consists of a receiver portion (evaporator), a working fluid that is in equilibrium with its own vapor or instead a phase change material and heat source heat exchanger portion (condenser). This is shown in Figure 2-15.

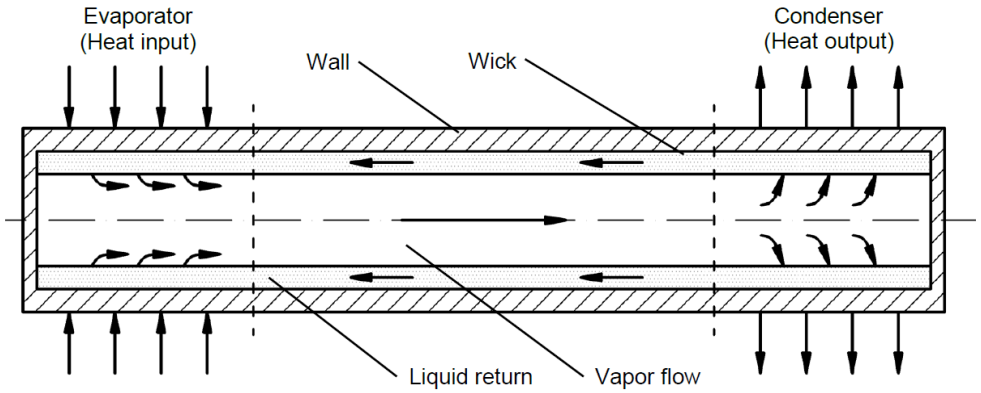

Figure 2-15: Cross section of a heat pipe receiver [32]

When heat is absorbed by the evaporator the temperature of the working fluid increases slightly triggering some of the fluid to evaporate. During this process, a temperature difference occurs that causes a change in vapor pressure of the fluid and this due to the saturation condition. Thus, resulted vapor flows to the condenser where it discharges its latent heat and liquefies again. After that, the liquid is forced to return to the evaporator portion.

During heating of the working fluid and during periods of solar incidence, a portion of the energy absorbed is stored as latent energy. The outstanding and not stored energy is transported to the condenser section of the receiver. During the passing of the clouds, the temperature pressure and temperature of the working fluid starts to decrease to supply the condenser for a certain period based on the volume and type the working fluid.

The main advantages of the heat pipe design are the high temperature capabilities in the range of 500-1000°C, the low-pressure stresses in high temperature component due to the operation at ambient pressure, and the experienced low pressure drop on the gas side due to large design flexibilities [33]. Moreover, the fluctuating of the supplied outlet temperature is minimal and this is due latent heat transfer by the working fluid. On the other hand, as per the heat pipe material, the outlet receiver temperature is limited up to 900°C. in addition to that, the receiver will not function at a lower operating limit of 400°C.

Other heat pipe receivers are the cavity and panel heat pipe receiver. Both are shown in Figure 2-16 and Figure 2-17. In the first type which was developed for the U.S. DOE and used in a Brayton cycle with electrical output of 10 MWe [33], the heat pipes are mounted on panels inside a cavity whereas in the second one the panels are arranged in a flat manner.

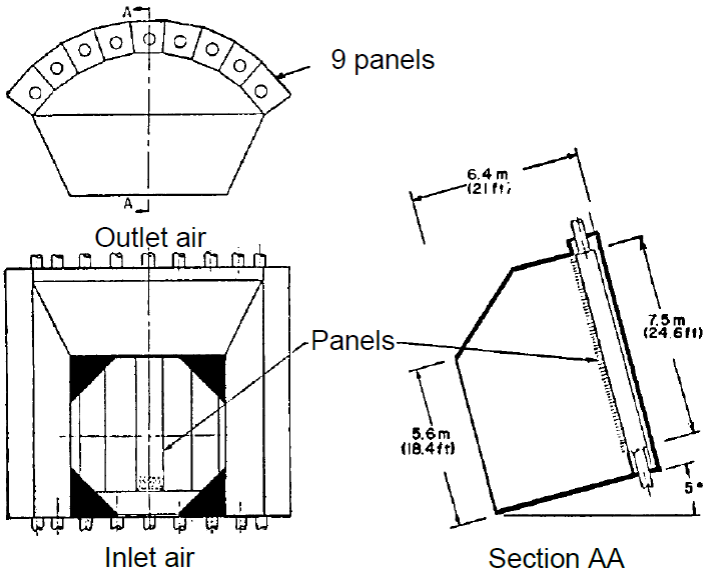

Figure 2-16: Cavity heat pipe receiver [33]

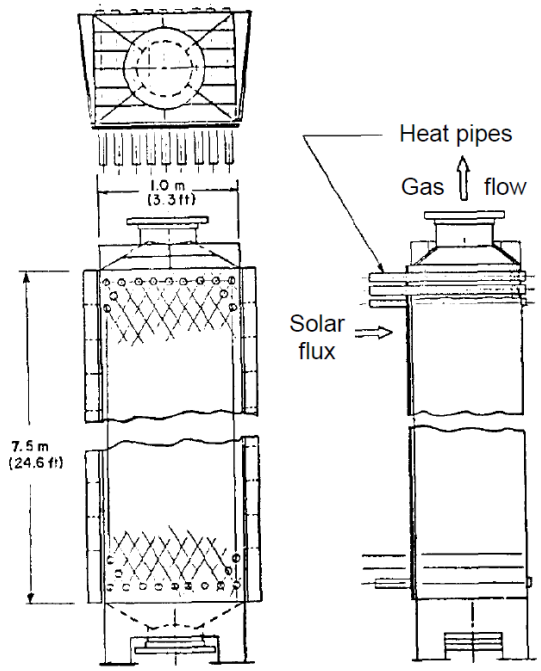

Figure 2-17: Panel heat pipe receiver [33]

2.3.2.4 Solid particle design

Sold particle design or the direct absorbing particle is another way of absorbing concentrated solar radiation. The concept behind this receiver is based on a falling solid particle curtain that absorbs directly the incident concentrated solar radiation. As shown in Figure 2-18. Usually the solid particles are made of ceramic and the temperature of the curtain can reach up to 1000°C [34]. The solid particles in this case are the heat transfer and the storage medium with no limits for the flux densities to the particles as the same medium absorbs and transfers the heat [27].

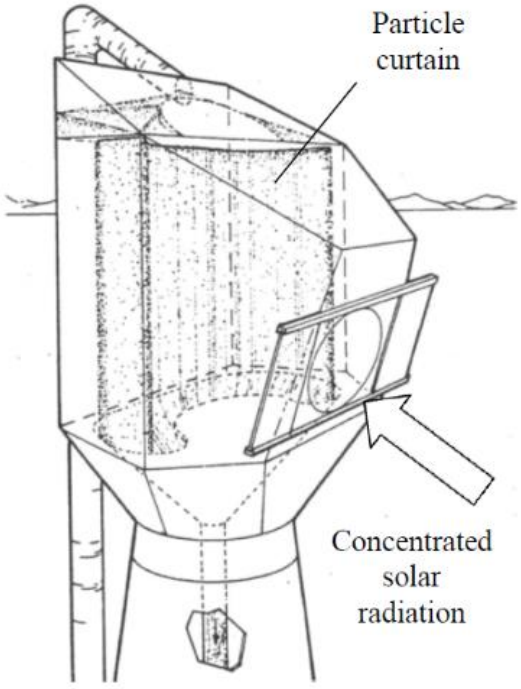

Figure 2-18: Solid particle receiver concept [35]

The solid particle receivers are used mainly as a heat source for chemical processes especially for solar driven water-splitting thermo-chemical (WSTC) cycles for hydrogen producing [34]. In the case of electricity generation, the system is shown in Figure 2-19. As can be noticed, the particles from the cold storage tank are pumped to the particle receiver at which they are heated up and subsequently stored within the hot storage to be used in the power block section with the use of dedicated heat exchanger. After that the particles completes the cycle when they are back in the cold storage tank.

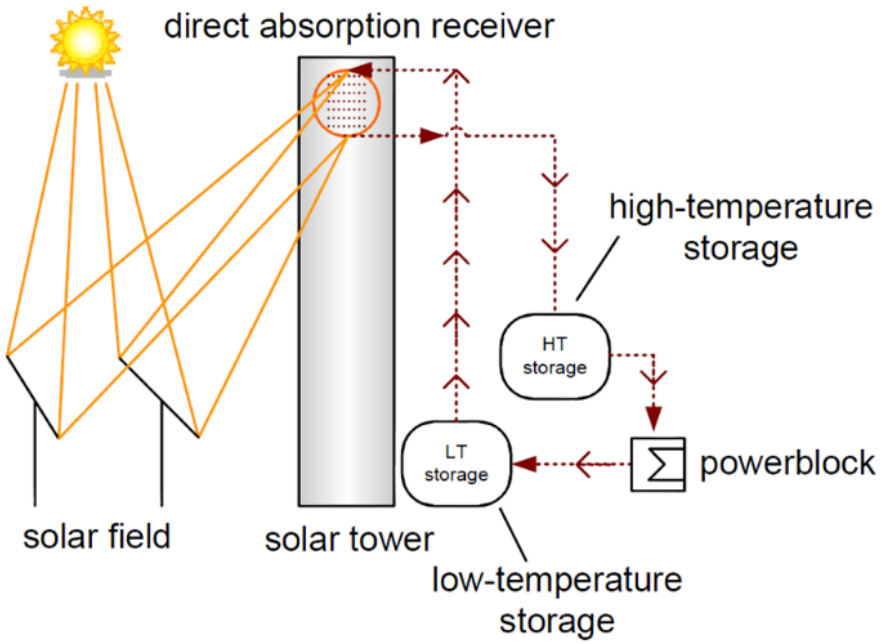

Figure 2-19: Solid particle receiver used in a solar power generating layout [27]

2.3.3 Heat transfer fluids

Heat transfer fluid is one of the main component of a typical CSP system. It is responsible to transfer the absorbed heat from the receiver to the power block section where power is generated and in some cases, where heat storage is applied, it is used to store heat for later use when sun rays are not available. For any CSP plant to operate, a large amount of heat transfer fluid is required. Thus, it is necessary to minimize it is cost and maximize its performance. The preferred characteristics of a typical heat transfer fluid include: low melting point, high boiling point and thermal stability, low vapor pressure (less than atmospheric pressure) at high temperature, low corrosion with the metal alloys that contains the heat transfer fluid, high heat capacity for energy storage, low viscosity, high thermal conductivity, and low cost [36]. In Figure 2-20, the working temperature ranges for thermal oils, molten-salts and liquid metals are shown.

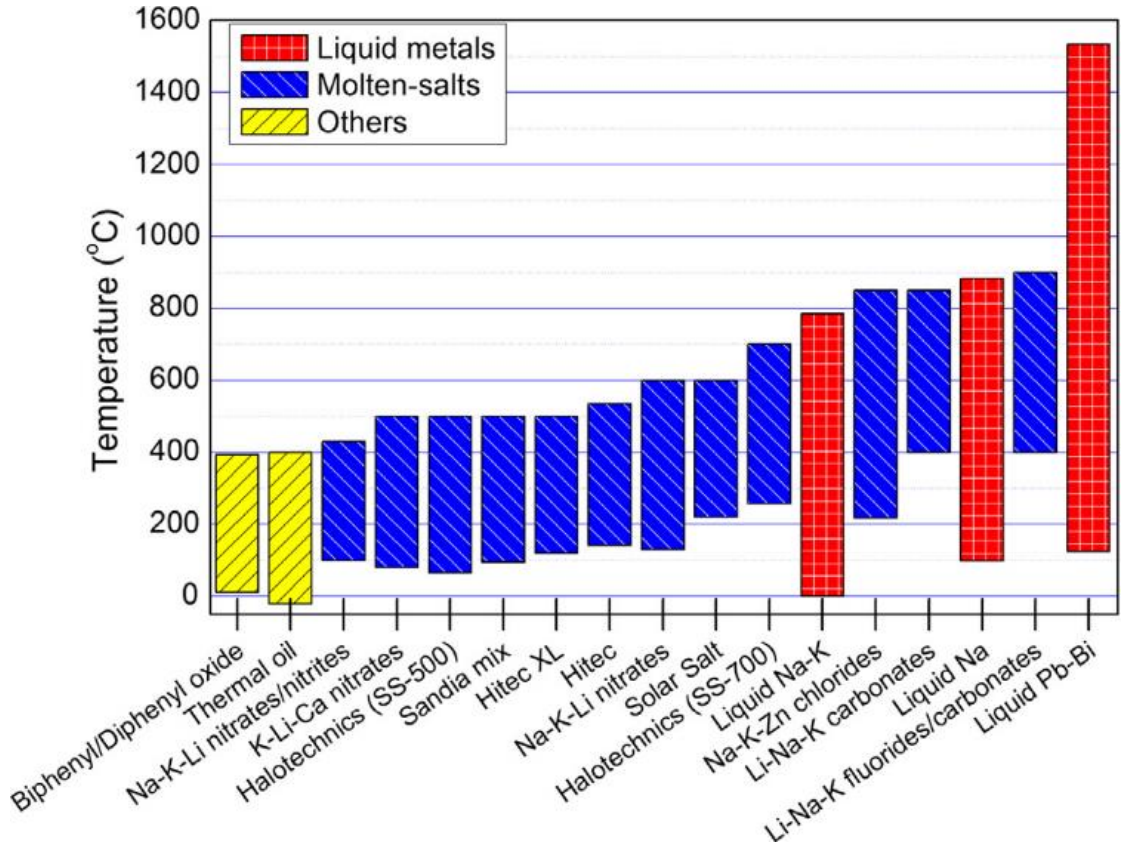

Figure 2-20: Operating temperature range for various heat transfer fluids [37].

Based on the material of the heat transfer fluid, it can be classified into six main groups: (1) air and other gases, (2) water/steam, (3) thermal oils, (4) organics, (5) molten-salts and (6) liquid metals [36]. As the liquid metals are still under study for the concentrated solar applications, it will not be considered.

2.3.3.1 Air

Air usage as a heat transfer fluid is still limited in large CSP plants. In 2009, a 1.5MWe plant was built in Jülich, Germany that utilizes air as the heat transfer fluid in the open volumetric receiver. The air is heated up to a temperature of 700°C at atmospheric pressure to generate steam in the power block section [38]. As the air is abundant and cost free, this technology is cost effective and has high efficiencies. Moreover, due to the very low dynamic viscosity related to other liquid metals heat transfer fluids, air has decent flow properties inside the pipelines in a CSP system [39] . One of the draw backs of using air is that it requires large volume of air.

2.3.3.2 Water/ Steam

Usually water/steam fluid is used as both heat transfer fluid and working fluid in plants where steam Rankine cycle is used to produce the electricity. This means that plant operated with less losses and costs associated with heat exchangers. The use of water/steam as both heat transfer fluid and working fluid in the power cycle simplifies the system and end up with improved efficiency and cost reduction of electricity production [40].

This heat transfer fluid is used currently in one of the world's largest CSP plant – the Ivanpah solar power facility that was launched in February 2014. Moreover, there are

seven commercial CSP plants in the world working with water/steam as the single fluid. Four plants are in Spain (Puerto Errado 1, PS10 solar power tower, PS20 solar power tower and Puerto Errado 2) and the other three are in California, USA (Kimberlina solar thermal energy plant, Bakersfield, Sierra sun tower, Lancaster and Ivanpah solar power facility, Ivanpah dry lake) [38].

Besides all of the less losses and cost reduction with using water/steam as both heat transfer fluid and working fluid, the system will require extra effort to control due to the phase change phenomena of the water and steam (evaporation) in the receiver [13]. Moreover, one of the major problem with using water/steam as a heat transfer fluid is the lack of water in desert regions CSP plants where large land area and high direct solar radiation intensity are available [41].

2.3.3.3 Thermal oils

Synthetic oils, silicone oil and mineral oil have been used as heat transfer fluids in CSP plants along time ago. Examples of such plants are the Andasol-3, Helioenergy, Aste, Solacor and Solnova plant located in Spain using parabolic trough collector [38]. They have the advantage of delivering predictable and stable receiver operation. Most of these oils have the same thermal conductivity and can be thermally stable only up to 400 °C and that is why they are not usually used for high temperature applications and very efficient solar thermal systems [38]. From Figure 2-20, it can be noticed that thermal oils

have limited operating temperatures compared to the molten salt and liquid metals. Moreover, they show a decomposing affect when operated at high temperature with fire hazards if leaking outside the pipes. Cost wise, these thermal oils are highly expensive [42].

2.3.3.4 Organics

Organic materials are also heat transfer fluids that are used in CSP systems. Biphenyl/Diphenyl, for example, is an oxide pair (also known as Therminol VP-1) that is usually used in total of eight commercial CSP systems, especially in thermal plants located in Spain [37]. Operating temperature range of this Biphenyl/ Diphenyl oxide is very narrow within 12–393 °C [38]. As the thermal oils, the operating temperatures are limited compared to molten salts and liquid metals.

2.3.3.5 Molten salts

Molten salt heat transfer fluid is a fluid that has the advantages of being a single phase fluid in the receiver, has a high specific heat, and has a thermal stability at high temperatures. Using the molten salt in the thermal energy storage sector has proven the its effectiveness with the use of insulated tanks. Moreover, molten salts also have properties similar to water at high temperature including similar viscosity and low vapor pressure [43]. Most of the used salts solidify at temperatures below 220 °C and this means that external heating is required to keep the salt away from solidification during

cols starts [13]. In addition, molten salts are corrosive and it reacts with air and water if leaks occur.

Molten salts are used in modern CSP systems with the earliest molten salt power tower systems operated back in 1984. These innovative systems were the THEMIS tower (2.5MWe) in France and Molten-salt Electric Experiment (1MWe) in the United States [37].

Most of the currently used salts are based on nitrates/nitrites among various heat transfer fluids. Solar salt, NaNO3 (60 wt%)–KNO3 (40 wt%), is a common used salt in many modern CSP systems. It melts at 223 °C and remains in thermally stable liquid phase at temperatures up to 600 °C [44]. The second commonly used salt is the Hitec salt. It consists of NaNO3 (7 wt%)–KNO3 (53 wt%)–NaNO2 (40 wt%) and it is mixture of alkali-nitrates/nitrites. The major advantage of Hitec salt is that its melting point (142°C) is much lower than that of Solar Salt [45]. This advantage will reduce the amount of energy required for heating to keep the salt from solidification.

2.3.4 Thermal energy storage

Concentrated solar plants can be designed with a heat storage system to produce electricity after sunset or with cloudy skies. There are two main types of thermal storage, direct or indirect storage. For direct storage arrangements and as shown in Figure 2-21

(a), the heat transfer fluid is the same as the storage medium. On the other hand, indirect storage arrangements utilize a heat exchanger to transfer thermal energy from the storage medium to the heat transfer fluid and it is shown in Figure 2-21 (b). Currently, thermal energy storage technology integrated into the parabolic trough and power tower plants is the two-tank sensible energy storage using a molten salt comprising of sodium nitrate and potassium nitrate (60–40 wt %) [46].

The cold HTF whether it is water/steam, molten salt or synthetic oil is firstly heated up in the solar field and then the thermal storage unit (either directly or indirectly) is charged by the hot HTF through heat exchangers. Based on the energy demand and when the stored energy is needed, the system operates in reverse to generate steam to run the power plant. In the case of molten salt as a HTF, the hot and cold molten salt is separately stored in the hot and cold tanks as shown in Figure 2-21. It was reported that at the Solar Two power tower demonstration the round-trip energy efficiency can achieve up to 98% for the storage system [47].

The range of the operating temperature of the storage system is dependent on the solar field technologies used. The current parabolic trough and power tower technology can provide HTF at temperatures of 393 °C and 565 °C, respectively, that result in a storage temperature range of 292–385 °C and 290–565 °C, respectively [48]. Higher operating temperature will enable the possibility to increase the overall solar-to-electricity

efficiency, reduce thermal storage volume and decrease the levelized cost of electricity [49].

Thermal storage can considerably improve the capacity factor that is defined as the ratio of the number of hours per year that the plant can produce electricity with respect to the maximum possible output for the same period. Moreover, thermal storages can improve the plant dispatchability that is defined as the ability of a certain plant to provide electricity based on the operator's demand. For instance, in the period of sunny hours, the excess of solar energy can be stored in a high thermal capacity fluid and then released based on the demand. This demand can be producing electricity either in the day time at the peak load or at the night time. Based on the targeted load the heat storage capacity is designed accordingly. To produce this required heat, the solar field, the mirrors and solar collectors, of the solar plant must produce higher than the nominal electric capacity of the plant.

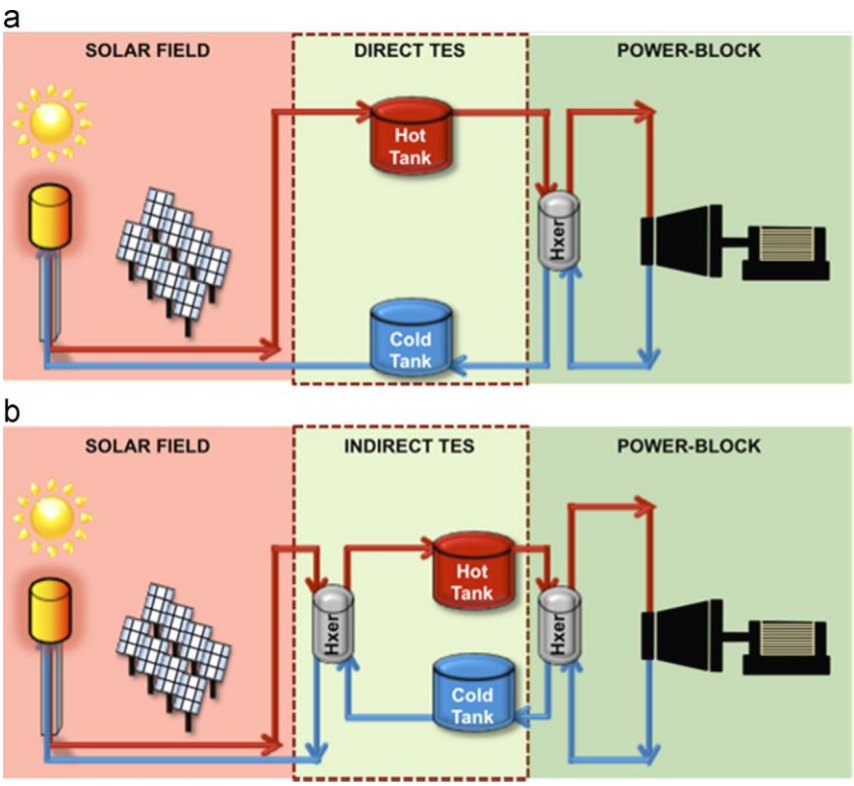

Figure 2-21: Thermal storage system integrated in the CSP plant with solar field and power block: (a) direct heat storage and (b) indirect heat storage [50].

In this regard, a parameter called the solar multiple (SM) that normalizes the size of the solar field to the power block of the plant. A system with an SM of 1 means that the solar collector is sized to provide the power block with only the enough energy to operate at its rated capacity under reference solar conditions. A larger SM indicates a larger solar collector area and in this case, any excess of thermal energy provided by the solar filed that is over the capacity rating of the power block has to be storied or removed from the system in another application. Currently, plants with no thermal storage have a SM

between 1.1-1.5 while plants with thermal storage may have solar multiples of 3-5 ([8].

2.3.5 Power cycle

Mainly, there are three thermos mechanical cycles that are being implemented with solar thermal power technologies. These are Rankine cycle, Brayton cycle and Stirling engine systems. These power cycles of a thermal CSP system are in many cases equivalent to those of conventional thermal power plants.

2.3.5.1 Rankine Cycle

A widely held of CSP plants are based on the Rankine cycle, that uses steam as a working fluid, with boilers and steam turbines as the major components. The same cycle is used extensively in coal or biomass fired plants. The cycle starts with pumping the water by a feed-water pump to the boiler to be boiled up and then superheated. Using a steam turbine, the superheated steam is expanded turning an electric generator. The low-pressure steam, exiting the turbine, is after that condensed in a heat exchanger that can be either air or water cooled. Finally, the water will be back to the feed-water pump to be reused again. Steam Rankine cycles have been, and continue to be, utilized with mainly parabolic trough and central receiver solar thermal power plants.

2.3.5.2 Brayton cycle

The Brayton cycle is the foundation of the gas turbine conventional cycle and it is used in a few tower and dish system and they have been tested in small scale and proposed for large-scale tower systems [13]. The cycle begins with an adiabatic compression of a gas by a compressor. Next, the heat is added to the gas at constant pressure. After that, the gas expanded at the turbine at adiabatic expansion. Finally, the air cooled at constant pressure. In a system that utilize fossil fuels, the heat is added in a combustion chamber and gases are exhausted to atmosphere after expansion, either with or without heat recovery. However, for solar applications, heat recovery is economically necessary for efficiency gains. Moreover, a gas fuel back up system is recommended for system control purposes [51].

2.3.5.3 Stirling Cycle

This cycle is being used for small module engines in the range of kW up to MW and specially for dish solar systems. Due to the possible achieved high process temperature using this cycle, the small sizes applications have high efficiency [13]. The Stirling cycle employs external heating and cooling of its working fluid to finish the cycle. It is mainly used in Dish/Stirling systems that produce very high net solar to electricity conversion efficiencies [51]. In solar applications, Stirling engines are the most engines that are working on this cycle and use commonly helium or hydrogen as the working fluid.

3 LITERATURE REVIEW

In this chapter, concentrated solar power plants, either operational, under construction, under contract or under development, around world are studied and described from different aspects. Parabolic trough, linear Fresnel reflector, power tower, and dish/engine systems are the four technologies available. These data, for all the plants under all different status, is compiled in tables. An example of a certain plant is shown in details for illustration. After that, the solar software packages that are used in this thesis, SolarPILOT and SAM, are described.

An important step prior to finding the most proper CSP technology and components for a certain location is to find how CSP plants are utilized around the world and which technology and components are used. Qatar doesn't have yet any large CSP facility that could provide information about the performance of the CSP systems in Qatar. Thus, an extensive data collection is required to choose the most proper CSP system.

3.1 CSP plants information

Currently, one of the most complete data source about the CSP plants in the world is the SolarPACES program that stands for Solar Power and Chemical Energy Systems. It is an

international program of the International Energy Agency, furthers collaborative development, testing, and marketing of CSP plants [52].

The available data includes CSP projects around the world that have plants that are either operational, under construction, under contract or under development. CSP technologies include parabolic trough, linear Fresnel reflector, power tower, and dish/engine systems. Moreover, background information, a listing of participants in the project, and data on the power plant configuration.

The total number of projects are 167 installed in 21 different countries from all over the world. The available material is updated regularly to include any new or updated information about the projects. In this thesis, all this information for the all CSP projects was compiled and grouped in one Microsoft Excel file for the ease of searching and comparing between the different projects and the file was last updated in Dec 2016. An example of the information compiled from SolarPACES for project Shams 1 located in United Arab Emirates is shown in Appendix B. The complete projects list, categorized as per the CSP technology, along with all the information is included in Appendix C.

3.1.1 Compiled information about CSP plants

Having more than 167 projects in different status in 21 different countries requires summary tables and graphs to understand the full picture of the projects and to know

which countries possess the highest number plants that are running with certain CSP technology and certain plant operation status.

In Figure 3-1, the total number of CSP plants installed per each country is illustrated. Spain has the highest number of CSP plants installed of more than 50 plants, then Unites States comes in the second place having 40 plants and China in the third place with more than 20 plants. The rest of the other countries are below the line of 10 plants except India.

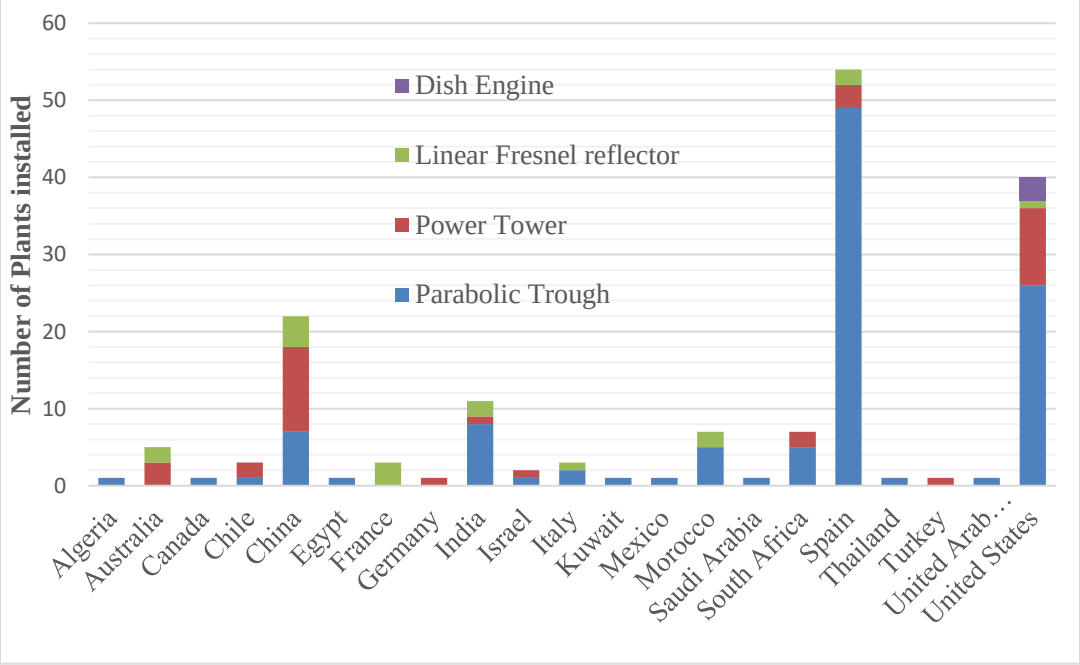

Figure 3-1: Total number of plants per country with the CSP technology used.

In Table 3-1 and Figure 3-2, the total number of plants of each CSP technology is illustrated. It is obvious that parabolic trough technology is the highest technology that is used with 67% of utilization and 112 plants. This is because the parabolic trough technology is the most mature among the CSP technologies and it is commercially proven. Next, power tower technology comes in the second place with utilization of 21% and 35 plants. It is worth to mention that power tower technology is the future trend of CSP technologies due to it is higher efficiency, heat transfer fluid's temperature and concentration ratio compared to other technologies. Then, the linear fresnel reflector and the dish engine.

Table 3-1: Total number of plants of each CSP technology

	CSP Technology			
	Parabolic Trough	Power Tower	Linear Fresnel reflector	Dish Engine
Total number of plants	112	35	17	3

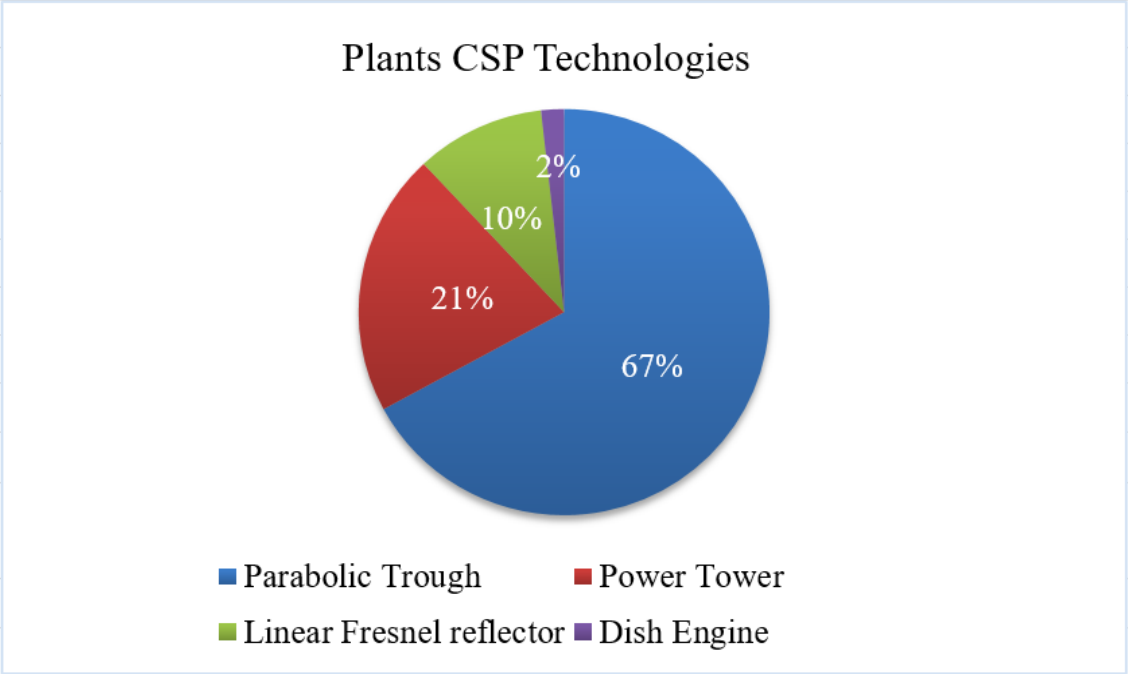

Figure 3-2: Total number of plants of each CSP technology

In Table 3-2 and Figure 3-3, the total number of plants of each operational status is illustrated. Plants at operational status represents most the plants with 73% and 182 plants. Then, 40 plants are under development and this represents 16%. The third highest percentage is the plants that are under construction and 3 plants only are non-operational and under contract.

Table 3-2: Total number of plants of each operational status

	Plants Status				
	Non-Operational	Operational	Under Construction	Under Contract	Under Development
Total number of plants	3	182	22	3	40

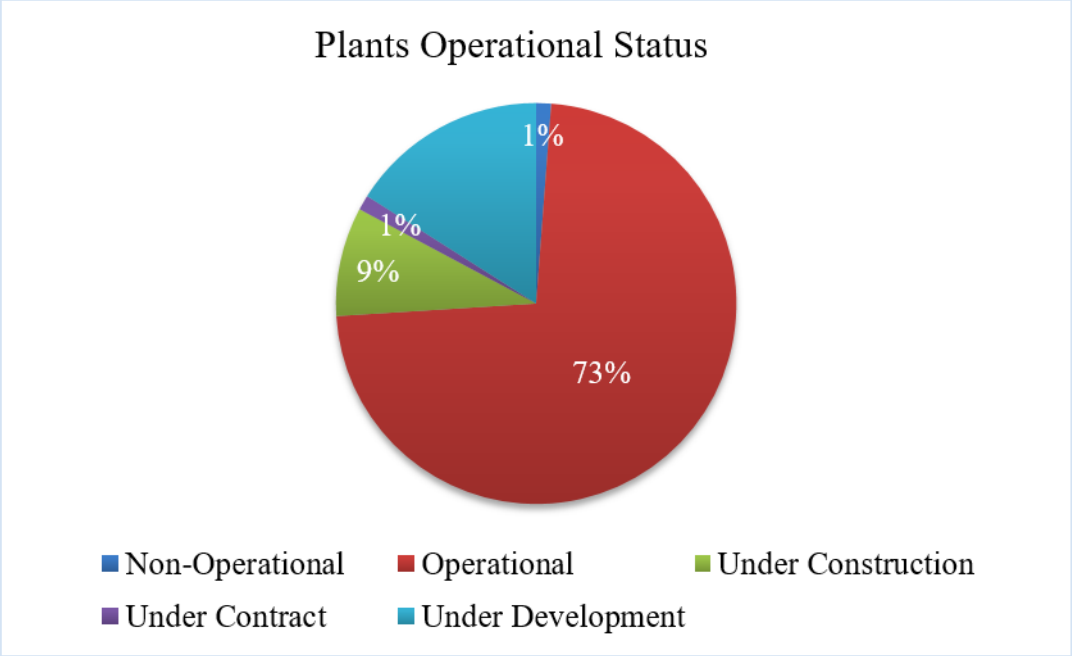

Figure 3-3: Total number of plants of each operational status

The CSP capacity of the operational and under construction plants categorized by receiver technologies and with/without storage is shown in Figure 3-4. Nearly less than half of the installed CSP capacity is integrated with thermal storage. Over than 80% of

the capacity under construction has energy storage and the majority is with molten salt storage technology. This percentage increases to 88% in trough and tower systems. While the current thermal storage technology used in linear Fresnel plants is a short term pressurized steam storage with less than an hour [46].

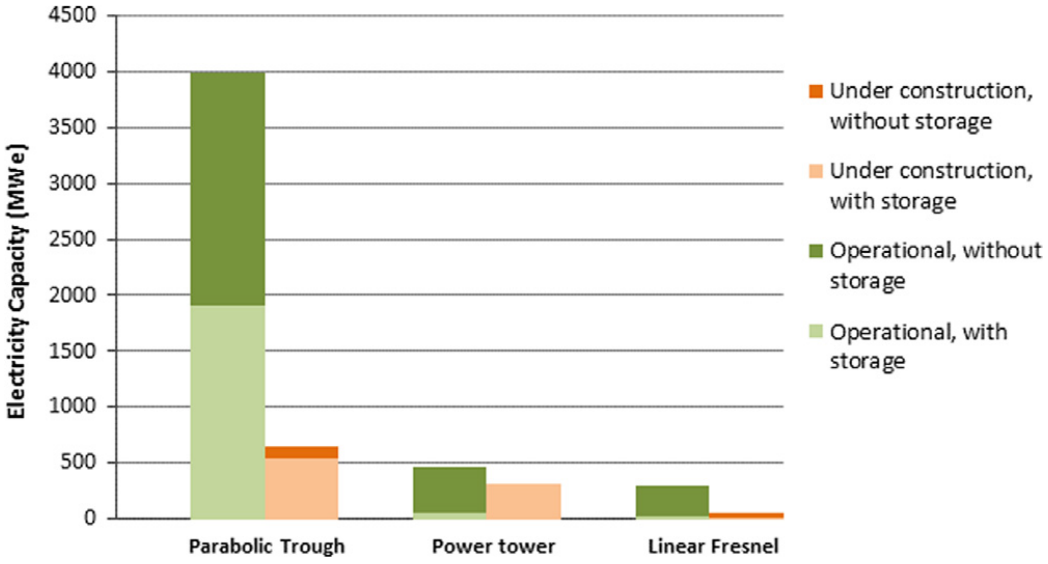

Figure 3-4: CSP capacity categorized by receiver technologies and with/without storage [46].

More details about the number of plants in each country with the 4 different technologies and their operational status are shown in Table 3-3, Table 3-4, Table 3-5 and Table 3-6. It can be shown from Table 3-3 that many countries from different continents have parabolic trough technology with most of them are in operational status. The rest of

plants are under development and under construction. Spain with 45 operational plant in in the top of the list.

Table 3-3: Number of plants in each country with parabolic trough technology and their operational Status.

Country	Parabolic Trough Plants				
	Non-Operational	Operational	Under Construction	Under Contract	Under Development
Algeria		1			
Canada		1			
Chile					1
China			1		6
Egypt		1			
India		3	5		
Israel					1
Italy		2			
Kuwait					1
Mexico			1		
Morocco		3	2		
Saudi Arabia			1		
South Africa		2	2		1
Spain		45	3	1	
Thailand		1			
United Arab Emirates		1			
United States	1	17			8
Total number of plants	1	77	15	1	18

Table 3-4: Number of plants in each country with power tower technology and their operational status

Country	Power Tower Plants				
	Non-Operational	Operational	Under Construction	Under Contract	Under Development
Australia		3			
Chile			1		1
China		1	2		8
Germany		1			
India		1			
Israel			1		
South Africa		1			1
Spain		3			
Turkey		1			
United States		3			7
Total number of plants	-	14	4	0	17

Table 3-5: Number of plants in each country with linear Fresnel refflector technology and their operational

Country	Linear Fresnel reflector Plants				
	Non-Operational	Operational	Under Construction	Under Contract	Under Development
Australia	1	1			
China					4
France		1	1	1	
India		1	1		
Italy		1			
Morocco			1	1	
Spain		2			
United States		1			
Total number of plants	1	7	3	2	4

The CSP plants that are currently operating and being constructed have been reviewed also by [39] and the details of the plants' solar collector configuration, solar field operating conditions, TES systems and cooling methods are summarized in Table 3-7.

Table 3-6: Number of plants in each country with dish engine technology and their operational status

	Dish Engine Plants				
Country	Non-Operational	Operational	Under Construction	Under Contract	Under Development
United States	1	1			1
Total number of plants	1	1	0	0	1

Table 3-7: Representative features of the different CSP technologies for current and future CSP plants [46].

	Current trough	**Current tower**	**Current linear Fresnel**	**Current dish**
Maturity	High, commercially proven	Medium, recently commercially proven	Medium, pilot plants, commercial pro-jects under construction	Low, demonstration projects
Typical plant capacity	100 (MW)	50–100 (MW)	50 (MW)	3–30 each (kW)
Operating temperature of solar field (°C)	290–390	290–565	250–390	550–750
Plant peak efficiency (%)	14–20	23–35	18	31.25
Annual average conversion efficiency (%)	13–15	14–18	9–13	22–24

Collector concentration (suns)	70–80	1000	> 60 (depends on secondary reflector)	>1300
Power block cycle and fluid conditions	Superheated steam Rankine, steam @380 °C / 100bar	Superheated steam Rankine, steam @ 540 °C / 100–160bar	Saturated steam Rankine (steam @ 270 °C / 55 bar), superheated steam Rankine (steam @ 380 °C / 50 bar)	Stirling / Brayton
Power cycle efficiency (%)	37.7	41.6	–	–
Heat transfer fluid	Synthetic oil, water/steam (DSG), molten salt (demonstration), air (demonstration)	Water/steam, molten salt, air (demonstration)	Water/steam	Air, hydrogen, helium
Annual capacity factor (%)	20–25 (no TES) 40–53 (6h TES)	40–45 (6–7.5h TES) 65–80 (12–15h TES)	22–24	~25
Storage system	Storage system Indirect two tank molten salt storage (293–393 °C)	Direct two-tank molten salt storage (290–565 °C),	Short-term pressurized water storage (Ruths tank)	No storage for Stirling dish, chemical storage under development
Capital cost (USD/kW)	4700–7300(no TES, OECD countries) 3100–4050 (no TES, non-OECD countries)	6400–10,700 (with TES)	–	–
LCOE (USD/kW h)	6400–10,700 (with TES) 0.26–0.37(no TES) 0.22–0.34 (with TES)	0.2–0.29 (6–7.5h TES) 0.17–0.24 (12–15h TES)	0.19–0.38 (no TES) 0.17–0.37(6h TES)	–
Cooling method	Wet	Wet, dry	Dry	Dry
Suitable for air cooling	Low to good	Good	Good	Best
Water requirement (m3/ MW h)	3 (wet) 0.4–1.7 (hybrid) 0.3 (dry)	1.8–2.8 (wet) 0.3–1 (hybrid) 0.3 (dry)	3.8 (wet)	~0.08 (mirror washing)

3.2 Annual solar to electricity efficiency

A significant parameter to evaluate a CSP system is the annual solar to electricity efficiency. A cost reduction is a major result of any efficiency improvement. In Figure 3-5**,** the estimated annual efficiency for various CSP technical options as well as the maturity of the technology is shown. In the current industrial CSP plants, tower systems with molten salt as both the HTF and the storage material are the most efficient option with annual efficiency of 17–18%. On the other hand, the lowest among those technical options is the annual efficiency of linear Fresnel systems with saturated/superheated steam, which is 9–13% [53].

The tower systems can have higher efficiency and that is expected to be increased from the current 18% to above 23%. This can be accomplished by firstly using supercritical steam or carbon dioxide as the HTF and secondly using pressurized air as the HTF to drive a combined cycle plant where the upper cycle is Brayton cycle and lower cycle is Rankine cycle [46]. However, those both systems are still under study and they are at a very early stage of development. The current feasibly options of tower systems are using saturated steam as HTF, superheated steam as HTF or molten salt as the HTF with storage. The usage of superheated steam as HTF system has the highest annual efficiency then the molten salt as the HTF with storage and finally the saturated steam as HTF. The latter is not commonly used anymore as other options have higher annual efficiency.

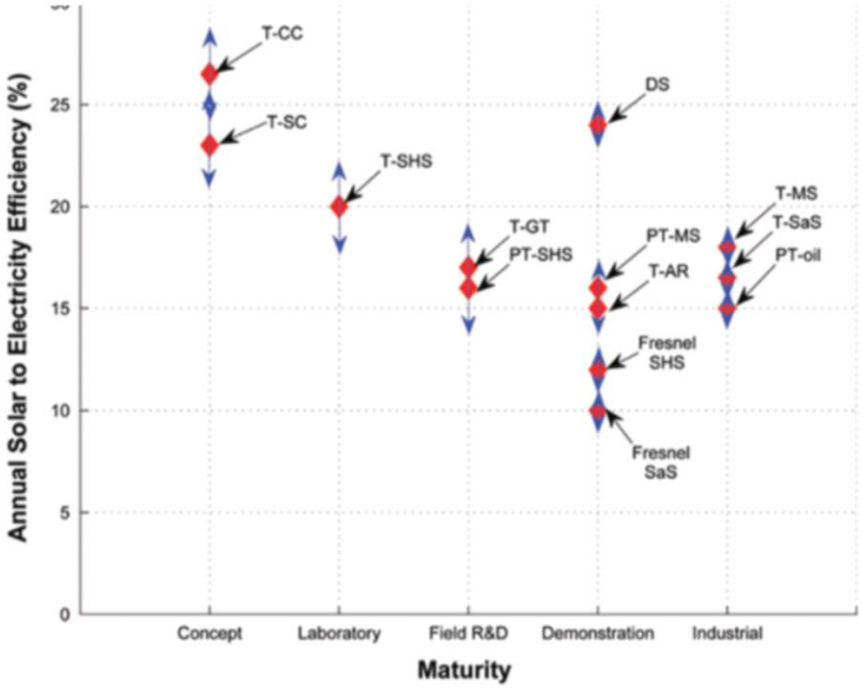

CSP technology	Technical options
Parabolic troughs (PT)	PT-oil: oil as HTF and molten salt storage
	PT-SHS: superheated steam as HTF
	PT-MS: molten salt as HTF and storage
Linear Fresnel systems (F)	Fresnel SaS: saturated steam as HTF
	Fresnel SHS: superheated steam as HTF
Towers (T)	T-SaS: saturated steam as HTF
	T-SHS: superheated steam as HTF
	T-MS: molten salt as HTF and storage
	T-AR: ambient pressure air as HTF and Rankine cycle
	T-GT: pressurised air as HTF and Brayton cycle
	T-SC: supercritical cycle
	T-CC: pressurised air as HTF and combined cycle
Parabolic dishes (DS)	DS: helium Stirling cycle

Figure 3-5: Annual solar-to-electricity efficiency as a function of development level [11]

3.3 Software packages

Currently, there are many software packages that have been developed for analyzing and optimizing either the entire solar thermal plant or only the heliostat field only. Examples of these software packages are HFLCAL, DELSOL3, CAMPO, SOLTRACE, SAM (System Advisor Model) and SolarPILOT. Many of these software packages are available as freeware for the public and providing the purpose of using it and the identity of the user are enough to have it. Moreover, many of them allow the user to have the freedom in choosing the variables that are required to be optimized. Although some software packages allow the user to specify the solar field layouts, currently it is shown that their optimization capabilities are restricted to cornfield or radial staggered layouts [54].

In this thesis, SolarPILOT software package (version: 2017.2.7), which is an integrated layout and optimization tool for solar power towers, is used for designing and optimizing the solar field layout of the plant and then the final design values are inserted in SAM software packages for designing and optimizing the entire solar plant from a financial and technical point of view.

SolarPILOT is developed by the National Renewable Energy Laboratory (NREL) and it generates and characterizes power tower systems only. SolarPILOT has implemented methods to reduce the overall computational efficiency of the number of heliostats while generating accurate and precise results. These methods have been developed as part of

the U.S. Department of Energy (DOE) SunShot Initiative research funding at NREL and are made available as part of this software. With SolarPILOT and as per the official website of the software packages [55].

On the other hand, SAM (version: 2017.1.17) is a performance and financial model designed to facilitate decision making for users involved in the renewable energy sector. SAM makes performance predictions and cost of energy estimates for grid-connected power projects based on installation and operating costs and system design parameters that user specifies as inputs to the model. Projects can be either on the customer side of the utility meter, buying and selling electricity at retail rates, or on the utility side of the meter, selling electricity at a price negotiated through a power purchase agreement [56].

SAM calculates the cost and performance of renewable energy projects using computer models developed at NREL, Sandia National Laboratories, the University of Wisconsin, and other organizations. Each performance model represents a part of the system, and each financial model represents a project's financial structure. The models require input data to describe the performance characteristics of physical equipment in the system and project costs. SAM's user interface makes it possible for people with no experience developing computer models to build a model of a renewable energy project, and to make cost and performance projections based on model results [56].

Currently and with low numbers of renewable projects in the middle east region, the data base of the performance and cost values of typical renewable project is not available to help in evaluating and estimating a new project. Both SolarPILOT and specially SAM provide a very good reference for a reasonable default values from many references and research work for the all types of concentrated solar power. Once a new case or file is created through those both softwares, inputs values are populated with default values about the specified design values. As the file or the case is refined and gets in more analysis, the input values could be changed to more appropriate values for the project scenario. Two of the main references that are used by SolarPILOT and SAM to determine the default values of CSP are the [57] and the [58].

4 WORK DESCRIPTION

In this chapter, the solar insolation model derivation and its validation are discussed. Then, the software validation of both software packages used in this project, SolarPILOT and SAM, is described and discussed. Third, the electrical consumption Souq Waqif is shown with considerations for plant location and selection and desalination process. After that, the considerations for heliostats cleaning, water demand, CO_2 gas emissions reduction and maintenance actives are discussed.

4.1 Solar Insolation Model

Determining the available solar energy of a certain location is the most important step in case of applying any solar application in that location. The available solar energy can be either measured or simulated. The measurement method is way costlier than the simulation method because of the high cost of the instruments in general. Moreover, its result is only valid for the studied location only at certain climate conditions and thus it has limited benefits and cannot be used to optimize the best location among two unless both are measure at the same time to get the same climate conditions. However, these drawbacks do not mean that measurement method is not valuable. It is required to validate the simulation method and assure that the simulation equations are accurate to the reality. On the other hand, the simulation method can be used easily to check the

location's solar availability at different seasons and at different climate conditions. Moreover, the same can be measured at different slope surface of the solar plate or mirror to find out the optimum angle.

In the current project work, a Microsoft Excel-based model has been built to determine the hourly available solar energy per square meter on a horizontal, sloped, one-axis tracking and two axis tracking surface in any location on earth. This model can find the optimum values of the controllable parameters that affect the capturing of the available solar energy. For example, the inclination and the azimuth angle of the surface. The model is based on the most accurate available relations for calculating available solar energy. These well-known theoretical relations have been clearly defined in section 2 in [59] and they have been tested in Japan and verified [60] [61].

In the current study, the cloudy sky approach is used that where the available solar energy at ground surface becomes a function of only the extraterrestrial radiation and the clearness index (KT). Both will be defined below in the equations section.

4.1.1 Model's equations

The model has many types of equations, the solar angles' equations, the horizontal surface's equations, the tilted surface's equations and the tracking surface's equations. The equations of these models are generating the insolation available at a certain location

at an average day of the month. In Table 4-1, the average day of the month of each month is mentioned.

Table 4-1: Recommended Average Days for Months and Values of n by Months

Month	***n* for *i*th Day of Month**	**For Average Day of Month**		
		Date	***n***	***δ***
January	i	17	17	−20.9
February	31 + i	16	47	−13.0
March	59 + i	16	75	−2.4
April	90 + i	15	105	9.4
May	120 + i	15	135	18.8
June	151 + i	11	162	23.1
July	181 + i	17	198	21.2
August	212 + i	16	228	13.5
September	243 + i	15	258	2.2
October	273 + i	15	288	−9.6
November	304 + i	14	318	−18.9
December	334 + i	10	344	−23.0

Before starting with the model's equations, an important variable should be defined which is the solar time. It is the time used in all the sun-angle relations and it does not overlap with local clock time. It is essential to convert the standard time to solar time by applying two corrections. The first one is shown in Equation (1) which is a constant correction for the difference between the location longitude and the meridian on which the local standard time is based. The difference between solar time and standard time is in minutes.

$$\text{Solar time} - \text{standard time} = 4(\text{Lst} - \text{Lloc}) + \text{E} \quad (1)$$

where:

- Lst is the standard meridian for the local time zone
- Lloc is the longitude of the location.

The second correction is shown in Equation (2) that is derived from the equation of time. It considers the disruption in the earth's rate of rotation.

$$\text{E} = 229.2(0.000075 + 0.001868\ \cos\text{B} - 0.032077\ \sin\text{B} - 0.014615\ \cos 2\text{B} - 0.04089\ \sin 2\text{B}) \quad (2)$$

where:

- E is the equation of time (in minutes).
- $\text{B} = (\text{n} - 1)\frac{360}{365}$.
- n is the day of the year.

4.1.1.1 Solar angles' Equations

The geometric relationships between a plane of any orientation relative to the earth at any time (whether that plane is fixed or moving relative to the earth) and the incoming beam

solar radiation, that is, the position of the sun relative to that plane, can be described in terms of several angles. These angles are indicated in Figure 4-1 [59].

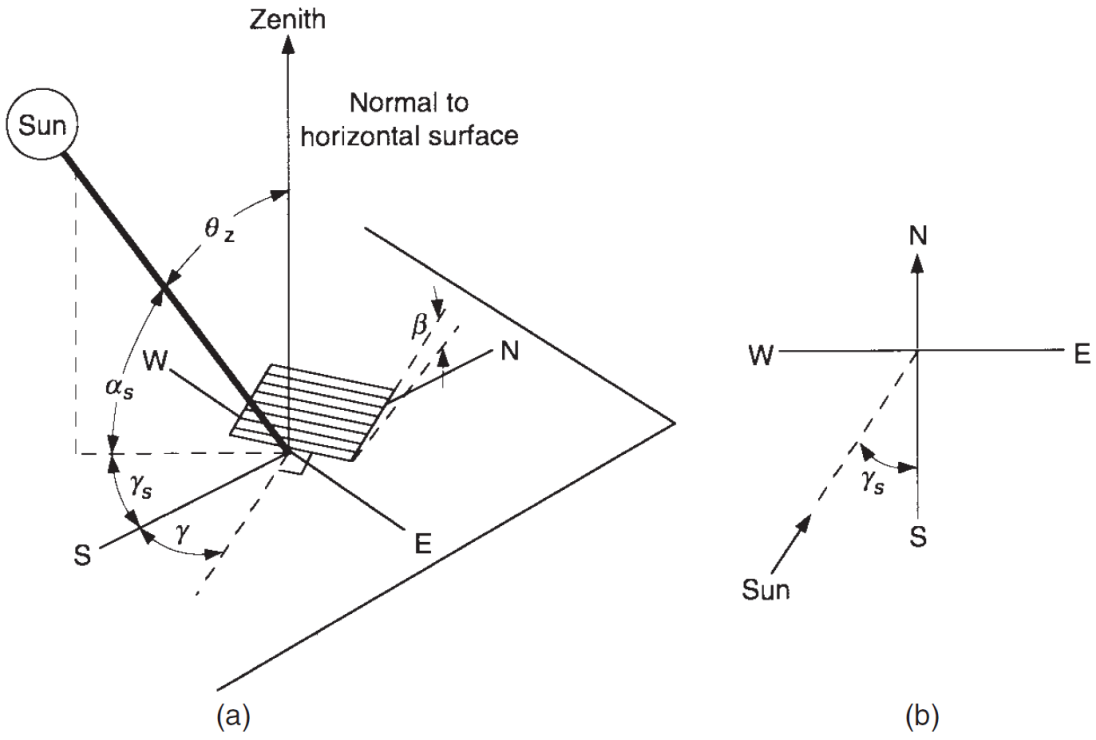

Figure 4-1: (a) Zenith angle, slope, surface azimuth angle, and solar azimuth angle for a tilted surface. (b) Plan view showing solar azimuth angle [59].

φ Latitude, the angular location north or south of the equator, north positive; $-90^\circ \leq \varphi \leq 90^\circ$.

δ Declination, the angular position of the sun at solar noon (i.e., when the sun is on the local meridian) with respect to the plane of the equator, north positive; $-23.45^\circ \leq \delta \leq 23.45^\circ$. The declination δ can be found from Equation (3)

$$\delta = 23.45 \sin\ (360\ \frac{284 + n}{365}) \qquad (3)$$

β Slope, the angle between the plane of the surface in question and the horizontal; $0^\circ \leq \beta \leq 180^\circ$. ($\beta > 90^\circ$ means that the surface has a downward-facing component.)

γ Surface azimuth angle, the deviation of the projection on a horizontal plane of the normal to the surface from the local meridian, with zero due south, east negative, and west positive; $-180^\circ \leq \gamma \leq 180^\circ$.

ω Hour angle, the angular displacement of the sun east or west of the local meridian due to rotation of the earth on its axis at 15° per hour; morning negative, afternoon positive. In other words, it is the difference between noon and the desired time of day in terms of a 360^o rotation in 24 hours. It can be found from Equation (4) [62]

$$\omega = \frac{12 - T}{24} \times 360^\circ = 15(12 - T)^\circ \qquad (4)$$

ωs Sunset Hour angle, the hour angle when the Zenith angle θz is 90^o. It can be found from Equation (5)

$$\cos \omega s = \frac{-\sin \varphi \sin \delta}{\cos \varphi \cos \delta} = -\tan \varphi \tan \delta \quad (5)$$

It also follows that the number of daylight hours N can be found from Equation (6)

$$= \frac{2}{15} \cos^{-1} (-\tan \varphi \tan \delta) \quad (6)$$

θ Angle of incidence, the angle between the beam radiation on a surface and the normal to that surface and can be found from Equation (7)

$$\cos \theta = \sin \delta \sin \varphi \cos \beta - \sin \delta \cos \varphi \sin \beta \cos \gamma + \cos \delta \cos \varphi \cos \beta \cos \omega + \cos \delta \sin \varphi \sin \beta \cos \gamma \cos \omega + \cos \delta \sin \beta \sin \gamma \sin \omega \quad (7)$$

Additional angles are defined that describe the position of the sun in the sky:

θz Zenith angle, the angle between the vertical and the line to the sun, that is, the angle of incidence of beam radiation on a horizontal surface. For horizontal surfaces, the angle of incidence is the zenith angle of the sun, θz is found from Equation (8)

$$\cos \theta z = \cos \varphi \cos \delta \cos \omega + \sin \varphi \sin \delta \quad (8)$$

γs Solar azimuth angle, the angular displacement from south of the projection of

beam radiation on the horizontal plane. Displacements east of south are negative and west of south are positive. The solar azimuth angle γs has values in the range of 180◦ to −180◦. The γs is negative when the hour angle is negative and positive when the hour angle is positive and can be found from Equation (9)

$$\gamma_s = \text{sign}\,(\omega)\left|\cos^{-1}\left(\frac{\cos\theta z \sin\varphi - \sin\delta}{\sin\theta z \cos\varphi}\right)\right| \quad (9)$$

αs Solar altitude angle, the angle between the horizontal and the line to the sun, that is, the complement of the zenith angle. The solar altitude angle αs is a function only of time of day and declination as shown in Equation (10)

$$\alpha s = \text{Arc}\sin\left(\cos\varphi\cos\delta\cos\omega + \sin\varphi\sin\delta\right) \quad (10)$$

ρ Ground reflectivity (Albedo), value of albedo for a certain surface is based on the type of that surface. In Qatar, the location of the proposed solar plant is assumed to be in an arid location. For a desert surface location, the value of albedo is given as 40% [63].

4.1.1.2 Horizontal surface's equations

The total solar radiation on a horizontal surface is split into its diffuse and beam

components. The usual approach is to correlate Id/I, the fraction of the hourly radiation on a horizontal plane which is diffuse, with kT , the hourly clearness index. The ratio of the diffused solar radiation to the total solar radiation is found by the following correlation (11)

$$\frac{I_d}{I} = \begin{cases} 1.0 - 0.09\,k_T & , \quad \text{for } k_T \leq 0.22 \\ 0.9511 - 0.1604k_T + 4.388k_T^2 - 16.638k_T^3 + 12.336k_T^4 & , \quad \text{for } 0.22 < k_T \leq 0.80 \\ 0.165 & , \quad \text{for } k_T > 0.8 \end{cases} \tag{11}$$

At any point in time, the solar radiation incident on a horizontal plane outside of the atmosphere is the normal incident solar radiation as given by equation (12). The value is then multiplied by the corresponding kT for the month to add the atmospheric effect.

$$Go = Gsc\,(1 + 0.033\cos\frac{360n}{365})(\cos\varphi\cos\delta\cos\omega + \sin\varphi\sin\delta) \tag{12}$$

Where:

- Gsc is the solar constant in watts per square meter and n is the day of the year

The diffused solar radiation is found by multiplying the total solar radiation available by the Id/I. The beam solar radiation is the remaining of the total solar radiation after

subtracting the diffused portion.

4.1.1.3 Tilted surface's equations

The ratio Gb,T /Gb that the beam component is given by Equation (13)

$$\mathrm{Rb} = \frac{\mathrm{Gb,T}}{\mathrm{Gb}} = \frac{\mathrm{Gb,n}\cos\theta}{\mathrm{Gb,n}\cos\theta\mathrm{z}} = \frac{\cos\theta}{\cos\theta\mathrm{z}} \qquad (13)$$

A surface tilted at slope β from the horizontal has a ratio of diffuse on the tilted surface to that on the horizontal surface Rd = (1 + cos β)/2. The tilted surface has a ratio of reflective on the tilted surface to that on the horizontal surface Rr = (1 − cos β)/2. If the surroundings have a diffuse reflectance of ρg for the total solar radiation, the reflected radiation from the surroundings on the surface will be I ρg(1 − cos β)/2.

$$\mathrm{I_T} = \mathrm{I_b R_b} + \mathrm{I_d}\left(\frac{1+\cos\beta}{2}\right) + \mathrm{I}\,\rho_g\left(\frac{1-\cos\beta}{2}\right) \qquad (14)$$

Thus, the total solar radiation, in Energy per meter square, on the tilted surface for an hour as the sum of three terms as shown in Equation (14)

4.1.1.4 Tracking surface's equations.

For the solar collector to follow the sun instead of being fixed, some form of tracking mechanism is usually used. This is done in varying degrees of modes and accuracy. In general, there are four main modes of tracking as indicated in Figure 4-2 [64]. Based on the type of the motion, the tracking can be about single axis or about two axes. In the case of two axes, full tracking mode is available (Figure 4-2(a)). In the case of a single axis mode, the motion can be in several ways, that is, east-west polar (Figure 4-2(b)), north–south (Figure 4-2(c)), or east–west (Figure 4-2(d)).

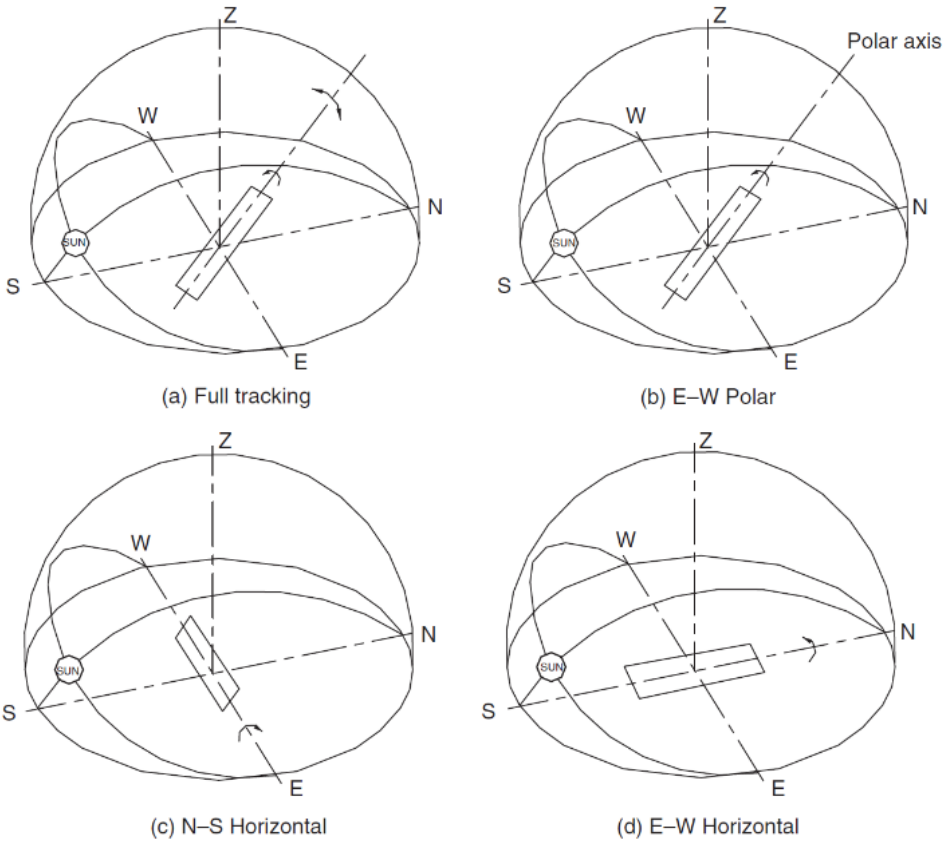

Figure 4-2: Collector geometry for various modes of tracking [64]

For a comparison purposes and to find the proper mode to be selected. As in [64] and for each mode, the amount of energy falling on a surface per unit area for the summer and winter solstices and the equinoxes for the latitude of 35° is investigated. This analysis has been completed with a radiation model, which is affected by the incidence angle and is dissimilar for each mode. The type of the model used here is not important as it is used for comparison purposes only.

Based on the mode of tracking selected, the amount of incident radiation falling on the collector surface is in proportion to the cosine of the incidence angle. Based on the four modes of tracking, the amount of energy falling on a surface per unit area for the summer and winter solstices and the equinoxes is shown in Table 4-2.

Full tracking mode collects the maximum amount of solar energy shown as 100% and the performance of the other various modes of tracking are compared to it. It can be noticed that the polar is the most suitable for one-axis tracking as its performance is very close to the full tracking.

Table 4-2: Comparison of energy received for various modes of tracking

	Solar energy received (kWh m-2)			**Percentage to full tracking**		
Tracking mode	E	SS	WS	E	SS	WS
Full tracking	8.43	10.60	5.70	100	100	100
E-W polar	8.43	9.73	5.23	100	91.7	91.7
N-S horizontal	7.51	10.36	4.47	89.1	97.7	60.9
E-W horizontal	6.22	7.85	4.91	73.8	74.0	86.2

Note: E, Equinoxes; SS, Summer solstice; WS, Winter solstice.

4.1.1.4.1 Full tracking (two axis tracking)

For a two-axis tracking mechanism, keeping the surface in question continuously oriented to face the sun will always have an angle of incidence θ equal to Cos(θ)=1 or θ = 0°. This of course depends on the accuracy of the mechanism. The full tracking configuration collects the maximum possible sunshine. The performance of this mode of tracking with respect to the amount of radiation collected during 1 day under standard conditions is shown in Figure 4-3. The slope of this surface (β) is equal to the solar zenith angle (Φ) and the surface azimuth angle (zs) is equal to the solar azimuth angle (z).

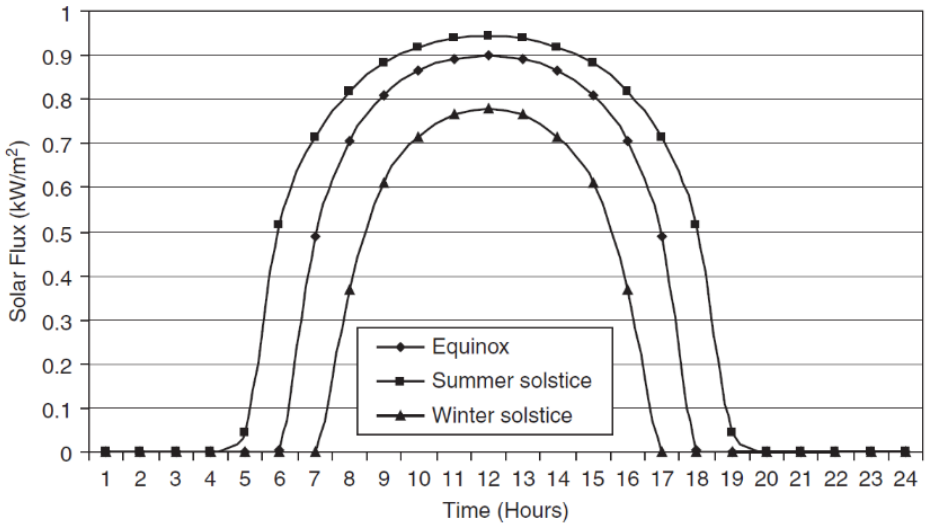

Figure 4-3: Daily variation of solar flux – full tracking [64]

4.1.1.4.2 N–S axis polar/E–W tracking

For a plane rotated about a north–south axis parallel to the earth's axis, with continuous adjustment, θ is equal to Cos(θ)= Cos (δ). This configuration is shown in Figure 4-2 (b). As can be seen, the collector axis is tilted at the polar axis, which is equal to the local latitude. For this arrangement, the sun is normal to the collector at equinoxes (δ = 0°) and the cosine effect is maximum at the solstices. The same comments about tilting of collector and shadowing effects applies here as in the previous configuration. The performance of this mount is shown in Figure 4-4.

The equinox and summer solstice performance, in terms of solar radiation collected, are essentially equal, that is, the smaller air mass for summer solstice offsets the small cosine projection effect. The winter noon value, however, is reduced because these two effects are combined. If it is desired to increase the winter performance, an inclination higher than the local latitude would be required, but the physical height of such configuration would be a potential penalty to be traded-off in cost-effectiveness with the structure of the polar mount. Another side effect of increased inclination is that of shadowing of the adjacent collectors, for multirow installations.

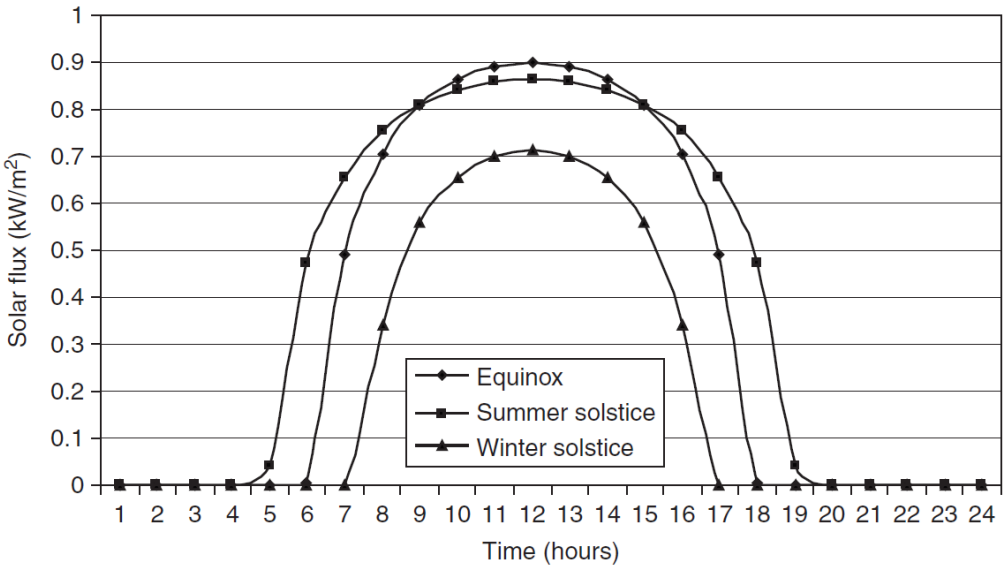

Figure 4-4: Daily variation of solar flux – N–S axis polar/E–W tracking [64]

The slope of the surface varies continuously and is given by Equation (15)

$$\tan(\beta) = \frac{\tan(L)}{Cos(Z_s)} \tag{15}$$

The surface azimuth angle is given by Equation (16)

$$Z_s = \ tan^{-1}\frac{\sin(\emptyset)\sin(z)}{\cos(\theta')\sin(L)} + 180C_1C_2 \tag{16}$$

where:

- $\cos(\theta') = \cos(\emptyset)\cos(L) + \sin(\emptyset)\sin(L)\cos(z)$

- $C_1 = \begin{cases} 0, \ if \ \left(\frac{\sin(\emptyset)\sin(z)}{\cos(\theta')\sin(L)}\right) z \geq 0 \\ 1, \ otherwise \end{cases}$

- $C_2 = \begin{cases} 1, \ if \ z \geq 0^{\circ} \\ -1, \ if \ z < 0^{\circ} \end{cases}$

4.1.2 Model interface

The excel model's interface has 6 sheets named as, input data, horizontal surface, fixed slope surface, one axis tracking surface, two axes tracking surface and comparison sheet. The model gives the complete radiation data and results for the 4 solar systems mentioned above in two ways. The first way is providing the all radiation components available for a certain day specified in the input data sheet. The second way is the total radiation available per day for a full year.

4.1.2.1 Input data sheet

In the input data sheet, the required data for the calculation is entered. These data are the location of the plant, the day of the year required, the slope angle for the fixed slope mode only, the albedo of the surface and the clearness index per month for the location. The sheet is shown in Table 4-3. The current location is the Al-Safliya island and the clearness index are for Qatar University location derived from Figure 4-6.

4.1.2.2 Horizontal surface sheet

In this sheet, shown in Table 4-4and Table 4-5, the surface and sun angles are shown along with the radiation components available (global, diffuse and beam) for each hour for the specified day. The total insolation available per day is calculated at the last column. This sheet will repeat at all the modes as it is the base for further calculations.

Table 4-3: The input data sheet of the excel model

Input system Information			
Location Latitude	25.35	N	Degrees
Location Longitude	51.58	E	Degrees
Location Elevation	4.00	m	
Location Standard Longitude	15.00	Degrees	
Day of the year	17.00	Day	
Slope angle	25.00	Degrees	"+" for N or "-" for S
Clearness Index, kt (fill below table)	0.60	-	
Month	0.57	Month	
Albedo, ρg	0.40	-	
Azimuth Angle, reference is south, "+" west of south and "-" west of south	0.00	Degrees	

Clearness Index per month *	Value
Jan	0.6
Feb	0.65
Mar	0.64
Apr	0.59
May	0.64
Jun	0.66
Jul	0.64
Aug	0.64
Sep	0.66
Oct	0.65
Nov	0.64
Dec	0.63

Clearness index at Qatar University

Table 4-4: The sun angles of the horizontal surface sheet of the excel model

Standard Time (hour)	Solar Time (hour)	Hour Angle (deg)	Solar Zenith, **Ø**, (deg)	Sun Altitude (deg)	Incidence angle, **θ,** (deg)	Solar Azimuth, **Z,** (deg)	Sunset hour angle, **Ws**, (deg)	**Id/I** (fraction of the total horizontal radiation)
0.00	1.28	-160.76	161.78	-71.78	161.78	-79.89	79.57	0.44
1.00	2.28	-145.76	148.28	-58.28	148.28	-89.14		
2.00	3.28	-130.76	134.74	-44.74	134.74	-85.02		
3.00	4.28	-115.76	121.31	-31.31	121.31	-79.96		
4.00	5.28	-100.76	108.08	-18.08	108.08	-74.88		
5.00	6.28	-85.76	95.18	-5.18	95.18	-69.29		
6.00	7.28	-70.76	82.80	7.20	82.80	-62.74		
7.00	8.28	-55.76	71.20	18.80	71.20	-54.65		
8.00	9.28	-40.76	60.88	29.12	60.88	-44.27		
9.00	10.28	-25.76	52.59	37.41	52.59	-30.73		
10.00	11.28	-10.76	47.43	42.57	47.43	-13.69		
11.00	12.28	4.24	46.45	43.55	46.45	5.47		
12.00	13.28	19.24	49.90	40.10	49.90	23.74		
13.00	14.28	34.24	56.97	33.03	56.97	38.82		
14.00	15.28	49.24	66.53	23.47	66.53	50.48		
15.00	16.28	64.24	77.64	12.36	77.64	59.46		
16.00	17.28	79.24	89.73	0.27	89.73	66.59		
17.00	18.28	94.24	102.43	-12.43	102.43	72.54		
18.00	19.28	109.24	115.54	-25.54	115.54	77.79		
19.00	20.28	124.24	128.89	-38.89	128.89	82.79		
20.00	21.28	139.24	142.40	-52.40	142.40	88.15		
21.00	22.28	154.24	155.94	-65.94	155.94	84.72		
22.00	23.28	169.24	169.17	-79.17	169.17	68.07		
23.00	24.28	184.24	174.10	-84.10	174.10	-42.25		

Table 4-5: The horizontal surface sheet of the excel model

Horizontal surface			
Go (W/m2) horizontal	Gd (W/m2) horizontal	Gb (W/m2) horizontal	Total Insolation on horizontal surface per day, H, (MJ/m2.day)
0.00	0.00	0.00	**14.36**
0.00	0.00	0.00	
0.00	0.00	0.00	
0.00	0.00	0.00	
0.00	0.00	0.00	
0.00	0.00	0.00	
106.12	46.64	59.48	
272.63	119.82	152.82	
411.76	180.96	230.80	
514.01	225.90	288.11	
572.42	251.57	320.85	
583.01	256.22	326.79	
545.05	239.54	305.51	
461.14	202.66	258.48	
336.99	148.10	188.89	
181.06	79.57	101.49	
3.98	1.75	2.23	
0.00	0.00	0.00	
0.00	0.00	0.00	
0.00	0.00	0.00	
0.00	0.00	0.00	
0.00	0.00	0.00	
0.00	0.00	0.00	
0.00	0.00	0.00	

The total radiation available using this horizontal mode for each day is calculated and added to a table made for later comparison with the other modes in the comparison sheet.

4.1.2.3 Fixed slope surface sheet

Utilizing the horizontal surface results described previously, the fixed slope surface's radiation components are shown in Table 4-6 and Table 4-7. The surface slope angle is entered on the input data sheet. Using the excel solver option, the surface angle that result in maximum collected solar radiation through the whole year is found to be ~25 degree.

Table 4-6: The solar components ratios of the fixed slope surface sheet of the excel model

Incidence Angle with azimuth(deg)	Beam component, Rb	Beam component, Rb	Difuse component, Rd	Reflected component, Rr
152.13	0.00	0.00	0.95	0.05
140.74	0.00	0.00		
127.73	0.00	0.00		
114.08	0.00	0.00		
100.16	0.00	0.00		
86.16	0.00	0.00		
72.20	2.44	2.44		
58.43	1.62	1.62		
45.14	1.45	1.45		
32.95	1.38	1.38		
23.72	1.35	1.35		
21.66	1.35	1.35		
28.39	1.37	1.37		
39.65	1.41	1.41		
52.58	1.53	1.53		
66.19	1.89	1.89		
80.09	36.58	2.50		
94.09	0.00	0.00		
108.06	0.00	0.00		
121.86	0.00	0.00		
135.21	0.00	0.00		
147.51	0.00	0.00		
156.90	0.00	0.00		
159.01	0.00	0.00		

Table 4-7: The solar components of the fixed slope surface sheet of the excel model

Gd (W/m2) Fixed slope	Gb (W/m2) Fixed slope	Gr (W/m2) Fixed slope	Gt for Fixed slope surfaces (W/m2)	Gt for Fixed slope surfaces (MJ/m2)	Gt (MJ/m2.day)
0.00	0.00	0.00	0.00	0.00	**18.05**
0.00	0.00	0.00	0.00	0.00	
0.00	0.00	0.00	0.00	0.00	
0.00	0.00	0.00	0.00	0.00	
0.00	0.00	0.00	0.00	0.00	
0.00	0.00	0.00	0.00	0.00	
44.45	145.00	1.99	191.44	0.69	
114.20	248.27	5.11	367.58	1.32	
172.48	334.56	7.72	514.75	1.85	
215.31	397.97	9.63	622.92	2.24	
239.78	434.20	10.73	684.71	2.46	
244.22	440.77	10.92	695.91	2.51	
228.32	417.23	10.21	655.76	2.36	
193.17	365.18	8.64	566.99	2.04	
141.16	288.18	6.31	435.66	1.57	
75.84	191.48	3.39	270.71	0.97	
1.67	5.58	0.07	7.32	0.03	
0.00	0.00	0.00	0.00	0.00	
0.00	0.00	0.00	0.00	0.00	
0.00	0.00	0.00	0.00	0.00	
0.00	0.00	0.00	0.00	0.00	
0.00	0.00	0.00	0.00	0.00	
0.00	0.00	0.00	0.00	0.00	
0.00	0.00	0.00	0.00	0.00	

4.1.2.4 One axis tracking surface sheet

Utilizing the horizontal surface results described previously, the surface slope and the surface azimuth angles are found, shown in Table 4-8, that are required to find the radiation components of this mode of tracking shown in Table 4-9 and Table 4-10.

Table 4-8: The one axis tracking surface sheet of the excel model – surface slope and surface azimuth angle

Surface Azimuth, Zs, (deg)	cos(θ')	C1	C2	Slope of surface, β (deg)
-139.26	-0.83	1.00	-1.00	90
-121.94	-0.77	1.00	-1.00	90
-110.25	-0.61	1.00	-1.00	90
-101.67	-0.41	1.00	-1.00	90
-94.65	-0.17	1.00	-1.00	90
-88.18	0.07	0.00	-1.00	86.16
-81.50	0.31	0.00	-1.00	72.67
-73.75	0.53	0.00	-1.00	59.43
-63.59	0.71	0.00	-1.00	46.80
-48.42	0.84	0.00	-1.00	35.51
-23.93	0.92	0.00	-1.00	27.39
9.84	0.93	0.00	1.00	25.68
39.20	0.88	0.00	1.00	31.43
57.84	0.77	0.00	1.00	41.66
69.75	0.61	0.00	1.00	53.84
78.33	0.41	0.00	1.00	66.88
85.35	0.17	0.00	1.00	80.29
91.82	-0.07	1.00	1.00	90
98.50	-0.31	1.00	1.00	90
106.25	-0.53	1.00	1.00	90
116.41	-0.71	1.00	1.00	90
130.48	-0.81	1.00	1.00	90
154.60	-0.86	1.00	1.00	90
-169.44	-0.87	1.00	-1.00	90

Table 4-9: The solar components ratios of the one axis tracking surface sheet of the excel model

Incidence Angle (deg)	Beam component, Rb	Beam component, Rb	Difuse component, Rd	Reflected component, Rr
72.93	0.00	0.00	0.50	0.50
58.30	0.00	0.00	0.50	0.50
44.74	0.00	0.00	0.50	0.50
31.31	0.00	0.00	0.50	0.50
18.08	0.00	0.00	0.50	0.50
9.02	0.00	0.00	0.53	0.47
10.13	7.85	2.50	0.65	0.35
11.77	3.04	2.50	0.75	0.25
14.08	1.99	1.99	0.84	0.16
17.08	1.57	1.57	0.91	0.09
20.03	1.39	1.39	0.94	0.06
20.77	1.36	1.36	0.95	0.05
18.46	1.47	1.47	0.93	0.07
15.31	1.77	1.77	0.87	0.13
12.69	2.45	2.45	0.79	0.21
10.77	4.59	2.50	0.70	0.30
9.44	209.59	2.50	0.58	0.42
12.43	0.00	0.00	0.50	0.50
25.54	0.00	0.00	0.50	0.50
38.89	0.00	0.00	0.50	0.50
52.40	0.00	0.00	0.50	0.50
66.38	0.00	0.00	0.50	0.50
82.21	0.00	0.00	0.50	0.50
90.56	0.00	0.00	0.50	0.50

Table 4-10: The solar components of the one axis tracking surface sheet of the excel model

Gd (W/m2) One Axis surface	Gb (W/m2) One Axis surface	Gr (W/m2) One Axis surface	Gt for One Axis surfaces (W/m2)	Gt for One Axis surfaces (MJ/m2)	Gt (MJ/m2.day)
0.00	0.00	0.00	0.00	0.00	**20.29**
0.00	0.00	0.00	0.00	0.00	
0.00	0.00	0.00	0.00	0.00	
0.00	0.00	0.00	0.00	0.00	
0.00	0.00	0.00	0.00	0.00	
0.00	0.00	0.00	0.00	0.00	
23.32	148.70	21.22	193.25	0.70	
59.91	382.04	54.53	496.48	1.79	
90.48	460.01	82.35	632.84	2.28	
112.95	453.36	102.80	669.11	2.41	
125.78	445.57	114.48	685.84	2.47	
128.11	443.44	116.60	688.15	2.48	
119.77	449.86	109.01	678.64	2.44	
101.33	457.43	92.23	650.99	2.34	
74.05	462.69	67.40	604.14	2.17	
39.79	253.72	36.21	329.72	1.19	
0.88	5.58	0.80	7.25	0.03	
0.00	0.00	0.00	0.00	0.00	
0.00	0.00	0.00	0.00	0.00	
0.00	0.00	0.00	0.00	0.00	
0.00	0.00	0.00	0.00	0.00	
0.00	0.00	0.00	0.00	0.00	
0.00	0.00	0.00	0.00	0.00	
0.00	0.00	0.00	0.00	0.00	

4.1.2.5 Two axes tracking surface sheet

In this sheet, the two axes tracking surface's irradiance components are shown in Table 4-11. Based on the initial result found using the set of equations described previously and the set of clearness indexes, the beam irradiance for the whole year shows a very low value compared to the global irradiance. Based on the literature review about solar measurement in Qatar, the only study that measured the direct beam irradiance was for a horizontal surface only not a tracked one [65]. Moreover, the total irradiance is the only solar value measured by the Qatar Meteorological Department by the several weather station sites. Thus, there is no a published data about the direct beam component of two axes tracked surface in Qatar.

Using the SAM data base and going through the available data for many locations, it is observed that the direct beam irradiance values for a certain location is in the range of the global horizontal irradiance of the horizontal surface of the same location. Thus, a correction factor was multiplied by the direct beam irradiance result to bring it in the range of the global horizontal irradiance. The correction factor is selected to be 1.5 of the original value. The results of the solar irradiance components are shown in Table 4-11 and Table 4-12.

Table 4-11: The solar components ratios of the two axes tracking surface sheet of the excel model

Incidence Angle (deg)	Beam component, Rb	Beam component, Rb	Difuse component, Rd	Reflected component, Rr
0.00	0.00	0.00	0.50	0.50
0.00	0.00	0.00	0.50	0.50
0.00	0.00	0.00	0.50	0.50
0.00	0.00	0.00	0.50	0.50
0.00	0.00	0.00	0.50	0.50
0.00	0.00	0.00	0.50	0.50
0.00	7.97	2.50	0.56	0.44
0.00	3.10	2.50	0.66	0.34
0.00	2.05	2.05	0.74	0.26
0.00	1.65	1.65	0.80	0.20
0.00	1.48	1.48	0.84	0.16
0.00	1.45	1.45	0.84	0.16
0.00	1.55	1.55	0.82	0.18
0.00	1.83	1.83	0.77	0.23
0.00	2.51	2.50	0.70	0.30
0.00	4.67	2.50	0.61	0.39
0.00	212.46	2.50	0.50	0.50
0.00	0.00	0.00	0.50	0.50
0.00	0.00	0.00	0.50	0.50
0.00	0.00	0.00	0.50	0.50
0.00	0.00	0.00	0.50	0.50
0.00	0.00	0.00	0.50	0.50
0.00	0.00	0.00	0.50	0.50
0.00	0.00	0.00	0.50	0.50

Table 4-12: The solar components of the two axes tracking surface sheet of the excel model

Gd (W/m2) Two Axes surface	Gb (W/m2) Two Axes surface	Gr (W/m2) Two Axes surface	Gt for Two Axes (W/m2)	Gt for Two Axes (MJ/m2)	Gt (MJ/m2.day)
0.00	0.00	0.00	0.00	0.00	**31.32**
0.00	0.00	0.00	0.00	0.00	
0.00	0.00	0.00	0.00	0.00	
0.00	0.00	0.00	0.00	0.00	
0.00	0.00	0.00	0.00	0.00	
0.00	0.00	0.00	0.00	0.00	
26.24	252.80	18.56	297.60	1.07	
79.21	649.48	36.96	765.65	2.76	
134.51	806.25	42.28	983.04	3.54	
181.56	806.25	40.35	1028.17	3.70	
210.88	806.25	37.03	1054.16	3.79	
216.38	806.25	36.26	1058.89	3.81	
196.92	806.25	38.79	1041.96	3.75	
156.56	806.25	41.96	1004.77	3.62	
103.54	802.78	40.55	946.88	3.41	
48.30	431.33	28.46	508.09	1.83	
0.88	9.49	0.79	11.16	0.04	
0.00	0.00	0.00	0.00	0.00	
0.00	0.00	0.00	0.00	0.00	
0.00	0.00	0.00	0.00	0.00	
0.00	0.00	0.00	0.00	0.00	
0.00	0.00	0.00	0.00	0.00	
0.00	0.00	0.00	0.00	0.00	
0.00	0.00	0.00	0.00	0.00	

4.1.2.6 Comparison sheet

In this sheet, the total available radiation for horizontal surface, fixed slope surface, one axis tracking surface and two axes tracking surface for each month of the year are shown. The numeric comparison of the results is shown in Table 4-13 and the graphical

comparison is shown in Figure 4-5. As expected, the two axes tracking surface throughout all months has the highest monthly total available radiation. Thus, for comparison purposes, the output of the latter is given 100% of the monthly radiation as shown in Table 4-13**Error! Reference source not found.**. The one axis tracking surface comes in second with almost 65% of the two axes tracking surface output. The fixed slope surface receives less radiation than the horizontal surface in April to August.

Table 4-13: The numeric comparison result of the comparison sheet

	Horizontal		**Fixed Slope**		**One Axis**		**Two Axes**	
Month	**Gt (kWh/m^2)**	**%**	**Gt (kWh/m^2)**	**%**	**Gt (kWh/m^2)**	**%**	**Gt (kWh/m^2)**	**%**
January	123.63	45.84	155.43	57.63	174.73	64.78	269.71	100.00
February	143.13	44.74	173.29	54.17	209.56	65.51	319.89	100.00
March	183.09	49.39	200.27	54.03	248.13	66.94	370.69	100.00
April	184.14	56.89	182.30	56.33	219.83	67.92	323.66	100.00
May	219.02	53.42	204.85	49.97	273.22	66.64	409.96	100.00
June	222.99	51.94	202.34	47.13	282.08	65.70	429.34	100.00
July	220.46	53.49	201.79	48.96	273.22	66.29	412.18	100.00
August	210.34	52.73	203.33	50.97	267.52	67.07	398.90	100.00
September	190.94	48.93	201.66	51.68	261.03	66.89	390.22	100.00
October	165.56	46.22	193.79	54.10	236.58	66.05	358.21	100.00
November	132.80	42.95	168.89	54.63	199.12	64.40	309.16	100.00
December	123.22	41.91	163.08	55.47	187.05	63.62	294.02	100.00
Total	**2119.33**	**49.45**	**2251.02**	**52.52**	**2832.06**	**66.08**	**4285.94**	**100.00**

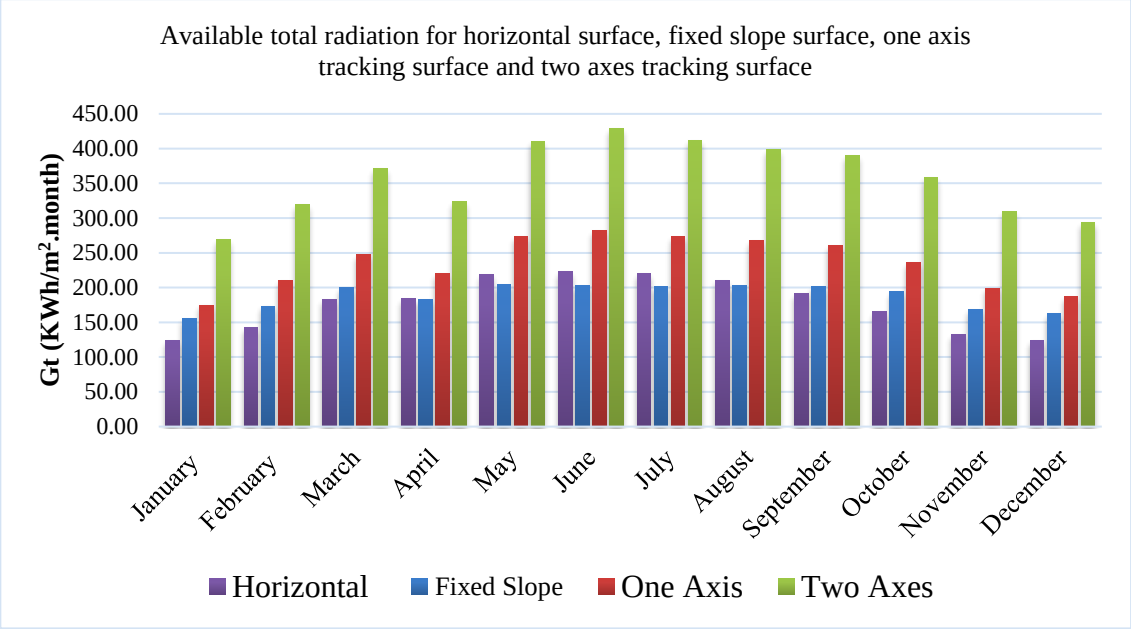

Figure 4-5: The graphical comparison result of the comparison sheet

4.1.3 Model validation

To validate the model prepared in this thesis for measuring the available solar radiation at a certain location. The model is compared with actual data collected by QEERI presented in a paper issued in 2015 [66]. In the mentioned paper, a study of up to six years of ground measurements of the total solar radiation arriving on a horizontal surface, collected by 12 automatic weather stations throughout Qatar. Moreover, the monthly clearness index is presented for each location. The location is selected to be Qatar University with longitude of 51.49° E and latitude of 25.38° N. For Qatar, the standard longitude is 52.50° E. From the paper mentioned, the monthly clearness index for Qatar University is shown in Figure 4-6. The values are extracted and presented in Table 4-14.

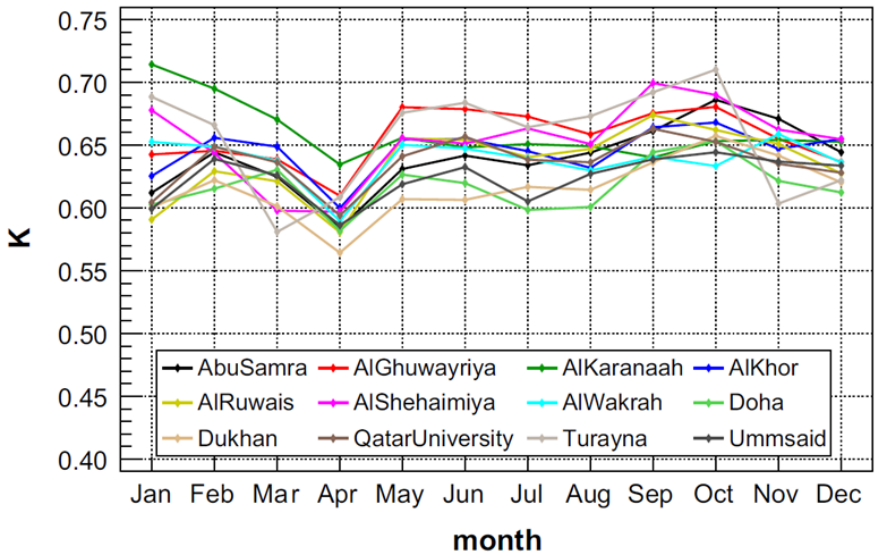

Figure 4-6: Monthly averages of clearness index for 12 locations in Qatar [66].

Table 4-14: Clearness Index per month of Qatar University [66]

Month	Clearness Index Value
Jan	0.6
Feb	0.65
Mar	0.64
Apr	0.59
May	0.64
Jun	0.66
Jul	0.64
Aug	0.64
Sep	0.66
Oct	0.65
Nov	0.64
Dec	0.63

Based on the actual stations' data, the year-to-year and monthly variations of daily global horizontal irradiation are calculated for each station and the average found to be 5.80 kWh/m2/day and a total of 2116 kWh/m^2/year.

By feeding Qatar University location's input data (latitude, longitude and clearness index) into the prepared model, the results are presented below:

1- Daily average horizontal irradiation: 20.87 MJ/m^2/day = 5.797 kWh/m^2/day
2- Yearly average horizontal irradiation: 2119.72 kWh/m^2/year

The results found by the model are very close to the actual results presented in the above paper [66]. Thus, the model is valid and can be used.

4.2 Software packages validation

Validation of the SolarPILOT and SAM is required to make sure that both software packages are precise and accurate in simulating the intended results so they can both be used to design a new solar power plant in any required location. For getting this step done, an already built solar power plant will be simulated and the results of the software will be compared with the actual results of the plant.

One of the newest solar power plants in USA is the Crescent Dunes Solar Energy Project in Tonopah, Nevada. It is a 110 MW plant with 10 hours thermal storage that started its production in Sep 2015. The plant is shown in Figure 4-7. It is the first utility scale CSP

plant with a central receiver tower and advanced molten salt energy storage technology from SolarReserve. This project is selected among other projects because most of its technical data and other information are made available to public. This information is shown in Appendix D.

Figure 4-7: Crescent Dunes Solar Energy Project [67]

4.2.1 Crescent Dunes Solar Energy Project overview

The proposed solar facility will use CSP technology. This specific technology uses heliostat (reflecting mirrors) to redirect sunlight on a receiver erected in the center of the solar field (called the central receiver). The facility is expected to produce approximately 110 MW of power.

This central receiver system consists of a series of tubes and a receiver that collects the redirected sun rays. The molten salt, which has the viscosity and appearance of water when heated, is routed to the receiver when solar energy is required to be collected. The molten salt passes through the receiver where it is heated by the reflected concentrated solar energy. After that, the molten salt is routed to a large insulated tank called the hot tank where it can be stored with minimal energy loss.

Once the electricity is to be generated, the hot molten salt is pumped and circulated through a series of heat exchangers to generate a high pressure superheated steam. This steam is then used to power a conventional Rankine cycle steam turbine with generator that produces electricity. At the end of the cycle, the turbine's exhaust steam is condensed and returned through feedwater pumps to the heat exchangers where the high pressure superheated steam is generated again. After the steam generation, the available energy in the molten salt is depleted and then it is routed to a tank called the cold tank where it is to be recycled again.

Major project components include the below components that are shown in Figure 4-8:

- A solar field consists of 10,347 heliostats that reflect the sun's solar energy into a central receiver or tower.
- A conventional steam turbine with generator to generate electricity
- Two thermal storage tanks to store the hot and cold molten salt

- A hybrid cooling system consists of an air-cooled condenser with a wet cooling augmentation system designed to minimize water consumption by use only during times of high electricity demand
- A water treatment system (reverse osmosis system) and evaporation ponds used to remove impurities from the groundwater and as a disposal point for waste water generated
- Equipment such as heat exchangers, pumps, transformers and buildings
- Linear facilities with a transmission line and access road

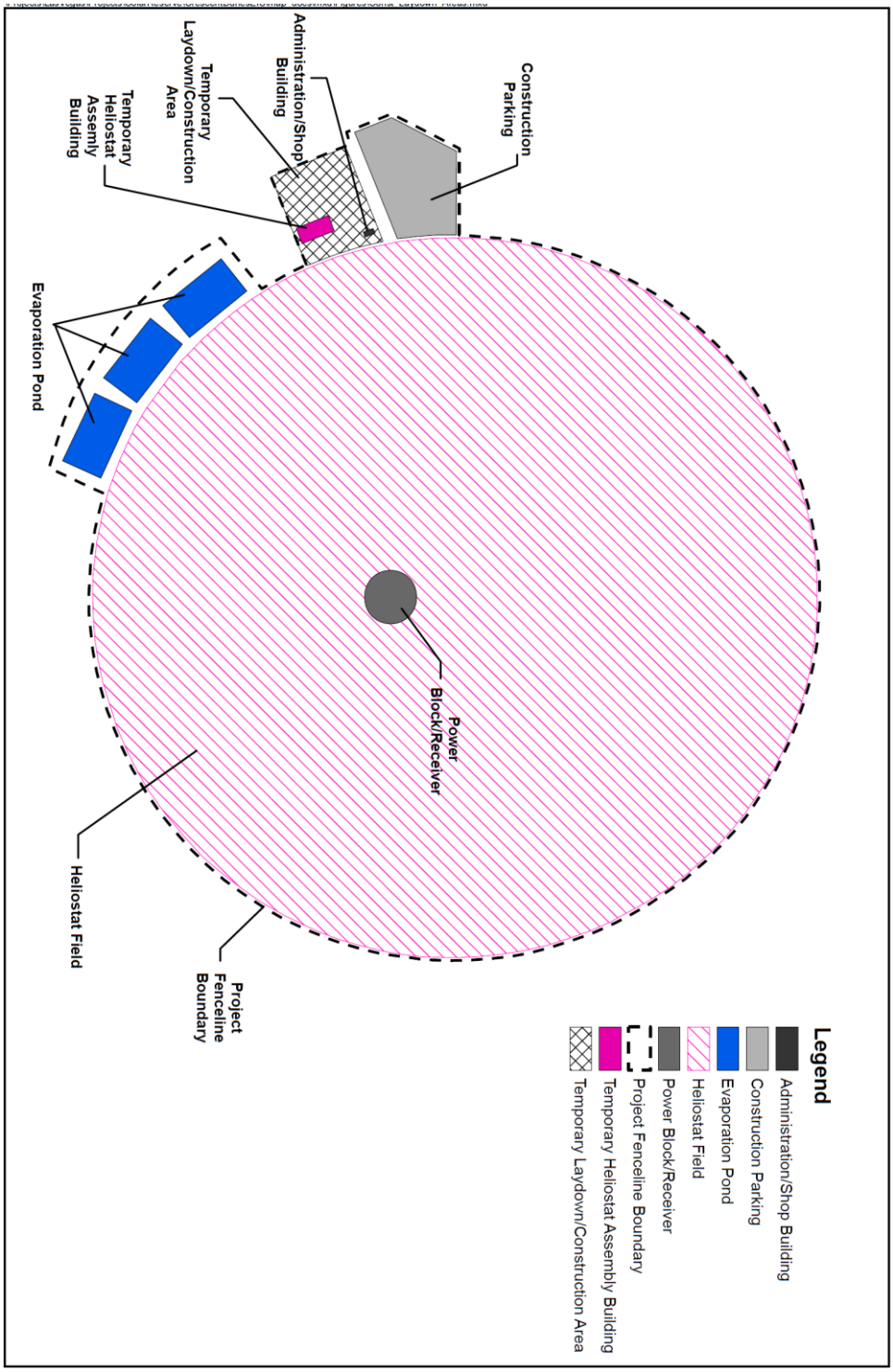

Figure 4-8: Crescent Dunes Solar Energy Project construction areas [68]

4.2.2 SolarPILOT validation

SolarPILOT is mainly used to find the heliostat field including the calculation of the heliostat positions and optimal values for the tower height, receiver height, and receiver aspect ratio (height / diameter). SolarPILOT and SAM have list of available location weather files for most of the world countries and with more focus on the United States of America. Each weather file for a certain location includes two rows of hourly information for a duration of one year. First row provides information about the Location, City, State, Country, Latitude, Longitude, Time Zone and Elevation of the location. Second row provides the below information

- Year: Four-digit number (e.g. 1988)
- Month: One- or two-digit number (e.g. 1=January, 11=November)
- Day: One- or two-digit number indicating the day of month.
- Hour: One- or two-digit number indicating the hour of day.
- GHI: Total global horizontal irradiance in W/m^2 at the end of the time step.
- DNI: Total direct normal irradiance in W/m^2 at the end of the time step.
- DHI: Total diffuse horizontal irradiance in W/m^2 at the end of the time step.
- Tdry: Dry-bulb temperature in °C.
- Tdew: Wet-bulb temperature in °C.
- RH: Relative humidity in %.
- Pres: Atmospheric pressure in millibar.
- Wspd: Wind speed at 10 m above the ground in m/s.

- Wdir: Wind direction at 10 m above the ground in degrees east of North, with zero degrees indicating wind from the north.
- Snow Depth: Snow depth in meters.

To find the heliostat field of the project, input values are entered through different interfaces. Climate, Layout setup, Plant, Heliostat, Receiver, Simulation - field layout and Results – field layout & system summary. These are discussed briefly below.

4.2.2.1 Climate

As the location of the Crescent Dunes Solar Energy Project in Nevada, Tonopah in USA, the climate weather file of the same location is selected. The atmospheric conditions are selected as shown in Figure 4-9. The sunshape model is selected to be point sun where sun is represented as a single point and incoming irradiation is modeled as uniform and parallel. The insolation model is selected to be the same as the hourly weather file data. The atmospheric attenuation model is selected to be the DELSOL3 clear day with visibility of 5 km. The DELSOL3 is a software from Sandia National Lab that combines several spacing correlations of azimuthal and radial spacing as a function of distance from the tower, heliostat width, heliostat height, heliostat geometry type, and receiver type. The resulted atmospheric attenuation is 8.6%.

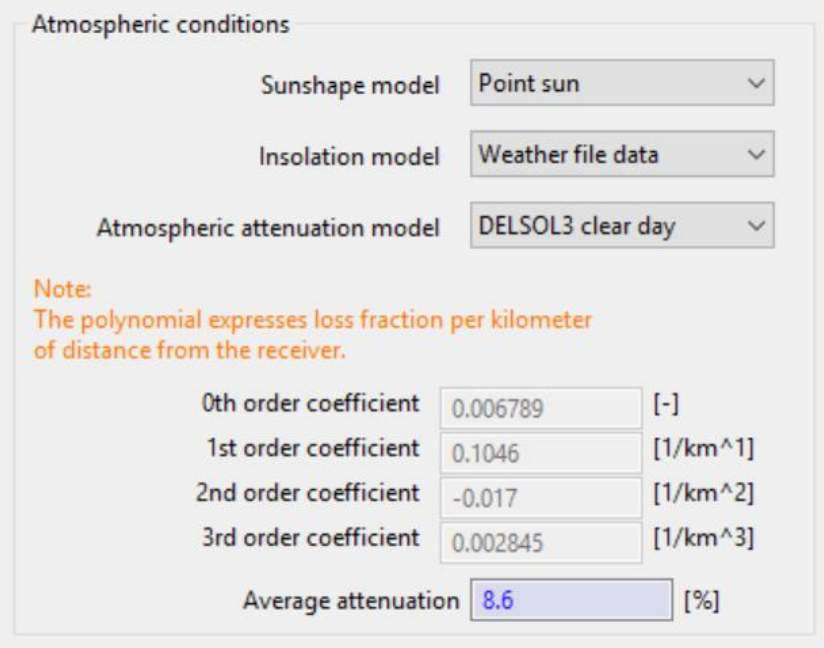

Figure 4-9: SolarPILOT validation, climate - Atmospheric conditions

4.2.2.2 Layout setup

In this interface the field layout, land boundaries, and tower height are configured. In the design point definition group shown in Figure 4-10, the heliostat selection criteria is specified which is a metric that will compare the heliostats over the design point simulation set. Power to receiver metric is selected that is based on the total power that is normalized by heliostat reflector area and delivered to the receiver over the simulation set. The second metric is the optimization simulations that will be included in the design assessment. Annual Simulation is selected in which each daylight hour of the year is simulated.

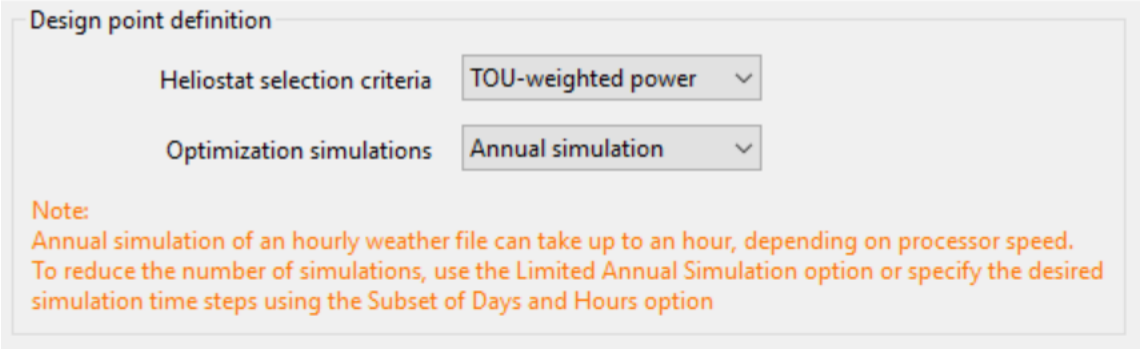

Figure 4-10: SolarPILOT validation, layout setup - design point definition

In the next interface, design values are shown in Figure 4-11, the desired total power delivered by the receiver at the reference design point is specified. This amount of power, shown in Equation (17), is equal to the power provided by the solar field minus the heat loss from the receiver and heat loss from tower runner piping, as

$$\dot{q}_{sf,des} = \dot{q}_{inc} \cdot \alpha - \dot{q}''_{hl} \cdot A_{rec} - \dot{q}_{pipe} \quad (17)$$

where:

- $\dot{q}_{sf,des}$ MW Thermal power delivered by the solar field
- $\dot{q}_{inc}$ MW Thermal power incident on the receiver (prior to emissive, convective, and reflective thermal loss)
- α - Receiver surface absorptivity

- $\dot{q}''_{hl}$ kW/m^2 Emissive and convective thermal loss per square meter of receiver area. This value is calculated using the receiver heat loss settings on the Receivers page(s).
- A_{rec} m^2 Absorptive surface area of the receiver
- $\dot{q}_{pipe}$ MW Thermal loss due to riser/downcomer piping. This value is calculated on the Receiver page(s) and may be a function of tower height.

The second parameter in this interface is the design point DNI value that is the solar resource available at the reference design point. The Solar Field Design Power must be met assuming this magnitude of available solar resource.

The third parameter is the sun location at design point. Summer solstice sun positon is selected for the chosen current weather file location (typically June 21st).

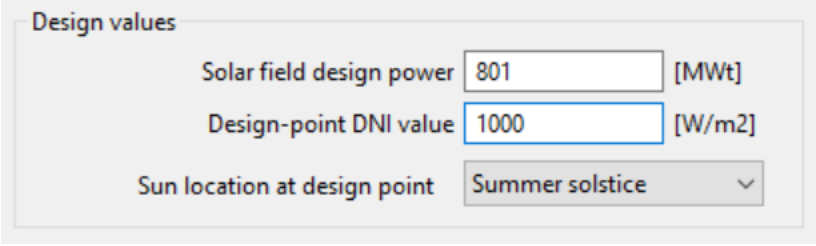

Figure 4-11: SolarPILOT validation, layout setup - design values

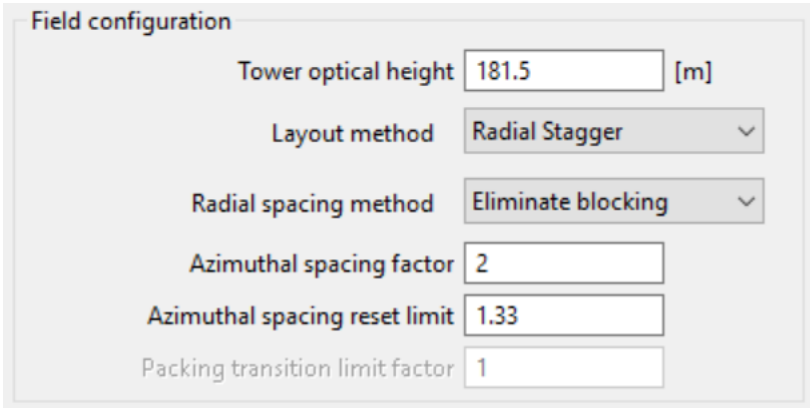

In Figure 4-12, the filed configuration group is filled. First parameter is the tower optical height parameter which is the distance between the heliostat pivot point and the midpoint of the receiver. Next parameter is the layout method for calculating the potential heliostat positions based on the design input values. Radial stagger method is selected as a layout method in which heliostat rows are placed alternatingly along iso-azimuthal lines at constant radius. Third parameter option, Radial Spacing Method, is selected to be eliminate blocking method.

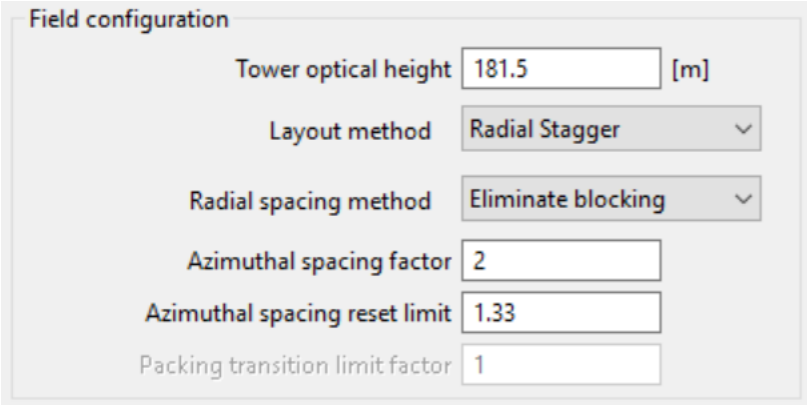

Figure 4-12: SolarPILOT validation, layout setup - field configuration

This concept is illustrated in Figure 4-13. The initial heliostat spacing between heliostats in a row is determined by the Azimuthal Spacing Factor which is specified in terms of heliostat structural widths and can be determined by dividing the azimuthal spacing between heliostats in a row by the minimum spacing. As rows are added radially, the spacing between neighboring heliostats in the same radial row increases and must be periodically reset to improve optical performance. Once the ratio of heliostat spacing to the original spacing exceeds the Azimuthal Spacing Reset Limit, the spacing resets to the original distance. This discontinuity is referred to as a slip plane. The Azimuthal Spacing Reset Limit is a ratio of spacing in any given row to the initial spacing that determines where the spacing will revert to the initial value. The separation of heliostats in a row after a slip plane or in the first row of the field is determined by multiplying the Azimuthal Spacing Factor by the Heliostat Width.

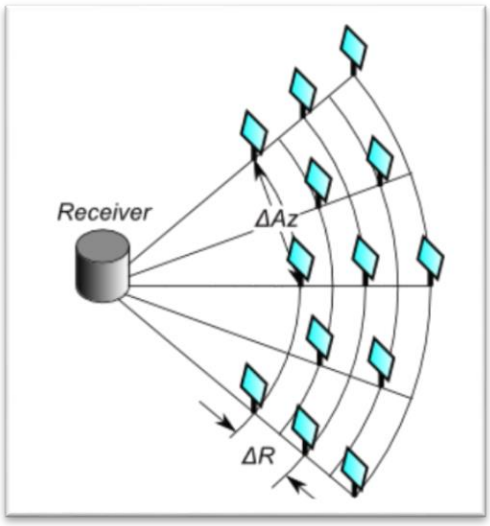

Figure 4-13: SolarPILOT validation, layout setup - radial stagger method

Regarding the third parameter, eliminate blocking option, it seeks to spread out rows radially such that heliostats along an iso-azimuthal line do not block reflected light from reaching the receiver. To get this done, the rows of the heliostats must be spaced adequately apart to prevent light reflected from the lowermost portion of the distal heliostat from being interrupted by the uppermost portion of the proximal heliostat, as illustrated in Figure 4-14. It can be noticed that as the radial position of the rows grows, the elevation angle θ of the tangent line decreases. In this case, the spacing between rows ΔR is essential also to be increased to prevent blocking. The ΔR mentioned represents the distance between alternating rows only not the intermediate rows that are offset azimuthally and does not contribute to blocking in this way.

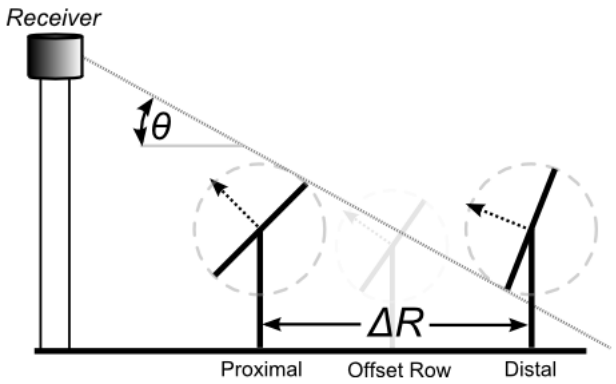

Figure 4-14: SolarPILOT validation, layout setup - field configuration - eliminate blocking option

Moreover, to avoid collisions between neighboring heliostat rows the row spacing must be sufficient. This is done by ensuring that collisions are avoided by calculating δmin for each row as shows in Figure 4-15

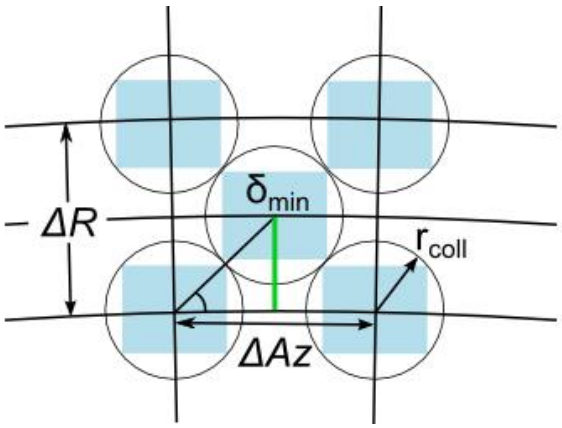

Figure 4-15: SolarPILOT validation, layout setup - field configuration - eliminate blocking option with collision avoidance

SolarPILOT offers several options for specifying the region of land where heliostats may be placed. The field boundary interface is shown in Figure 4-16. One of the options is to use the land boundary array that specifies the area by using the polygonal shapes from Google Earth PRO as shown in Figure 4-17. After selecting the field area, the tower location is selected and imported to the land boundary array. Eventually, the table of the polygonal coordinates that consists of X coordinate (East + and West -) and Y coordinate (North + and South -) is formed.

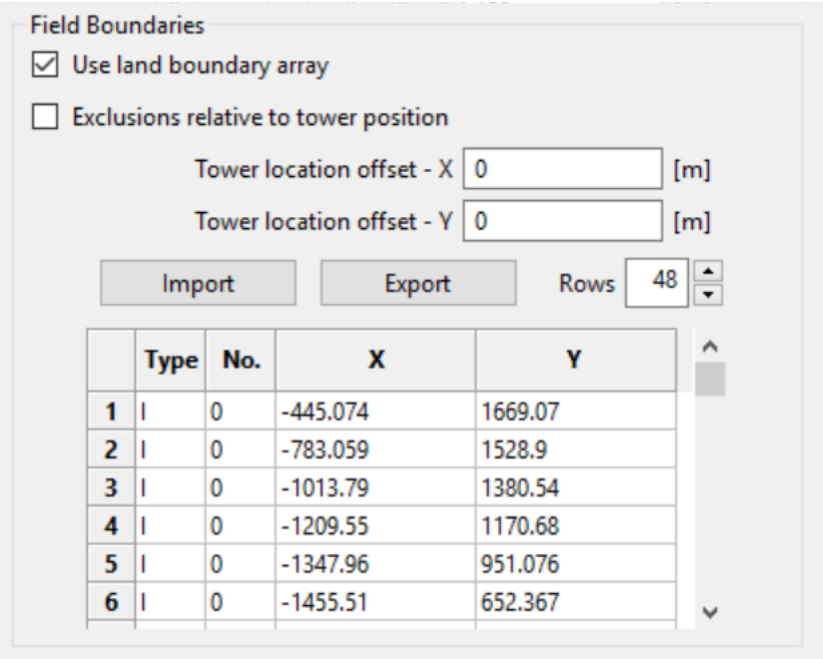

	Type	No.	X	Y
1	I	0	-445.074	1669.07
2	I	0	-783.059	1528.9
3	I	0	-1013.79	1380.54
4	I	0	-1209.55	1170.68
5	I	0	-1347.96	951.076
6	I	0	-1455.51	652.367

Figure 4-16: SolarPILOT validation, layout setup - field boundaries

Figure 4-17: SolarPILOT validation, layout setup - field land boundary array of the actual project (picture originally from Google earth PRO)

4.2.2.3 Plant sizing

The Plant page delivers information and sizing calculations for the power cycle and thermal energy storage systems. In Figure 4-18, the plant sizing parameters are shown. The Solar Field Design Power parameter is already specified in the layout setup page. The Solar Multiple parameter is the ratio of thermal power delivered by the solar field to thermal power consumed by the power cycle at reference conditions. This ratio determines the relative sizing of the solar field and the power cycle for purposes of introducing thermal storage. It is selected 3 to match the Design Turbine Gross Output of 110 MWe and 10 hours of thermal storage. All other parameters are kept as suggested by SolarPILOT.

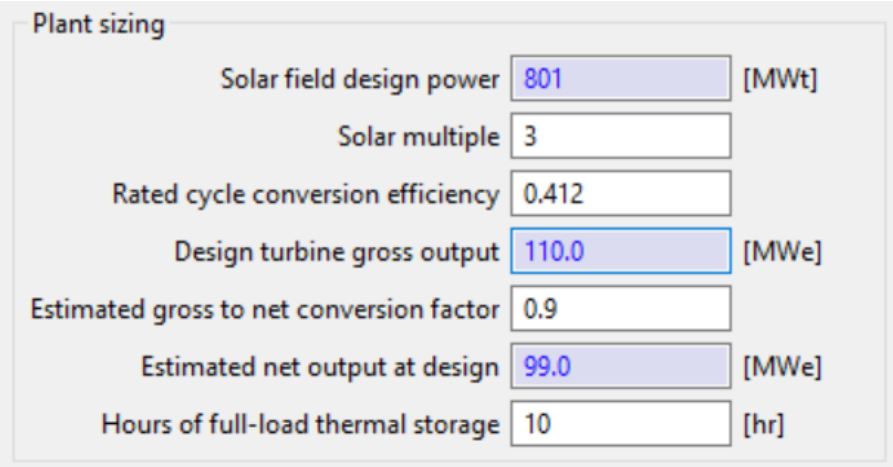

Figure 4-18: SolarPILOT validation, plant sizing

The Design Power Block Thermal Input can be found using Equation (18). The calculated value indicates the thermal input required by the cycle at reference conditions.

$$\dot{Q}_{cycle} = \frac{\dot{Q}_{sf}}{SM} \tag{18}$$

where:

- SM : Solar Multiple
- $\dot{Q}_{sf}$: Solar field design power [MWt]

Thus, the Design Turbine Gross Output can be found which is equal to cycle thermal power input times cycle conversion efficiency using Equation (19)

$$\dot{W}_{cycle} = \dot{Q}_{cycle}\eta_{cycle} \tag{19}$$

The Estimated Gross to Net Conversion Factor is an estimated ratio of net output to the grid divided by gross output from the cycle. This provides an estimate of the parasitic losses associated with plant operation on average. After that, the Estimated Net Output at Design can be found using Equation (20). This value is the net output of the plant after all the parasitic losses.

$$\dot{W}_{net} = \dot{W}_{cycle} r_{GrossToNet} \quad (20)$$

Finally, the Hours of Full Load Thermal Storage parameter is specified using Equation (21) which is equal to the number of hours of full load cycle operation that can be delivered by the thermal energy storage system when no energy is available from the solar field.

$$U_{tes}[MWh] = N_{hr,tes} \dot{Q}_{cycle} \quad (21)$$

where:

- U_{tes} : Thermal capacity of the TES system [MWh]
- $N_{hr,tes}$: Hours of full-load thermal storage [hr]

4.2.2.4 Heliostat

Heliostat geometry page includes macroscopic dimensions and parameters to specify heliostat facets. Relevant dimensions are shown in the Figure 4-19 and are filled in Figure 4-20.

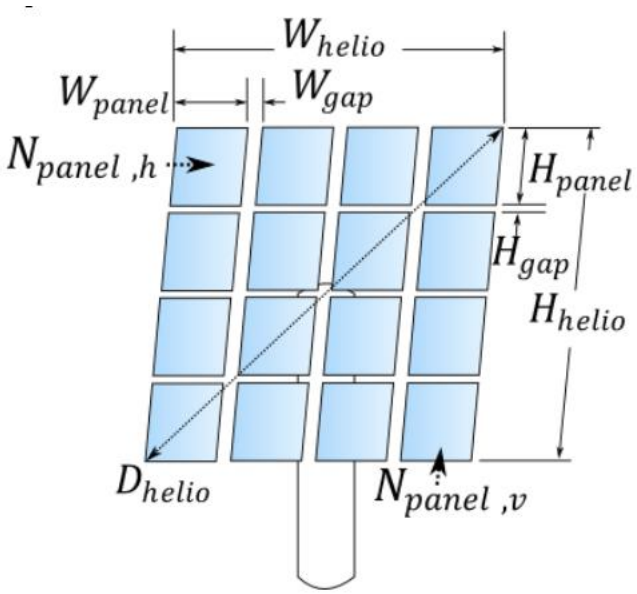

Figure 4-19: SolarPILOT validation, Heliostats - heliostat geometry dimensions (Source: SolarPILOT)

The dimensions are as below:

1- Structure Width: Physical extent in the width direction of the heliostat structure.

2- Structure Height: Physical extent in the height direction of the heliostat structure.

3- Heliostat Footprint Diameter: The maximum physical extent of the heliostat.

Equal to the diagonal length of the heliostat and can be found using Equation (22)

$$D_{helio} = \sqrt{W_{helio}^2 + H_{helio}^2} \tag{22}$$

4- No. Horizontal Panels: The number of panel facets in the horizontal (width) dimension.
5- No. Vertical Panels: The number of panel facets in the vertical (height) dimension.
6- Cant Panel Horiz. Gap: Specified gap length between panels in the horizontal dimension.
7- Cant Panel Vert. Gap: Specified gap length between panels in the vertical dimension.

A heliostat can be composed of multiple mirror facets, each of which may be mounted on the heliostat structure at a preferred orientation to maximize optical performance. This practice is called canting and several techniques are available for determining the orientation of each facet. The on axis at slant canting method is selected in which each facet is adjusted such that the normal vector intercepts the receiver at the heliostat aim point.

Another parameter is the Heliostat focusing type in which the focal point radius of the heliostat is specified. The At slant option is selected in which the heliostat focal length is equal to the distance between the heliostat pivot point and the receiver centroid.

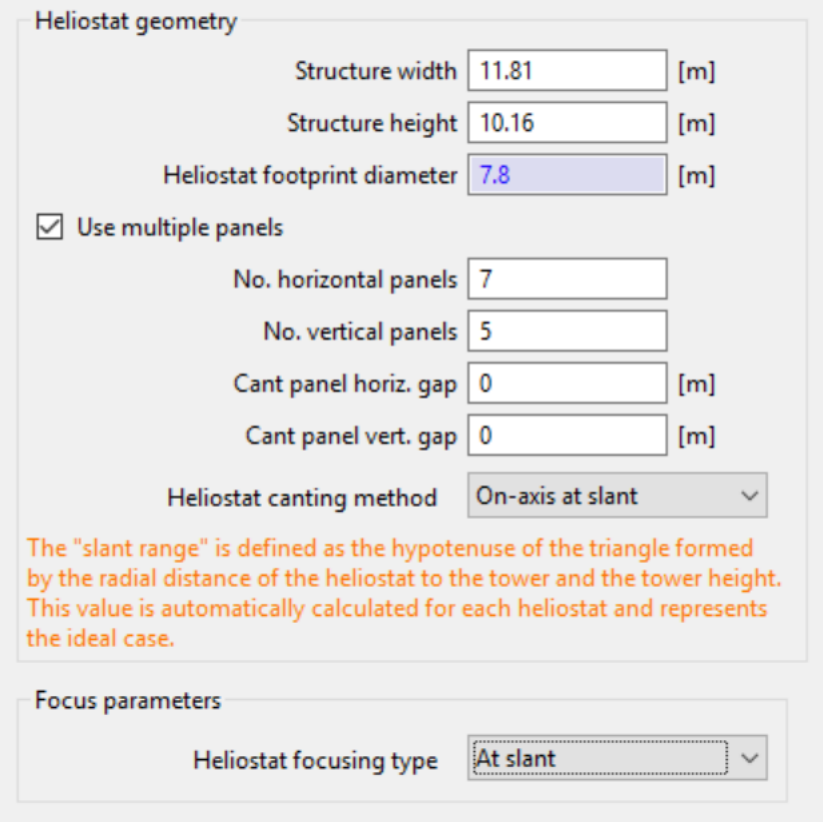

Figure 4-20: SolarPILOT validation, Heliostats - heliostat geometry

In the side of Mirror Performance Parameters that are shown in Figure 4-21, the Reflective surface ratio is the ratio of active reflective area to total structural area and it is directly affecting the power delivered by the heliostat. The effective reflective area is equal to the product of the Structure width, Structure height, and Reflective surface ratio. The second parameter affecting directly the power delivered is the Mirror reflectivity. The third parameter is the Soiling Factor that is accounting for any fraction of light that is reflected due to surface soiling.

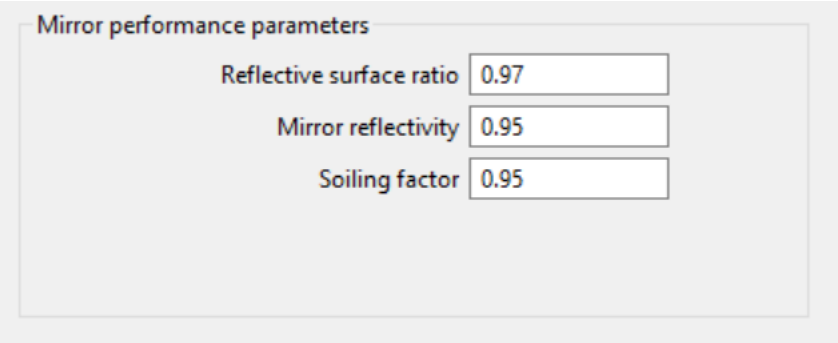

Figure 4-21: SolarPILOT validation, Heliostats - mirror performance parameters

The total optical reflectance of the heliostat after accounting for the Mirror reflectivity and the Soiling factor is equal to the product of the mirror reflectivity and the soiling factor.

4.2.2.5 Receivers

In the Receiver Geometry interface in Figure 4-22, the type of the receiver is selected that is external cylindrical and its dimensions, the receiver height and diameter. The Receiver aspect ratio is defined as the height of the receiver divided by its width, where the width is equal to the specified width for a flat plate receiver or the specified diameter for a cylindrical receiver. Then, the Receiver absorber area that is the heat absorbing surface area of the receiver. For external cylindrical receivers, this is equal to the diameter times the height times Pi. For flat plate receivers, this is equal to the width times the height.

Finally, the Receiver optical height that is already inserted in the Layout Setup page.

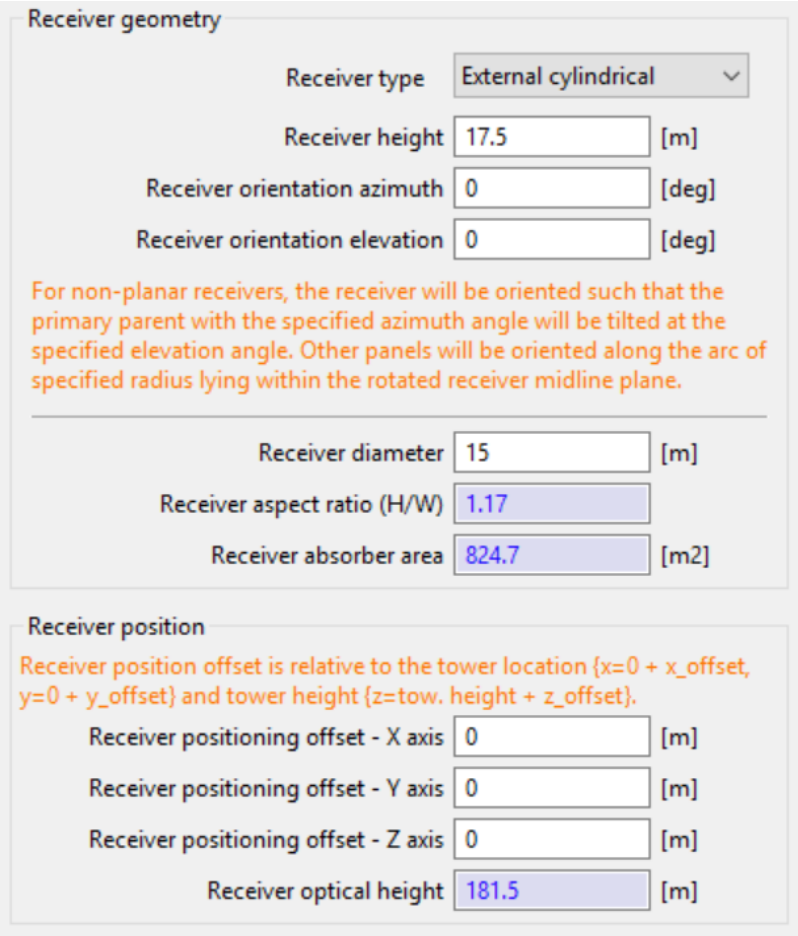

Figure 4-22: SolarPILOT validation, Receivers - receiver geometry and position

In the optical properties interface shown in Figure 4-23, the Allowable peak flux is used only for optimization and it specifies the maximum flux allowed at any point on the

receiver surface. The second parameter is the Receiver thermal absorptance that specifies the fraction of light that is absorbed when striking the receiver before radiative and convective losses. This value typically indicates the absorptivity of the receiver surface coating.

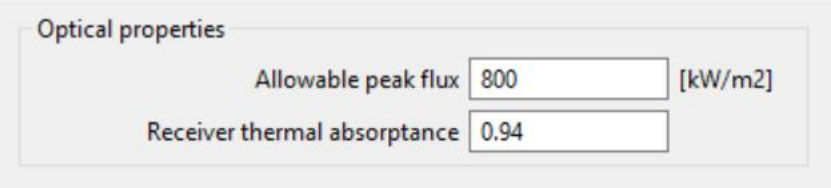

Figure 4-23: SolarPILOT validation, Receivers - optical properties

The receiver thermal losses contain convective and radiative loss from the absorbing surface of the receiver and piping loss from the riser and down comer. The thermal losses are estimated using a design point value with the receiver absorptive area as shown in Figure 4-24. The total thermal power delivered to the receiver must equal the specified Solar field design power on the Layout Setup page plus the design-point thermal loss plus the fractional loss due to the receiver thermal absorptance fraction. Thus, the power delivered by the heliostats will typically surpass the specified Solar field design power.

The design point thermal loss is the total rate of thermal loss due to convection and

radiation at reference conditions. The design point thermal loss is added to the Solar field design power and the fractional loss due to imperfect absorption to determine the total required power to be delivered by the heliostat field at the reference condition.

In the piping thermal losses side, the Receiver piping loss coefficient determines the loss from the receiver piping per meter of the tower height. In case there is a constant loss from the piping arrangement that is not depends on the system arrangement, a Receiver piping loss constant can be inserted. However, it is not filled in this project due to lack of information in this regard.

Finally, the Receiver piping loss is calculated which indicates the total receiver piping loss, including constant loss and loss that scales with tower height. The receiver piping loss is calculated as shown in Equation (23):

$$\dot{Q}_{piping} = H_{tower} C_{piping,s} + C_{piping,f} \tag{23}$$

where:

- H_{tower} : Tower height, in m
- $C_{piping,s}$: Receiver piping loss coefficient, in kW/m
- $C_{piping,f}$: Receiver piping loss constant, in kW

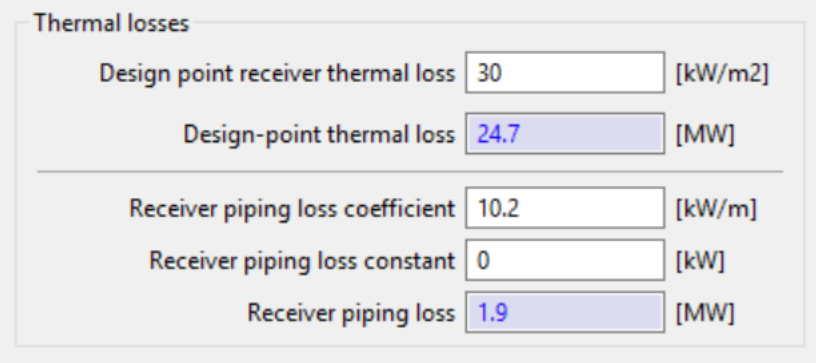

Figure 4-24: SolarPILOT validation, Receivers - thermal losses

4.2.2.6 Simulation field layout

In this page, the performance simulation will be evaluated. It consists of evaluating the current heliostat field layout and receiver geometry for optical and thermal performance. Moreover, it calculates the optical performance of each heliostat to determine the overall field performance. The simulation requires two steps to be accomplished. The generation of the aim points for each heliostat according to the method selected in the Simulation parameters group and the calculation of the performance of each heliostat in the layout, and the generation of the information on individual heliostat and the total system performance. The field layout result is shown in Figure 4-25. The number of heliostats of the solar field is found to be 10216 heliostats. Filed layout result shows information on the individual heliostat locations, focusing parameters, and aim points.

Field Layout

Heliostats 10216 Import Export

	Template	Loc. X [m]	Loc. Y [m]	Loc. Z [m]	Slant [m]	Rad. pos [m]	Az. pos [deg]	Focal X [m]	Focal Y [m]	Cant vect. <i>	Cant vect. <j>	Cant vect. <k>	Aim pt. X [m]	Aim pt. Y [m]	Aim pt. Z [m]
1	Crescent Dunes	1165.3	-723.7	0.0	1376.2	1371.7	121.84	1376.2	1376.2	0.000	0.000	1.000	6.79	-3.19	181.50
2	Crescent Dunes	1212.3	-641.8	0.0	1376.2	1371.7	117.90	1376.2	1376.2	0.000	0.000	1.000	6.79	-3.19	181.50
3	Crescent Dunes	1311.5	-402.0	0.0	1376.2	1371.7	107.04	1376.2	1376.2	0.000	0.000	1.000	7.37	-1.41	181.50
4	Crescent Dunes	1370.7	-53.7	0.0	1376.2	1371.7	92.24	1376.2	1376.2	0.000	0.000	1.000	7.49	0.47	180.80
5	Crescent Dunes	704.2	-715.6	0.0	1012.9	1004.0	135.46	1012.9	1012.9	0.000	0.000	1.000	5.78	-4.78	180.10
6	Crescent Dunes	768.3	-646.3	0.0	1012.9	1004.0	130.07	1012.9	1012.9	0.000	0.000	1.000	5.78	-4.78	180.10
7	Crescent Dunes	633.8	-778.6	0.0	1012.9	1004.0	140.85	1012.9	1012.9	0.000	0.000	1.000	4.41	-6.07	180.10
8	Crescent Dunes	557.9	-834.7	0.0	1012.9	1004.0	146.24	1012.9	1012.9	0.000	0.000	1.000	4.41	-6.07	180.10
9	Crescent Dunes	477.0	-883.5	0.0	1012.9	1004.0	151.64	1012.9	1012.9	0.000	0.000	1.000	2.76	-6.97	180.10
10	Crescent Dunes	825.7	-571.2	0.0	1012.9	1004.0	124.68	1012.9	1012.9	0.000	0.000	1.000	5.78	-4.78	180.10
. . . . .															
10206	Crescent Dunes	-85.8	222.4	0.0	293.7	238.4	-21.08	293.7	293.7	0.000	0.000	1.000	-1.87	7.26	187.80
10207	Crescent Dunes	-57.9	231.3	0.0	293.7	238.4	-14.05	293.7	293.7	0.000	0.000	1.000	-1.87	7.26	175.20
10208	Crescent Dunes	-76.4	300.6	0.0	352.9	310.2	-14.26	352.9	352.9	0.000	0.000	1.000	-1.87	7.26	175.90
10209	Crescent Dunes	-109.5	279.4	0.0	344.3	300.0	-21.40	344.3	344.3	0.000	0.000	1.000	-1.87	7.26	187.10
10210	Crescent Dunes	-101.1	293.3	0.0	352.9	310.2	-19.02	352.9	352.9	0.000	0.000	1.000	-1.87	7.26	187.10
10211	Crescent Dunes	-93.1	241.4	0.0	309.9	258.7	-21.08	309.9	309.9	0.000	0.000	1.000	-1.87	7.26	187.80
10212	Crescent Dunes	-62.8	251.0	0.0	309.9	258.7	-14.05	309.9	309.9	0.000	0.000	1.000	-1.87	7.26	175.20
10213	Crescent Dunes	-85.9	287.5	0.0	344.3	300.0	-16.64	344.3	344.3	0.000	0.000	1.000	-1.87	7.26	187.10
10214	Crescent Dunes	-70.1	275.7	0.0	331.1	284.5	-14.26	331.1	331.1	0.000	0.000	1.000	-1.87	7.26	175.20
10215	Crescent Dunes	-75.0	237.0	0.0	301.8	248.6	-17.57	301.8	301.8	0.000	0.000	1.000	-1.87	7.26	187.80
10216	Crescent Dunes	-81.2	256.3	0.0	318.2	268.9	-17.57	318.2	318.2	0.000	0.000	1.000	-1.87	7.26	187.80

Figure 4-25: SolarPILOT validation, Simulation field layout

4.2.2.7 Results

In this page, the solar field generated from the performance simulation is shown in Figure 4-26. It is very close to the actual solar field arrangement of the Crescent Dunes Solar Energy project shown in Figure 4-17. Moreover, the number of heliostats of the solar field generated by SolarPILOT is found to be 10216 heliostats, which is only 1.3 % less than the actual number of the heliostats of Crescent Dunes Solar Energy's solar filed that is 10347 heliostats. The final simulation summary results are shown in Figure 4-27. Proper comparison cannot be made with the actual results due to the lack of information available about the actual Crescent Dunes Solar Energy's solar filed project.

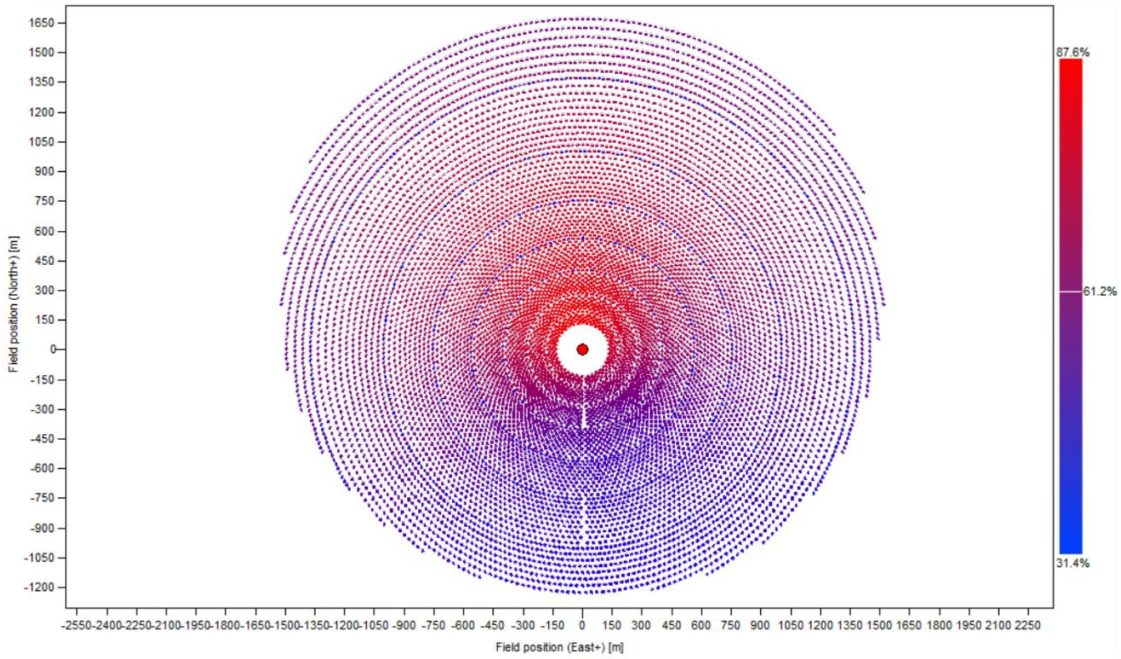

Figure 4-26: SolarPILOT validation, Results - layout results

Flux simulation results summary

Export to CSV | Copy to clipboard

	Units	Mean	Minimum	Maximum	Std. dev
Simulated heliostat area	m^2	1189039.3			
Simulated heliostat count	-	10216			
Power incident on field	kW	1189039.3			
Power absorbed by the receiver	kW	683490.2			
Power absorbed by HTF	kW	656898.9			
Solar field optical efficiency	%	61.2	31.4	87.6	0.000
Optical efficiency incl. reciever	%	57.5	29.5	82.3	0.000
Cosine efficiency	%	78.2	49.9	100.0	13.798
Blocking efficiency	%	98.5	51.8	100.0	5.746
Shading efficiency	%	100.0	100.0	100.0	0.000
Attenuation efficiency	%	91.3	85.2	97.1	3.078
Reflection efficiency	%	90.3			
Image intercept efficiency	%	96.5	80.0	100.0	3.966
Cloudiness efficiency	%	100.0	100.0	100.0	0.000
Absorption efficiency	%	94.0			
Incident flux	kW/m2	881.7	89.1	1488.7	372.364

Figure 4-27: SolarPILOT validation, Results - flux simulation results summary

4.2.3 SAM validation

As discussed earlier, SAM is a performance and financial model designed to facilitate decision making for users involved in the renewable energy sector. SAM makes performance predictions and cost of energy estimates for grid-connected power projects based on installation and operating costs and system design parameters that user specifies as inputs to the model. As mentioned earlier, the technical information available about the project is compiled from SolarPACES references and if not, the SAM prediction is used.

4.2.3.1 System design

The first step in constructing the model after selecting the weather file of the location is filling the design parameters in the design point parameters page shown in Figure 4-28.

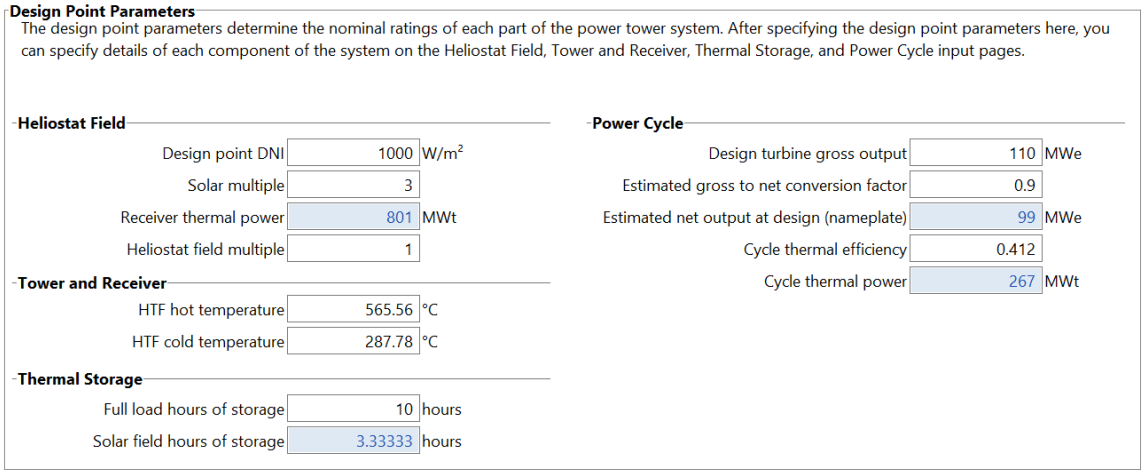

Figure 4-28: SAM validation, System design

4.2.3.2 Heliostat field

The heliostats positions of the solar field are exported from SolarPILOT and imported into SAM interface page as shown in Figure 4-29. The heliostats properties and dimensions are filled in the heliostats properties page as shown in Figure 4-30.

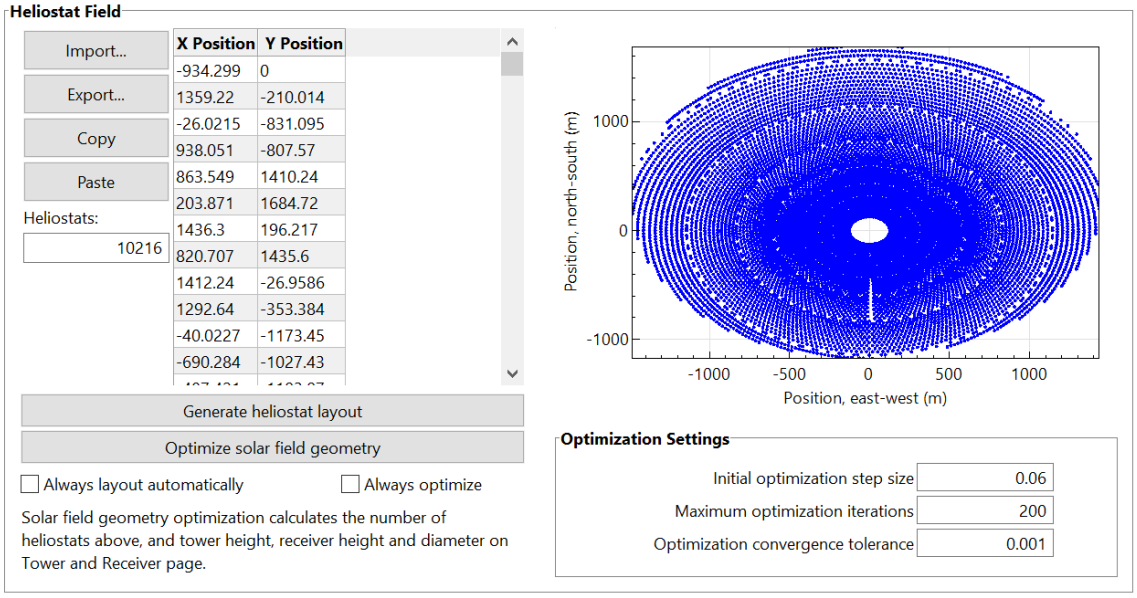

Figure 4-29: SAM validation, Heliostat Field

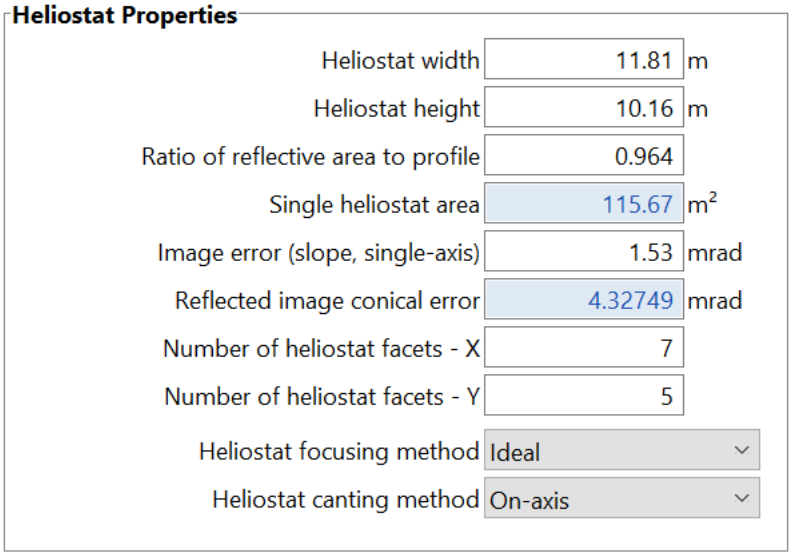

Figure 4-30: SAM validation, Heliostat Field - heliostat properties

In the heliostats operation interface page shown in Figure 4-31, four parameters are defined. The first parameter is the heliostat stow/ deploy angle which is compared to the instant solar elevation angle in degrees. Once the latter is found to be below the set angle the heliostat field will not operate and will go onto stowed position. The heliostat stow/ deploy angle is selected to be 8 deg.

The second parameter is the wind stow speed which is responsible to defocus the heliostats and force them to the stowed position. The wind velocities are available from the weather file of the location. At wind speeds above the specified stow speed, SAM assumes that the heliostats move into stow position to protect the mirror surface and support structure from any wind damage. SAM considers the parasitic tracking power required to stow the heliostats and to re-focus them when the wind speed falls below the stow speed. The stow speed is selected to be 15 m/s.

The third parameter is the heliostat startup energy, in kWe-hr, that is responsible for the energy required to bring a single heliostat out of stow position to operation positon. It is selected to be 0.025 kWe-hr. The fourth parameter is the heliostat tracking energy, in kWe, that is responsible for power required to operate a single heliostat.

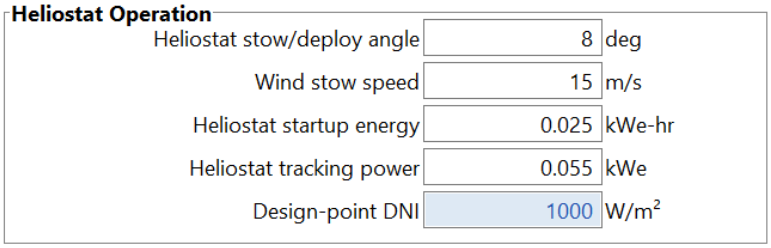

Figure 4-31: SAM validation, Heliostat Field - heliostat operation

The maximum and minimum tower height ratios, tower height and maximum and minimum distance from the tower are filled in the solar filed layout constraints interface as shown in Figure 4-32.

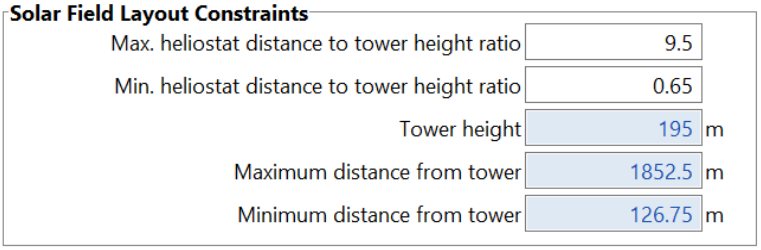

Figure 4-32: SAM validation, Heliostat Field - solar field layout constraints

The heliostats cleaning schedule is determined in the mirror washing interface as shown in Figure 4-33. The average consumption of water per m^2 is 0.7 liter and the number of washes per year are 63 washes. This means approximately a wash per week.

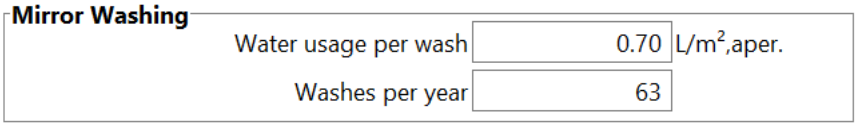

Figure 4-33: SAM validation, Heliostat Field - mirror washing

In the heliostat field availability interface shown in Figure 4-34. In the edit losses window a constant loss can be defined. This loss affects the solar field optical efficiency by increasing or decreasing the efficiency correspondingly based on the value(s) entered. This input may be beneficial in characterizing heliostat downtime, washing schedules, or other effects where field production may not match the ideal calculation. For this project, no constant losses are assigned.

The mirror reflectance and soiling input is the solar weighted specular reflectance related to the type of the mirrors that are in use. The solar weighted specular reflectance is defined as the fraction of incident solar radiation reflected into a given solid angle about the specular reflection direction. The mirror reflectance and soiling is selected to be 0.9.

Heliostat availability is an adjustment factor that take into consideration the reduction in energy output due to downtime of some heliostats in the field for repair, maintenance or cleaning activity. A value of 1 means that each heliostat in the field operates whenever enough solar energy is available. The solar field output for each hour is multiplied by the

availability factor. Heliostat availability for this project is selected to be 0.9.

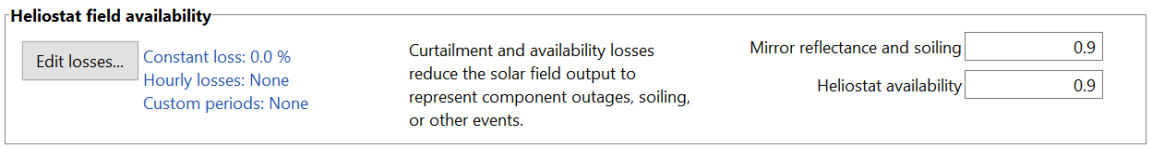

Figure 4-34: SAM validation, Heliostat Field - heliostat field availability

4.2.3.3 Tower and receiver

The tower and receiver dimensions are filled in the tower and receiver dimensions' interface shown in Figure 4-35.

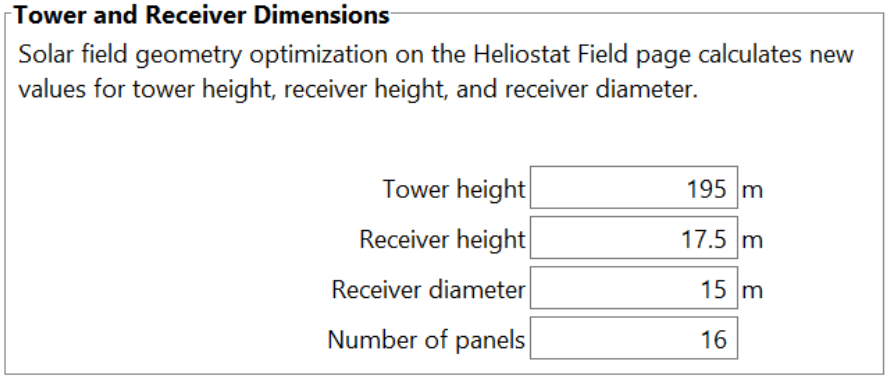

Figure 4-35: SAM validation, Tower and Receiver - tower and receiver dimensions

The type of the heat transfer fluid salt is selected as 60% NaNO3 and 40% KNO3 as shown in Figure 4-36. The material type of the pipes and the flow pattern are assumed to be stainless steel and pattern 1, respectively.

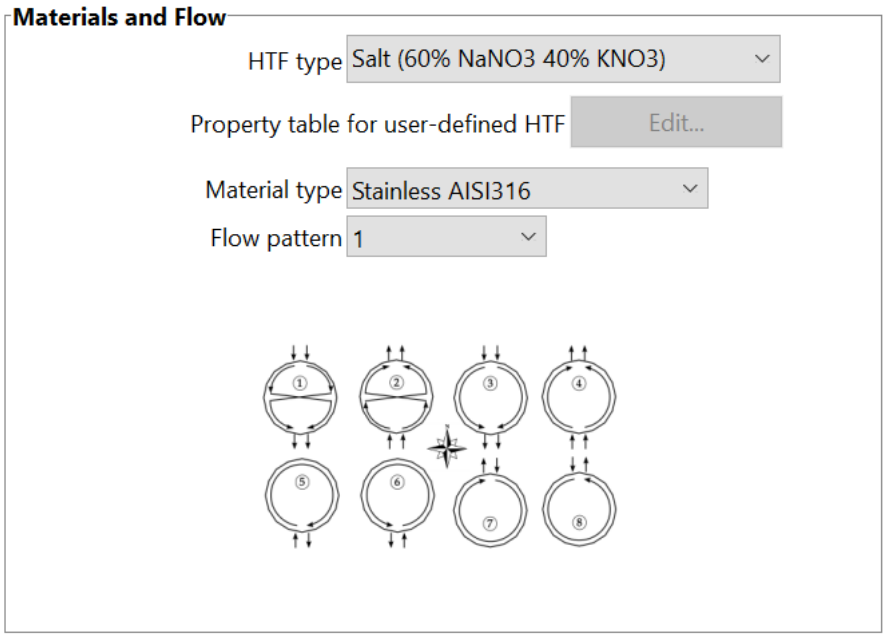

Figure 4-36: SAM validation, Tower and Receiver - materials and flow

The receiver heat transfer properties mentioned in Figure 4-37 are default values referenced from SAM.

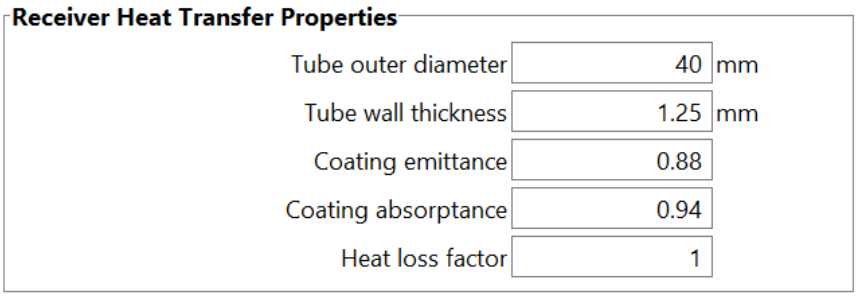

Figure 4-37: SAM validation, Tower and Receiver - receiver heat transfer properties

Regarding the modeling of the receiver flux, The maximum allowable incident flux on the receiver, before reflection, re-radiation, or convection losses.

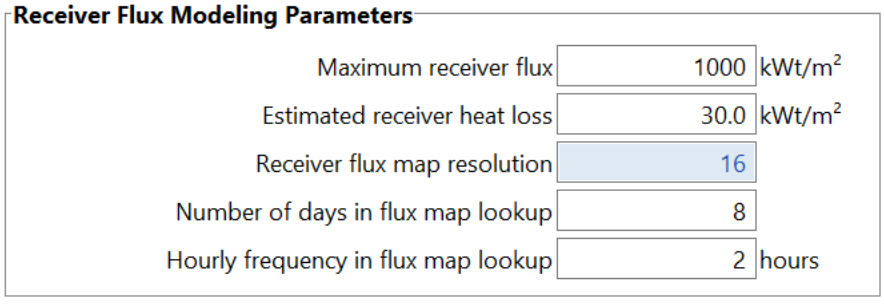

Figure 4-38: SAM validation, Tower and Receiver - receiver flux modeling parameters

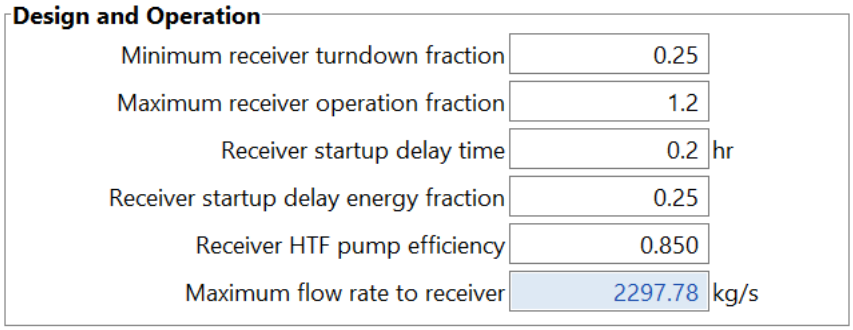

Figure 4-39: SAM validation, Tower and Receiver - design and operation

In the piping losses interface shown in Figure 4-40, the piping heat loss coefficient is specified. This value indicates the thermal energy loss per meter length of piping between the tower and thermal storage system, including both hot and cold header piping. The thermal losses due to convection, emission, or reflection are not included. The piping length constant is assumed to be zero. The piping length multiplier factor is selected to be 2.6 m that is used to find the total piping length by multiplying its value by the tower height. Note that this piping length is used only in the calculation of thermal energy loss from the receiver and is not used for pumping parasitic power or pressure loss requirement calculations. The final value mentioned is the total piping loss which is found by multiplying the piping length by the piping heat loss coefficient.

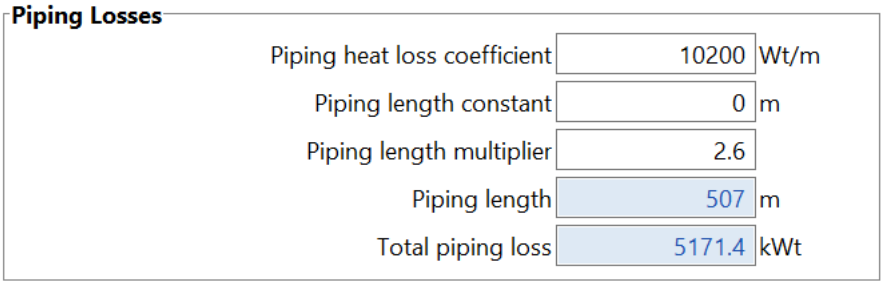

Figure 4-40: SAM validation, Tower and Receiver - piping losses

4.2.3.4 Power cycle

In Figure 4-41, the general design parameters of the power cycle are shown. The pumping power for the HTF through power block is a coefficient that is used to calculate the electric power consumed by pumps to move heat transfer fluid through the power cycle. The fraction of thermal power is needed for keeping the power cycle in standby mode. This thermal energy is not converted into electric power and the default is 0.2. The power block startup time in hours is the time through which the system consumes energy at the startup fraction before it begins producing electricity. The default is 0.5 hours. The fraction of thermal power needed for startup is the fraction of the turbine's design thermal input required by the system during startup. The default is 0.75 and this thermal energy is not converted to electric power.

The minimum turbine operation is the fraction of the nameplate electric capacity below which the power block does not produce electricity and at that time the solar field is defocused. For systems with storage as our case, solar field energy is delivered to storage until storage is full. The default value is 0.25. The maximum turbine over design operation is the fraction of the electric nameplate capacity into which some heliostats in the solar field are defocused to limit the power block output to the maximum load if there is no storage system or the storage is full. The default value is 1.05.

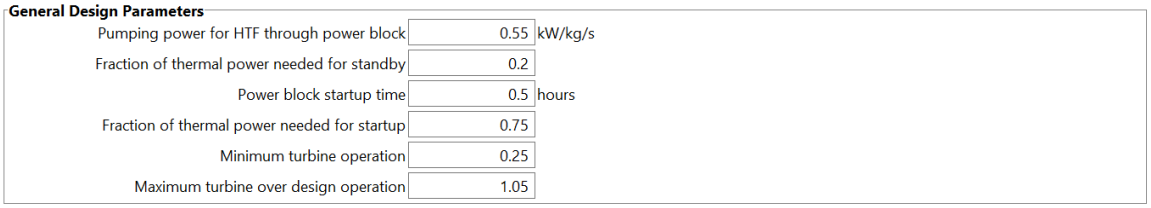

Figure 4-41: SAM validation, Power cycle - general design parameters

The Rankine cycle page, shown in Figure 4-42, shows variables that specify the design operating conditions for the steam Rankine cycle used to convert thermal energy to electricity.

The boiler operating pressure in bars is the saturation pressure of the steam as it is

transformed from liquid to vapor in the boiler. This value is used to determine the steam's saturation temperature and consequently the superheating capability of the heat exchangers. The default value is 115 bars.

The Steam cycle blowdown fraction is the fraction of the steam mass flow rate in the power cycle that is extracted and replaced by fresh water. This blowdown is defined as the removal of water from the power cycle for controlling the water parameters within prescribed limits to minimize corrosion, scale, carryover and other specific problems. Moreover, blowdown is also used to eliminate suspended solids present in the system. For determining the total required quantity of power cycle makeup water, the fraction is multiplied by the steam mass flow rate in the power cycle for each hour of plant operation. A default value for the hybrid cooling system is 0.02.

Turbine inlet pressure control value determines the power cycle working fluid pressure during off-design loading and fixed value is selected where the the power block maintains the design high pressure of the power cycle working fluid during off-design loading. The condenser type is a hybrid cooling system where a wet cooling system and dry cooling share the heat rejection load.

The ambient temperature at design in ºC is the temperature at which the power cycle operates at its design point rated cycle conversion efficiency. Initial temperature

difference (ITD) is used for the air cooled condensers only. It is the difference between the temperature of steam at the turbine outlet/ the condenser inlet and the ambient dry-bulb temperature.

The reference condenser water dT in ºC is for the evaporative condenser type only. The temperature rise of the cooling water through the condenser under design conditions is used to calculate the cooling water mass flow rate at design and the steam condensing temperature. The Approach temperature in ºC is also used for the evaporative type only. It is the temperature difference between the circulating water at the condenser inlet and the wet bulb ambient temperature. It is used with the ref. condenser water dT value to determine the condenser saturation temperature and thus the turbine back pressure.

The condenser pressure ratio is for the air-cooled type only. It is used to calculate the pressure drop across the condenser and the corresponding parasitic power required to sustain the air flow rate.

Minimum condenser pressure in inches of mercury prevents the condenser pressure from dropping below the level selected to avoid physical damage to the system. For hybrid systems, the default value is 2 inches of mercury. Cooling system part load levels tells how many discrete operating points there are for the heat rejection system. A value of 8 is selected.

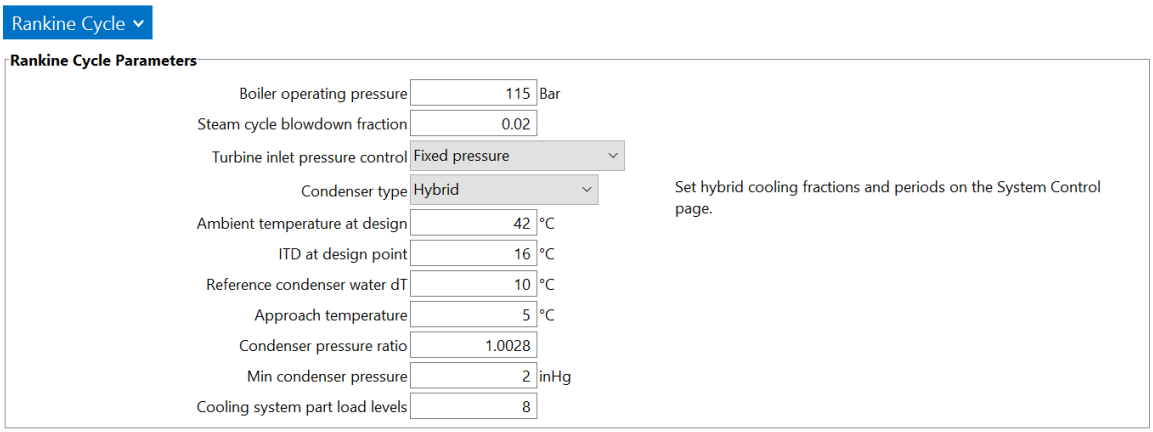

Figure 4-42: SAM validation, Power cycle - Rankine cycle parameters

4.2.3.5 Thermal storage

The parameters on the thermal storage page, shown in Figure 4-43, describe the properties of the thermal energy storage system. The storage type is selected to be a two tanks storage system with separate hot and cold storage tanks. The nominal thermal storage capacity of the storage system is found by multiplying the hours of storage by the cycle thermal input power and both at power cycle full capacity. Based on the total fluid volume and the number of tanks, the cylindrical shaped tank height and diameter are specified. The tank fluid minimum height, in meters, is the minimum allowable height of fluid in the storage tank determined by the mechanical limits of the tank. The default value is 1 meter.

The parallel tank pairs number is the number of the parallel hot and cold storage tanks pairs. The wetted loss coefficient, in Wt/m²/K, is the thermal loss coefficient related to the portion of the storage tank holding the storage heat transfer fluid. The default value is 0.4 Wt/m²/K and it is used to find the estimated heat loss amount.

Both hot and cold tanks have electric heaters to add sufficient thermal energy to storage to reach the set point. The cold tank heater temperature set point is set at 280 °C and the heater capacity is 15 MWe. On the other hand, the hot tank heater temperature set point is 500 °C and heater capacity is 30 MWe. The tank heater efficiency is selected to be 99%. Last value found is the density of the heat transfer fluid.

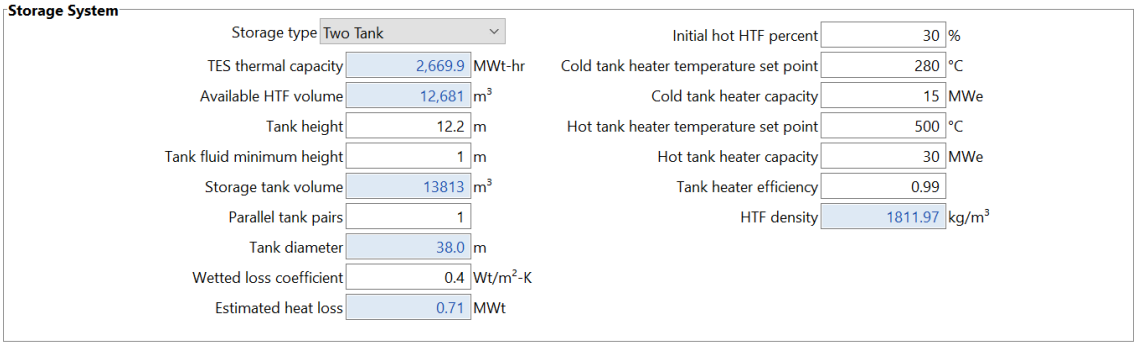

Figure 4-43: SAM validation, Thermal Storage - storage system

4.2.3.6 System costs

CSP plants in general are capital intensive, but have virtually zero fuel costs. The total installed cost of the project is the total summation of two main cost categories. The direct and the indirect capital costs. The direct capital costs represent the expenses for the specific pieces of equipment or the installation services prior the commissioning of the plant. It is in $/kWe of gross power block capacity rather than nameplate capacity because the size and cost of the power block is determined by the gross capacity, not the net capacity. The indirect capital costs represent any cost that cannot be identified with a specific piece of equipment or installation service. It is in $/Wac of nameplate power block capacity because those costs that use the entire plant as the basis, not just the power block. In the case of the total installed cost, the cost is also in $/kWe of the nameplate capacity.

As mentioned before, the default cost values that are selected are based on realistic references for CSP plants. The cost data are meant to be realistic, but not to represent actual costs for a specific project.

The direct capital costs interface is shown in Figure 4-44. Under the heliostat field category, the site improvement cost is the cost per square meter of total reflective area from of the solar field to account for expenses related to site preparation and other equipment not included in the heliostat field cost category. The default value is 16 $/m^2.

The heliostat field cost is per square meter of the total reflective area from the solar field to account for expenses related to installation of the heliostats, including heliostat parts, field wiring, drives, labor, and equipment. The default value is 145 $/m^2.

Under the tower category, the fixed tower cost accounts for costs related to tower construction, materials and labor. It is a multiplier in the tower cost scaling equation. The tower cost scaling exponent defines the nonlinear relationship between tower cost and tower height. Thus, the total tower cost is found by Equation (24)

$$\text{Total Tower Cost} = \text{Fixed Tower Cost x } e^{(\text{Tower Cost Scaling Exponent } (\text{Tower Height} - \text{Receiver Height} \div 2 + \text{Heliostat Height} \div 2))} \quad (24)$$

Under the receiver category, the receiver reference cost is the cost per receiver reference area, on which the receiver reference cost is based, to account for receiver installation costs, including labor and equipment. The receiver cost scaling exponent defines the nonlinear relationship between receiver cost and receiver area based on the reference cost conditions provided as per Equation (25)

$$\text{Receiver Cost} = \text{Receiver Ref. Cost x } \left(\frac{\text{Receiver Area}}{\text{Receiver Ref. Area}}\right)^{\text{Receiver Cost Scaling Exponent}} \quad (25)$$

Under the Storage category, the thermal energy storage cost is per thermal megawatt-hour of storage capacity to account for the installation of a thermal energy storage system, including equipment and labor.

Under the power cycle category, there is no fossil backup in this project and thus there is no cost is assigned. The balance of plant is the cost per electric kilowatt of power cycle gross capacity expenses related to installation of the balance of plant components and controls, and construction of buildings, including labor and equipment. The power cycle cost is per electric kilowatt of power cycle gross capacity expenses related to installation of the power block components, including labor and equipment.

Last cost variable in the direct capital costs is the Contingency percentage that is a percentage of the sum of the site improvements, heliostat field, balance of plant, power block, storage system, fixed solar field, total tower, and total receiver costs to account for expected uncertainties in direct cost estimates. In most of the cases the contingency is always less than 10%. In this project, it is 7%.

The total direct cost is the sum of improvements, site improvements, heliostat field, balance of plant, power block, storage system, fixed solar field, total tower, total receiver, and contingency costs. It is found to be $ 539,703,680.00.

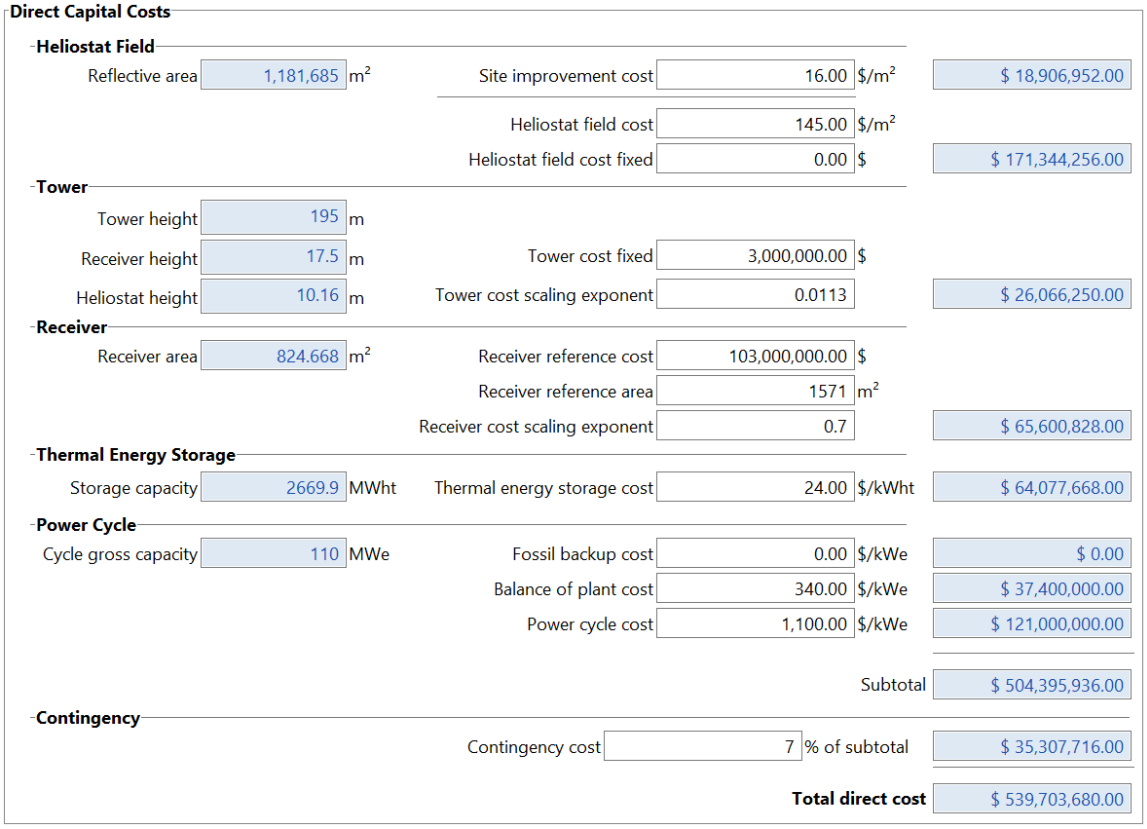

Figure 4-44: SAM validation, System Cost - direct capital cost

The second main component of the total installed cost is the indirect capital cost. It is typically the cost that cannot be identified with a specific piece of equipment or installation service. The interface is shown in Figure 4-45. The EPC (engineer-procure-construct) and owner costs are associated with the design and construction of the project. Typical costs that may be appropriate to include in the EPC and Owner category are: permitting, consulting, management or legal fees, geotechnical and environmental surveys, spare parts inventories, commissioning costs, and the owner's engineering and

project development activities. The common practice in determining this type of cost is by a percentage from the direct cost. The default value is 13%. The total land cost is associated with land purchases per are. The land in Nevada states is assumed to be $ 10,000 per acre.

As the project was constructed in U.S.A., sales tax is an important factor to be considered. The total sales tax amount is found by multiplying the sales tax rate, that is selected by default as 5%, by the percentage of direct costs that is selected by default as an 80% of the direct cost. At the end the total indirect cost is the sum of EPC costs, project-land-miscellaneous costs, and sales tax.

Indirect Capital Costs

Total land area	3,211 acres		Cycle net (nameplate) capacity	99 MWe	
	$/acre	% of direct cost	$/We	$	
EPC and owner cost	0.00	13	0.00	0.00	$ 70,161,480.00
Total land cost	10,000.00	0	0.00	0.00	$ 32,113,414.00
Sales Tax					
Sales tax basis	80	% of direct cost	Sales tax rate	5 %	$ 21,588,146.00
				Total indirect cost	$ 123,863,040.00

Figure 4-45: SAM validation, System cost - indirect capital costs

Finally, the total installed cost is the sum of all the direct and indirect capital costs that are specified in the above sections as shown in Figure 4-46. Thus, the total installed cost of the project is $ 663,566,720. In comparison to this value, the U.S. department of energy has issued in Sep 2011 a $ 737,000,000 loan guarantee to finance Crescent Dunes project [69]. There is no further information about the breakdown of this loan. The difference between the expected cost from SAM and the issued load is less than $ 75,000,000. This difference can be due to unknown source of costs or not that accurate estimation from SAM.

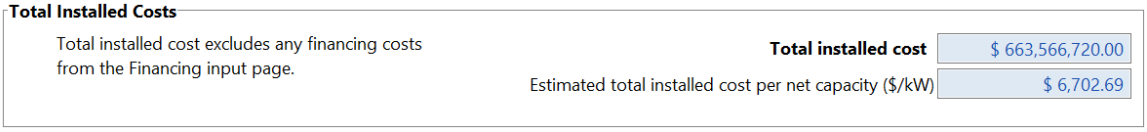

Figure 4-46: SAM validation, System cost - total installed costs

4.2.3.7 Results

After simulating the results using all the inputs values, the summary tab displays the metrics table with a selection of results for each case in the project file. This table is shown in Figure 4-47 and it has two sets of data, the performance metrics and the financial metrics. Looking at the performance metrics, the annual energy produced by the plant is shown to be around 430,000 MWh and the capacity factor is 49.6%. Moreover,

the monthly energy production for the first year of operation can be extracted from SAM and it is shown in Figure 4-48. Summer seasons are having the highest energy production.

Metric	Value
Annual energy (year 1)	429,785,440 kWh
Capacity factor (year 1)	49.6%
Annual Water Usage	84,024 m^3
PPA price (year 1)	6.40 ¢/kWh
PPA price escalation	1.00 %/year
Levelized PPA price (nominal)	14.36 ¢/kWh
Levelized PPA price (real)	11.29 ¢/kWh
Levelized COE (nominal)	13.27 ¢/kWh
Levelized COE (real)	10.44 ¢/kWh
Net present value	$49,442,068
Internal rate of return (IRR)	11.00 %
Year IRR is achieved	20
IRR at end of project	12.59 %
Net capital cost	$730,396,800
Equity	$364,694,048
Size of debt	$365,702,784

Figure 4-47: SAM validation, Results - Summary table

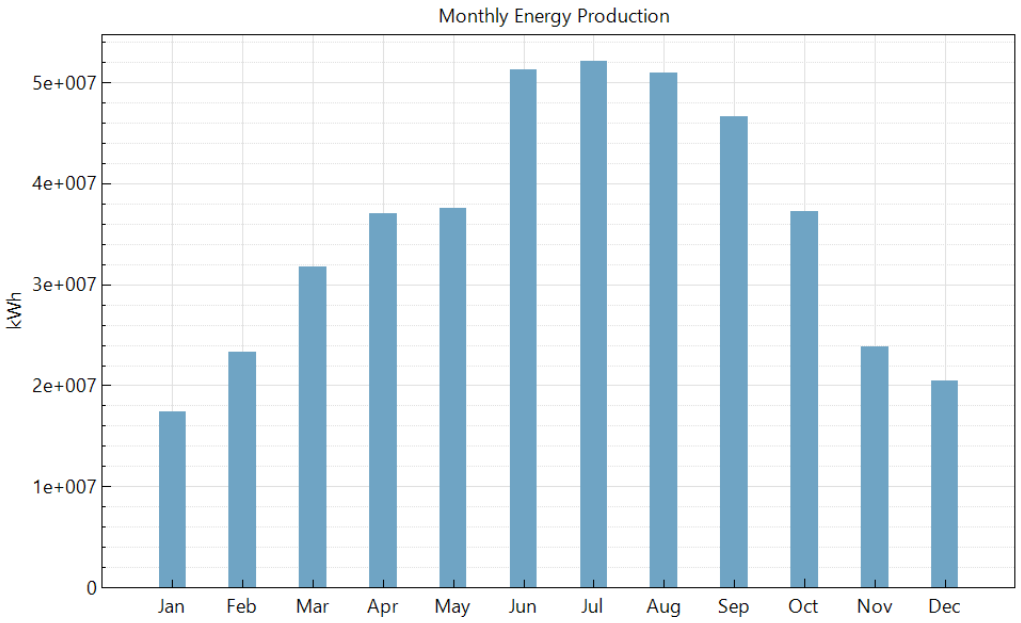

Figure 4-48: SAM validation, Results - monthly energy production

As mentioned before, the annual energy production of Crescent Dunes Solar Energy Project is expected to be 500,000 MWh. The actual monthly energy production of the plant since commissioning on Feb 2016 is shown in Table 4-15 and there is no any information about the performance status of the plant during these months. If the expected annual energy production of the project is compared with SAM result, then there is a difference of 70,000 MWh, i.e. SAM is less by 14%. However, based on the actual monthly production numbers of the project, specially July, August and September, SAM's result shows higher energy production numbers. More than 45,000 MWh for the latter each mentioned months. Due to the lack of actual performance information about

Crescent Dunes Solar Energy Project, a final conclusion about validity of SAM result cannot be derived. However, based on the avavilable information of the project, SAM is considered close to the expected annual energy production.

Table 4-15: Monthly energy production of Crescent Dunes Solar Energy project [70]

Month	Energy production in year 2015 (MWh)	Energy production in year 2016 (MWh)
Jan	-	1,504
Feb	-	9,095
Mar	-	7,099
Apr	-	2,158
May	-	11,485
Jun	-	6,216
Jul	-	25,560
Aug	-	28,267
Sep	-	30,514
Oct	1,703	5,410
Nov	1,831	0
Dec	0	0
Total Energy Production (MWh)	**3,534**	**127,308**

4.3 Considerations for the electrical demand in key locations in Doha

In line with Qatar National Vision 2030 and all the current plans to transfer the sole dependence on fossil fuels to renewable energy resources, some renewable powered initiations should be made in the state. Two of key locations in Doha with high electricity demand potential are the Al-Jasra and Msheireb down town Doha city zones. Msheireb

area is still not completed and many sites are still under construction. Thus, the electrical consumption data cannot be determined. However, the second area, Al-Jasra, contains Souq Waqif which was built a hundred years ago and it was restored in 2006 to preserve its traditional architectural style. This Souq is considered one of the top tourist destinations in Qatar where thousands of people from all over the world visit it. This is called a Souq where traditional clothes, spices, handicrafts, and souvenirs are sold, however it hosts several events, art galleries, and local and global concerts. Moreover, it contains dozens of local and worldwide restaurants.

Those two areas are selected, to be powered by the CSP plant, due to their importance in the country and to convey to the whole world that Qatar is seriously considering the gradual transformation from fossil fuels to renewable resources.

To design the required capacity of the CSP plant, the electrical consumptions data should be identified in the first place. Currently and as mentioned before, the electrical consumption data can be determined for Souq Waqif only. For that reason, the information technology department in Qatar General Electricity & Water Corporation (Kahramaa) was contacted and the readings for more than 600 shops in Souq Waqif for the year of 2014 and 2015 was provided on monthly basis as shown in Table 4-16 and Figure 4-49.

Table 4-16: Souq Waqif electrical consumption of year 2014 and 2015

Month	2014 Consumption, kWh, Monthly	2015 Consumption, kWh, Monthly	Average consumption, kWh, Monthly
Jan	435,292	468,331	451,812
Feb	330,966	334,723	332,845
Mar	350,866	436,516	393,691
Apr	546,928	552,972	549,950
May	760,861	833,902	797,382
Jun	864,223	619,984	742,104
Jul	1,046,369	1,007,851	1,027,110
Aug	1,048,554	1,010,271	1,029,413
Sep	1,012,682	1,102,627	1,057,655
Oct	1,092,261	946,546	1,019,404
Nov	661,226	775,200	718,213
Dec	566,989	546,915	556,952
Total consumption	8,717,217	8,635,838	8,676,528

It is worth to mention that collecting the electrical consumption readings from the shops' electrical meters is done manually by a meter man. This may affect the accuracy of the reading per month if the reading is not recorded at the end of the month. Moreover, some shops for certain months are not rented and this may affect the data in comparison with the same month of the other year. It can be shown that the maximum monthly electrical consumption occurred in month of September with value of 1,057,655 kWh. In addition of that, the maximum daily electrical consumption of both years was found to be 36,754.23 kWh. The total averaged annual consumption is 8,676,528 kWh that is almost 8.7 GWh.

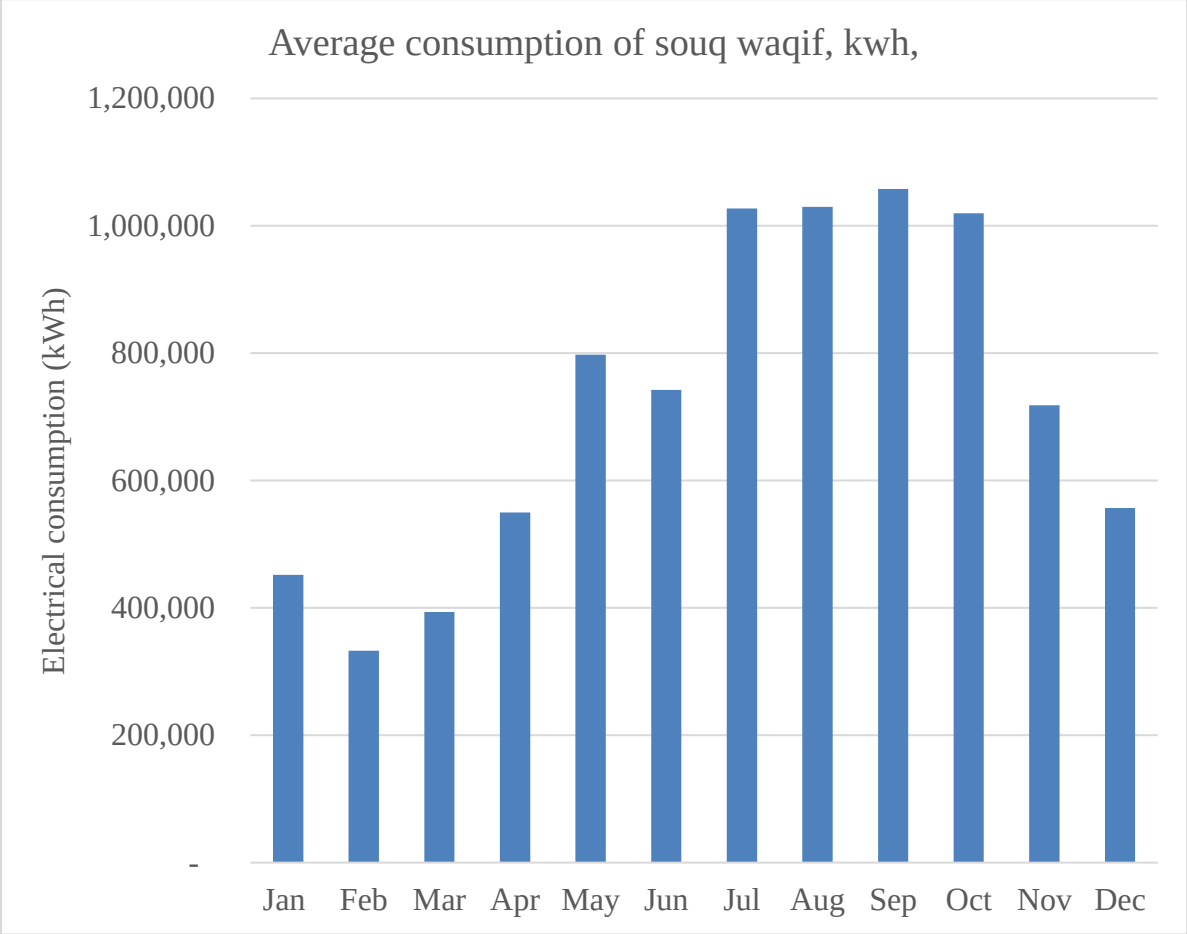

Figure 4-49: Souq Waqif electrical consumption of year 2014 and 2015 averaged with each corresponding month

4.4 Considerations for plant location selection

The selection of the CSP plant's location is an important step in the designing stage. Based on this decision, many related issues will rise such as the distance between the plant and the planned electrical consumption area and the site preparation steps required

for the selected location and how large it is. All these issues will definitely affect the plant's electricity net output and the total cost. In this thesis, the location will be selected based on two major criterions. The plant should be close enough to the electrical consumption area to reduce the total losses in electricity transmission and distribution. Then, the location should reflect the interest of the government in utilizing the renewable resources in providing electricity to the state.

Meeting the above two criterions, Al-Safliya island is selected. It is 1.26 km^2 in area and it is geographically located around 25.345 degrees North and 51.577 degrees East. As shown in Figure 4-50. It is less than 8.5 km far from the electrical consumption area which is in the heart of Doha and the island in the same time is very near from Hamad International Airport and it can be easily seen during the departures and arrivals flights. Many solar power plants are built on islands, examples of these are the solar power plant built on Al-Farasan Island in Saudi Arabia [71] and the solar power plant built on the island of Annobón in Annobón Province [72]. Moreover, an example of the solar power plants that are under study is the solar power plant on the island of Kauai in Hawaii [73].

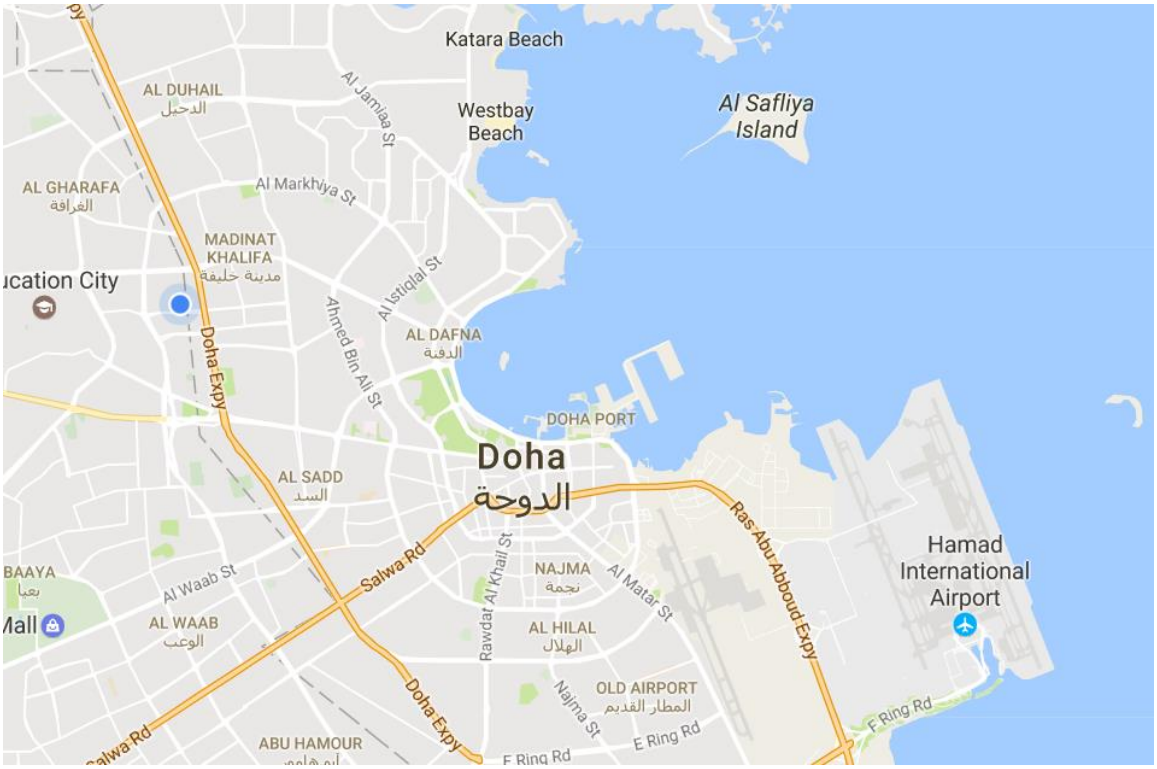

Figure 4-50: Safliya island location (picture is from Google Maps)

The designed CSP plant will not utilize the whole island's area. Currently, people are attracted to Al Safliya island for fishing and playing with water scooter during the summer months. These activates are done on the coast of the island only. Thus, building the CSP plant on the land core of the island will not interfere with the tourism activates mentioned above. The CSP plant will utilize only 0.46 km^2 of the island total area (i.e. less than 40% of the total area) as shown in Figure 4-51.

Figure 4-51: CSP plant area in Al-Safliya island (picture is originally from Google earth PRO)

4.5 Considerations for desalination process

Desalination simply means the process of removing salt from saline water. There are many methods for this process. The major processes that are in use currently are based on either a membrane process or a thermal process.

The thermal processes are based on distilling the water. In other words, to heat the saline water until it vaporizes and then remove the resulted vapor to a different container with condensation by cooling. As a natural example of distillation is the rainfall phenomena. Multi-stage flash (MSF), Multi-effect distillation (MEF) and Vapor compression are the

most used thermal processes. One of the disadvantage of using these applications is the huge water input required and energy consumption compared to the membranes applications [74].

The membrane technology applications are using, on the other hand, mechanical pressure, electrical potential, or a concentration gradient as the driving forces across a semi-permeable membrane barrier to separate the salt from water [75]. Two of the most famous membrane technologies are the Reverse Osmosis (RO) and the Membrane Distillation (MD). Commercially, the most dominant and worldwide competitive technologies are based on RO processes with approximately 65% use in the world [76]. On the other hand, the MD processes are not mature enough with less than 2% of the total usage in the world [76].

In Qatar, a study was conducted by QEERI to compare between seawater RO and the MSF system [74]. The result was found that MSF system which is mostly used for desalting seawater in Qatar has negative impacts on the environment, because of the solely dependent on fossil fuels, in comparison with the seawater RO. Moreover, for a supply of 1.2 Mm3/ day of desalted water, the study showed that seawater intake would be reduced about 3 times when utilizing the reverse osmosis as well as the energy use with up to 75%. Thus, the seawater intake to product ratio for the reverse osmosis is 3 with 4 kWh/m3 of pumping energy.

In this thesis, the membrane technology is utilized instead of the thermal processes because of the above discussed reasons and more specifically the RO technology as it is more mature than the MD technology.

It is observed that there is a tremendous decrease in desalination costs in the last decades with the new technologies that are invented and under continuous development. The installed cost of a desalination plant is approximately $1m for every 1,000 cubic meters per day of installed capacity [77]. The costs of infrastructure to distribute water must be added to this estimated cost. Moreover, the operational cost of desalinated seawater has dropped below US$0.50/$m^3$ for a large-scale seawater reverse osmosis plant at a certain location and conditions while in other locations the cost is 50% higher (US$1.00/$m^3$) for an alike facility [78].

4.6 Considerations for heliostats cleaning

The power tower solar plants have a huge number of heliostats whose reflective surfaces are composed of mirrors. The reflectivity levels of these mirrors are of a vital importance. Any reduction in the reflectivity levels, due to accumulation of dust and dirt, has a direct and substantial effect upon the plant's efficiency and thus the overall productivity capacity of the plant. This is translated to important losses in plant revenues and profits. To take a full benefit of solar energy available at the plant's solar field, it is enormously important to maintain maximum reflectivity of these mirrors always. Thus, a regular

cleaning system is crucial for maintaining desired productivity levels.

There are two main cleaning systems for such applications. The cleaning system by water jet cleaning and the wet brushing cleaning. In comparison between the both systems, the latter has a higher cleaning efficiency with minimizing the water and fuel consumption. In Spain, a test was conducted by exposing solar reflectors outdoor and applying different cleaning methods [79]. As per the obtained results, the most attractive cleaning method is the one based on wet brushing cleaning, with an average efficiency of 98.8 % in rainy periods and 97.2 % in dry seasons.

The cleaning system can be applied manually by either utilizing a truck with proper cleaning arm with brush, as shown in Figure 4-52 ,or utilizing an autonomous cleaning system using robots as shown in Figure 4-53. The first option has proven its validity with parabolic trough plants and it can be used also with power tower plants. The second is still under testing and the leader in these systems is SENER company with their patented HECTOR (Heliostat Cleaning Team Oriented Robot). As shown in Figure 4-53, HECTOR is an autonomous cleaning system based on a fleet of individual cleaning robots.

Figure 4-52: Truck with cleaning arm with brush [80]

Figure 4-53: HECTOR device [81]

4.7 Considerations of water demand for running CSP plant

Any running CSP plant with hybrid cooling system would requires water for three primary uses:

1- Steam cycle makeup

Although the steam cycle for the CSP plant is a closed system, some water should be removed during operational steam blow down. This removal is to control the water parameters within the recommended limits to minimize corrosion, scale and other specific problems. Moreover, this water blowdown is also required to remove any suspended solids present in the system. Thus, makeup water during plant operation is required to recover this blowdown loss. This loss is estimated at 125,000 m^3 per year [68].

2- Heliostat washing activities

As the solar field heliostats collect dust and other particles, their efficiency and reflectivity would decrease. This results in reduction in the ability to generate electricity. Thus, a continual heliostat wash program is required to be implemented on a continual basis. Based on Qatar environment, the program will be repeated twice a week with 0.7 liter per m^2 of a single heliostat. The program will utilize a truck with proper cleaning arm with brush, as shown in Figure 4-52.

3- Hybrid cooling system augmentation

During periods of high electrical demand and temperatures, the cooling system will be operated in hybrid mode. This mode consists of heat rejection through air cooled condenser as well as heat rejection through evaporative cooler (i.e. cooling tower). The hybrid mode of operation will increase the efficiency of the plant and will allow the plant to produce additional electricity during times of high electricity demand and high temperatures. In this CSP project, the heat rejection using the cooling tower will be used based on the need and actual measurement of the steam cycle. However, for the worst-case scenario of the water consumption, the mode of operation will be using the cooling tower at 75% at all time of operation and the rest is the air-cooled method.

4.8 Considerations of maintenance activities for CSP plant

The long-term operation of the CSP facility should include periodic maintenance and major overhaul of many solar facility equipment such as the steam turbine generator, all types of the used pumps, piping, etc., in accordance with manufacturer recommended schedules. Moreover, to maintain the desired heliostat reflectivity, a periodic cleaning of the heliostats with demineralized water is necessary. Regarding the transmission line and substations, routine inspections is necessary to be conducted by certified site personnel monthly or as needed under emergency conditions [68]. In addition of that, all the substation structures should be inspected from the ground on an annual basis for corrosion and foundation condition. The frequency of inspection could vary depending on

factors such as the structure type and age of the system. Based on the recent report from U.S. Energy Information Administration published on April 2013 [87], the most of the thermal solar operators treat operating and maintenance on a fixed basis that is $67.26/kW-year.

4.9 Considerations of CO_2 reduction of a CSP plant

As discussed previously, most of the electricity all over the world is generated utilizing the fossil fuels and CO_2 gas emission is one of the major gas emissions the that is considered as the primary greenhouse gas. One of the most efficient power generation process in generating electricity is the combined cycle gas turbine process. In this process, the power is generated much more efficiently than in a single gas turbine cycle where the hot exhaust gases of the gas turbine are utilized to produce steam through a heat exchanger that generates electricity in a steam turbine cycle. In this combined cycle, the plant efficiency can reach up to 58 % [82]. The CO_2 gas emissions of the most efficient combined cycle gas turbine process is estimated by The Parliamentary Office of Science and Technology in London to be 200 gCO_2eq/kWh [83]. Thus, using this number and the energy produced by the designed CSP plant, the reduction in CO_2 gas emissions can be found.

5 RESULTS AND DISCUSSION

In this chapter, the weather file of the selected location and the results from both the software packages that are used, SolarPILOT and SAM, are discussed.

5.1 Weather file of the selected location

As mentioned in SolarPILOT validation section, a weather file for the selected location should be prepared as an input information about the location's weather and solar status. In this thesis, the weather file for Al-Safliya island has the solar irradiance data (total global horizontal irradiance, total direct normal irradiance and total diffuse horizontal irradiance) from the prepared Microsoft excel model shown in Table 4-3 to Table 4-12 and Figure 4-5. The other weather data (dry-bulb temperature, relative humidity, atmospheric pressure, wind speed and direction) are taken from [84] that was based on a satellite-based values measured for Doha International Airport on 2011. The wet-bulb temperature is generated from a Microsoft Excel program provided from www.the-snowman.com using the available dry-bulb temperatures and relative humidity values. A sample of the weather file on the first day of year 2016 is shown in Figure 5-1.

Source	Location	City	State	Country	Latitude	Longitude	Time Zone	Elevation						
TMY2	-	Doha	-	Qatar	25.3455	51.5773	3	4						
Year	Month	Day	Hour	GHI	DNI	DHI	Tdry	Tdew	RH	Pres	Wspd	Wdir	Snow Dep	
2016	1	1	0	0	0	0	16.4	14.7	78	1017.2	1.5	230	0	
2016	1	1	1	0	0	0	16	14.8	82	1018.1	1.5	240	0	
2016	1	1	2	0	0	0	16	14.2	77	1018.1	1.5	250	0	
2016	1	1	3	0	0	0	15.8	14.5	81	1018.1	2.6	250	0	
2016	1	1	4	0	0	0	16	14.2	77	1018.1	2.6	250	0	
2016	1	1	5	0	0	0	16	14.2	77	1018.1	2.1	270	0	
2016	1	1	6	109.0766	152.8498	47.93674	18.6	14.1	59	1019.9	2.6	250	0	
2016	1	1	7	270.9921	379.7428	119.0949	21	12.9	40	1018.1	3.1	250	0	
2016	1	1	8	404.7776	474.9097	177.8907	22	14.2	43	1018.1	3.6	250	0	
2016	1	1	9	501.3159	474.9097	220.3171	23.1	15.2	44	1017.6	2.6	260	0	
2016	1	1	10	554.028	474.9097	243.4829	23	15.1	44	1017.6	3.1	310	0	
2016	1	1	11	559.3218	474.9097	245.8094	24	15.9	44	1017.6	4.6	310	0	
2016	1	1	12	516.8364	474.9097	227.138	23.5	17	52	1016.4	5.1	310	0	
2016	1	1	13	429.4673	474.9097	188.7412	23	18.3	61	1018.2	4.6	320	0	
2016	1	1	14	303.1683	424.8316	133.2357	22	18.1	65	1018.2	4.6	320	0	
2016	1	1	15	146.5467	205.3567	64.40397	20.5	17.5	70	1018	4.6	320	0	
2016	1	1	16	0	0	0	20	17.5	73	1018.2	4.1	310	0	
2016	1	1	17	0	0	0	19	16.5	73	1018.2	4.6	310	0	
2016	1	1	18	0	0	0	18.9	15.7	68	1018.5	4.1	310	0	
2016	1	1	19	0	0	0	19	16.5	73	1018.2	5.1	300	0	
2016	1	1	20	0	0	0	18	17	83	1018.2	4.6	300	0	
2016	1	1	21	0	0	0	17.4	16.2	82	1017.8	4.6	300	0	
2016	1	1	22	0	0	0	17	16	83	1018.2	4.6	300	0	
2016	1	1	23	0	0	0	17	15.1	77	1018.2	4.6	300	0	

Figure 5-1: Weather file sample of Al-Safliya island

5.2 SolarPILOT result

After the location of the CSP plant is selected and the weather file for the same is prepared, a new SolarPILOT file is created for the thesis project following the same inputs and steps followed in the validation section from Figure 4-9 to Figure 4-27 otherwise mentioned. The SolarPILOT has an inbuilt optimization tool, however the current version that is used (version: 2017.2.7) and the previous versions cannot get it activated due to a bug. NREL has been communicated regarding this issue and they have assured that the problem is under rectifying and they will update it in the newer version. In this case, a parametric study is the only available option to get the maximum production of the CSP plant by optimizing the parameters of the solar field. These parameters are tower optical height, structure width and height, number of horizontal and vertical panels and receiver height and diameter.

5.2.1 Parameters optimization

To get the parametric study done, initial values for the solar field's parameters are assumed and then they will be optimized later one by one. First, the land boundary array option is selected and the solar field area is chosen for the CSP plant as shown in Figure 5-2. Second, the design point DNI value based on the weather file is 700 W/m^2 as per the weather file and the values in Table 5-1 are inserted as initial values.

Figure 5-2: SolarPILOT results, boundary array - solar filed of the CSP plant

Table 5-1: Initial values for solar field's parameters

Initial values for solar field's parameters	**Value**
Tower optical height, m	220
Heliostats structure width, m	8
Heliostats structure height, m	8
Number of heliostat horizontal panels	2
Number of heliostat vertical panels	8
Receiver height, m	3
Receiver diameter, m	10

The simulations for a new layout of the solar field and the performance simulation are generated. The solar field design power will be changed until the heliostats are filling the whole selected area. After many iterations, the optimum solar field design power is found as shown in Table 5-2. It can be noticed that as the solar field design power increases as all the mentioned parameters in the table increases till a limit of the power absorbed by the solar field. This limit is found at 55 MW of design power with absorbed power by the receiver of 58,171 kW.

Table 5-2: Optimum solar field design power and related performance parameters for the initial solar field's parameters values

	Solar field design power, MWt		
Performance parameters	54	55	56
Simulated heliostat area, m^2	169,603	169,851	169,851
Simulated heliostat count	2732	2736	2736
Power incident on field, kW	118,722	118,896	118,896
Power absorbed by the receiver, kW	58,110	58,171	58,171
Power absorbed by HTF, kW	53,039	53,100	53,100
Solar field optical efficiency, %	52.1	52	52

5.2.1.1 Tower optical height optimization

Tower height is an important parameter that will affect the layout of the solar field. As the tower increases, the adjacent heliostats from the tower at smallest radius will have

difficulty in directing the sun rays to the receiver and vice versa. In Figure 5-3, the relation between the power absorbed by the receiver versus the tower optical height is shown for the current simulation stage. The optimum tower height is 150 m at which maximum power can be absorbed by the receiver, 63,863 kW. Thus, 150 m is the tower height selected for the solar tower.

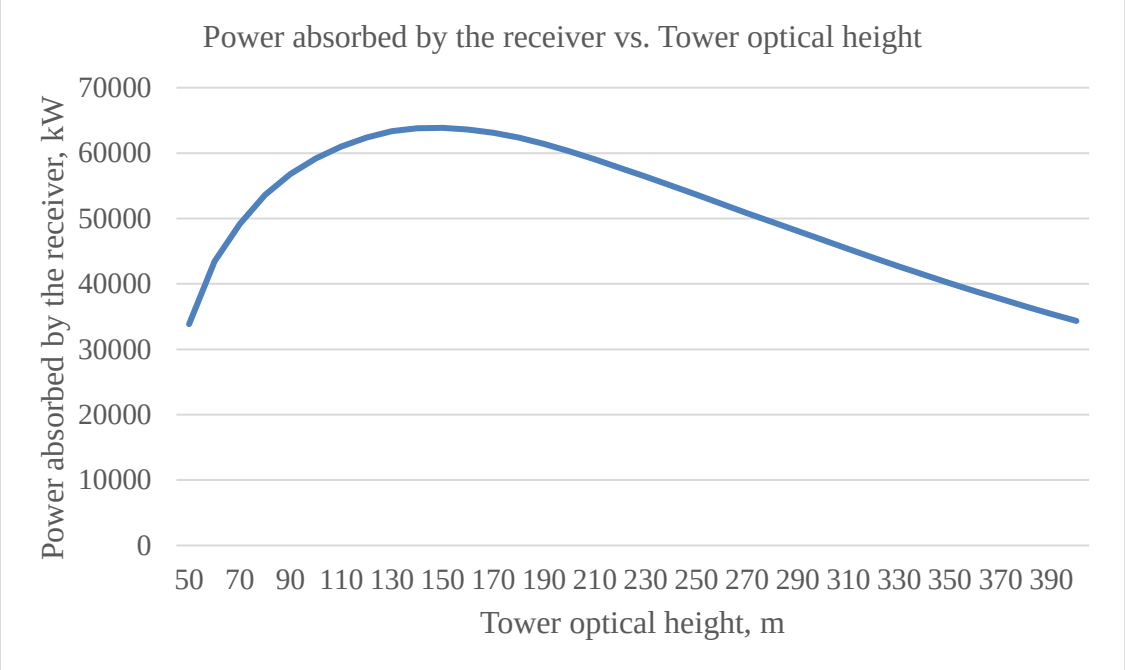

Figure 5-3: Power absorbed by the receiver versus the tower optical height

5.2.1.2 Structure width and height optimization

Another important parameter that will affect the solar field reflective area and the count of heliostats is the heliostat structure width and height. Both can be shown in Figure 4-19. As the width and height increases as the reflective area of the heliostat increases. For a fixed solar field area like the case of this CSP plant, as the area of a single heliostat increases as the total number of heliostats required decreases, power reflected to the receiver decrease, less separate cleaning activates, and less number of mechanism components and control equipment. All of this will reduce the total direct and operational cost of the project. However, both parameters should have an upper limit in size to avoid a substantial loss in the power produced by the solar field and the very low solar field total efficiency. In Table 5-3, different heliostat structure widths and heights versus solar filed performance parameters are shown for the CSP plant.

It is obvious that decreasing the area of the single heliostat increases the number of the solar filed heliostats rapidly. This is accompanied with increase in all the performance parameters mentioned. However, there will be a huge difference in the controlling system and the number of mechanisms required between, for example, 2,736 heliostats in the case of 8 m by 8 m and 4,985 heliostats in the case of 6 m by 6 m. Moreover, the difference in the solar field design power for both cases is only 1 MWt which do not worth all the extra cost and the added complexity of the mechanism. Thus, 8 m by 8 m is selected.

Table 5-3: Different heliostat structure widths and heights versus solar filed performance parameters

	Structure width and height			
Mean simulation results	4m x 4m	6m x 6m	8m x 8m	10m x 10m
Solar Field Design Power, MWt	60	56	55	54
Simulated heliostat area, m^2	185,169	174,076	169,851	169,168
Simulated heliostat count	11931	4985	2736	1744
Power incident on field, kW	129,618	121,853	118,896	118,418
Power absorbed by the receiver, kW	64,681	60,370	58,171	57,453
Power absorbed by HTF, kW	59,610	55,298	53,100	52,382

5.2.1.3 Number of horizontal and vertical panels optimization

The number of horizontal and vertical panels of a heliostat is considered as part of the multiple panels heliostat geometry dimensions as shown in Figure 4-19. Multiple panels of a heliostat are mounted on the heliostat structure at a preferred orientation to maximize optical performance of the heliostat. To get the optimum combination number of both horizontal and vertical panels to produce the maximum power absorbed by the receiver, the relation is shown in Figure 5-4. The relation is found for all the combinations from two panels up to six panels.

The maximum power absorbed is at 2 & 2 combination however this option is not cost effective and will have manufacturing difficulty to get it done. Moreover, large panels are very expensive to replace if crack in the surface occurs. Thus, this combination is not recommended. The all next combinations have the same power value which is next maximum power absorbed point is 58,031 kW. Any combination can be selected and combination 5 & 4 is selected.

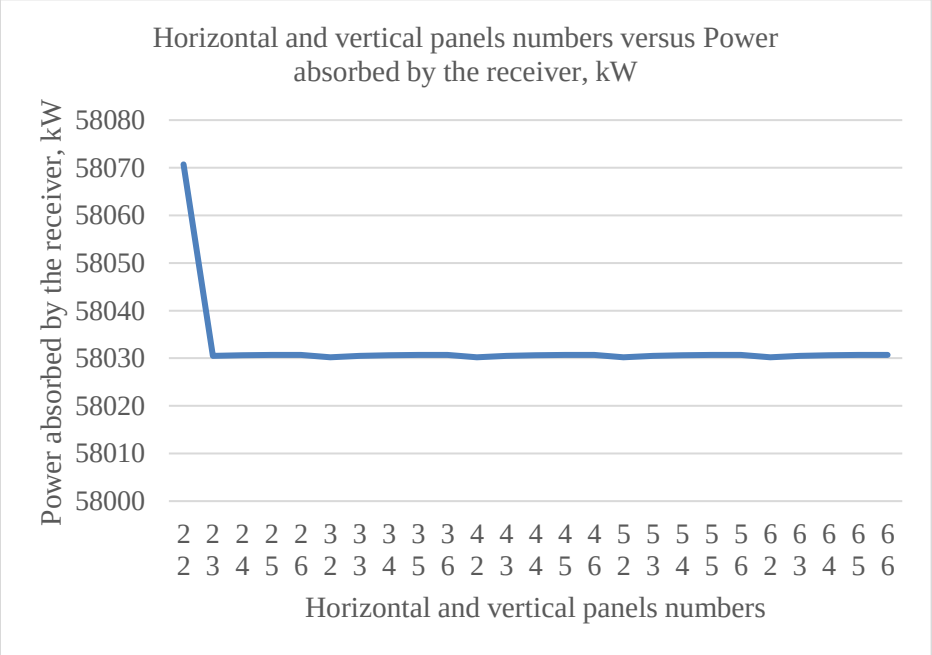

Figure 5-4: Horizontal and vertical panels numbers versus power absorbed by the receiver

5.2.1.4 Receiver height and diameter optimization

In this CSP project the external cylindrical receiver type is selected. It is defined as a cylinder of specified diameter and height. To find the relation between the receiver height and diameter and the power absorbed by the receiver, four different diameters against eight heights for each diameter are studied in Figure 5-5. The diameters are from 2 m to 6 m and the heights are from 1 m to 3 m. As the diameter of the receiver increases, as the power absorbed by the receiver increases and converges to a maximum value. This value is already reached with diameter 6 m. Thus, there is no point of having more than 6 m diameter. Regarding the height of the receiver, as the selected height increases as the power absorbed increases. However, due to a convergence error in solving the equations of the simulation steps, the maximum height that can be selected is 3 m for the above selected range of diameters. Thus, the height of 3 m is the maximum height that can be chosen with diameters of 2 m to 6 m. The cost related to the receiver panels of any CSP tower is considered the most expensive component among the other capital cost items, thus any reduction in the size of the receiver is recommended. The difference in the power absorbed between the receiver of 3 m height and diameter 6 m and diameter 5 m is less than 0.9 kW. Thus, the receiver with diameter of 5 m and height of 3 m is selected.

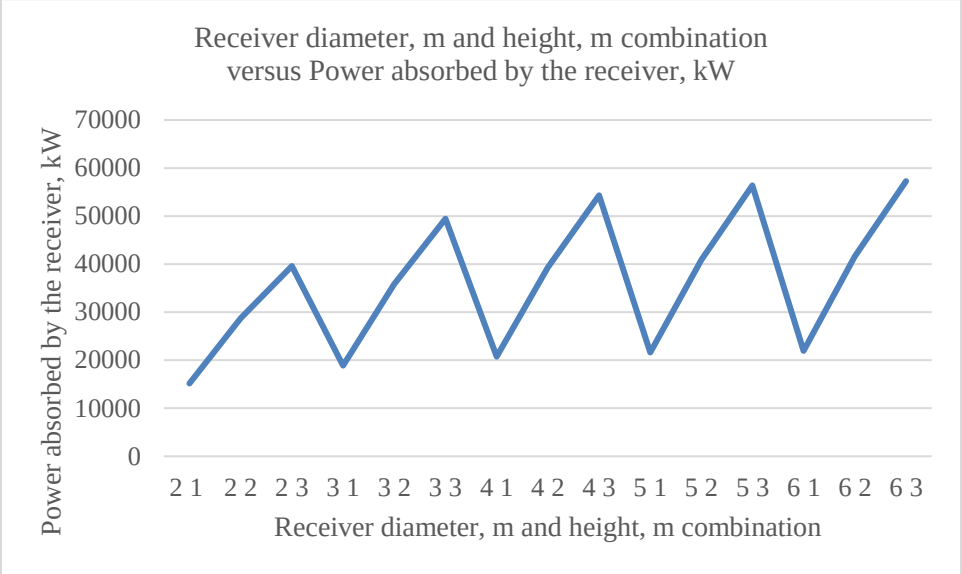

Figure 5-5: Receiver diameter and height combination versus power absorbed by the receiver.

5.2.2 Parameter optimization summary

Following to the same steps done in the manual optimization for the 1st optimized values, the final optimized values are found and tabulated in Table 5-4 along with the initial values and the 1st optimized of the solar field's parameters. The tower optical height converged from 220 m to 140 m which means that optimization steps converges toward the most optimal value. The number of heliostat of the optimized solar field, that is 2736, did not change from the initial value due to the same heliostat structure width and height. The heliostats distribution with optical efficiency for each is shown in Figure 5-6. The nearest three rows of heliostats have less efficiency than the later rows due to the difficulty of controlling the aim point of the heliostat toward the receiver. The last rows

have lesser efficiency due to optical losses from the relatively far distance from the receiver. The final optimized solar field design power is the highest as expected and it is 61 MWt and this means 8 MWe estimated net output power at design. In Table 5-5, the final optimized solar filed performance parameters are shown.

Table 5-4: Optimized values versus the initial values of solar field's parameters

Parameter	**Initial values**	**1st optimized values**	**Final Optimized values**
Tower optical height, m	220	150	140
Heliostat structure width, m	8	8	8
Heliostat structure height, m	8	8	8
Heliostat horizontal panels number	2	5	5
Heliostat vertical panels number	8	4	4
Receiver height, m	3	3	3
Receiver diameter, m	10	5	5
Number of heliostats	2736	2736	2736
Solar field design power, MWt	55	60	61

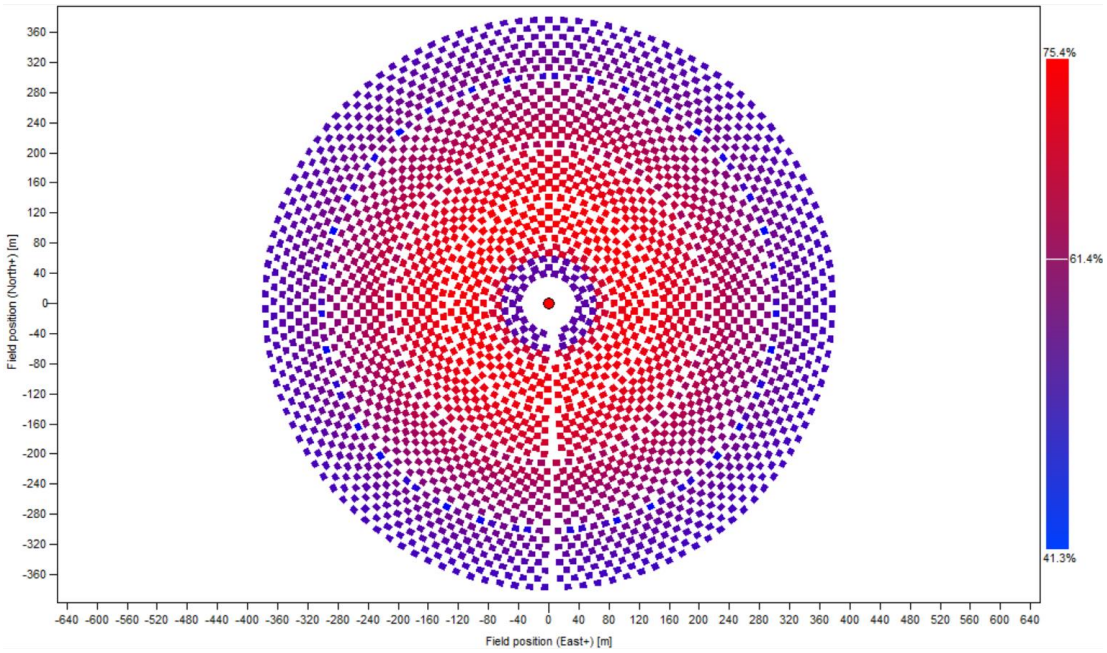

Figure 5-6: SolarPILOT results, the final optimized solar field of the CSP plant

Table 5-5: SolarPILOT results, final optimized solar filed performance parameters

Mean simulation performance parameters	**Value**
Solar Field Design Power, MWt	61
Simulated heliostat area, m	156,255
Power incident on field, kW	109,379
Power absorbed by the receiver, kW	60,976
Power absorbed by HTF, kW	58,134
Solar field optical efficiency, %	59.3
Optical efficiency incl. receiver, %	55.7

5.3 SAM result

The result from SolarPILOT software package regarding the solar field parameters and the weather file prepared for the location are feed into SAM software package for performance and cost simulation of the CSP plant. The system design, heliostat field, tower and receiver parameters are discussed. Moreover, the thermal storage parameters along with water demand required for determining the desalination capacity of the plant are shown. Finally, the annually and monthly expected electrical production with the CO_2 emissions reduction are shown with the breakdown of the total expected cost.

5.3.1 System design

The design parameters of the CSP plant system is shown in Figure 5-7. The receiver thermal power is 61 MWt and the Estimated net output at design is 8 MWe.

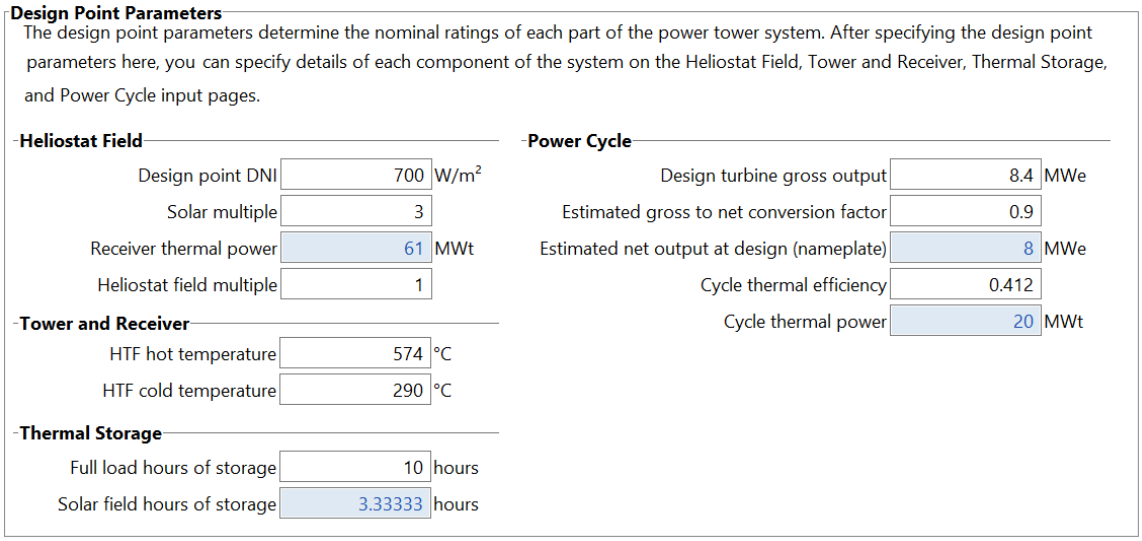

Figure 5-7: SAM results, system design point parameters

SAM generates the general arrangement of the CSP plant in Figure 5-8. This arrangement includes the heliostat field, tower and receiver, power cycle and thermal storage. The solar field of the CSP plant is presented on location, Al-Safliya Island, in Figure 5-9 and Figure 5-10. In the latter Figure, the whole components of the CSP plant are shown in their expected location and at their expected size. These components are the solar tower, hot and cold storage tank of the molten salt, the steam generation building, steam turbine and generator area and the hybrid condensing system area. Moreover, the electrical building and the water treatment area are showed.

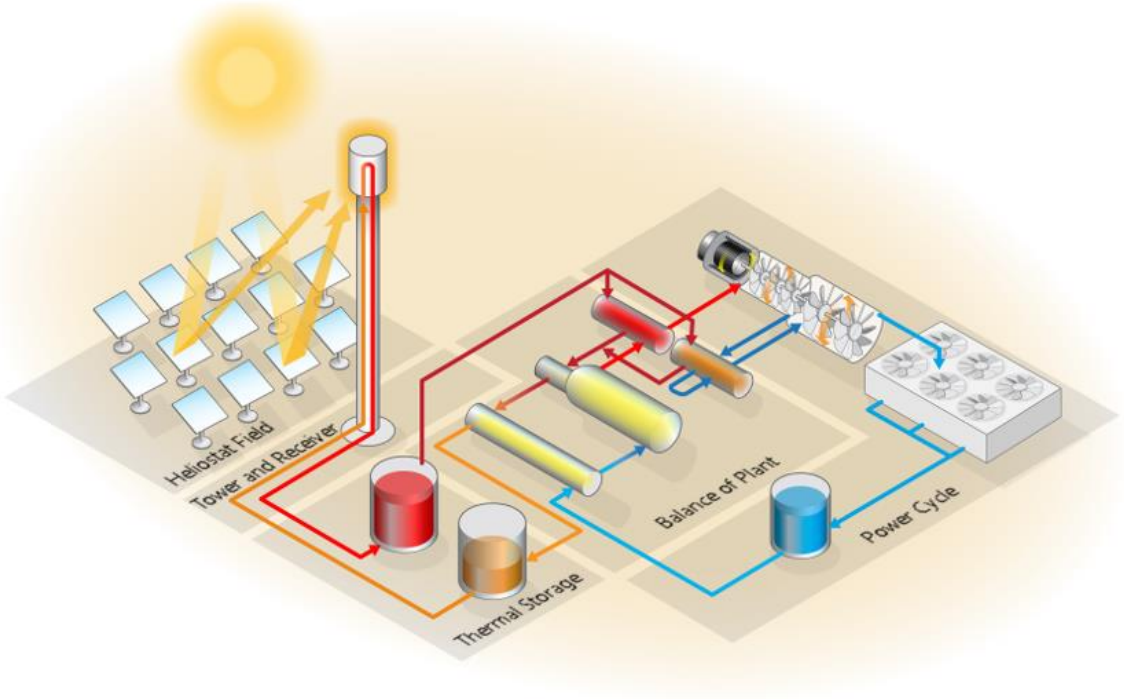

Figure 5-8: CSP plant arrangement resulted from SAM

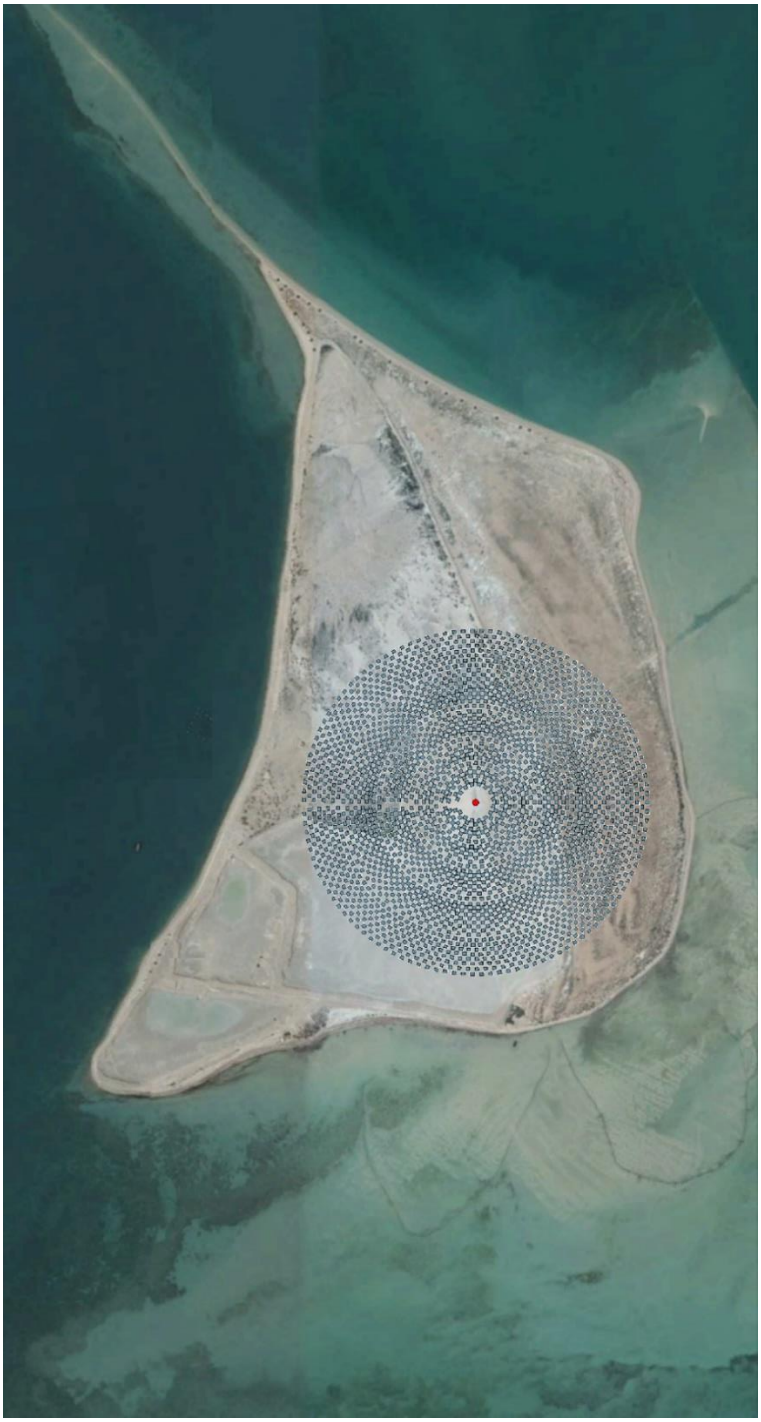

Figure 5-9: Solar field of the CSP plant on Al-Safliya island (picture is originally from Google earth PRO)

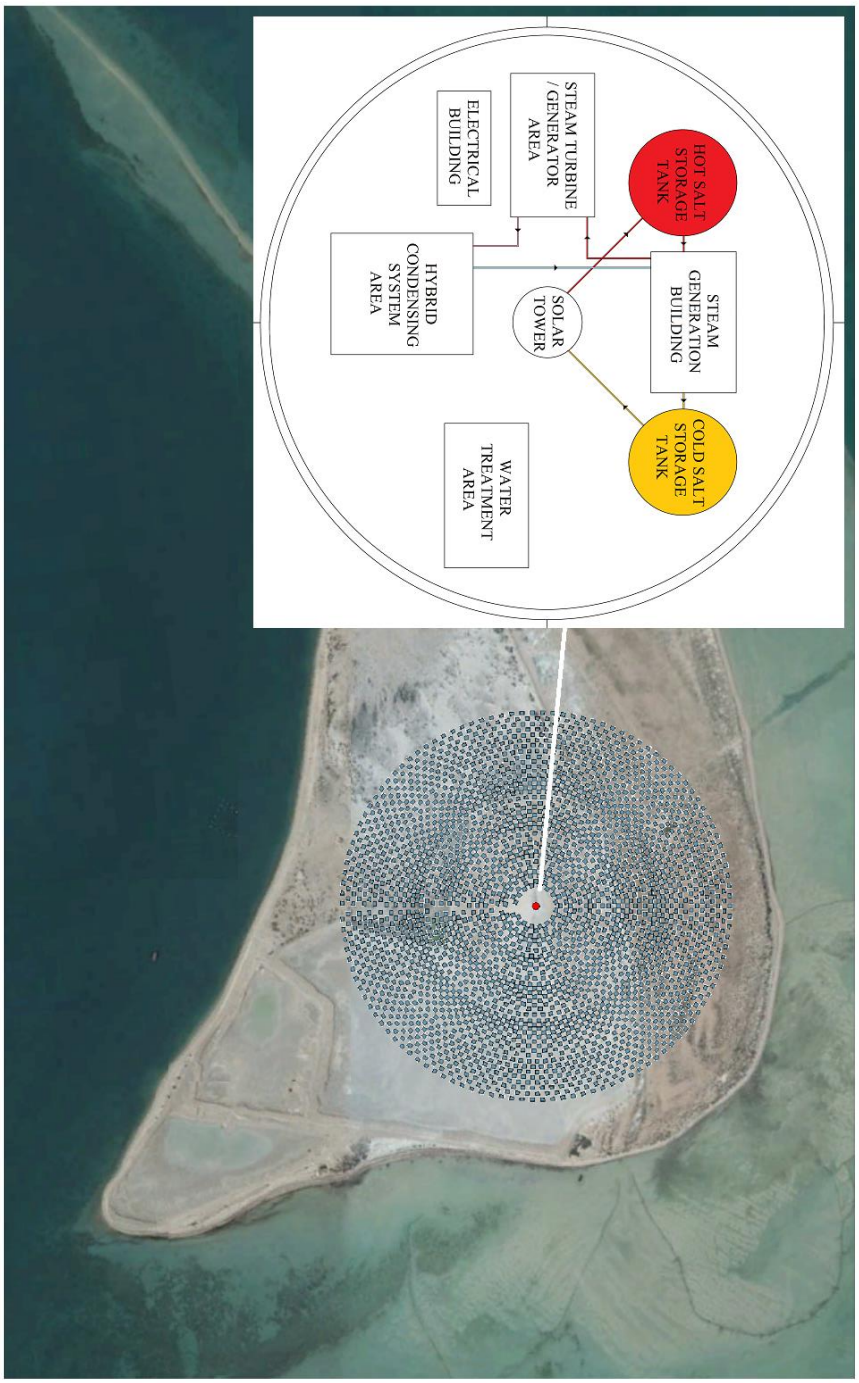

Figure 5-10: All components of the CSP plant on Al-Safliya island (picture is originally from Google earth PRO)

5.3.2 Heliostat field parameters

The positions of the imported heliostats from SolarPILOT to SAM are shown in Figure 5-11. The heliostats' positions map is the same as expected and as shown previously with SolarPILOT. The heliostat properties, operation and washing frequency are shown in Figure 5-12. The heliostat dimensions are the optimized results from SolarPILOT shown in Table 5-4. The heliostat operation parameters are selected as per the recommended values by SAM. Twice a week is the expected washing activities program of the whole solar field heliostats.

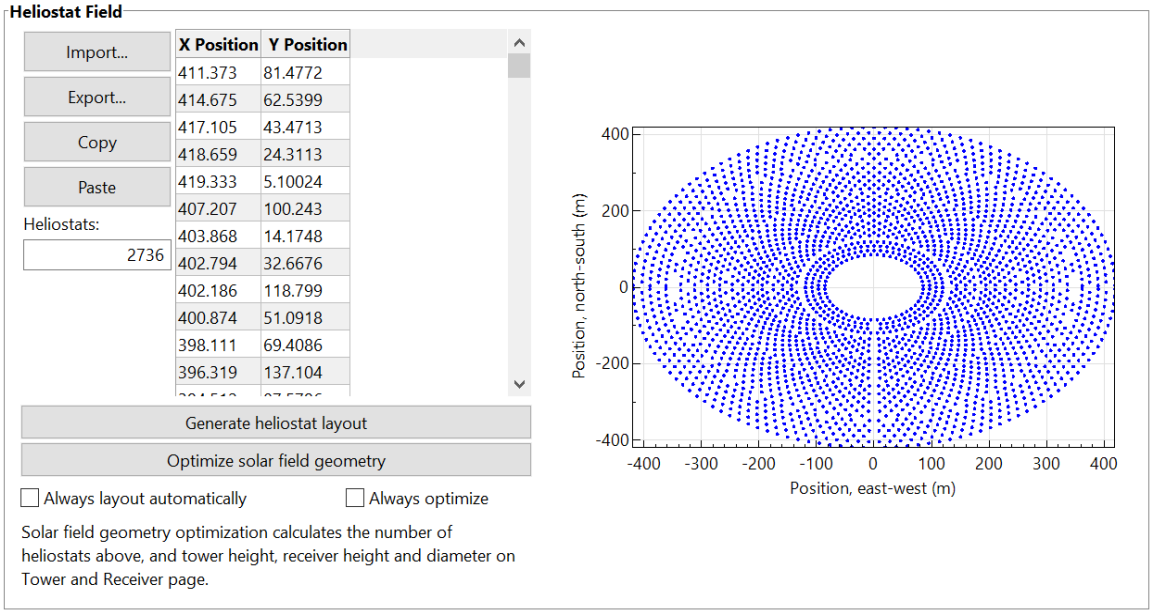

Figure 5-11: SAM results, positions of the imported heliostats from SolarPILOT to SAM

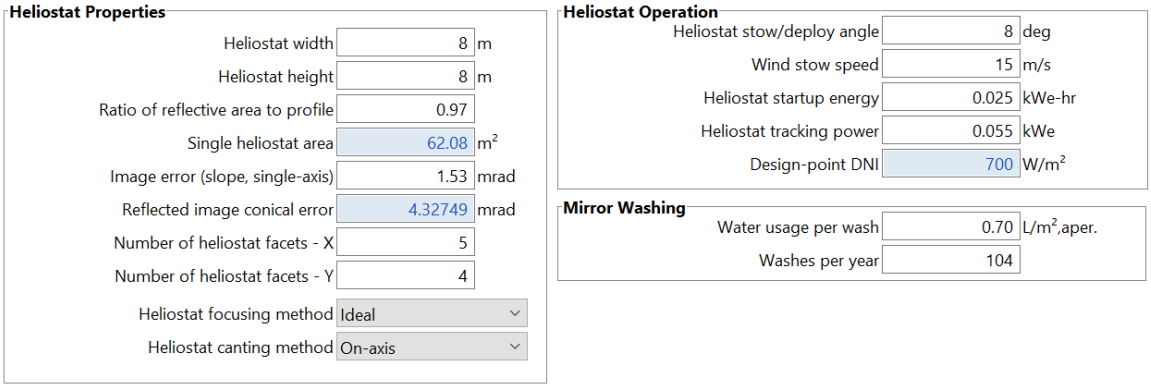

Figure 5-12: SAM results, heliostat properties, operation and washing frequency

5.3.3 Tower and receiver parameters

The solar tower and receiver dimensions, heat transfer proprieties and materials selected are shown in Figure 5-13. The tower and receiver dimensions are the optimized results from SolarPILOT shown in Table 5-4. The tower and receiver design and operation, piping losses and receiver flux modeling parameters are selected as per the recommended values by SAM and are shown in Figure 5-14.

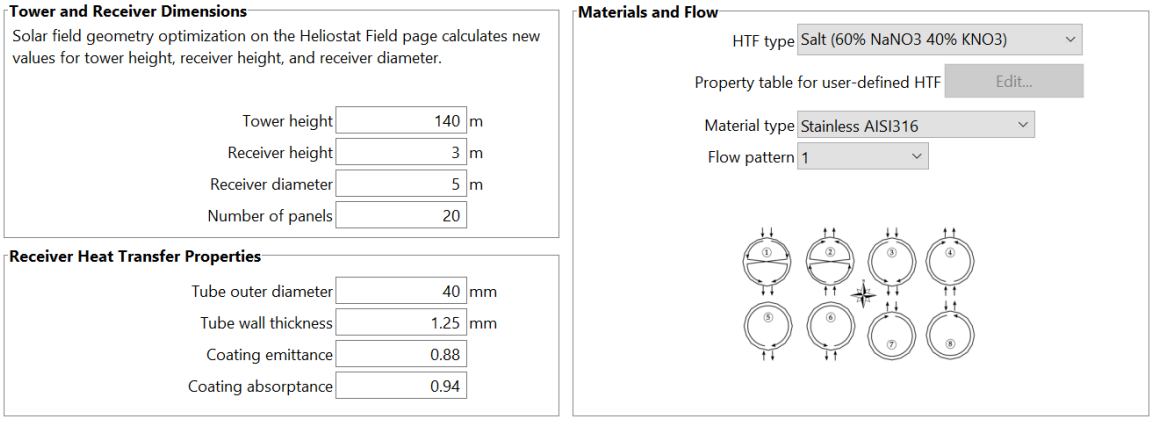

Figure 5-13: SAM results, tower and receiver dimensions, heat transfer proprieties and materials selected.

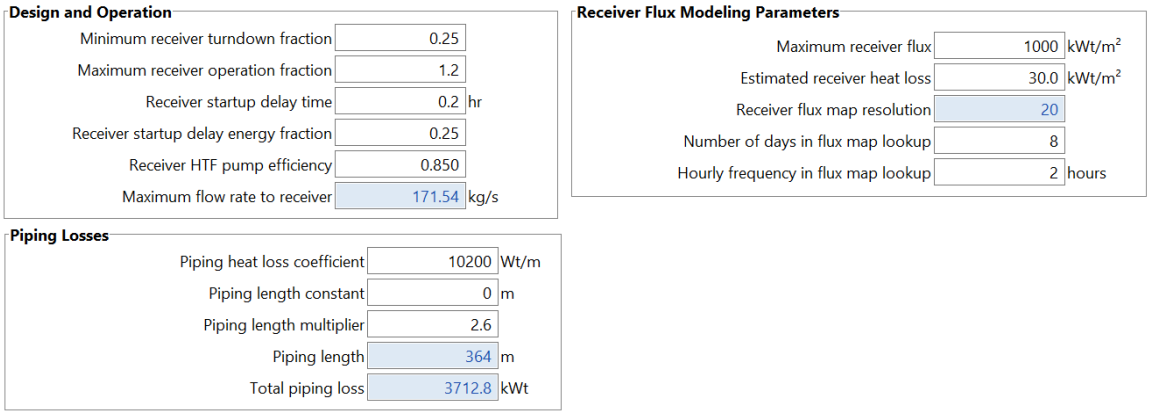

Figure 5-14: SAM results, tower and receiver design and operation, piping losses and receiver flux modeling parameters

5.3.4 Power cycle parameters

Power cycle design parameters and Rankine cycle parameters are shown in Figure 5-15.

The condenser type is selected to be hybrid mode of operation with the usage of the

cooling tower at 75% at all time of operation and the rest is the air-cooled method. However, in the actual operation of the project, the air-cooled condenser will be running all the time and the cooling tower will be in operation during high demand and high temperatures. The other parameters are selected as per the recommended values by SAM.

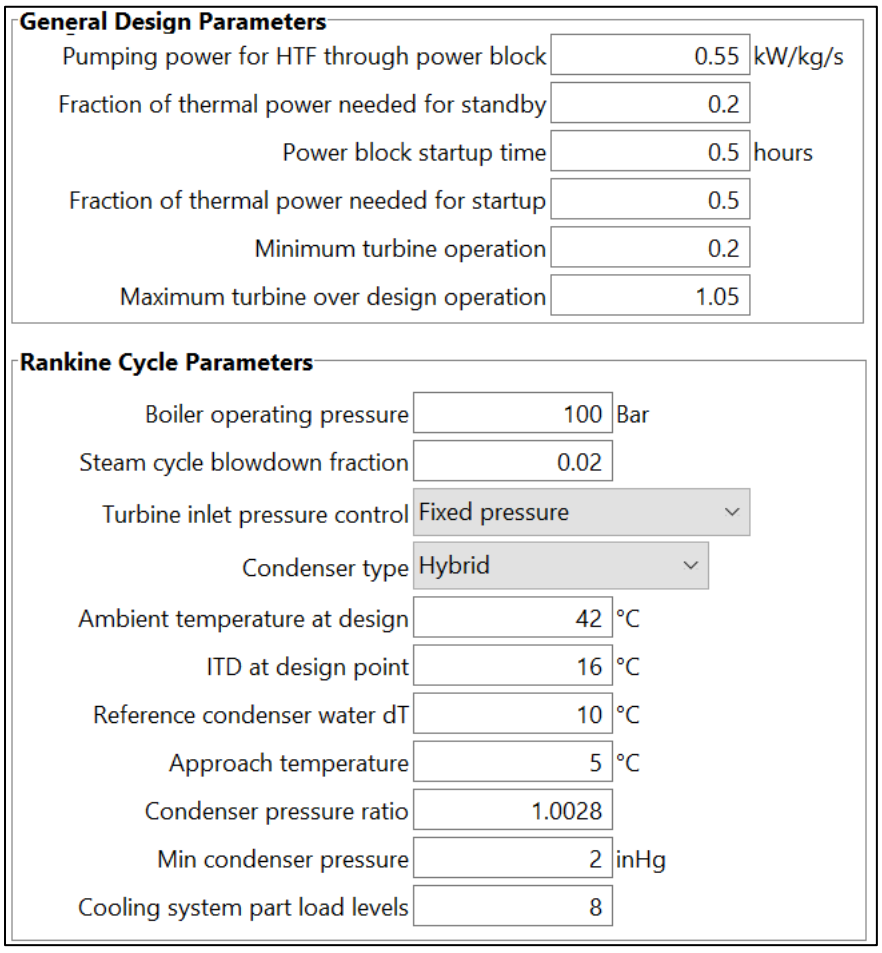

Figure 5-15, SAM results, power cycle design parameters and Rankine cycle parameters

5.3.5 Thermal storage parameters

The parameters of the thermal energy storage system are shown in Figure 5-16. Some of these parameters are the capacity of the system, tank dimensions and the heaters of the tanks along with their efficiencies.

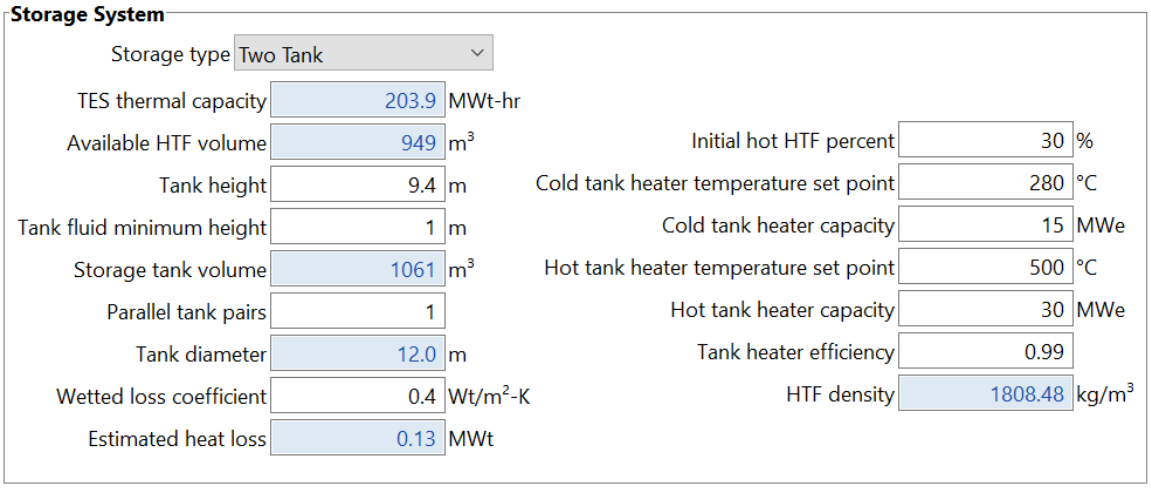

Figure 5-16: SAM results, plant thermal storage system parameters

5.3.6 Water demand and desalination requirements

As discussed before in the section of considerations of water demand for running CSP plant, there are three primary uses for water. Heliostat washing activities, steam cycle make up and hybrid cooling system augmentation. The expected consumption of each on monthly basis is discussed separately in the below sections.

5.3.6.1 Heliostat washing activities

As discussed before, twice a week is the expected washing activities program of the whole solar field heliostats. The total area of heliostats based on the total heliostat count is 169,851 m^2 and the water requirement for each wash is 119 m^3. It is expected that 0.7 liters is required for each 1 m^2 of the heliostat. The monthly water volume required for heliostat washing activates is shown in Table 5-6.

Table 5-6: Monthly water volume required for heliostat washing activates

Month	Number of washes per month	Total water volume required monthly, m^3
January	8	951
February	8	951
March	8	951
April	10	1,189
May	8	951
June	8	951
July	10	1,189
August	8	951
September	8	951
October	10	1,189
November	8	951
December	10	1,189

5.3.6.2 Steam cycle make up and hybrid cooling system augmentation

The water requirement related to the steam cycle makeup and the hybrid cooling is simulated by SAM on hourly basis for the whole year in Kg per hour. The weight of 1 m^3 of water volume is assumed to be 1000 kg. Thus, the monthly rate is found and tabulated in Table 5-7. The water consumption is normally distributed with July as the maximum month.

Table 5-7: Water requirement of steam cycle makeup and hybrid cooling

Month	Water consumption monthly, Kg/hr	Water consumption monthly, m^3
January	5,731,973	5,732
February	5,964,641	5,965
March	7,184,844	7,185
April	7,499,304	7,499
May	7,803,732	7,804
June	7,731,246	7,731
July	8,145,072	8,145
August	7,816,574	7,817
September	7,286,268	7,286
October	6,714,035	6,714
November	5,751,033	5,751
December	5,585,181	5,585
Total	83,213,903	83,214

5.3.6.3 Total water consumption

The monthly total plant water requirement for the steam cycle makeup, hybrid cooling and heliostat washing activates are shown in Table 5-8. It can be seen from Figure 5-17 that the water consumption related to steam and hybrid cooling follows the temperature profile of the location and it is maximum in July. Annually, heliostat washing activates consumes around 15% only in comparison to steam makeup and hybrid cooling consumption.

Table 5-8: Total water requirement of the plant

Month	Heliostat washing activities, m^3	Steam Makeup and hybrid cooling, m^3	Total water consumption, m^3
January	951	5,732	6,683
February	951	5,965	6,916
March	951	7,185	8,136
April	1,189	7,499	8,688
May	951	7,804	8,755
June	951	7,731	8,682
July	1,189	8,145	9,334
August	951	7,817	8,768
September	951	7,286	8,237
October	1,189	6,714	7,903
November	951	5,751	6,702
December	1,189	5,585	6,774
Total	12,365	83,214	95,579

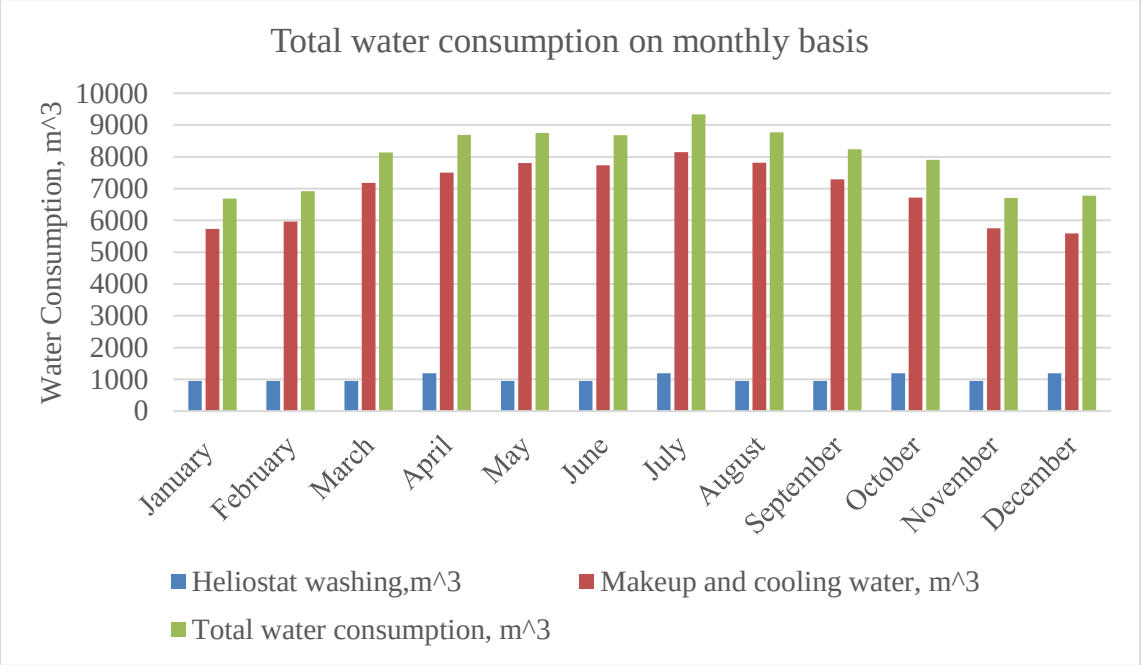

Figure 5-17: Total water consumption on monthly basis

5.3.7 Desalination electrical requirements

In the considerations for desalination process section, it is mentioned that using reverse osmosis for sea water desalination consume 4 kWh per m^3 and the installed cost is approximately $1m for every 1,000 cubic meters per day of installed capacity. Using the total water consumption tabulated in Table 5-8, the monthly electrical consumption of the plant using reverse osmosis is shown in Table 5-9. The maximum daily consumption of water occurs in 21 July and it is approximated to be 386 m^3 daily (267 m^3 for steam makeup and hybrid cooling water and 119 m^3 for heliostat washing). Thus, the capacity of the reverse osmosis system is selected to be 400 m^3 and it will cost around $ 400,000.

Table 5-9:Electrical consumption of the desalination system

Month	Water consumption, m^3	Electrical consumption, kWh
January	6,683	26,733
February	6,916	27,663
March	8,136	32,544
April	8,688	34,753
May	8,755	35,020
June	8,682	34,730
July	9,334	37,336
August	8,768	35,071
September	8,237	32,950
October	7,903	31,612
November	6,702	26,809
December	6,774	27,097
Total	95,579	382,316

5.3.8 Plant monthly energy production

The electricity production and consumption of the plant on monthly basis is shown in Figure 5-18 and Table 5-10. The highest production of the plant is in July, which is 3,621,950 kWh and the highest excess of electrical energy is in March, which is 2,946,965 kWh. This excess of energy is assumed to be enough to provide electricity to Msheireb Downtown Doha zone that is still under construction. A degradation rate of 1% per year is selected. The degradation for January is shown in Figure 5-19. The maximum production loss is at year of 35 which is 1,000,000 kWh for each month. With the highest consumption month of Souq Waqif, an excess of more than 1,500,000 kWh is available.

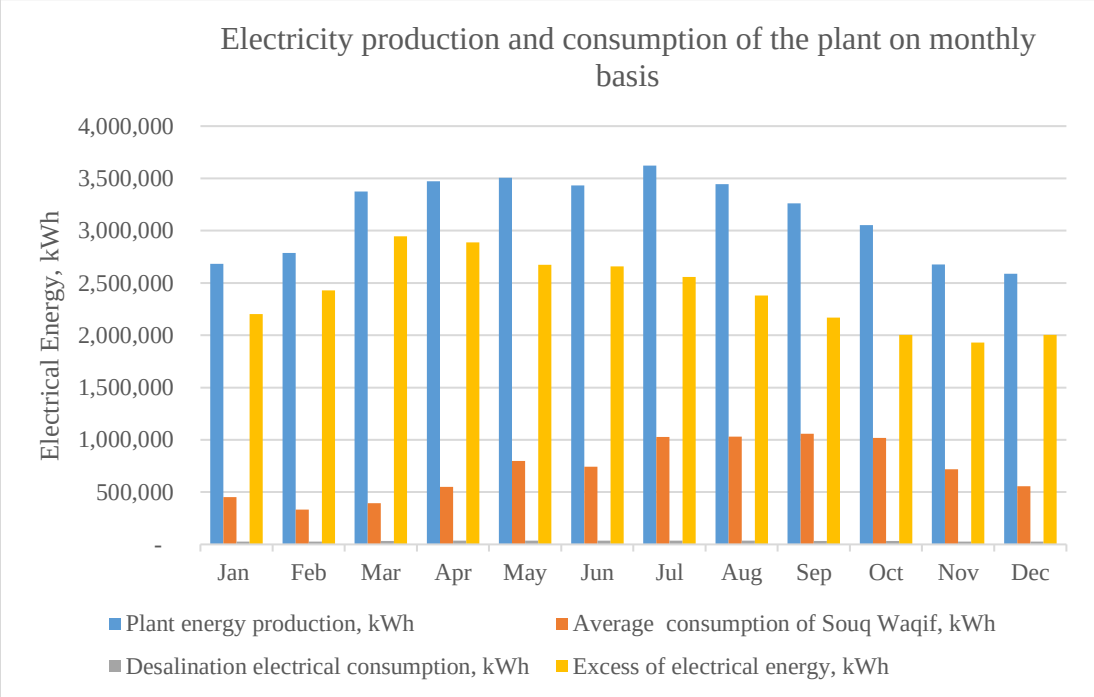

Figure 5-18: Electricity production and consumption of the plant on monthly basis

Table 5-10: Electricity production and consumption of the plant on monthly basis

Month	Plant energy production, kWh	Average consumption of Souq Waqif, kWh	Desalination electrical consumption, kWh	Excess of electrical energy, kWh
Jan	2,682,480	451,812	26,733	2,203,936
Feb	2,788,540	332,845	27,663	2,428,032
Mar	3,373,200	393,691	32,544	2,946,965
Apr	3,473,260	549,950	34,753	2,888,557
May	3,507,390	797,382	35,020	2,674,989
Jun	3,434,140	742,104	34,730	2,657,307
Jul	3,621,950	1,027,110	37,336	2,557,504
Aug	3,444,600	1,029,413	35,071	2,380,117
Sep	3,260,140	1,057,655	32,950	2,169,536
Oct	3,054,640	1,019,404	31,612	2,003,625
Nov	2,676,350	718,213	26,809	1,931,328
Dec	2,588,140	556,952	27,097	2,004,091
Total	**37,904,830**	**8,676,528**	**382,316**	**28,845,986**

5.3.9 CO_2 gas emissions reductions of the CSP plant

As discussed previously, the CO_2 gas emissions of the most efficient combined cycle gas turbine process is estimated by The Parliamentary Office of Science and Technology in London to be 200 gCO_2eq/kWh [83]. Thus, multiplying this number with the energy produced by the designed CSP plant, the reduction in CO_2 gas emissions can be found. In these calculations, the ton of CO_2 is equal 1,000,000 gCO_2. The estimated emissions reduced by utilizing the designed CSP plant in first year instead of combined cycle gas turbine process is found in Table 5-11. The total CO_2 emissions reduced is 7,581 ton CO_2.

Table 5-11: CO_2 gas emissions reductions of the CSP plant

Month	Plant energy production, kWh	CO_2 gas emissions reductions, tonCO_2
Jan	2,682,480	536.50
Feb	2,788,540	557.71
Mar	3,373,200	674.64
Apr	3,473,260	694.65
May	3,507,390	701.48
Jun	3,434,140	686.83
Jul	3,621,950	724.39
Aug	3,444,600	688.92
Sep	3,260,140	652.03
Oct	3,054,640	610.93
Nov	2,676,350	535.27
Dec	2,588,140	517.63
Total	**37,904,830**	**7,581**

5.3.10 System cost analysis

The cost of the system consists of the total system installed cost, the financial parameters selected and the system cash flow diagram.

5.3.10.1 Total system installed costs

As mentioned in the validation section, the total system installed cost consists of direct capital costs, indirect capital costs and operation and maintenance costs. The costs of the different plant components are selected as per the recommended values by SAM.

Regarding the cost of the desalination unit and as per the water consumption calculation, the highest water consumption occurs on 8th of June and it is 384 m^3. The cooling and makeup water consumption at that day is 265 m^3 and it is assumed that heliostats washing is done also on the same day. The maximum water consumption is thus approximated to be 400 m^3 and as per [77], the installed cost of a desalination plant is approximated to be $1m for every 1,000 cubic meters per day of installed capacity. Thus, the desalination unit cost is approximated to be $ 400,000. In SAM, the only section in the cost interface where a fixed cost can be added is in the heliostat field fixed cost. For that reason, the related cost is added there as shown in Figure 5-20.

Based on the available operational experience for CSP plants, the life time of a CSP plant may be more than 30 years [13]. In this thesis, the life time of the CSP plant is selected to be 35 years. The degradation rate of the plant is selected to be 1% each year up to the 35th year. The annual energy production of the plant with degradation is shown in Figure 5-19. The plant annual production in the month of January in the 35th year is 2,471,270 kWh instead of 3,477,960 kWh in the first year.

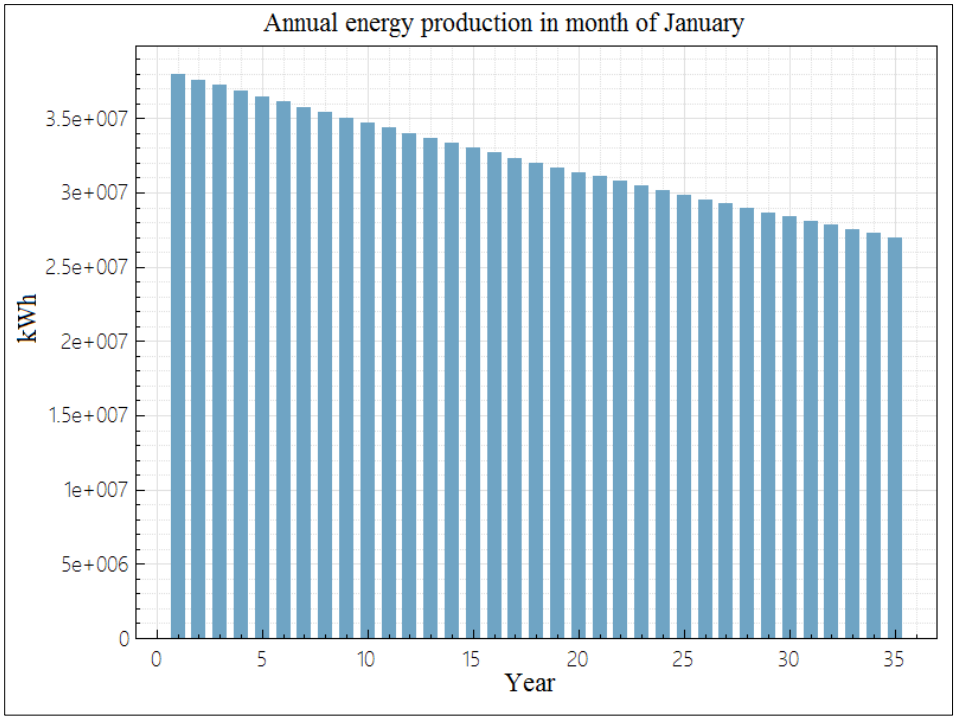

Figure 5-19: SAM results, annual energy production of the plant in month of January with degradation rate of 1% every year

The typical operating and maintenance expenses for a CSP plant include mirror washing, repair, and replacement and major equipment maintenance activities (as per the equipment manufacturer recommendations) that are approximately done every 5 to 7 years. Based on the recent report from U.S. Energy Information Administration published on April 2013 [87], the most of the thermal solar operators treat operating and maintenance on a fixed basis that is $67.26/kW-year. Considering a 3% per year inflation rate from 2013 to 2017, the fixed operating and maintenance expenses in 2017 is expected to be $75.70/kW-year. Moreover, the contingency cost is selected to be 7% of the subtotal cost of the direct capital cost. From Figure 5-20, the total direct capital cost is found to be $ 73,395,696.

Regarding the indirect capital costs, total installed cost and operation and maintenance costs and taxes are not considered in the calculations as Qatar State has no taxes. Moreover, the cost of the plant's dedicated land is assumed to be 10,000 $/acre. As the land is 113 acres, then the total cost is $ 1,132,751. From Figure 5-21**Error! Reference source not found.**, the total indirect cost of the plant is $ 10,674,192. Adding together the direct and the indirect capital costs, the total installed cost of the project is found to be $ 84,069,896. Thus, the estimated total installed cost per net capacity is $ 11,120 /kW. This result falls in high end of the range provided in Table 3-7 in the literature chapter.

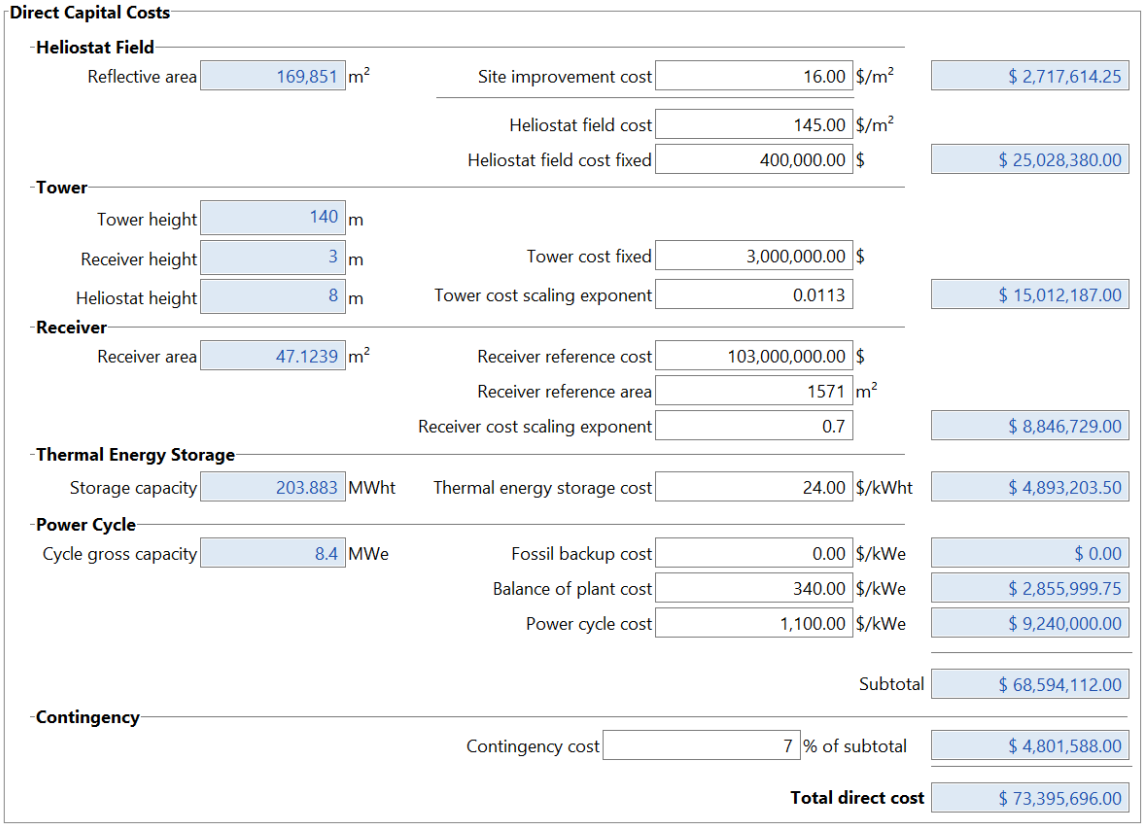

Figure 5-20: SAM results, System Cost - direct capital costs

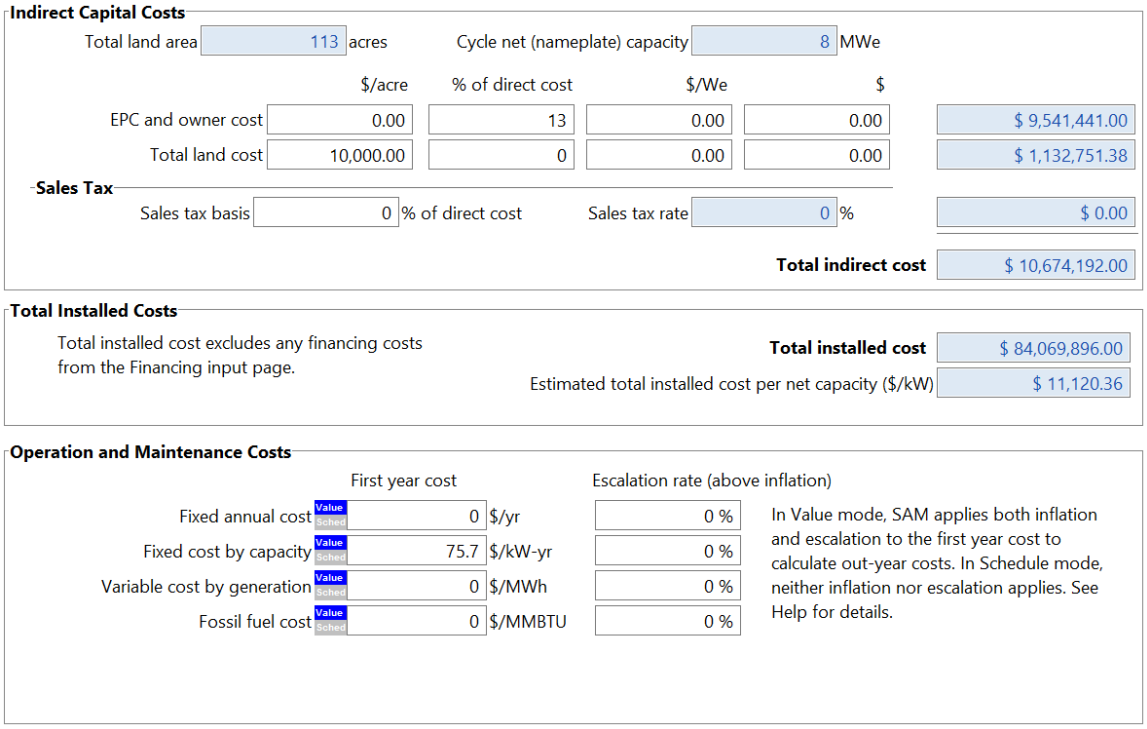

Figure 5-21: SAM results, System Cost – indirect capital costs, total installed costs and operation and maintenance costs

5.3.10.2 Financial parameters

In SAM, the PPA price is the bid price in a power purchase agreement (PPA), and it is defined as the price that the project gains for each unit of electricity that the system generates. The internal rate of return (IRR) of the project is a measure of how much the project is profitable, and it is defined as the rate that leads to a net present value of zero. The latter value is the difference between the plant's energy cost and price. The IRR target year is the year at which the IRR target specified will be achieved with net present

value of zero. In this thesis as shown in Figure 5-22, the IRR target is selected as 11% and the IRR target year is 20 years. At this point of time, the system total cost shall be paid back and the plant will start make profit.

In terms of the analysis parameters shown in Figure 5-22, the analysis period of the project is the same as the expected life time of the project and it is 35 years. The inflation rate is selected to be 3% per year and the real discount rate to be 5.5% per year. As discussed before, taxes in all forms are not considered in this thesis. The annual insurance rate is selected to be 0.5% of the installed cost. Finally, the net salvage value of the plant when decommissioned is selected to be 10% of the installed cost with the end of analysis period value of $ 8,406,990.

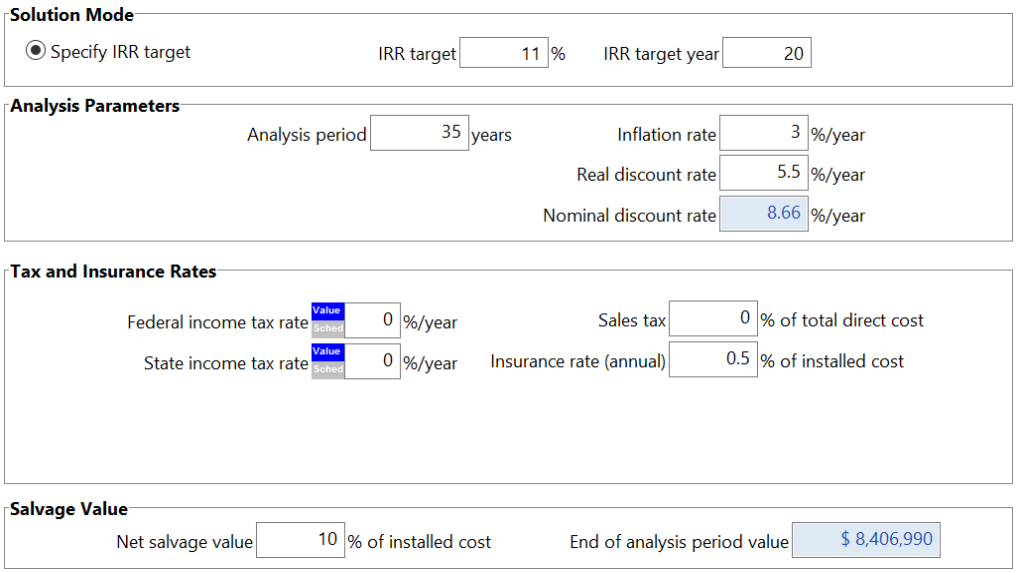

Figure 5-22: SAM results, System cost – financial parameters

5.3.10.3 Summary results and system cash flow diagram

The summary results of the system cost with financial parameters are shown in Table 5-12. The levelized cost signifies the total project lifecycle costs. It is expressed as the present value of project costs in cents per kilowatt-hour of electricity generated by the system over its life.

The capacity factor of the plant is found to be 57.40% in year 1. For the real levelized cost, the real IRR is used and it is found to be 18.65 ¢/kWh. Similarly, for the nominal levelized cost, the nominal IRR is used and it is found to be 25.72 ¢/kWh. As discussed before, the project's net present value is a measure of a project's economic feasibility that contains both revenue and cost. In general, a positive net present value indicates an economically feasible project, while a negative net present value indicates an economically infeasible project. In this thesis, $26,057,166 is the net present value of the project. Thus, the project is economically feasible with receiving profit starting from the 20th year of operation.

In Figure 5-23, the project cash flow is shown with the total installed in year 0 with negative value. Then the both the project revenues and costs are shown through the operational years of the plant. At the final year, the salvage value is added. The details of the project cash flow are shown in Table 5-13 for the project’s revenues and Table 5-14 for the project’s operating expenses for the project life time.

Table 5-12: SAM result, summary cost data

Metric	Value
Annual energy (year 1)	37,992,020 kWh
Capacity factor (year 1)	57.40%
Annual Water Usage	95,579 m^3
PPA price (year 1)	15.76 ¢/kWh
Levelized COE (nominal)	25.72 ¢/kWh
Levelized COE (real)	18.65 ¢/kWh
Net present value	$26,057,166
Internal rate of return (IRR)	11.00%
Year IRR is achieved	20
IRR at end of project	12.10%
Net capital cost	$84,069,896

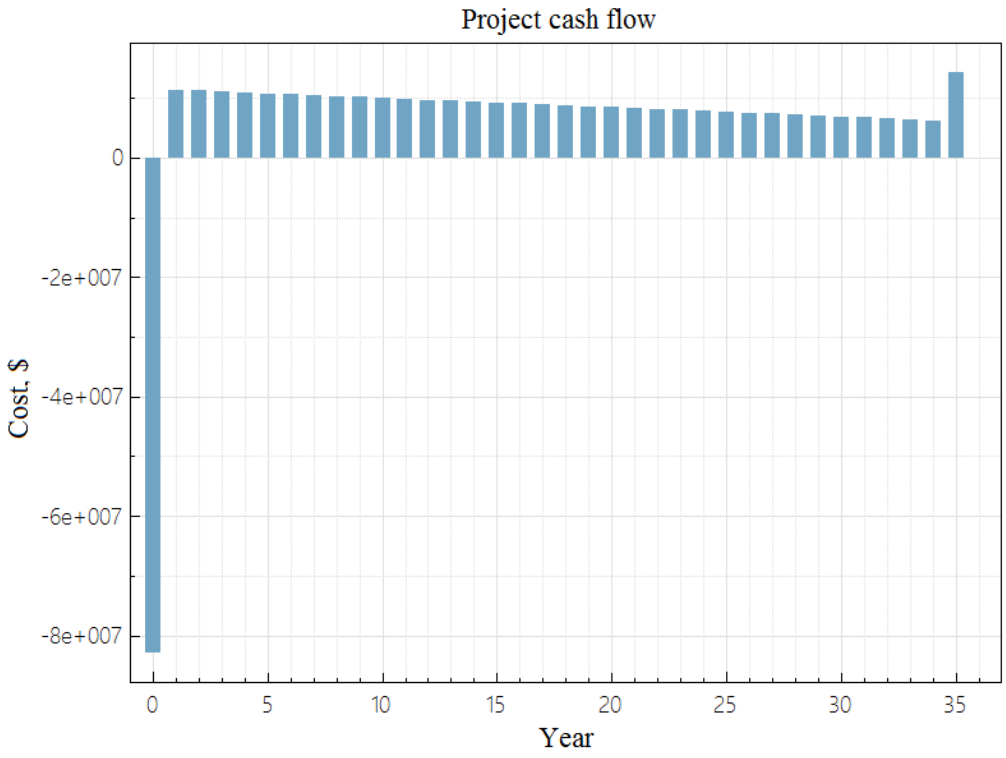

Figure 5-23: SAM result, project cash flow

Table 5-13: SAM results, cash flow table for revenues for the project life time

Year	Production energy (kWh)	PPA price (cents/kWh)	PPA revenue ($)	Salvage value ($)	Total revenue ($)
0	0	0	0	0	0
1	37,992,020	15.75	12,354,626	0	12,354,626
2	37,612,100	15.75	12,231,079	0	12,231,079
3	37,235,976	15.75	12,108,768	0	12,108,768
4	36,863,620	15.75	11,987,681	0	11,987,681
5	36,494,980	15.75	11,867,804	0	11,867,804
6	36,130,032	15.75	11,749,126	0	11,749,126
7	35,768,732	15.75	11,631,635	0	11,631,635
8	35,411,044	15.75	11,515,318	0	11,515,318
9	35,056,936	15.75	11,400,165	0	11,400,165
10	34,706,364	15.75	11,286,164	0	11,286,164
11	34,359,300	15.75	11,173,302	0	11,173,302
12	34,015,708	15.75	11,061,569	0	11,061,569
13	33,675,552	15.75	10,950,953	0	10,950,953
14	33,338,796	15.75	10,841,444	0	10,841,444
15	33,005,408	15.75	10,733,029	0	10,733,029
16	32,675,354	15.75	10,625,699	0	10,625,699
17	32,348,600	15.75	10,519,442	0	10,519,442
18	32,025,114	15.75	10,414,248	0	10,414,248
19	31,704,862	15.75	10,310,105	0	10,310,105
20	31,387,814	15.75	10,207,004	0	10,207,004
21	31,073,936	15.75	10,104,934	0	10,104,934
22	30,763,196	15.75	10,003,885	0	10,003,885
23	30,455,564	15.75	9,903,846	0	9,903,846
24	30,151,010	15.75	9,804,807	0	9,804,807
25	29,849,498	15.75	9,706,759	0	9,706,759
26	29,551,004	15.75	9,609,692	0	9,609,692
27	29,255,494	15.75	9,513,595	0	9,513,595
28	28,962,938	15.75	9,418,459	0	9,418,459
29	28,673,310	15.75	9,324,274	0	9,324,274
30	28,386,576	15.75	9,231,031	0	9,231,031
31	28,102,710	15.75	9,138,721	0	9,138,721
32	27,821,684	15.75	9,047,334	0	9,047,334
33	27,543,466	15.75	8,956,861	0	8,956,861
34	27,268,032	15.75	8,867,292	0	8,867,292
35	26,995,352	15.75	8,778,619	8,406,990	17,185,609

Table 5-14: SAM results, cash flow table for operating expenses for the project life time

Year	O&M capacity-based expense ($)	Insurance expense ($)	Total operating expenses ($)	Earnings ($)	Total installed cost ($)
0	0	0	0	0	-84069896
1	572,292	414,686	9,869,78	11,367,648	0
2	589,461	427,126	1,016,587	11,214,492	0
3	607,145	439,940	1,047,085	11,061,684	0
4	625,359	453,138	1,078,497	10,909,184	0
5	644,120	466,732	1,110,852	10,756,952	0
6	663,443	480,734	1,144,178	10,604,948	0
7	683,347	495,156	1,178,503	1,0453,132	0
8	703,847	510,011	1,213,858	1,0301,460	0
9	724,962	525,311	1,250,274	1,0149,891	0
10	746,711	541,071	1,287,782	9,998,382	0
11	769,113	557,303	1,326,416	9,846,886	0
12	792,186	574,022	1,366,208	9,695,361	0
13	815,951	591,243	1,407,194	9,543,759	0
14	840,430	608,980	1,449,410	9,392,034	0
15	865,643	627,249	1,492,892	9,240,137	0
16	891,612	646,067	1,537,679	9,088,020	0
17	918,361	665,449	1,583,809	8,935,633	0
18	945,911	685,412	1,631,324	8,782,924	0
19	974,289	705,975	1,680,263	8,629,842	0
20	1,003,517	727,154	1,730,671	8,476,333	0
21	1,033,623	748,969	1,782,592	8,322,343	0
22	1,064,632	771,438	1,836,069	8,167,816	0
23	1,096,571	794,581	1,891,151	8,012,695	0
24	1,129,468	818,418	1,947,886	7,856,922	0
25	1,163,352	842,971	2,006,322	7,700,437	0
26	1,198,252	868,260	2,066,512	7,543,180	0
27	1,234,200	894,308	2,128,508	7,385,088	0
28	1,271,226	921,137	2,192,363	7,226,096	0
29	1,309,363	948,771	2,258,134	7,066,141	0
30	1,348,644	977,234	2,325,878	6,905,154	0
31	1,389,103	1,006,551	2,395,654	6,743,068	0
32	1,430,776	1,036,748	2,467,524	6,579,811	0
33	1,473,699	1,067,850	2,541,549	6,415,312	0
34	1,517,910	1099,886	2,617,796	6,249,497	0
35	1,563,447	1,132,882	2,696,330	14,376,004	0

6 CONCLUSIONS AND FUTURE RECOMMENDATIONS

In this chapter, the thesis conclusion and the future recommendations related to the designed CSP plant are discussed.

6.1 Conclusion

In this thesis, CSP power tower plant with 8 MWe capacity was designed to power Al-Jasra and Msheireb down town Doha city zones. The location of the CSP plant, Al-Safliya island, offered a site that is less than 10 km in distance from the targeted zones and very near from Hamad International Airport where the plant can be easily seen during the departures and arrivals flights. The plant has a thermal energy storage for 10 hours with hybrid steam condensing system. The solar filed of the plant was designed to be 0.45 km^2 in area with 2736 heliostats. The solar tower height was 140 m with receiver's height of 3 m and diameter of 5 m. A heliostat washing program was considered with twice a week frequency of washing. The water that is required for the plant operation, heliostat washing activities, steam cycle make up and hybrid cooling system augmentation, is estimated to be 95,579 m^3 per year. A desalination unit was designed to provide this required volume of sea water based on the highest water demand on daily basis. This desalination unit extracts the water from the sea and it desalinates it using a reverse osmosis water treatment system. The maximum monthly water consumption was in July and it was 9,334 m^3.

The total electrical production of the plant was found to be 37,904,830 kWh with excess of electrical energy of 28,845,986 kWh, after subtracting the consumption of Souq Waqif. This excess of energy is assumed to be enough for Msheireb Downtown Doha zone. The maximum monthly electrical production was in July and it was 3,621,950 kWh. The capacity factor of the plant is found to be 57.40% in year 1. The life time of the CSP plant was selected to be 35 years and a degradation rate of 1% per year was selected. The maximum production loss was at year of 35 which is 1,000,000 kWh for each month. With the highest consumption month of Souq Waqif, an excess of more than 1,500,000 kWh was still available for Msheireb Downtown Doha zone.

The total system installed cost was found to be $ 84,069,896. It was broken down as total direct capital cost of $ 73,395,696 and total indirect cost of $ 10,674,192. The estimated total installed cost per net capacity was found to be $ 11,120 /kW. The fixed operating and maintenance expenses in 2017 was expected to be $75.70/kW-year with inflation rate of 3% per year. The IRR target was selected to be 11% and the IRR target year was 20 years. The real discount rate was found to be 5.5% per year. The annual insurance rate was selected to be 0.5% of the installed cost with the end of analysis period value of $ 8,293,715. The net present value of the project was found to be $26,057,166. Moreover, the net salvage value of the plant when decommissioned was selected to be 10% of the installed cost with the end of analysis period value of $ 8,406,990.

6.2 Future recommendation

1- One of the main future recommendations is to build an immediate solar and weather station in Qatar at many locations that measures the actual three components of the available solar irradiance on both horizontal and dual axes tracking surface to simulate the actual irradiance received by the heliostat. Moreover, the station should measure all the climatic factors that will influence the energy output of the plant. Such influences that need to be recorded are the fog, dust, dirt, cloud cover and humidity duration and severity. This is a vitally important step to build a real solar and climate data base for more precise and accurate design of any solar plant in Qatar, either CSP or photovoltaic.

2- Currently, the published information related to the cost of the CSP plant components are very little and not enough to build a firm conclusion. A study should be held to determine the cost of each component separately by communicating with the vendors of these components.

3- The electrical consumption of Al-Jasra and Msheireb down town Doha city zones is to be studied in more details.

4- The ebb and flow phases of Al-Safliya Island should be studied to specify the maximum permissible land area for the plant.

5- The site preparation required for Al-Safliya Island should be studied. This include the site clearing activities, site surveying activities, soil testing and site plan design.

REFERENCES

[1] "BP Statistical Review of World Energy," British Petroleum, London SW1Y 4PD, June 2016.

[2] "Renewable Energy Market Analysis: The GCC Region," The International Renewable Energy Agency (IRENA), Abu Dhabi, 2016.

[3] "Renewable Energy Statistics," The International Renewable Energy Agency (IRENA), Abu Dhabi, 2016.

[4] "Key world energy statistics," International Energy Agency (IEA), Paris, 2016.

[5] "An oasis of green technologies (Qatar)," 28 Jan 2014. [Online]. Available: http://saharaforestproject.com/qatar/. [Accessed 9 12 2016].

[6] "QNV2030," 2016. [Online]. Available: http://www.mdps.gov.qa/en/qnv/Documents/QNV2030_English_v2.pdf. [Accessed 11 Oct 2016].

[7] T. Finn, "Qatar plans to build around 1,000 megawatts of solar power," 22 Feb 2016. [Online]. Available: http://energy.economictimes.indiatimes.com/news/renewable/qatar-plans-to-build-around-1000-megawatts-of-solar-power/51085083. [Accessed 15 Oct 2016].

[8] "Concentrating Solar Power - Technology Brief," International Energy Agency

(IEA), Energy Technology Systems Analysis Programme (ETSAP) and International Renewable Energy Agency (IRENA), 2013.

[9] R. Pitz-Paal, Solar Energy - Concentrating Solar Power, Cologne: Elsevier Ltd., 2014.

[10] "Concentrating Solar Power," 2016. [Online]. Available: http://www.sbcenergyinstitute.com/Publications/SolarPower.html. [Accessed 29 Jan 2017].

[11] "Concentrating solar power: its potential contribution to a sustainable energy future," The European Academies Science Advisory Council (EASAC), Halle - Germany, 2011.

[12] B. Hoffschmidt, S. Alexopoulos, C. Rau, J. Sattler, A. Anthrakidis, C. Boura, B. O'Connor and P. Hilger, Concentrating Solar Power, Jülich: Elsevier Ltd., 2012.

[13] E. Pihl, "Concentrating Solar Power," The Energy Committee of the Royal Swedish Academy of Sciences, Stockholm, 2009.

[14] B. Norton, "SOLAR ENERGY," 8 Feb 2011. [Online]. Available: http://www.thermopedia.com/content/1136/). [Accessed 16 Mar 2016].

[15] S. Kalogirou, Solar Thermal Systems: Components and Applications – Introduction, Limassol, Cyprus: Elsevier Ltd., 2012.

[16] Á. Marín, "Volumetric receivers in Solar Thermal Power Plants with Central Receiver System technology," *Solar Energy*, pp. 891-910, 2011.

[17] M. Romero, R. Buck and J. Pacheco, "An Update on Solar Central Receiver, Projects, and Technologies,," *Solar Energy Engineering*, pp. 98-108, 2002.

[18] SolarPACES, "Technology Characterization Solar Power Tower," 2016. [Online]. Available: http://www.solarpaces.org/csp-technology/csp-technology-general-information. [Accessed 30 Apr 2016].

[19] Ctein, "Ctein's Online Gallery," 2016. [Online]. Available: www.ctein.com. [Accessed 30 Apr 2016].

[20] "SOLGATE Solar hybrid gas turbine electric - final publishable report," Publication office of European Commission (EC), 2002.

[21] "Final Report - SOLHYCO (Solar-Hybrid Power and Cogeneration Plants)," 03 Nov 2011. [Online]. Available: http://cordis.europa.eu/publication/rcn/13318_en.html. [Accessed 30 Apr 2016].

[22] J. Jedamski, L. Amsbeck, R. Buck, R. Couturier, P. Heller, P. Tochon, R. Uhlig and F. Vasquez, "Development of a Profiled Multilayer Tube for High Temperature Solar Receivers and Heat Exchangers," in *2010 14th International Heat Transfer Conference*, Washington, DC, 2010.

[23] "SOLUGAS homepage," 2015. [Online]. Available: http://www.cspworld.org/cspworldmap/solugas. [Accessed Apr 30 2016].

[24] L. Aichmayer, "Solar Receiver Design and Verification for," KTH School of Industrial Engineering and Management, Stockholm, 2011.

[25] J. Karni, A. Kribus, P. Doron, R. Rubin, A. Fiterman and D. Sagie, "A High-Pressure, High-Temperature Solar Receiver, Journal of Solar Energy," *Solar Energy*, pp. 74-78, 1997.

[26] F. Incropera, D. DeWitt , T. Bergmann and A. Lavine, Fundamentals of heat and mass transfer, Hoboken, USA: Wiley and Sons Inc., 2007.

[27] B. Hoffschmidt, "Receivers for Solar Tower System," 25 Jun 2014. [Online]. Available: http://elib.dlr.de/94540/1/SFERA2014_SolarTowerReceivers_final.pdf. [Accessed 30 Apr 2016].

[28] A. Kribus, P. Doron, R. Rubin, R. Reuven, E. Taragan, S. Duchan and J. Karni, "Performance of the Directly-Irradiated Annular Pressurized Receiver (DIAPR)," *Solar Energy Engineering*, pp. 10-17, 2001.

[29] E. Augsten, "Make the desert bloom," *Sun and Wind Energy*, pp. 2052-2055, 2009.

[30] R. Buck, T. Bräuning , T. Denk , M. Pfänder , P. Schwarzbözl and F. Téllez,

"Solar-Hybrid Gas Turbine-based Power Tower Systems (REFOS)," *Solar Energy Engineering,* pp. 2-9, 2002.

[31] G. Xiaohong , S. Xiange , Z. Miao and T. Dawei , "Influence of void ratio on thermal stress of PCM canister for heat pipe receiver," *Applied Thermal Engineering,* pp. 615-621, 2016.

[32] Z. Bearbeitete, 2006. [Online]. Available: http://www.vdi.eu/index.php?tx_mnogosearch_pi1%5Bq%5D=heat+pipe+receiver. [Accessed 16 Nov 2016].

[33] W. Bienert, "The heat pipe and its application to solar receivers, Electric Power," *Electric Power,* pp. 111-123, 1980.

[34] K. Kima, N. Siegelb, G. Kolbb, V. Rangaswamyc and S. Moujaes, "A study of solid particle flow characterization in solar particle receiver," *Solar Energy,* pp. 1784-1793, 2009.

[35] G. Evans , W. Houf , R. Greif and C. Crowe , "Gas-Particle Flow Within a High Temperature Solar Cavity Receiver Including Radiation Heat Transfer," *Solar Energy Engineering,* pp. 134-142, 1987.

[36] J. Pacio and T. Wetzel, "Assessment of liquid metal technology status and research paths for their use as efficient heat transfer fluids in solar central receiver systems," *Solar Energy,* pp. 11-22, 2013.

[37] b. X. X. a. A. A. c. K. H. a. A. K. K. Vignarooban a, "Heat transfer fluids for concentrating solar power systems – A review," *Applied Energy*, pp. 383-396, 2015.

[38] Y. Tian and C. Zhao , "A review of solar collectors and thermal energy storage in solar thermal applications," *Appl Energy*, pp. 538-553, 2013.

[39] M. Liu, M. Belusko, N. Tay and F. Bruno, "Impact of the heat transfer fluid in a flat plate phase change thermal storage unit for concentrated solar tower plants.," *Solar Energy*, pp. 220-231, 2014.

[40] A. Modi and F. Haglind, "Performance analysis of a Kalina cycle for a central receiver solar thermal power plant with direct steam generation.," *Applied Thermal Energy*, pp. 201-208, 2014.

[41] L. Pistocchini and M. Motta, "Feasibility study of an innovative dry-cooling system with phase-change material storage for concentrated solar power multi-MW size power plant. z," *Solar Energy Engineering*, 2011.

[42] A. Gil , M. Medrano, I. Martorell, A. Lazaro, P. Dolado and B. Zalba, "State of the art on high temperature thermal energy storage for power generation.," *Renewable and Sustainable Energy Reviews*, pp. 31-55, 2010.

[43] Q. Peng, X. Wei, J. Ding, J. Yang and X. Yang, "High-temperature thermal stability of molten salt materials," *International Journal of Energy Research*, pp. 1164-1174, 2008.

[44] R. I. Dunn, P. J. Hearps and M. N. Wright, "Molten-Salt Power Towers: Newly Commercial Concentrating Solar Storage," *IEEE,* pp. 504-515, 2011.

[45] Q. Peng, J. Ding, X. Wei, J. Yang and X. Yang, "The preparation and properties of multi-component molten salts," *Applied Energy,* pp. 2812-2817, 2010.

[46] M. Liu, T. S. N.H., S. Bell, M. Belusko, R. Jacob, G. Will, W. Saman and F. Bruno, "Review on concentrating solar power plants and new developments in high temperature thermal energy storage technologies," *Renewable and Sustainable Energy Reviews,* p. 1411–1432, 2016.

[47] J. Pacheco, "Final Test and Evaluation Results from the Solar Two Project," Sandia National Laboratories, Albuquerque, NM, 2002.

[48] M. Liu, W. Saman and F. Bruno, "Review on storage materials and thermal performance enhancement techniques for high temperature phase change thermal storage systems," *Renewable and Sustainable Energy Reviews,* pp. 2118-2132, 2012.

[49] C. Kutscher, M. Mehos, C. Turchi and G. Glatzmaier, "Line-Focus Solar Power Plant Cost Reduction Plan," National Renewable Energy Laboratory (NREL), Golden, Colorado, 2010.

[50] J. Stekli, . L. Irwin and R. Pitchumani, "Technical Challenges and Opportunities for Concentrating Solar Power With Thermal Energy Storage,"

Journal of Thermal Science and Engineering Applications, p. 5:021011, 2013.

[51] A. Luzzi and K. Lovegrove, "Solar Thermal Power Generation," *Encyclopedia of Energy*, pp. 669-683, 2004.

[52] "Concentrating Solar Power Projects - NREL," 2016. [Online]. Available: http://www.nrel.gov/csp/solarpaces/index.cfm. [Accessed 9 Dec 2016].

[53] "Concentrating solar power: its potential contribution to a sustainable energy future," The European Academies Science Advisory Council (EASAC), Halle - Germany, 2011.

[54] J. E. Hoffmann, "ON THE OPTIMIZATION OF A CENTRAL RECEIVER SYSTEM," Stellenbosch University, Stellenbosch, South Africa, 2016.

[55] "Integrated Layout and Optimization Tool for Solar Power Towers," [Online]. Available: https://www.nrel.gov/csp/solarpilot.html. [Accessed 29 Jan 2017].

[56] "System Advisor Model (SAM)," 5 April 2010. [Online]. Available: https://sam.nrel.gov/. [Accessed 29 Jan 2017].

[57] C. Turchi and G. Heath, "Molten Salt Power Tower Cost Model for the System Advisor Model (SAM)," NREL, Denver, 2013.

[58] P. Kurup and C. Turchi, "Parabolic Trough Collector Cost Update for the System Advisor Model (SAM)," NREL, Denver, 2015.

[59] J. Duffie and W. Beckman, Solar Engineering of Thermal Processes, New

Jersey: John Wiley & Sons, Inc., 2013.

[60] M. Basunia , H. Yoshiob and T. Abec , "Simulation of solar radiation incident on horizontal and inclined surfaces," *Journal of Engineering Research*, pp. 27-35, 2012.

[61] L. El Chaar and L. Lamont, "Global solar radiation: Multiple on-site assessments in Abu Dhabi, UAE," *Renewable Energy*, pp. 1596-1601, 2010.

[62] R. Messenger and J. Ventre, Photovoltaic systems engineering, New York: CRC Press LLC, 2004.

[63] 2016. [Online]. Available: https://scied.ucar.edu/sites/default/files/teaching-box-files/albedo_answer_key.pdf. [Accessed 15 Dec 2016].

[64] S. Kalogirou, Solar Thermal Systems: Components and Applications – Introduction, Limassol,: Elsevier Ltd., 2012.

[65] P. Astudillo and D. Bachour, "DNI, GHI and DHI ground measurements in Doha, Qatar," *Energy Procedia*, pp. 2398-2404, 2013.

[66] D. Perez-Astudillo and D. Bachour, "Variability of measured Global Horizontal Irradiation throughout Qatar," *Solar Energy*, pp. 169-178, 2015.

[67] "Crescent Dunes," SolarReserve, 2017. [Online]. Available: http://www.solarreserve.com/en/global-projects/csp/crescent-dunes. [Accessed 21 Jan 2017].

[68] "Proposed Crescent Dunes Solar Energy Project," [Online]. Available: https://www.blm.gov/style/medialib/blm/nv/field_offices/battle_mountain_field/blm_information/nepa/crescent_dunes_scoping.Par.41942.File.dat/Crescent%20Dunes%20DEIS%20Chapters%201%20and%202_508.pdf. [Accessed 15 Feb 2017].

[69] "CRESCENT DUNES PROJECT," [Online]. Available: https://energy.gov/lpo/crescent-dunes. [Accessed 18 Mar 2017].

[70] "Electricity Data Browser," U.S. Energy Information Admministration (iea) , 8 Mar 2017. [Online]. Available: https://www.eia.gov/electricity/data/browser/#/plant/57275/?pin=ELEC.PLANT.GEN.57275-SUN-ALL.M&linechart=ELEC.PLANT.GEN.57275-SUN-ALL.M. [Accessed 27 Mar 2017].

[71] A. AL-ZILA'I, "Saudi Arabia's first solar power station inaugurated on Farasan Island," 5 Oct 2011. [Online]. Available: https://www.alarabiya.net/articles/2011/10/05/170310.html. [Accessed 28 Jan 2017].

[72] "A solar energy power plant is to be installed on the island of Annobón," Embassy of the Republic of Equatorial Guinea, , [Online]. Available: http://embassyofequatorialguinea.co.uk/a-solar-energy-power-plant-is-to-be-installed-on-the-island-of-annobon/. [Accessed 28 Jan 2017].

[73] J. Golson, "Tesla built a huge solar energy plant on the island of Kauai," The verge, 8 Mar 2017. [Online]. Available: http://www.theverge.com/2017/3/8/14854858/tesla-solar-hawaii-kauai-kiuc-powerpack-battery-generator. [Accessed 31 Mar 2017].

[74] M. Darwish, A. H. Hassabou and B. Shomar, "Using Seawater Reverse Osmosis (SWRO) desalting system for less environmental impacts in Qatar," *Desalination,* pp. 113-124, 2013.

[75] R. Deng, L. Xie, H. Lina, J. Liuc and W. Hana, "Integration of thermal energy and seawater desalination," *Energy,* vol. 35, no. 11, pp. 4368-4374, 2010.

[76] S. Gorjian and B. Ghobadian, "Solar desalination: A sustainable solution to water crisis in Iran," *Renewable and Sustainable Energy Reviews,* vol. 48, pp. 571-584, 2015.

[77] R. McGovern, "How much does a water desalination plant cost?," 13 Feb 2017. [Online]. Available: https://smipp.wordpress.com/2017/02/13/how-much-does-a-water-desalination-plant-cost/. [Accessed 14 Mar 2017].

[78] N. Ghaffour, T. Missimer and G. Amy, "Technical review and evaluation of the economics of water desalination: Current and future challenges for better water supply sustainability," *Desalination,* pp. 197-207, 2013.

[79] A. Fernández-García, L. Álvarez-Rodrigo, L. Martínez-Arcos, R. Aguiar and J. Márquez-Payés, "Study of different cleaning methods for solar reflectors used

in CSP plants," *Energy Procedia,* pp. 80-89, 2014.

[80] D. Levitan, "How Do You Clean 250 Thousand Solar Thermal Mirrors? Trucks With Robot Arms!," 18 Mar 2013. [Online]. Available: http://spectrum.ieee.org/energywise/green-tech/solar/how-do-you-clean-258048-solar-thermal-mirrors-trucks-with-robot-arms. [Accessed 18 Jan 2017].

[81] "HECTOR successfully completes qualification tests," Senser, 2012. [Online]. Available: http://www.sener.es/revista-sener/en/n44/up-to-date__new_markets.html. [Accessed 2 Mar 2017].

[82] "EFFICIENCY IN ELECTRICITY GENERATION," EURELECTRIC, Boulevard de l'Impératrice,, 2003.

[83] "Carbon Footprint of Electricity Generation," June 2011. [Online]. Available: https://www.parliament.uk/documents/post/postpn_383-carbon-footprint-electricity-generation.pdf. [Accessed 17 Apr 2017].

[84] M. A. Taha, "On The Chemical Mixture Methodologies for Estimation of the Integrated Health Effects.," Texas A & M University, 2014.

[85] "The SmartGrids European Technology Platform," European Technology Platform, 2013. [Online]. Available: http://www.smartgrids.eu/ETPSmartGrids. [Accessed 24 Jan 2017].

[86] "Incorporating Renewables Into The Electric Grid: Expanding Opportunities

For Smart Markets And Energy Storage," Council of Economic Advisers, 2016.

[87] "Smart Power Grids In Qatar Soon," *The Peninsula qatar,* 10 Jan 2013.

[88] M. Kezunovic , "About TEES Smart Grid Center," 2016. [Online]. Available: http://smartgridcenter.tamu.edu/sgc/web/. [Accessed 16 Oct 2016].

[89] "Workshop Focuses on Transition of Power System to Smart Grid," *Gulf Times,* 12 Jan 2016.

[90] H. Trabish, "SolarReserve's 110-megawatt Crescent Dunes concentrated solar power tower is due to come on-line this year," 6 Mar 2014. [Online]. Available: http://helioscsp.com/solarreserves-110-megawatt-crescent-dunes-concentrated-solar-power-tower-is-due-to-come-on-line-this-year/. [Accessed 5 Feb 2017].

[91] "Updated Capital Cost Estimates for Utility Scale Electricity Generating Plants," U.S. Energy Information Administration (EIA), Washington, DC, 2013.

APPENDIX A: SMART GRID TECHNOLOGY

Smart grid is defined by European Technology Platform Smart Grid (ETPSG) as a concept and vision that captures a range of advanced information, sensing, communications, control, and energy technologies in which the electric power system can intelligently integrate the actions of all connected users to efficiently deliver sustainable, economic, and secure electricity supplies [85]. In other words, a smart grid is an electrical grid that contains a diversity of operational and energy measures including smart appliances, smart meters and renewable and efficient energy resources. Smart grids will reduce in general the operational costs and will enable the effective control and remote monitoring.

Smart grid and its importance

A smart grid is a combination of diverse types of power stations such as solar, thermal, wind, gas and other types. These power stations interconnect with each other through the smart grid without human intervention to choose automatically which power station should be in service depending on the area demand and the supplying capacity of the available power stations.

Solar energy is one of the most in use renewable energy resource that provide variable energy output depending on the location, season, weather factors, time of the day and

other technical factors. Because of the above uncontrollable factors and the variations in output energy, the energy output is imperfectly predictable and cannot be connected directly into the existing electricity grid with the current level of smartness. Thus, to be able to penetrate high levels of renewables onto the grid, its management services, temporary storage capacity, technology and response during high times of load should be improved gradually with the level of renewable penetration.

Moreover, the global trend in the meantime is directed toward increasing the penetration of renewables into the public electricity grid to increase the dependability on renewables instead of fossil fuels. For that reason, a new smart grid is required to accommodate this approach. In the case of increased penetration of the solar energy into an existing electricity grid, the net electricity load, defined as the electricity demand of a typical day after subtracting the variable renewable resource of that day, can be plotted during a day period in a shape of duck and this is called the duck curve. This can be shown in Figure A- where the 2020 forecast for the net electricity load throughout a typical spring day in California is illustrated.

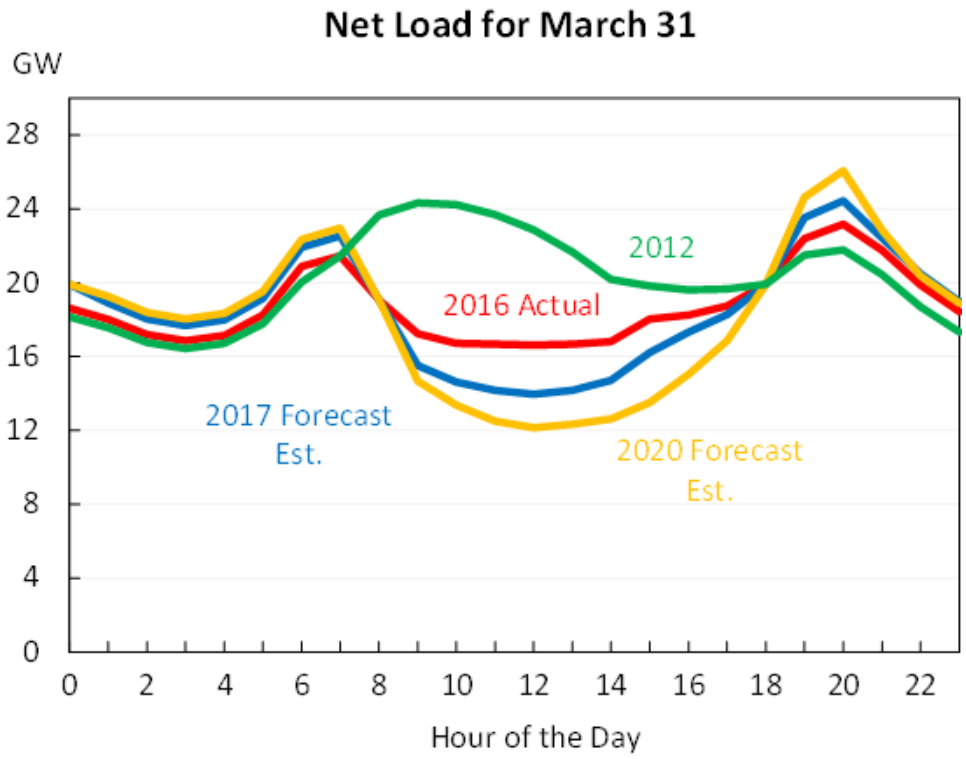

Figure A-1: 2020 forecast for the net electricity load throughout a typical spring day in California [86]

The curve describes two steep ramps of net load, one downward in the morning as the sun rises and one upwards in the evening as the sun sets. It can be concluded from the curve that with more renewable energy penetration, from 2016 to 2020, the curve becomes deeper with higher steep in the morning and evening period and subsequently rise the need for increasing the smartness of the grid management system to handle this difference in net electricity load smoothly.

Some regions in the world have already succeed to manage extremely high penetration of renewable energy into the grid. For instance, in May 2016, Portugal succeeded to run for complete four days on 100 percent on solar, wind, and hydropower, and in Feb 2016 Texas in USA has achieved a 45 percent of instantaneous penetration from wind generation during one evening [86].

Qatar smart grid status

Qatar is undergoing a quick growth in economic and demand for energy. To reduce the sole dependency on the limited sources of fossil fuels and to reduce the greenhouse gasses emitted, penetration of renewable resources, such as solar energy resource, onto the electric grid is becoming an important and attractive solution. Moreover, to be in line with Qatar National Vision [6], a sustainable infrastructure system that is consistent with international environment standards is required to be constructed. All those factors are driving the attention of leaders of energy producing companies in Qatar to build a smart grid that is penetrated by renewables.

Responding to this need, Saleh Hamad Al Marri, head of renewable energy technologies in Qatar General Water and Electricity Corporation (KAHRAMAA), told The Peninsula [87] on the sidelines of the 4th General Conference of Arab Union of Electricity and Exhibition that was held on Jan 2013 that a pilot project is going to be built to introduce a smart power grid system in Qatar. This project shall be located in Duhail and will be

implemented in cooperation with Iberdrola, a Spanish private multinational electric utility company. Moreover, Qatar Environment and Energy Research Institute (QEERI) and Qatar Science and Technology Park (QSTP) are also in cooperation for the project.

One of the major centers that is active in this area of research is The Smart Grid Center in Qatar. It is a branch within the Texas A&M Engineering Experiment Station (TEES), found with a mission to expand on the smart grid associated efforts of TEES in an area of intense national interest in confirming the reliability, sustainability, and security of the electric energy supply [88]. The center has held four smart grid workshops till now, in April 17, 2013, April 8, 2014, April 21, 2015 and April 28, 2016, with the objective of discussing the latest development in smart grid systems and how to implement it in Qatar. Moreover, the center has arranged the first workshop on smart grid and renewable energy on March 22-23, 2015 and the objectives were discussing the importance of the smart grid and renewable energy resources integration in Qatar with further exploring the viability of this technology. In addition of exchanging information on medium to long term smart grid and future challenges.

The college of engineering in Qatar university on the other hand held a workshop on Jan, 2016 to discuss the developments, solutions and challenges for the transition of Qatar's power system to a smart grid. As per the Gulf-times [89], the workshop was themed a the "Qatar Power System Transition to a Smart Grid". The event was part of a research

project sponsored by Qatar National Research Fund, and supported by its collaborating research institutions such as Qatar Mobility and Innovations Centre (QMIC), QEERI, Virginia Tech, and University of Sheffield and industrial partners, Qatar General Electricity and Water Corporation (Kahramaa), Siemens, and Iberdrola. The event aimed to deliver a discussion platform for industry experts and local and international researchers on launching a research initiative for an effective transition of Qatar power system to a smart grid.

Currently, smart grid option in Qatar is still not yet implemented on a large scale. However, based on the substantial interest shown by Qatar's government and all related corporations toward this smart option, the implementation rate is expected to be high and on high priority.

APPENDIX B: AN EXAMPLE OF THE INFORMATION COMPILED ABOUT CSP PLANTS

An example of the information compiled from SolarPACES is project Shams 1 located in United Arab Emirates.

1- Project raw number in the Microsoft Excel file: 127

2- Plant Name: Shams 1

3- Status Date: 21 Oct 2016

4- Background

- Technology: Parabolic trough
- Status: Operational
- Country: United Arab Emirates
- City: Madinat Zayed
- Region: 120 km southwest of Abu Dhabi
- Latitude/Longitude Location: 23°34′ 13.0″ North, 53°42′ 56.0″ East
- Land Area: 250 hectares
- Electricity Generation: 210,000 MWh/yr
- Solar Resource: 1,934 kWh/m2/yr
- Start Production: 3/17/2013
- Cost (approx.): 600,000,000 USD
- Project Type: Commercial

5- Participants

- Developers: Masdar, Total and Abengoa Solar
- EPC contractors: Abener and Teyma
- Owners: Masdar (80%) and Total (20%)

6- Solar Field

- Solar-Field Aperture Area: 627,840 m²
- Number of Solar Collector Assemblies: 768
- Number of Loops: 192
- Number of SCAs per Loop: 4
- Number of Modules per SCA: 12
- SCA Length1: 150 m
- SCA Manufacturer (Model): Abengoa Solar (ASTRO)
- Number of Heat Collector Elements (HCEs): 27,648
- HCE Manufacturer (Model): Schott (PTR 70)

7- Heat Transfer Fluid

- HTF Type: Therminol VP-1
- Solar-Field Inlet Temperature: 300°C
- Solar-Field Outlet Temperature: 400°C
- HTF Company: Solutia

8- Power Block

- Turbine Capacity (Gross): 100.0 MW

- Output Type: Steam Rankine\
- Turbine Manufacturer: Man
- Cooling Method: Dry cooling
- Fossil Backup Type: Natural gas

9- Thermal Storage

- None

APPENDIX C: COMPLETE CSP PROJECTS LISTS CATEGORIZED AS PER THE CSP TECHNLOGY.

1- Plants with parabolic trough CSP technology

S/N	Plant Name	Status Date	Technology	Status	Country	City	Region	Lat/Long Location	Land Area	Electricity Generation	Solar Resource	Company	Start Production	Cost (approx)	Project Type	Developer(s)	Owner(s) (%)	Operator(s)	Solar-Field Aperture Area	# of Solar Collector Assemblies (SCAs)	# of Loops	# of SCAs per Loop	# of Modules per SCA	SCA Aperture Area	SCA Length
1	ISCC Hassi R'mel	4/15/2015	Parabolic trough	Operational	Algeria	Hassi R'mel	Hassi R'mel	33°7′ 27.0″ North, 3°21′ 25.0″ East	64 hectares	-	-	Abener	7/14/2011	315,000,000 Euro	Commercial	Abener	Sonatrach (100%)	Abener	183,860 m^2	224	56	4	-	-	150 m
2	City of Medicine Hat ISCC Project	8/3/2015	Parabolic trough	Operational	Canada	Medicine Hat	Alberta	50°2′ 24.0″ North, 110°43′ 12.0″ West	-	1,500 MWh/yr (Estimated)	-	-	11/1/2014	9,000,000 USD	ISCC Demonstration	City of Medicine Hat	City of Medicine Hat	-	5,248 m^2	8	2	4	-	656 m^2	115 m
3	Pedro de Valdivia	2/12/2013	Parabolic trough	Under development	Chile	Maria Elena	Antofagasta	22°43′ 4.0″ South, 69°35′ 10.0″ West	1,982 hectares	2,108,000 MWh/yr (Estimated)	-	-	1/1/2015	2,610,000,000 USD	Commercial	Grupo Ibereolica	Grupo Ibereolica (100%)	-	-	5376	1344	4	-	-	-
4	Chabei 64MW Molten Salt Parabolic Trough project	9/29/2016	Parabolic trough	Under development	China	Chabei	Hebei Province	-	-	-	-	-	-	-	-	SkyFuel Contact: Webmaster Solar	Zhongyang Zhangjiakou Chabei	-	-	-	-	-	-	-	-
5	Delingha Solar Thermal Power Project	9/28/2016	Parabolic trough	Under construction	China	Delingha	Qinghai Province	-	-	-	1,976 kWh/m2/yr	-	1/1/2017	-	Commercial	CGN Delingha Solar Energy	CGN Delingha Solar Energy	-	-	-	190	-	-	-	-
6	Gansu Akesai 50MW Molten Salt Trough project	9/28/2016	Parabolic trough	Under development	China	Akesai	Gansu Province	-	-	-	-	-	-	-	-	Tianjin Binhai Concentrating Solar Power Investment Co., Ltd.	Shenzhen Jinfan Energy Technology Co., Ltd.	-	-	-	-	-	-	-	-
7	Gulang 100MW Thermal Oil Parabolic Trough project	9/29/2016	Parabolic trough	Under development	China	Wuwei	Gansu Province	-	-	-	-	-	-	-	-	Changzhou Royal Tech Solar Thermal Equipment Co., Ltd.	OECEP Gansu Weiwu Solar Technology Co., Ltd	-	-	-	-	-	-	-	-
8	Urat Middle Banner 100MW Thermal Oil Parabolic Trough project	9/28/2016	Parabolic trough	Under development	China	Urat Middle Banner	Inner Mongolia	-	-	-	-	-	-	-	-	Changzhou Royal Tech Solar Thermal Equipment Co., Ltd.	Inner Mongolia Royal Tech New Energy Co., Ltd.	-	-	-	-	-	-	-	-
9	Yumen 50MW Thermal Oil Trough CSP project	9/28/2016	Parabolic trough	Under development	China	Yumen	Gansu Province	-	-	-	-	-	-	-	-	Royal Tech CSP Limited	Royal Tech CSP Limited	-	-	-	-	-	-	-	-
10	Yumen East Town 50MW Thermal Oil Trough project	9/28/2016	Parabolic trough	Under development	China	Yumen	Gansu Province	-	-	-	-	-	-	-	-	Rayspower Energy Group Co., Ltd.	Rayspower Energy Group Co., Ltd.	-	-	-	-	-	-	-	-
11	ISCC Kuraymat	2/12/2013	Parabolic trough	Operational	Egypt	Kuraymat	100 km south of Cairo	29°16′ 43.0″ North, 31°14′ 56.0″ East	-	34,000 MWh/yr (Expected) Expected generation is based on solar fraction of anticipated total generation of 852,000 MWh/yr.	2,431 kWh/m2/yr	NREA	6/1/2011	-	Commercial	NREA	NREA (100%)	-	130,800 m^2	160	40	4	12	-	-
12	Abhijeet Solar Project	7/27/2015	Parabolic trough	Under construction	India	Phalodi	Rajasthan	26°49′ 40.0″ North, 70°55′ 11.0″ East	388 acres	-	-	Ener-t International Ltd.	1/1/2015	-	Commercial	Shriram EPC Ltd Chennai	NTPC Vidyut Vyapar Nigam Limited	-	-	-	-	-	-	-	-
13	Diwakar	2/12/2013	Parabolic trough	Under construction	India	Askandra	Rajasthan	27°21′ 53.0″ North, 71°43′ 53.0″ East	-	-	-	-	3/1/2013	-	Commercial	Lanco Solar	Lanco Infratech (100%)	-	-	-	290	-	-	-	-
14	Godawari Solar Project	2/13/2014	Parabolic trough	Operational	India	Nokh	Rajhastan	27°36′ 5.0″ North, 72°13′ 26.0″ East	150 hectares	118,000 MWh/yr (Estimated)	-	-	6/5/2013	-	Commercial	Godawari Green Energy Limited	Godawari Green Energy Limited (100%)	-	392,400 m^2	480	120	4	12	817 m^2	144 m
15	Gujarat Solar One	2/12/2014	Parabolic trough	Under construction	India	Kutch	Gujarat	23°34′ 45.0″ North, 70°39′ 0.0″ East	-	130,000 MWh/yr (Expected)	-	-	1/1/2014	-	Commercial	Cargo Solar Power	Cargo Solar Power (100%)	-	326,800 m^2	400	100	4	12	817 m^2	144 m
16	KVK Energy Solar Project	2/12/2013	Parabolic trough	Under construction	India	Askandra	Rajasthan	27°22′ 55.0″ North, 71°46′ 23.0″ East	-	-	-	-	3/1/2013	-	Commercial	KVK Energy Ventures Ltd	KVK Energy Ventures Ltd (100%)	-	-	-	290	-	-	-	-
17	Megha Solar Plant	11/21/2014	Parabolic trough	Operational	India	Anantapur	Andhra Pradesh	16°59′ 19.0″ North, 80°8′ 36.0″ East	242 hectares	110,000 MWh/yr (Expected/Planned)	-	-	11/13/2014	8,480,000,000 Rs	Commercial	Megha Engineering and Infrastructure	Megha Engineering and Infrastructure (100%)	-	366,240 m^2	448	112	4	12	817 m^2	150 m
18	National Solar Thermal Power Facility	2/13/2014	Parabolic trough	Operational	India	Gurgaon	-	28°25′ 39.0″ North, 77°9′ 33.0″ East	-	-	-	-	10/1/2012	-	Demonstration	IIT Bombay	IIT Bombay (100%)	IIT Bombay	8,000 m^2	12	3	4	10	-	120 m
19	Rajasthan Solar One	12/23/2010	Parabolic trough	Under construction	India	Rajasthan	-	-	-	-	-	-	1/1/2020	-	-	Entegra EPC Techint/Solare XXI	-	-	-	-	-	-	-	-	-
20	Ashalim	7/21/2015	Parabolic trough	Under development	Israel	Ashalim	Negev Desert	-	-	-	-	-	1/1/2018	1,000,000,000 USD	-	Negev Energy Ltd. (Abengoa and Shikun & Binui)	Negev Energy Ltd. (100%)	-	-	-	-	-	-	-	-
21	Archimede	8/3/2012	Parabolic trough	Operational	Italy	Priolo Gargallo	Sicily	37°8′ 3.12″ North, 15°13′ 0.15″ East	8 hectares	9,200 MWh/yr (Expected/Planned)	1,936 kWh/m2/yr	ENEL	7/14/2010	-	-	ENEL	ENEL (100%)	ENEL	31,860 m^2	54	9	6	8	590 m^2	100 m
22	ASE Demo Plant	1/22/2015	Parabolic trough	Operational	Italy	Massa Martana	-	42°43′ 47.0″ North, 12°31′ 45.0″ East	3 hectares	275 MWh/yr	1,527 kWh/m2/yr	-	1/1/2013	-	Demonstration	Archimede Solar Energy	Archimede Solar Energy	-	3,398 m^2	6	-	-	-	-	-
23	Shagaya CSP Project	11/25/2015	Parabolic trough	Under development	Kuwait	Kuwait City	-	-	-	-	-	-	12/1/2017	-	-	Kuwait Institute for Scientific Research (KISR)	Kuwait Institute for Scientific Research (KISR)	-	-	-	-	-	-	-	-
24	Agua Prieta II	10/30/2013	Parabolic trough	Under construction	Mexico	Agua Prieta	Sonora State	31°19′ 33.0″ North, 109°32′ 56.0″ West	60 hectares	34,000 MWh/yr	-	-	1/1/2014	-	Commercial	Abengoa Solar	Federal Electricity Commission (100%)	-	85,000 m^2	104	26	4	-	-	150 m
25	Airlight Energy Ait-Baha Pilot Plant	2/16/2015	Parabolic trough	Operational	Morocco	Ait Baha	Agadir	30°13′ 3.0″ North, 9°8′ 57.0″ West	24 hectares	2,390 MWh/yr (Estimated) Computed if it were a stand alone plant	2,200 kWh/m2/yr	Airlight Energy	6/1/2014	-	Pilot	Airlight Energy	Cimar, Italcementi Group (100%)	Cimar, Italcementi Group	6,159 m^2	3	1	3	12	2,053 m^2	215 m
26	ISCC Ain Beni Mathar	1/24/2013	Parabolic trough	Operational	Morocco	Ain Beni Mathar	Ain Beni Mathar	34°3′ 50.0″ North, 2°6′ 0.0″ West	-	55,000 MWh/yr	-	Abener	5/1/2010	-	Commercial	Abener	ONE (Office National de l'Electricite) (100%)	Abengoa Solar / ONE	183,120 m^2	224	56	4	-	-	150 m
27	NOOR I	5/10/2016	Parabolic trough	Operational	Morocco	Ouarzazate	-	30°59′ 40.0″ North, 6°51′ 48.0″ West	-	-	2,635 kWh/m2/yr	-	12/1/2015	1,042,000 Euro	Commercial	ACWA Power, Aries and TSK	ACWA Power Ouarzazate	-	-	-	-	-	-	-	-
28	NOOR II	11/16/2015	Parabolic trough	Under construction	Morocco	Ouarzazate	-	-	-	-	-	-	1/1/2017	-	-	ACWA	-	-	-	-	-	-	-	-	-
29	ISCC Duba 1	2/25/2016	Parabolic trough	Under construction	Saudi Arabia	Duba	-	-	-	-	-	-	1/1/2017	-	-	Saudi Electricity Co.	Saudi Electricity Co.	-	-	-	-	-	-	-	-
30	Bokpoort	11/22/2016	Parabolic trough	Operational	South Africa	Globershoop	Northern Cape Province	28°46′ 53.0″ South, 21°57′ 22.0″ East	100 hectares	230,000 MWh/yr (Estimated)	-	-	3/14/2016	565,000,000 USD	Commercial	ACWA Power EPC Acciona, Sener and TSK	ACWA Power Solafrica Bokpoort CSP Power Plant (Pty) Ltd	-	588,600 m^2	-	-	-	-	-	-
31	Ilanga I	2/16/2015	Parabolic trough	Under development	South Africa	Upington	-	-	-	-	-	-	1/1/2017	-	Commercial	Emvelo and Cobra	-	-	-	-	-	-	-	-	-
32	Kathu Solar Park	6/1/2016	Parabolic trough	Under construction	South Africa	Kathu	-	-	-	-	-	-	1/1/2018	-	Commercial	Engie	Kathu Solar Park Consortium	-	-	-	-	-	-	-	-
33	KaXu Solar One	4/14/2015	Parabolic trough	Operational	South Africa	Poffader	Northern Cape	28°54′ 6.0″ South, 19°37′ 15.0″ East	-	330,000 MWh/yr (Expected)	-	Abengoa Solar	3/2/2015	860,000,000 USD	Commercial	Abengoa Solar - IDC	Abengoa Solar (51%)	-	800,000 m^2	1200	300	4	10	-	-
34	Xina Solar One	9/8/2016	Parabolic trough	Under construction	South Africa	Pofadder	Northern Cape Province	-	-	-	-	-	1/1/2017	880,000,000 USD	-	ACWA ; Solar Reserve	ACWA	-	-	-	-	-	-	-	-
35	Andasol-1(AS-1)	11/16/2015	Parabolic trough	Operational	Spain	Aldeire	Granada	37°13′ 50.83″ North, 3°4′ 14.08″ West	200 hectares	158,000 MWh/yr (Expected/Planned)	2,136 kWh/m2/yr	ACS/Cobra Group	11/26/2008	-	Commercial	ACS/Cobra Group	Total (20%)	Cobra O&M	510,120 m^2	624	156	4	12	817 m^2	144 m
36	Andasol-2(AS-2)	1/25/2013	Parabolic trough	Operational	Spain	Aldeire y La Calahorra	Granada	37°13′ 50.83″ North, 3°4′ 14.08″ West	200 hectares	158,000 MWh/yr (Expected/Planned)	2,136 kWh/m2/yr	ACS/Cobra Group	6/1/2009	-	Commercial	ACS/Cobra Group	ACS/Cobra Group (100%)	Cobra O&M	510,120 m^2	624	156	4	12	817 m^2	144 m
37	Andasol-3(AS-3)	10/8/2013	Parabolic trough	Operational	Spain	Aldeire	Granada	37°13′ 42.7″ North, 3°4′ 6.73″ West	200 hectares	175,000 MWh/yr (Estimated)	2,200 kWh/m2/yr	-	8/1/2011	315,000,000 Euro	-	Ferrostaal AG	Ferrostaal/Solar Millennium/RWE/Rhein E./SWM (100%)	-	510,120 m^2	624	156	4	12	817 m^2	150 m
38	Arcosol 50(Valle 1)	7/3/2015	Parabolic trough	Operational	Spain	San José del Valle	Cádiz	36°39′ 40.0″ North, 5°50′ 0.0″ West	230 hectares	175,000 MWh/yr (Expected)	2,097 kWh/m2/yr	Torresol	12/1/2011	270,000,000 Euro	-	Torresol	Torresol (100%)	Torresol	510,120 m^2	624	156	4	-	817 m^2	-
39	Arenales	1/13/2014	Parabolic trough	Operational	Spain	Morón de la Frontera	Sevilla	37°9′ 43.0″ North, 5°32′ 54.0″ West	220 hectares	166,000 MWh/yr (Estimated)	-	-	11/1/2013	-	Commercial	RREF/OHL	RREF/OHL (100%)	OHL	510,120 m^2	936	156	6	-	545 m^2	96 m
40	Aste 1A	6/10/2014	Parabolic trough	Operational	Spain	Alcázar de San Juan	Ciudad Real	39°10′ 34.0″ North, 3°14′ 4.0″ West	180 hectares	170,000 MWh/yr (Expected/Planned)	2,019 kWh/m2/yr	-	1/1/2012	-	Commercial	Elecnor/Aries/ABM AMRO	Elecnor/Aries/ABM AMRO (100%)	-	510,120 m^2	624	156	4	12	817 m^2	150 m
41	Aste 1B	6/10/2014	Parabolic trough	Operational	Spain	Alcázar de San Juan	Ciudad Real	39°10′ 34.0″ North, 3°14′ 4.0″ West	180 hectares	170,000 MWh/yr (Expected/Planned)	2,019 kWh/m2/yr	-	1/1/2012	-	Commercial	Elecnor/Aries/ ABM AMRO	Elecnor/Aries/ ABM AMRO (100%)	-	510,120 m^2	624	156	4	12	817 m^2	150 m
42	Astexol II	6/10/2014	Parabolic trough	Operational	Spain	Olivenza	Badajoz	38°48′ 36.0″ North, 7°3′ 9.0″ West	160 hectares	170,000 MWh/yr	2,052 kWh/m2/yr	-	1/1/2012	-	Commercial	Elecnor/Aries/ABM AMRO	Elecnor/Aries/ABM AMRO (100%)	-	510,120 m^2	624	-	4	12	817 m^2	149 m
43	Borges Termosolar	9/27/2013	Parabolic trough	Operational	Spain	Les Borges Blanques	Lleida	41°31′ 44.0″ North, 0°47′ 60.0″ East	96 hectares	98,000 MWh/yr (Estimated)	-	Abantia	12/1/2012	153,000,000 Euro	Commercial	Abantia	Abantia (50%)	-	183,120 m^2	336	56	6	8	545 m^2	96 m
44	Casablanca	2/4/2014	Parabolic trough	Operational	Spain	Talarrubias	Badajoz	39°14′ 22.0″ North, 5°18′ 49.0″ West	200 hectares	160,000 MWh/yr (Estimated)	-	COBRA	1/1/2013	-	Commercial	ACS - COBRA group	ACS - COBRA group (100%)	-	510,120 m^2	624	156	4	12	817 m^2	144 m
45	Enerstar(Villena)	2/14/2014	Parabolic trough	Operational	Spain	Villena	Alicante	38°43′ 43.0″ North, 0°55′ 19.0″ West	214 hectares	100,000 MWh/yr (Estimated)	-	FCC Energy	9/26/2013	-	Commercial	FCC Energy	FCC Energy (100%)	-	339,506 m^2	420	105	4	12	-	150 m
46	Extresol-1(EX-1)	1/20/2011	Parabolic trough	Operational	Spain	Torre de Miguel Sesmero	Badajoz	38°39′ North, 6°44′ West	200 hectares	158,000 MWh/yr (Expected/Planned)	2,168 kWh/m2/yr	ACS/Cobra Group	1/1/2010	-	Commercial	ACS/Cobra Group	ACS/Cobra Group (100%)	Cobra O&M	510,120 m^2	624	156	4	12	817 m^2	144 m
47	Extresol-2(EX-2)	5/13/2011	Parabolic trough	Operational	Spain	Torre de Miguel Sesmero	Badajoz	38°39′ North, 6°44′ West	200 hectares	158,000 MWh/yr (Expected/Planned)	2,168 kWh/m2/yr	ACS/Cobra Group	1/1/2010	-	Commercial	ACS/Cobra Group	ACS/Cobra Group (100%)	Cobra O&M	510,120 m^2	624	156	4	12	817 m^2	144 m
48	Extresol-3(EX-3)	3/18/2013	Parabolic trough	Operational	Spain	Torre de Miguel Sesmero	Badajoz	38°39′ North, 6°44′ West	200 hectares	158,000 MWh/yr (Expected/Planned)	2,168 kWh/m2/yr	ACS/Cobra Group	8/1/2012	-	Commercial	ACS/Cobra Group	ACS/Cobra Group (100%)	Cobra O&M	510,120 m^2	624	156	4	12	817 m^2	144 m
49	Guzmán	3/18/2013	Parabolic trough	Operational	Spain	Palma del Río	Córdoba	37°9′ 7.0″ North, 5°16′ 16.0″ West	200 hectares	104,000 MWh/yr (Estimated)	-	FCC Energy	7/1/2012	-	Commercial	FCC Energy	FCC Energy (70%)	-	310,406 m^2	384	96	4	12	817 m^2	150 m
50	Helioenergy 1	8/24/2012	Parabolic trough	Operational	Spain	Écija	Sevilla	37°34′ 55.0″ North, 5°6′ 57.0″ West	110 hectares	95,000 MWh/yr (Expected/Planned)	-	Abengoa Solar	9/1/2011	-	Commercial	Abengoa Solar ; EON	Abengoa Solar (50%)	Abengoa	300,000 m^2	360	-	4	12	-	150 m
51	Helioenergy 2	8/24/2012	Parabolic trough	Operational	Spain	Écija	Sevilla	37°34′ 55.0″ North, 5°6′ 57.0″ West	110 hectares	95,000 MWh/yr (Expected/Planned)	-	Abengoa Solar	1/1/2012	-	Commercial	Abengoa Solar ; EON	Abengoa Solar (50%)	Abengoa Solar	300,000 m^2	360	-	4	12	-	150 m
52	Helios I	3/18/2013	Parabolic trough	Operational	Spain	Puerto Lápice	Ciudad Real	39°14′ 24.0″ North, 3°28′ 12.0″ West	260 hectares	97,000 MWh/yr (Expected/Planned)	2,217 kWh/m2/yr	Helios I HYPERION Energy Investments, S.L.	6/1/2012	-	Commercial	Helios I HYPERION Energy Investments, S.L.	Caja Castilla La Mancha Corporación, S.A. (5%)	-	300,000 m^2	360	90	4	12	-	150 m
53	Helios II	8/19/2015	Parabolic trough	Operational	Spain	Puerto Lápice	Ciudad Real	39°14′ 24.0″ North, 3°28′ 12.0″ West	260 hectares	97,000 MWh/yr (Expected/Planned)	2,217 kWh/m2/yr	Helios II HYPERION Energy Investments, S.L.	8/1/2012	-	Commercial	Helios II HYPERION Energy Investments, S.L.	Caja Castilla La Mancha Corporación, S.A. (5%)	-	300,000 m^2	360	90	4	12	-	150 m
54	Ibersol Ciudad Real (Puertollano)	1/30/2013	Parabolic trough	Operational	Spain	Puertollano	Castilla-La Mancha	38°38′ 36.19″ North, 3°58′ 29.6″ West	150 hectares	103,000 MWh/yr (Expected/Planned)	2,061 kWh/m2/yr	-	1/1/2009	200,000,000 Euro	-	IBERCAM (Iberdrola Renovables Castilla-La Mancha)	IBERCAM (Iberdrola Renovables Castilla-La Mancha) (90%)	Iberdrola Renovables	287,760 m^2	352	88	4	12	-	-
55	La Africana	11/24/2012	Parabolic trough	Operational	Spain	Posadas	Córdoba	37°44′ 52.0″ North, 5°6′ 56.0″ West	252 hectares	170,000 MWh/yr (Estimated)	1,950 kWh/m2/yr	-	11/21/2012	387,000,000 Euro	Commercial	Ortiz/TSK/Magtel	Ortiz/TSK/Magtel (100%)	-	550,000 m^2	672	168	4	12	-	150 m
56	La Dehesa	1/30/2013	Parabolic trough	Operational	Spain	La Garrovilla	Badajoz	38°57′ 6.14″ North, 6°27′ 48.36″ West	200 hectares	175,000 MWh/yr (Estimated)	-	Renovables SAMCA	2/1/2011	-	-	Renovables SAMCA	Renovables SAMCA (100%)	Renovables SAMCA	552,750 m^2	672	168	4	12	822 m^2	150 m
57	La Florida	8/14/2012	Parabolic trough	Operational	Spain	Badajoz	Badajoz	38°49′ 1.11″ North, 6°49′ 45.49″ West	200 hectares	175,000 MWh/yr (Estimated)	-	Renovables SAMCA	6/1/2010	-	-	Renovables SAMCA	Renovables SAMCA (100%)	Renovables SAMCA	552,750 m^2	672	168	4	12	822 m^2	150 m

S/N	SCA Manufacturer (Model)	Mirror Manufacturer	# of Heat Collector Elements (HCEs)	HCE Manufacturer (Model)	HCE Type (Length)	HTF Type	Solar-Field Inlet Temp	Solar-Field Outlet Temp	Solar-Field Temp Difference	HTF Company	Turbine Capacity (Gross)	Turbine Capacity (Net)	Output Type	Turbine Manufacturer	Turbine Efficiency	Power Cycle Pressure	Cooling Method	Cooling Method Description	Fossil Backup Type	General	Storage Type	Storage Capacity	Thermal Storage Description
1	Abengoa Solar (ASTR-Ø)	Rioglass	8,064	Schott (PTR 70)	-	Thermal oil	293°C	393°C	100°C	-	20.0 MW	20.0 MW	Steam Rankine	Siemens SST-900	-	-	Dry cooling	Aero condensers	-	-	None	-	-
2	-	-	-	-	-	Xceltherm®SST	-	-	-	Radco Industries	1.1 MW	1.1 MW	-	-	-	-	-	-	-	-	None	-	-
3	-	-	-	-	-	Thermal Oil	293°C	393°C	100°C	-	360.0 MW	360.0 MW	-	-	-	-	Dry cooling	-	Natural gas	-	2-tank indirect	10.5 hours	Molten Salt
4	-	-	-	-	-	Molten Salt	-	-	-	-	64.0 MW	64.0 MW	Steam Rankine	-	-	-	-	-	-	-	2-tank direct	16 hours	Molten salt
5	-	-	-	-	-	Thermal oil	293°C	393°C	100°C	-	50.0 MW	50.0 MW	Steam Rankine	-	-	-	Wet cooling	-	-	-	2-tank indirect	7.5 hours	Molten salt
6	-	-	-	-	-	-	-	-	-	-	50.0 MW	50.0 MW	Steam Rankine	-	-	-	-	-	-	-	2-tank direct	15 hours	Molten salt
7	-	-	-	-	-	-	-	-	-	-	100.0 MW	100.0 MW	Steam Rankine	-	-	-	-	-	-	-	2-tank indirect	7 hours	Molten Salt
8	-	-	-	-	-	-	-	-	-	-	100.0 MW	100.0 MW	Steam Rankine	-	-	-	-	-	-	-	2-tank indirect	4 hours	Molten Salt
9	-	-	-	-	-	-	-	-	-	-	50.0 MW	50.0 MW	Steam Rankine	-	-	-	-	-	-	-	2-tank indirect	7 hours	Molten Salt
10	-	-	-	-	-	-	-	-	-	-	50.0 MW	50.0 MW	Steam Rankine	-	-	-	-	-	-	-	2-tank indirect	7 hours	Molten Salt
11	Flagsol (SKAL-ET)	-	-	Schott (PTR 70)	-	Therminol VP-1	293°C	393°C	100°C	Solutia	20.0 MW	20.0 MW	Steam Rankine	Siemens	-	-	Wet cooling	Cooling tower	-	-	None	-	-
12	Ener-t International Ltd (ES-3.5)	Rioglass	-	Siemens (UVAC 2010)	-	Therminol VP-1	-	-	-	Solutia	50.0 MW	50.0 MW	Steam Rankine	Siemens SST-700	-	-	Wet cooling	-	-	-	none	-	-
13	SENERtrough (SNT0)	-	-	-	-	Synthetic Oil	-	-	-	-	100.0 MW	100.0 MW	-	Siemens SST-700	-	-	Wet cooling	-	-	-	2-tank indirect	4 hours	1010 MWht, Molten Salt
14	-	Flabeg (RP3)	-	Schott (PTR-70)	Evacuated (4 m)	Dowtherm A	293°C	390°C	100°C	Dow Chemical	50.0 MW	50.0 MW	-	Siemens SST-700	-	-	Wet cooling	-	-	-	None	-	-
15	-	Flabeg (RP-3)	-	Schott (PTR-70)	Evacuated (4 m)	Diphyl	293°C	393°C	100°C	Lanxess	28.0 MW	25.0 MW	Steam Rankine	-	-	-	Wet cooling	Cooling tower	-	-	2-tank indirect	9 hours	Molten Salt
16	SENERtrough (SNT0)	-	-	-	-	Synthetic Oil	-	-	-	-	100.0 MW	100.0 MW	-	Siemens SST-700	-	-	Wet cooling	-	-	-	2-tank indirect	4 hours	1010 MWht, Molten Salt
17	-	-	16,128	Siemens (UVAC 2010)	Evacuated (4 m)	Xceltherm®MK1	293°C	393°C	100°C	Radco Industries	50.0 MW	50.0 MW	Steam Rankine	GE	-	-	Wet cooling	Cooling tower	-	-	None	-	-
18	Shrijee Structures	-	360	Schott (PTR-70)	-	Therminol VP-1	293°C	393°C	100°C	Solutia	1.0 MW	1.0 MW	Steam Rankine	-	-	-	-	-	-	-	None	-	-
19	-	-	-	-	-	-	-	-	-	-	10 MW	-	Steam Rankine	-	-	-	-	-	-	-	-	8 hours	-
20	-	-	-	-	-	-	-	-	-	-	110.0 MW	110.0 MW	Steam Rankine	-	-	-	-	-	-	-	2-tank indirect	4.5 hours	Molten salt
21	-	Ronda Reflex	1,296	Archimede Solar Energy	-	Molten salt (60% $NaNO_3$, 40% KNO_3)	290°C	550°C	260°C	-	5.0 MW	4.72 MW	-	Tosi	39.3% @ full load	93.83 bar	Wet cooling	-	-	The plant produces steam that is sent to the CC steam turbine, rated at 130 MW; the 4.72 MW datum is the calculated capacity added by the solar steam, Annual Solar-to-Electricity Efficiency (Gross): 15.6%	2-tank direct	8 hours	Total of 1,580 tons of molten salt. 60% sodium nitrate, 40% potassium nitrate. Capacity 100 MWh (thermal). Tanks are 6.5 m high and 13.5 m in diameter.
22	-	-	-	-	-	Molten salt	290°C	550°C	260°C	-	0.35 MW	-	Steam Rankine	Siemens	15.61% @ full load	-	-	-	-	-	2-tank direct	4.27 MWh-t	Molten salt
23	-	-	-	-	-	-	-	-	-	-	50.0 MW	50.0 MW	Steam Rankine	-	-	-	-	-	-	-	2-tank indirect	10 hours	Molten salt
24	Abengoa Solar (ASTRO)	Rioglass	-	-	-	Thermal Oil	-	-	-	-	14.0 MW	12.0 MW	Steam Rankine	-	-	-	-	-	-	-	None	-	-
25	-	Airlight Energy (Pneumatic mirror)	108	Airlight Energy	-	Air at ambient pressure	270°C	570°C	300°C	-	3.0 MW	3.0 MW	Organic Rankine	-	-	-	-	-	-	Turboden, The solar field feeds 3 MWth to an existing 12 MWe ORC turbine, 3.9 MWth Peak thermal power	Other	5 hours	Packed-bed of rocks
26	Abengoa Solar (ASTR-Ø)	Rioglass	-	Schott (PTR70)	-	Therminol VP-1	-	393°C	-	-	20.0 MW	20.0 MW	Steam Rankine	-	-	-	Wet cooling	-	-	-	None	-	-
27	Sener (SenerTrough)	FE GmbH (formerly Flabeg GmbH, Germany) (Rp3, annealed)	-	-	-	Dowtherm A	293°C	393°C	100°C	DOW	170.0 MW	160.0 MW	Steam Rankine	-	-	-	Wet cooling	-	LFO Boiler System	-	2-tank indirect	3 hours	Molten Salt
28	-	-	-	-	-	Thermal oil	293°C	393°C	100°C	-	200.0 MW	200.0 MW	Steam Rankine	-	-	-	-	-	-	-	2-tank indirect	7 hours	Molten salt
29	Flabeg (Ultimate Trough)	-	-	-	-	-	-	-	-	-	43.0 MW	43.0 MW	Steam Rankine	-	-	-	-	-	-	-	None	-	-
30	Sener (SenerTrough)	FE GmbH (formerly Flabeg GmbH, Germany) (Rp3, annealed)	-	Schott (PTR 70)	-	Dowtherm A	293°C	393°C	100°C	DOW	55.0 MW	50.0 MW	Steam Rankine	Siemens (SST-800)	-	-	Wet cooling	-	LFO Boiler System (2x5 MWht)	-	2-tank indirect	9.3 hours	Molten salts (1300 MWht)
31	-	-	-	-	-	Thermal oil	293°C	393°C	100°C	-	100.0 MW	100.0 MW	Steam Rankine	-	-	-	-	-	-	-	2-tank indirect	4.5 hours	Molten salt
32	-	-	-	-	-	Thermal oil	293°C	393°C	100°C	-	100.0 MW	100.0 MW	Steam Rankine	-	-	-	-	-	-	-	2-tank indirect	4.5 hours	Molten salt
33	Abengoa Solar (E2)	Rioglass	-	-	Evacuated (4 m)	Thermal oil	-	-	-	-	100.0 MW	100.0 MW	Steam Rankine	Siemens	-	100.0 bar	Dry cooling	-	-	-	2-tank indirect	2.5 hours	Molten salt
34	-	-	-	-	-	Thermal oil	-	-	-	-	100.0 MW	100.0 MW	Steam Rankine	Siemens	-	-	-	-	-	-	2-tank indirect	5 hours	Molten salt
35	-	Flabeg (RP3)	11,232	Schott (PTR70) Solel (UVAC 2008)	-	Dowtherm A	293°C	393°C	100°C	-	50.0 MW	49.9 MW	Steam Rankine	Siemens	38.1% @ full load	100.0 bar	Wet cooling	Cooling tower	HTF heater	Annual Solar-to-Electricity Efficiency (Gross): 16%, Backup Percentage: 12%	2-tank indirect	7.5 hours	28,500 tons of molten salt. 60% sodium nitrate, 40% potassium nitrate. 1,010 MWh. Tanks are 14 m high and 36 m in diameter.
36	-	Flabeg (RP3)	11,232	Schott (PTR70) Solel (UVAC 2008)	-	Dowtherm A	293°C	393°C	100°C	-	50.0 MW	49.9 MW	Steam Rankine	Siemens SST-700	38.1% @ full load	100.0 bar	Wet cooling	Cooling tower	HTF heater	Annual Solar-to-Electricity Efficiency (Gross): 16%, Backup Percentage: 12%	2-tank indirect	7.5 hours	28,500 tons of molten salt. 60% sodium nitrate, 40% potassium nitrate. 1,010 MWh. Tanks are 14 m high and 36 m in diameter.
37	-	Rioglass	-	-	-	Thermal Oil	293°C	393°C	100°C	-	50.0 MW	50.0 MW	Steam Rankine	-	-	100.0 bar	Wet cooling	-	-	-	2-tank indirect	7.5 hours	Molten salt
38	Sener (SenerTrough)	-	-	-	-	Diphenyl/Diphenyl oxide	293°C	393°C	100°C	-	49.9 MW	49.9 MW	Steam Rankine	-	38.1% @ full load	100.0 bar	Wet cooling	-	Natural gas	-	2-tank indirect	7.5 hours	28,500 tons of molten salt. 60% sodium nitrate, 40% potassium nitrate.
39	Siemens (SunField 6)	-	-	Siemens (UVAC 2010)	Evacuated (4 m)	Diphyl	293°C	393°C	100°C	LanXess	50.0 MW	50.0 MW	Steam Rankine	GE	37% @ full load	-	Wet cooling	-	HTF Boiler	Backup Percentage: 12%	2-tank indirect	7 hours	Molten salts; 60% Sodium Nitrate, 40% Potassium Nitrate
40	-	Flabeg (RP3)	22,464	Siemens (UVAC 2010)	-	Dowtherm A	293°C	393°C	100°C	-	50.0 MW	50.0 MW	Steam Rankine	-	-	100.0 bar	Wet cooling	Cooling tower	HTF Boiler	Annual Solar-to-Electricity Efficiency (Gross): 15%, Backup Percentage: 12%	2-tank indirect	8 Hours	Molten salts; 60% Sodium Nitrate, 40% Potassium Nitrate
41	-	Flabeg (RP3)	22,464	Siemens (UVAC 2010)	-	Dowtherm A	293°C	393°C	100°C	-	50.0 MW	50.0 MW	Steam Rankine	-	-	100.0 bar	Wet cooling	Cooling tower	HTF Boiler	Annual Solar-to-Electricity Efficiency (Gross): 15%, Backup Percentage: 12%	2-tank indirect	8 Hours	Molten salts; 60% Sodium Nitrate, 40% Potassium Nitrate
42	Flagsol (SKAL-ET 150)	-	-	-	-	Thermal Oil	293°C	393°C	100°C	-	50.0 MW	50.0 MW	Steam Rankine	-	-	100.0 bar	Wet cooling	Cooling tower	HTF Boiler	Annual Solar-to-Electricity Efficiency (Gross): 15%	2-tank indirect	8 Hours	60% Sodium Nitrate, 40% Potassium Nitrate
43	-	-	8,064	Siemens (UVAC 2010)	Evacuated (4 m)	Thermal Oil	293°C	393°C	-	-	25.0 MW	22.5 MW	Steam Rankine	-	37% @ full load	-	Wet cooling	Cooling tower	Biomass (2x22MWt)	-	None	-	-
44	-	Flabeg (RP3)	22,464	Solel (UVAC 2008)	Evacuated (4 m)	-	293°C	393°C	-	Diphenyl/Biphenyl oxide	50.0 MW	50.0 MW	Steam Rankine	Siemens	38.1% @ full load	100.0 bar	Wet cooling	Cooling tower	HTF heater	Backup Percentage: 12%	2-tank indirect	7.5 hours	60% Sodium Nitrate, 40% Potassium Nitrate
45	Sener (SenerTrough)	-	-	Schott (PTR70)	-	Thermal Oil	293°C	393°C	100°C	-	50.0 MW	50.0 MW	Steam Rankine	Man-Turbo, 3 extractions	-	100.0 bar	Wet cooling	Cooling tower	HTF Heaters (3x15MWt)	Backup Percentage: 12%	None	-	-
46	-	Flabeg (RP3)	22,464	Schott (PTR 70)	Evacuated (4 m)	Diphenyl/Biphenyl oxide	293°C	393°C	100°C	-	50.0 MW	-	Steam Rankine	Siemens	38.1% @ full load	100.0 bar	Wet cooling	Cooling tower	HTF heater	Annual Solar-to-Electricity Efficiency (Gross): 16%, Backup Percentage: 12%	2-tank indirect	7.5 hours	28,500 tons of molten salt. 60% sodium nitrate, 40% potassium nitrate. 1,010 MWh. Tanks are 14 m high and 36 m in diameter.
47	-	Flabeg (RP3)	22,464	Solel (UVAC 2008)	Evacuated (4 m)	Diphenyl/Biphenyl oxide	293°C	393°C	100°C	-	49.9 MW	49.9 MW	-	Siemens	38.1% @ full load	100.0 bar	Wet cooling	Cooling tower	HTF heater	Annual Solar-to-Electricity Efficiency (Gross): 16%, Backup Percentage: 12%	2-tank indirect	7.5 hours	28,500 tons of molten salt. 60% sodium nitrate, 40% potassium nitrate. 1,010 MWh. Tanks are 14 m high and 36 m in diameter.
48	-	Flabeg (RP3)	22,464	Solel (UVAC 2008)	Evacuated (4 m)	Diphenyl/Biphenyl oxide	293°C	393°C	100°C	-	50.0 MW	50.0 MW	-	Siemens	38.1% @ full load	100.0 bar	Wet cooling	Cooling tower	HTF heater	Annual Solar-to-Electricity Efficiency (Gross): 16%, Backup Percentage: 12%	2-tank indirect	7.5 hours	28,500 tons of molten salt. 60% sodium nitrate, 40% potassium nitrate. 1,010 MWh. Tanks are 14 m high and 36 m in diameter.
49	-	Flabeg (RP3)	13,824	Schott (PTR-70)	-	Dowtherm A	293°C	393°C	100°C	-	50.0 MW	50.0 MW	Steam Rankine	Man-Turbo, 5 extractions	-	100.0 bar	Wet cooling	Cooling tower	HTF Heaters (3x15MWt)	Backup Percentage: 12%	None	-	-
50	Abengoa Solar (ASTRØ)	-	12,960	-	-	Thermal Oil	293°C	393°C	100°C	-	50.0 MW	50.0 MW	Steam Rankine	Siemens SST-700 (Germany)	-	100.0 bar	Wet cooling	Cooling tower	HTF Boiler	-	None	-	-
51	Abengoa Solar (ASTRØ)	-	12,960	-	-	Thermal Oil	293°C	393°C	100°C	-	50.0 MW	50.0 MW	Steam Rankine	Siemens SST-700 (Germany)	-	100.0 bar	Wet cooling	Cooling tower	HTF Boiler	-	None	-	-
52	Abengoa Solar (ASTRØ)	-	-	Schott	-	Thermal Oil	293°C	393°C	100°C	-	50.0 MW	50.0 MW	Steam Rankine	Siemens	-	100.0 bar	Wet cooling	Cooling tower	-	-	None	-	-
53	Abengoa Solar (ASTRØ)	-	-	Schott	-	Xceltherm®MK1	293°C	393°C	100°C	Radco Industries	50.0 MW	50.0 MW	Steam Rankine	Siemens	-	100.0 bar	Wet cooling	Cooling tower	-	-	None	-	-
54	Iberdrola (Iberdrola Collector)	Flabeg	6,336	Schott (PTR70) Solel	-	Diphenyl/Biphenyl oxide - Dowtherm A	304°C	391°C	87°C	Dow Chemical	50.0 MW	50.0 MW	Steam Rankine	Siemens	38.9% @ full load	100.0 bar	Wet cooling	-	HTF heater (gas-fired)	-	None	-	-
55	Sener (SenerTrough)	-	-	-	-	-	293°C	393°C	100°C	-	50.0 MW	50.0 MW	Steam Rankine	-	-	-	Wet cooling	-	-	-	2-tank indirect	7.5 hours	60% Sodium Nitrate, 40% Potassium Nitrate
56	-	Rioglass	24,192	Schott (PTR70)	-	Diphenyl/Biphenyl oxide	298°C	393°C	95°C	-	49.9 MW	49.9 MW	Steam Rankine	Siemens (Sweden)	38.13% @ full load	100.0 bar	Wet cooling	-	HTF heater	Annual Solar-to-Electricity Efficiency (Gross): 13.81%, Backup Percentage: 12%	2-tank indirect	7.5 hours	29,000 tons of molten salt. 60% sodium nitrate, 40% potassium nitrate.
57	-	Rioglass	24,192	Schott	-	Diphenyl/Diphenyl oxide	298°C	393°C	95°C	Dow Chemical	50.0 MW	50.0 MW	Steam Rankine	Siemens (Sweden)	38.13% @ full load	100.0 bar	Wet cooling	-	HTF heater	Annual Solar-to-Electricity Efficiency (Gross): 13.81%, Backup Percentage: 12%	2-tank indirect	7.5 hours	29,000 tons of molten salt. 60% sodium nitrate, 40% potassium nitrate.

58	La Risca(Alvarado I)	3/20/2013	Parabolic trough	Operational	Spain	Alvarado	Badajoz	38°49′ 37.0″ North, 6°49′ 34.0″ West	135 hectares	105,200 MWh/yr (Estimated)	2,174 kWh/m2/yr	Acciona Energía	6/1/2009	-	-	Acciona Energía	Acciona Energía (100%)	Acciona Energía	352,854 m^2	768	96	8	-	-	-	Acciona Solar	Flabeg (RP2)	-	-	-	Biphenyl/Diphenyl oxide	293°C	393°C	-	-	50.0 MW	50.0 MW	Steam Rankine	Siemens SST-700	-	100.0 bar	Wet cooling	-	HTF Heater, 35 MWt	Backup Percentage: 12%	None	-	-
59	Lebrija 1(LE-1)	8/14/2012	Parabolic trough	Operational	Spain	Lebrija	Sevilla	37°0′ 10.8″ North, 6°2′ 52.0″ West	188 hectares	120,000 MWh/yr (Expected/Planned)	1,993 kWh/m2/yr	Soleval	12/27/2011	-	-	Solucia Renovables 1, S.L.	Solel Solar Systems, LTD. (50%)	Soleval Renovables, S.L.	412,020 m^2	756	-	-	-	545 m^2	95 m	Solel	Solel	18,144	-	-	Therminol VP-1	-	395°C	-	-	50.0 MW	50.0 MW	-	-	-	100.0 bar	Wet cooling	-	HTF heater	Backup Percentage: 12%	None	-	-
60	Majadas I	3/20/2013	Parabolic trough	Operational	Spain	Majadas de Tiétar	Cáceres	39°58′ 5.0″ North, 5°44′ 32.0″ West	135 hectares	104,500 MWh/yr (Estimated)	2,142 kWh/m2/yr	Acciona Energía	10/1/2010	-	-	Acciona Energía	Acciona Energía (100%)	Acciona Energía	372240 m^2	792	99	8	12	470 m^2	100 m	-	-	-	-	-	Biphenyl/Diphenyl oxide	-	393°C	-	-	50.0 MW	50.0 MW	Steam Rankine	-	38.7% @ full load	-	Wet cooling	-	-	-	None	-	-
61	Manchasol-1	3/30/2011	Parabolic trough	Operational	Spain	Alcazar de San Juan	Ciudad Real	39°11′ 17.08″ North, 3°18′ 33.71″ West	200 hectares	158,000 MWh/yr (Expected/Planned)	2,208 kWh/m2/yr	ACS/Cobra Group	1/1/2011	-	Commercial	ACS/Cobra Group	ACS/Cobra Group (100%)	Cobra O&M	510,120 m^2	624	156	4	12	817 m^2	144 m	-	Flabeg (RP3)	11,232	Schott Solel	-	Diphenyl/Diphenyl oxide	293°C	393°C	100°C	-	49.9 MW	49.9 MW	-	Siemens	38.1% @ full load	100.0 bar	Wet cooling	Cooling tower	HTF heater	Annual Solar-to-Electricity Efficiency (Gross): 16%, Backup Percentage: 12%	2-tank indirect	7.5 hours	28,500 tons of molten salt. 60% sodium nitrate, 40% potassium nitrate. 375 MWh. Tanks are 14 m high and 36 m in diameter.
62	Manchasol-2	8/14/2012	Parabolic trough	Operational	Spain	Alcazar de San Juan	Ciudad Real	39°10′ 55.5″ North, 3°18′ 48.96″ West	200 hectares	158,000 MWh/yr (Expected/Planned)	2,208 kWh/m2/yr	ACS/Cobra Group	4/1/2011	-	Commercial	ACS/Cobra Group	ACS/Cobra Group (100%)	Cobra O&M	510,120 m^2	624	156	4	12	817 m^2	144 m	-	Flabeg (RP3)	11,232	Schott Solel	-	Diphenyl/Diphenyl oxide	293°C	393°C	100°C	-	50.0 MW	50.0 MW	-	Siemens	38.1% @ full load	100.0 bar	Wet cooling	Cooling tower	HTF heater	Annual Solar-to-Electricity Efficiency (Gross): 16%, Backup Percentage: 12%	2-tank indirect	7.5 hours	28,500 tons of molten salt. 60% sodium nitrate, 40% potassium nitrate. 375 MWh. Tanks are 14 m high and 36 m in diameter.
63	Morón	8/13/2012	Parabolic trough	Operational	Spain	Morón de la Frontera	Seville	37°8′ 23.0″ North, 5°28′ 16.0″ West	160 hectares	100,000 MWh/yr (Estimated)	-	-	5/1/2012	295,000,000 Euro	Commercial	Ibereólica Solar	Ibereólica Solar (100%)	-	380,000 m^2	464	-	4	-	-	-	-	-	-	-	-	Thermal Oil	293°C	393°C	100°C	-	50.0 MW	50.0 MW	Steam Rankine	Siemens, 5 extractions	-	100.0 bar	Wet cooling	Cooling tower	HTF Boiler	-	None	-	-
64	Olivenza 1	3/18/2013	Parabolic trough	Operational	Spain	Olivenza	Badajoz	38°48′ 37.0″ North, 7°3′ 32.0″ West	160 hectares	100,000 MWh/yr (Estimated)	-	-	9/1/2012	284,000,000 Euro	Commercial	Ibereólica Solar	Ibereólica Solar (100%)	-	402,210 m^2	738	123	6	-	545 m^2	96 m	Siemens (SunField 6)	-	17,712	Siemens (UVAC 2010)	Evacuated (4 m)	Thermal Oil	293°C	393°C	100°C	-	50.0 MW	50.0 MW	Steam Rankine	Siemens, 5 extractions	-	100.0 bar	Wet cooling	Cooling tower	HTF Boiler	Backup Percentage: 12%	None	-	-
65	Orellana	3/18/2013	Parabolic trough	Operational	Spain	Orellana	Badajoz	38°59′ 31.0″ North, 5°32′ 56.0″ West	186 hectares	118,000 MWh/yr (Estimated)	-	-	8/1/2012	240,000,000 Euro	Commercial	Acciona	Acciona (100%)	-	405,500 m^2	416	124	-	-	-	-	Sener (SENERtrough)	-	-	-	-	Thermal Oil	293°C	393°C	100°C	-	50.0 MW	50.0 MW	Steam Rankine	-	-	-	Wet cooling	-	-	-	None	-	-
66	Palma del Río I	3/18/2013	Parabolic trough	Operational	Spain	Palma del Río	Córdoba	37°38′ 42.0″ North, 5°15′ 29.0″ West	135 hectares	114,500 MWh/yr (Estimated)	2,291 kWh/m2/yr	Acciona Energía	7/1/2011	-	-	Acciona Energía	Acciona Energía (100%)	Acciona Energía	372240 m^2	792	99	8	12	470 m^2	100 m	-	-	-	-	-	Biphenyl/Diphenyl oxide	-	393°C	-	-	50.0 MW	50.0 MW	Steam Rankine	-	-	-	Wet cooling	-	-	-	None	-	-
67	Palma del Río II	3/18/2013	Parabolic trough	Operational	Spain	Palma del Río	Córdoba	37°38′ 42.0″ North, 5°15′ 29.0″ West	135 hectares	114,500 MWh/yr (Estimated)	2,291 kWh/m2/yr	Acciona Energía	12/1/2010	-	-	Acciona Energía	Acciona Energía (100%)	Acciona Energía	372,240 m^2	792	99	8	12	470 m^2	100 m	-	-	-	-	-	Biphenyl/Diphenyl oxide	-	393°C	-	-	50.0 MW	50.0 MW	Steam Rankine	-	-	-	Wet cooling	-	-	-	None	-	-
68	Solaben 1	10/3/2013	Parabolic trough	Operational	Spain	Logrosán	Cáceres	39°13′ 29.0″ North, 5°23′ 26.0″ West	110 hectares	100,000 MWh/yr (Estimated)	-	Abengoa Solar	8/1/2013	-	Commercial	Abengoa	Abengoa (100%)	Abengoa	300,000 m^2	360	-	4	12	-	150 m	Abengoa (ASTRØ)	-	12,960	-	-	Thermal Oil	293°C	393°C	100°C	-	50.0 MW	50.0 MW	Steam Rankine	-	-	100.0 bar	Wet cooling	Cooling tower	HTF Boiler	-	None	-	-
69	Solaben 2	10/3/2013	Parabolic trough	Operational	Spain	Logrosán	Cáceres	39°13′ 29.0″ North, 5°23′ 26.0″ West	110 hectares	100,000 MWh/yr (Estimated)	-	Abengoa Solar	10/1/2012	-	Commercial	Abengoa ; ITOCHU	Abengoa (70%)	Abengoa	300,000 m^2	360	-	4	12	-	150 m	Abengoa (ASTRØ)	-	12,960	-	-	Thermal Oil	293°C	393°C	100°C	-	50.0 MW	50.0 MW	Steam Rankine	-	-	100.0 bar	Wet cooling	Cooling tower	HTF Boiler	-	None	-	-
70	Solaben 3	10/3/2013	Parabolic trough	Operational	Spain	Logrosán	Cáceres	39°13′ 29.0″ North, 5°23′ 26.0″ West	110 hectares	100,000 MWh/yr (Estimated)	-	Abengoa Solar	6/1/2012	-	Commercial	Abengoa ; ITOCHU	Abengoa (70%)	Abengoa	300,000 m^2	360	-	4	12	-	150 m	Abengoa (ASTRØ)	-	12,960	-	-	Thermal Oil	293°C	393°C	100°C	-	50.0 MW	50.0 MW	Steam Rankine	-	-	100.0 bar	Wet cooling	Cooling tower	HTF Boiler	-	None	-	-
71	Solaben 6	10/3/2013	Parabolic trough	Operational	Spain	Logrosán	Cáceres	39°13′ 29.0″ North, 5°23′ 26.0″ West	110 hectares	100,000 MWh/yr (Estimated)	-	Abengoa Solar	8/1/2013	-	Commercial	Abengoa	Abengoa (100%)	Abengoa	300,000 m^2	360	-	4	12	-	150 m	Abengoa (ASTRØ)	-	12,960	-	-	Thermal Oil	293°C	393°C	100°C	-	50.0 MW	50.0 MW	Steam Rankine	-	-	100.0 bar	Wet cooling	Cooling tower	HTF Boiler	-	None	-	-
72	Solacor 1	8/24/2012	Parabolic trough	Operational	Spain	El Carpio	Córdoba	37°54′ 54.0″ North, 4°30′ 9.0″ West	110 hectares	100,000 MWh/yr (Estimated)	-	Abengoa Solar	2/1/2012	-	Commercial	Abengoa Solar ; JGC	Abengoa Solar (74%)	Abengoa Solar	300,000 m^2	360	-	4	12	-	150 m	Abengoa Solar (ASTRØ)	-	12,960	-	-	Thermal Oil	293°C	393°C	100°C	-	50.0 MW	50.0 MW	Steam Rankine	-	-	100.0 bar	Wet cooling	Cooling tower	HTF Boiler	-	None	-	-
73	Solacor 2	8/24/2012	Parabolic trough	Operational	Spain	El Carpio	Córdoba	37°54′ 54.0″ North, 4°30′ 9.0″ West	110 hectares	100,000 MWh/yr (Estimated)	-	Abengoa Solar	3/9/2012	-	Commercial	Abengoa Solar ; JGC	Abengoa Solar (74%)	Abengoa Solar	300,000 m^2	360	-	4	12	-	150 m	Abengoa Solar (ASTRØ)	-	12,960	-	-	Thermal Oil	293°C	393°C	100°C	-	50.0 MW	50.0 MW	Steam Rankine	-	-	100.0 bar	Wet cooling	Cooling tower	HTF Boiler	-	None	-	-
74	Solnova 1	8/24/2012	Parabolic trough	Operational	Spain	Sevilla	Sanlúcar la Mayor	37°26′ 30.97″ North, 6°14′ 59.98″ West	115 hectares	113,520 MWh/yr (Expected/Planned), Gross generation	2,012 kWh/m2/yr	Abengoa Solar	1/1/2009	-	Commercial	Abengoa Solar	Abengoa Solar	Abengoa Solar	300,000 m^2	360	-	4	-	833 m^2	150 m	Abengoa Solar (Astro)	Rioglass	-	Schott	-	Thermal oil	-	393°C	-	-	50.0 MW	50.0 MW	Steam Rankine	-	-	100.0 bar	Wet cooling	-	HTF boiler	-	None	-	-
75	Solnova 3	8/24/2012	Parabolic trough	Operational	Spain	Sevilla	Sanlúcar la Mayor	37°26′ 30.97″ North, 6°14′ 59.98″ West	115 hectares	113,520 MWh/yr (Expected/Planned), Gross generation	2,012 kWh/m2/yr	Abengoa Solar	1/1/2009	-	Commercial	Abengoa Solar	Abengoa Solar	Abengoa Solar	300,000 m^2	360	-	4	-	833 m^2	150 m	Abengoa Solar (Astro)	Rioglass	-	Schott	-	Thermal oil	-	393°C	-	-	50.0 MW	50.0 MW	Steam Rankine	-	-	100.0 bar	Wet cooling	-	HTF boiler	-	None	-	-
76	Solnova 4	8/24/2012	Parabolic trough	Operational	Spain	Sevilla	Sanlúcar la Mayor	37°26′ 30.97″ North, 6°14′ 59.98″ West	115 hectares	113,520 MWh/yr (Expected/Planned), Gross generation	2,012 kWh/m2/yr	Abengoa Solar	1/1/2009	-	Commercial	Abengoa Solar	Abengoa Solar	Abengoa Solar	300,000 m^2	360	-	4	-	833 m^2	150 m	Abengoa Solar (Astro)	Rioglass	-	Schott	-	Thermal oil	-	393°C	-	-	50.0 MW	50.0 MW	Steam Rankine	-	-	100.0 bar	Wet cooling	-	HTF boiler	-	None	-	-
77	Termesol 50(Valle 2)	7/3/2015	Parabolic trough	Operational	Spain	San José del Valle	Cádiz	36°39′ 40.0″ North, 5°50′ 50.0″ West	230 hectares	175,000 MWh/yr (Expected)	2,097 kWh/m2/yr	Torresol	12/1/2011	270,000,000 Euro	-	Torresol	Torresol (100%)	Torresol	510,120 m^2	624	156	4	-	817 m^2	-	Sener (SenerTrough)	-	-	-	-	Diphenyl/Diphenyl oxide	293°C	393°C	100°C	-	49.9 MW	49.9 MW	Steam Rankine	-	38.1% @ full load	100.0 bar	Wet cooling	-	Natural gas	-	2-tank indirect	7.5 hours	28,500 tons of molten salt. 60% sodium nitrate, 40% potassium nitrate.
78	Termosol 1	3/14/2013	Parabolic trough	Operational	Spain	Navalvillar de Pela	Badajoz	39°11′ 35.0″ North, 5°34′ 34.0″ West	200 hectares	180,000 MWh/yr (Estimated)	-	-	3/1/2013	-	Commercial	NextEra, FPL	NextEra, FPL (100%)	-	523,200 m^2	640	160	4	-	817 m^2	-	Sener (SENERtrough)	Flabeg (RP3)	-	-	-	Thermal Oil	293°C	393°C	100°C	-	50.0 MW	50.0 MW	Steam Rankine	-	-	-	Wet cooling	-	HTF Heaters (3x16MWt)	-	2-tank indirect	9 hours	60% Sodium Nitrate, 40% Potassium Nitrate
79	Termosol 2	3/14/2013	Parabolic trough	Operational	Spain	Navalvillar de Pela	Badajoz	39°11′ 35.0″ North, 5°34′ 34.0″ West	200 hectares	180,000 MWh/yr (Estimated)	-	-	3/1/2013	-	Commercial	NextEra, FPL	NextEra, FPL (100%)	-	523,200 m^2	640	160	4	-	817 m^2	-	Sener (SENERtrough)	Flabeg (RP3)	-	-	-	Thermal Oil	293°C	393°C	100°C	-	50.0 MW	50.0 MW	Steam Rankine	-	-	-	Wet cooling	-	HTF Heaters (3x16MWt)	-	2-tank indirect	9 hours	60% Sodium Nitrate, 40% Potassium Nitrate
80	Andasol-4 (AS-4)	11/23/2010	Parabolic trough	Under construction	Spain	Puebla de Don Fadrique	Granada	-	200 hectares	158,000 MWh/yr (Expected/Planned)	2,136 kWh/m2/yr	ACS/Cobra Group	1/1/2020	-	Commercial	ACS/Cobra Group Cobra Instalaciones y Servicios	ACS/Cobra Group (100%)	Cobra O&M	510,120 m^2	624	156	4	12	817 m^2	144 m	Cobra Instalaciones y Servicios (SENERTROUGH)	Flabeg (RP3)	22,464	Solel (UVAC 2008)	Evacuated (4 m)	Diphenyl/Biphenyl oxide	293°C	393°C	100°C	-	50.0 MW	49.9 MW	Steam Rankine	-	-	100.0 bar	Wet cooling	Cooling tower	HTF heater	Annual Solar-to-Electricity Efficiency (Gross): 16%, Backup Percentage: 12%	2-tank indirect	7.5 hours	28,500 tons of molten salt. 60% sodium nitrate, 40% potassium nitrate. 1,010 MWh. Tanks are 14 m high and 36 m in diameter.
81	Caceres	2/20/2013	Parabolic trough	Under construction	Spain	Valdeobispo	Caceres	40°3′ 38.0″ North, 6°16′ 32.0″ West	200 hectares	170,000 MWh/yr (Expected)	-	COBRA	3/1/2013	-	Commercial	ACS - COBRA group	ACS - COBRA group (100%)	-	510,120 m^2	624	156	4	12	817 m^2	144 m	Sener (SenerTrough)	Flabeg (RP3)	22,464	Solel (UVAC 2008)	Evacuated (4 m)	-	293°C	393°C	-	Diphenyl/Biphenyl oxide	50.0 MW	50.0 MW	Steam Rankine	SST-700 Siemens	38.1% @ full load	100.0 bar	Wet cooling	Cooling tower	HTF heater	Backup Percentage: 12%	2-tank indirect	7.5 hours	60% Sodium Nitrate, 40% Potassium Nitrate
82	EL REBOSO II 50-MW Solar Thermal Power Plant	8/27/2009	Parabolic trough	Under construction	Spain	Sevilla	La Puebla del Río	37°4′ 57.0″ North, 6°3′ 5.0″ West	160 hectares	110,006 MWh/yr (Expected/Planned)	2,200 kWh/m2/yr	Bogaris	-	-	Commercial	Bogaris	Bogaris (100%)	Bogaris	319,057 m^2	-	96	4	-	865 m^2	150 m	(SKALET 150)	Flabeg	-	-	-	Diphenyl/Biphenyl oxide	296°C	393°C	97°C	-	50.0 MW	-	Steam Rankine	-	34% @ full load	100.0 bar	Wet cooling	Cooling tower	Natural gas	Electricity Efficiency (Gross): 17% Backup Percentage: 0%	None	-	-
83	EL REBOSO III 50-MW Solar Thermal Power Plant	8/27/2009	Parabolic trough	Under contract	Spain	Sevilla	Utrera	37°4′ 20.0″ North, 5°56′ 57.0″ West	242 hectares	181,120 MWh/yr (Expected/Planned)	3,622 kWh/m2/yr	Bogaris	-	-	Commercial	Bogaris	Bogaris (100%)	Bogaris	518,469 m^2	-	156	4	12	865 m^2	150 m	(SKALET 150)	-	-	-	-	Diphenyl/Biphenyl oxide	296°C	393°C	97°C	-	50.0 MW	-	Steam Rankine	-	34% @ full load	100.0 bar	Wet cooling	Cooling tower	Natural gas	Electricity Efficiency (Gross): 17% Backup Percentage: 0%	Other	116 MWH	28,500 tons of molten salt (60% sodium nitrate, 40% potassium nitrate). Tanks are 14 m high and 11,9 m in diameter.
84	Thai Solar Energy 1	1/23/2015	Parabolic trough	Operational	Thailand	Huai Kachao	Kanchanaburi Province	14°20′ 1.0″ North, 99°42′ 33.0″ East	110 hectares	8,000 MWh/yr (Expected)	-	Solarlite GmbH	1/25/2012	-	Commercial	Solarlite GmbH	Thai Solar Energy Co.Ltd. (100%)	Thai Solar Energy Co.Ltd.	45,000 m^2	86	19	-	10	-	120 m	Solarlite GmbH (SL 4600)	Guardian & AGC	-	-	-	Water/Steam	201°C	340°C	139°C	-	5.0 MW	5.0 MW	-	MAN (MARC 2)	-	30.0 bar	Wet cooling	Cooling tower	-	Annual Solar-to-Electricity Efficiency (Gross): 12%	None	-	-
85	Shams 1	10/21/2016	Parabolic trough	Operational	United Arab Emirates	Madinat Zayed	120 km southwest of Abu Dhabi	23°34′ 13.0″ North, 53°42′ 56.0″ East	250 hectares	210,000 MWh/yr	1,934 kWh/m2/yr	-	3/17/2013	600,000,000 USD	Commercial	Masdar/Total/Abengoa Solar EPC Abener/Teyma	Masdar (80%) Total (20%)	-	627,840 m^2	768	192	4	12	-	150 m	Abengoa Solar (ASTRO)	-	27,648	Schott (PTR 70)	-	Therminol VP-1	300°C	400°C	100°C	Solutia	100.0 MW	100.0 MW	Steam Rankine	Man	-	-	Dry cooling	-	Natural gas	-	None	-	-
86	Saguaro Power Plant	6/10/2015	Parabolic trough	Operational	United States	Red Rock	Southwest USA, Arizona, Pinal County	32°32′ 52.0″ North, 111°17′ 34.0″ West	16 acres	2,000 MWh/yr (Expected/Planned)	2,636 kWh/m2/yr	Arizona Public Service (APS)	1/1/2006	6,000,000 USD	Production	Arizona Public Service	Arizona Public Service (100%)	Arizona Public Service	10,340 m^2	24	3	8	12 and 8	-	97 m	Starnet (LS-2)	Flabeg	528	Schott Glass (Schott PTR70)	Evacuated (4 m)	Xceltherm 600 (solar field); n-pentane (ORC working fluid)	248°F	572°F	324°F	Radco Industries	1.16 MW	1.0 MW	Organic Rankine	Ormat (Israel)	20.7% @ full load	323.0 psi	Wet cooling	-	-	Design-Point Solar-to-Electricity Efficiency: 12.1% Design-Point Conditions: Nominal ambient temp dry=80°F, relative humidity=30%, wet-bulb temp=60°F Annual Solar-to-Electricity Efficiency (Gross): 7.5%	None	-	-
87	Solana Generating Station	8/19/2015	Parabolic trough	Operational	United States	Phoenix	Southwest USA, Gila Bend, Arizona, Maricopa	32°55′ 0.0″ North, 112°58′ 0.0″ West	780 hectares	944,000 MWh/yr	-	Abengoa Solar	10/7/2013	2,000,000,000 USD	Commercial	Abengoa Solar	Abengoa Solar	-	2,200,000 m^2	3232	808	4	10	-	-	Abengoa Solar (E2)	-	-	-	-	Therminol VP-1 --- Xceltherm MK1	293°C	393°C	-	Solutia --- Radco Industries	280.0 MW (2x140 MW)	250.0 MW	Steam Rankine	-	-	100.0 bar	Wet cooling	-	Natural gas	-	2-tank indirect	6 hours	Molten salt
89	Genesis Solar Energy Project	4/25/2014	Parabolic trough	Operational	United States	Blythe	California, Riverside	33°40′ North, 114°59′ West	1,950 acres	580,000 MWh/yr (Expected/Planned)	-	NextEra Energy Resources	3/1/2014	-	Commercial	Genesis Solar, LLC ; NextEra Energy Resources, LLC	Genesis Solar, LLC	Genesis Solar, LLC	-	1840	460	4	-	-	-	Sener (SenerTrough)	Flabeg (RP3)	-	-	-	Therminol VP-1	-	740°F	-	Solutia	250.0 MW (2x125 MW)	250.0 MW	Steam Rankine	-	-	-	Dry cooling	Air cooled condenser	-	-	None	-	-
90	Mojave Solar Project	7/1/2015	Parabolic trough	Operational	United States	Harper Dry Lake	California, San Bernardino	35°1′ North, 117°20′ West	1,765 acres	600,000 MWh/yr (Expected/Planned)	-	Abengoa Solar	12/1/2014	1,600,000 USD	Commercial	Mojave Solar, LLC ; Abengoa Solar, Inc.	Mojave Solar, LLC	-	-	-	-	-	-	-	-	Abengoa Solar	Rioglass	-	Schott (PTR70)	-	Therminol VP-1	-	-	-	-	280.0 MW (2x140 MW)	250.0 MW	Steam Rankine	-	-	-	Wet cooling	Cooling tower	-	-	None	-	-
91	Solar Electric Generating Station I	5/22/2009	Parabolic trough	Operational	United States	Daggett	California, San Bernardino, Mojave Desert	34°51′ 47.0″ North, 116°49′ 37.0″ West	-	-	2,725 kWh/m2/yr	Cogentrix	12/20/1984	-	-	Luz	Cogentrix (100%)	Cogentrix	82,960 m^2	-	-	-	-	-	-	Luz (LS-1)	-	-	-	-	-	-	307°C	-	-	13.8 MW	13.8 MW	MHI regenerative steam turbine	-	31.5% @ full load	40.0 bar	-	-	-	-	2-tank direct	3 hours	Storage system was damaged by fire in 1999 and was not replaced
92	Solar Electric Generating Station II	12/3/2013	Parabolic trough	Operational	United States	Daggett	California, San Bernardino, Mojave Desert	34°51′ 47.0″ North, 116°49′ 37.0″ West	-	-	2,725 kWh/m2/yr	Cogentrix	1/1/1985	-	-	Luz	Cogentrix (100%)	Cogentrix	190,338 m^2	-	-	-	-	-	-	Luz (LS-1)	-	-	-	-	-	-	316°C	-	-	33.0 MW	30.0 MW	-	-	29.4% @ full load	40.0 bar	-	-	Natural gas	-	-	-	-
93	Solar Electric Generating Station III	10/1/2015	Parabolic trough	Operational	United States	Kramer Junction	California, San Bernardino, Mojave Desert	35°0′ 51.0″ North, 117°33′ 32.0″ West	-	-	2,725 kWh/m2/yr	NextEra Energy	12/31/1985	-	-	Luz	NextEra (50%)	NextEra	230,300 m^2	-	-	-	-	-	-	Luz (LS-2)	-	-	Solel Solar Systems (Solel UVAC)	Evacuated (4 m)	Therminol	-	349°C	-	-	33.0 MW	30.0 MW	-	-	30.6% @ full load	40.0 bar	-	-	Natural gas	-	-	-	-
94	Solar Electric Generating Station IV	10/1/2015	Parabolic trough	Operational	United States	Kramer Junction	California, San Bernardino, Mojave Desert	35°0′ 51.0″ North, 117°33′ 32.0″ West	-	-	2,725 kWh/m2/yr	NextEra Energy	2/1/1989	-	-	Luz	NextEra (38%)	NextEra	230,300 m^2	-	-	-	-	-	-	Luz (LS-2)	-	-	Solel Solar Systems (Solel UVAC)	Evacuated (4 m)	Therminol	-	349°C	-	-	33.0 MW	30.0 MW	-	-	30.6% @ full load	40.0 bar	-	-	Natural gas	-	-	-	-
95	Solar Electric Generating Station V	10/1/2015	Parabolic trough	Operational	United States	Kramer Junction	California, San Bernardino, Mojave Desert	35°0′ 51.0″ North, 117°33′ 32.0″ West	-	-	2,725 kWh/m2/yr	NextEra Energy	2/1/1989	-	-	Luz	NextEra (46%)	NextEra	250,500 m^2	-	-	-	-	-	-	Luz (LS-2)	-	-	Solel Solar Systems (Solel UVAC)	Evacuated (4 m)	Therminol	-	349°C	-	-	33.0 MW	30.0 MW	-	-	30.6% @ full load	40.0 bar	-	-	Natural gas	-	-	-	-
96	Solar Electric Generating Station VI	10/1/2015	Parabolic trough	Operational	United States	Kramer Junction	California, San Bernardino, Mojave Desert	35°0′ 51.0″ North, 117°33′ 32.0″ West	-	-	2,725 kWh/m2/yr	NextEra Energy	2/1/1989	-	-	Luz	NextEra (41%)	NextEra	188,000 m^2	-	-	-	-	-	-	Luz (LS-2)	-	-	Solel Solar Systems (Solel UVAC)	Evacuated (4 m)	Therminol	-	390°C	-	-	35.0 MW	30.0 MW	-	-	37.5% @ full load	100.0 bar	-	-	Natural gas	-	-	-	-
97	Solar Electric Generating Station VII	10/1/2015	Parabolic trough	Operational	United States	Kramer Junction	California, San Bernardino, Mojave Desert	35°0′ 51.0″ North, 117°33′ 32.0″ West	-	-	2,725 kWh/m2/yr	NextEra Energy	2/1/1989	-	-	Luz	NextEra (50%)	NextEra	194,280 m^2	-	-	-	-	-	-	Luz (LS-2)	-	-	Solel Solar Systems (Solel UVAC)	Evacuated (4 m)	Therminol	-	390°C	-	-	35.0 MW	30.0 MW	-	-	37.5% @ full load	100.0 bar	-	-	Natural gas	-	-	-	-
98	Solar Electric Generating Station VIII	10/1/2015	Parabolic trough	Operational	United States	Harper Dry Lake	California, San Bernardino, Mojave Desert	35°1′ 54.0″ North, 117°20′ 53.0″ West	-	-	2,725 kWh/m2/yr	NextEra Energy	12/1/1989	-	-	Luz	NextEra (50%)	NextEra	464,340 m^2	-	-	-	-	-	-	Luz (LS-3)	-	-	Solel Solar Systems (Solel UVAC)	Evacuated (4 m)	Therminol	-	390°C	-	-	89.0 MW	80.0 MW	-	-	37.6% @ full load	100.0 bar	-	-	Natural gas	-	-	-	-
99	Solar Electric Generating Station IX	10/1/2015	Parabolic trough	Operational	United States	Harper Dry Lake	California, San Bernardino, Mojave Desert	35°1′ 54.0″ North, 117°20′ 53.0″ West	-	-	2,725 kWh/m2/yr	NextEra Energy	10/1/1990	-	-	Luz	NextEra (50%)	NextEra	483,960 m^2	-	-	-	-	-	-	Luz (LS-3)	-	-	Solel Solar Systems (Solel UVAC)	Evacuated (4 m)	Therminol	-	390°C	-	-	89.0 MW	80.0 MW	-	-	37.6% @ full load	100.0 bar	-	-	Natural gas	-	-	-	-
100	Colorado Integrated Solar Project	11/21/2013	Parabolic trough	Currently Non-Operational	United States	Palisade	Colorado	39°8′ 54.96″ North, 108°19′ 5.1234″ West	6 acres	-	-	Xcel Energy	1/1/2010	4,500,000 USD	Demonstration	Xcel Energy ; Abengoa Solar	Xcel Energy (100%)	Xcel Energy	6,540 m^2	8	4	2	-	817 m^2	150 m	-	-	-	-	-	Xceltherm® 600	190°C	300°C	110°C	-	2.0 MW	2.0 MW	Solar hybrid	-	-	-	Wet cooling	-	-	-	None	-	-
101	Martin Next Generation Solar Energy Center	1/25/2013	Parabolic trough	Operational	United States	Indiantown	Florida, Martin, South Florida	27°3′ 13.0″ North, 80°33′ 46.0″ West	500 acres	155,000 MWh/yr (Estimated)	-	Florida Power & Light Company	12/1/2010	476,300,000 USD	-	Florida Power & Light Co.	Florida Power & Light Co. (100%)	Florida Power & Light Co.	464,908 m^2	1136	142	8	6	-	72 m	Gossamer Space Frames (LAT 1)	-	-	Solel (UVAC 2008)	-	Dowtherm A	-	-	-	-	75.0 MW	75.0 MW	Steam Rankine	-	-	-	Wet cooling	-	-	-	None	-	-
102	Holaniku at Keahole Point	8/20/2015	Parabolic trough	Operational	United States	Keahole Point	Hawaii	19°43′ North, 156°2′ West	3 acres	4,030 MWh/yr	-	-	12/1/2009	-	-	Keahole Solar Power, LLC ; Sopogy	Keahole Solar Power, LLC	Sopogy, Inc.	-	1008	-	-	-	-	-	Sopogy (SopoNova®)	-	-	-	-	Xceltherm® 600	93°C	176°C	83°C	Radco Industries	2.0 MW	2.0 MW	Steam Rankine	-	-	-	Wet cooling	-	-	2 MW thermal power; at ~350 F, can theoretically produce 200 kW electric power at 10% thermal-to-electric efficiency factor	Other	2 Hours	-
103	Nevada Solar One	9/7/2011	Parabolic trough	Operational	United States	Boulder City	Nevada, Clark	35°48′ North, 114°59′ West	400 acres	134,000 MWh/yr (Expected/Planned)	2,606 kWh/m2/yr	Acciona Energía	6/1/2007	266,000,000 USD	Commercial	Acciona Solar Power	Acciona Energía (100%)	Acciona Solar Power	357,200 m^2	760	-	8	-	470 m^2	100 m	Acciona Solar Power (SGX-2)	Flabeg	18,240	Schott/Solel	-	DOWTHERM A	318°C	393°C	75°C	Dow Chemical	75.0 MW	72.0 MW	-	-	-	-	Wet cooling	-	-	-	0.5 hour(s)	-	0.5 hours full-load storage
104	Stillwater GeoSolar Hybrid Plant	10/21/2016	Parabolic trough	Operational	United States	Fallon	Nevada	39°32′ 53.0″ North, 118°33′ 20.0″ West	21 acres	3,000 MWh/yr (Estimated)	-	NREL	3/1/2015	-	-	Enel Green Power	Enel Green Power	Enel Green Power	-	-	-	-	8	656 m^2	115 m	SkyFuel (SkyTrough®)	SkyFuel (ReflecTech®)	-	-	-	-	-	-	-	Demineralised water	2.0 MW	2.0 MW	Organic Rankine	-	-	-	-	-	-	-	None	-	-
105	Fort Irwin Solar Power Project	3/18/2011	Parabolic trough	Under development	United States	California Ft. Irwin	Mojave Desert	-	14,000 acres	125,000 MWh/yr (Expected/Planned)	-	Acciona Solar	-	2,000,000,000 dollars	-	Acciona Solar Power ; Clark Energy Group	Acciona Solar Power (100%)	-	-	-	-	-	-	-	-	-	-	-	-	-	-	-	-	-	-	500.0 MW	-	Steam Rankine	-	-	-	-	-	-	-	-	-	-
106	Mt. Signal Solar Plant - tentative	1/21/2011	Parabolic trough	Under development	United States	California Imperial County	-	-	-	-	-	-	1/1/2020	-	-	MMR Power Solutions	-	-	-	-	-	-	-	-	-	-	-	-	-	-	-	-	-	-	-	50.0 MW	-	Steam Rankine	-	-	-	-	-	-	-	-	-	-
107	NextEra Beacon Solar Energy Project	1/21/2011	Parabolic trough	Under development	United States	California Kern	-	35°16′ North, 118°0′ 30.0″ West	2,012 acres	-	-	-	-	1,000,000,000 USD	-	NextEra Energy	-	-	-	-	-	-	-	-	-	-	-	-	-	-	-	-	-	-	-	250.0 MW	-	Steam Rankine	-	-	-	-	-	-	-	-	-	-
108	Palmdale Hybrid Power Plant	10/20/2011	Parabolic trough	Under development	United States	California Victorville	-	-	377 acres	-	-	Inland Energy, Inc.	-	-	-	Inland Energy, Inc.	City of Palmdale	-	-	-	-	-	-	-	-	-	-	-	-	-	-	-	-	-	-	50.0 MW	-	Steam Rankine	-	-	-	Wet cooling	-	-	-	-	-	-
109	Ridgecrest Solar Power Project	1/21/2011	Parabolic trough	Under development	United States	California Ridgecrest	-	-	1,440 acres	-	-	-	-	-	-	Solar Millennium, LLC	-	-	-	-	-	-	-	-	-	-	-	-	-	-	-	-	-	-	-	250.0 MW	-	Steam Rankine	-	-	-	Dry cooling	-	-	-	-	-	-
110	Sonoran Solar Energy Project	2/17/2011	Parabolic trough	Under development	United States	Arizona Little Rainbow Valley	-	-	13,440 acres	-	-	-	1/1/2020	-	-	Boulevard Associates LLC	-	-	-	-	-	-	-	-	-	-	-	-	-	-	-	-	-	-	-	375.0 MW	-	Steam Rankine	-	-	-	-	-	-	-	-	-	-
111	UA Tech Park Thermal Storage Demonstration Project	10/20/2011	Parabolic trough	Under development	United States	Arizona Tucson	-	-	200 acres	-	-	UA Tech Park	-	32,000,000 USD	-	Bell Independent Power Corp.	Bell Independent Power Corp.	-	-	-	-	-	-	-	-	-	-	-	-	-	-	-	-	-	-	5.0 MW	-	Steam Rankine	-	-	-	-	-	-	-	-	-	-
112	Victorville 2 Hybrid Power Plant	10/20/2011	Parabolic trough	Under development	United States	California Victorville	-	-	-	-	-	Inland Energy, Inc.	-	-	-	-	-	-	-	-	-	-	-	-	-	-	-	-	-	-	-	-	-	-	-	50.0 MW	-	Steam Rankine	-	-	-	-	-	-	-	-	-	-
1	ISCC Hassi R'mel	4/15/2015	Parabolic trough	Operational	Algeria	Hassi R'mel	Hassi R'mel	33°7′ 27.0″ North, 3°21′ 25.0″ East	64 hectares	-	-	Abener	7/14/2011	315,000,000 Euro	Commercial	Abener	Sonatrach (100%)	Abener	183,860 m^2	224	56	4	-	-	150 m	Abengoa Solar (ASTR-Ø)	Rioglass	8,064	Schott (PTR 70)	-	Thermal oil	293°C	393°C	100°C	-	20.0 MW	20.0 MW	Steam Rankine	Siemens SST-900	-	-	Dry cooling	Aero condensers	-	-	None	-	-

2- Plants with power tower CSP technology

S/N	Plant Name	Status Date	Technology	Status	Country	City	Region	Lat/Long Location	Land Area	Electricity Generation	Solar Resource	Company	Start Production	Cost (approx)	Project Type	Developer(s)	Owner(s) (%)	Operator(s)	Heliostat Solar-Field Aperture Area	# of Heliostats	Heliostat Aperture Area	Heliostat Manufacturer	Heliostat Description	Tower Height	Receiver Manufacturer	Receiver Type	General	HTF Type	Solar-Field Inlet Temp	Solar-Field Outlet Temp	Solar-Field Temp Difference	HTF Company	Turbine Capacity (Gross)	Turbine Capacity (Net)	Output Type	Turbine Manufacturer	Turbine Efficiency	Power Cycle Pressure	Cooling Method	Cooling Method Description	Fossil Backup Type	General	Storage Type	Storage Capacity	Thermal Storage Description	S/N	Plant Name	Status Date
1	Jemalong Solar Thermal Station	7/25/2016	Power tower	Operational	Australia	Jemalong	New South Wales	33°24' South, 148°6' East	10 hectares	2,200 MWh/yr	-	Vast Solar	1/1/2016	10,000,000 AUD	Pilot	Vast Solar	Vast Solar	Vast Solar	15,000 m²	3,500	-	Vast Solar	Standard AziEle	30 m	Vast Solar	-	-	Liquid sodium	270°C	560°C	290°C	-	1.1 MW	-	Steam Rankine	-	-	-	Dry cooling	MACCSOL Air Cooled Condenser	-	-	2-tank direct	3 hours	Liquid sodium	1	Jemalong Solar Thermal Station	7/25/2016
2	Lake Cargelligo	5/8/2014	Power tower	Operational	Australia	Lake Cargelligo	New South Wales	33°19' 42.0" South, 146°24' 15.0" East	-	-	-	-	5/1/2011	-	Demonstration	Lloyd Energy Systems Pty Ltd	Graphite Energy (100%)	Graphite Energy	6,080 m²	620	9.8 m²	-	-	-	Lloyd Energy Systems Pty Ltd	Graphite solar storage receiver	-	Water/Steam	200°C	500°C	300°C	-	3.0 MW	3.0 MW	Steam Rankine	-	-	50.0 bar	-	-	-	-	Other	-	Core graphite thermal-storage technology	2	Lake Cargelligo	5/8/2014
3	Sundrop CSP Project	10/26/2016	Power tower	Operational	Australia	Port Augusta	-	32°35' 38.0" South, 137°51' 21.0" East	-	1,700 MWh/yr	-	Webmaster Solar	10/6/2016	-	-	Aalborg CSP	Sundrop Farms EPC John Holland	Aalborg CSP	51,505 m²	23,712	-	eSolar (SCSS)	-	127 m	-	-	-	Water/Steam	-	-	-	-	1.5 MW	1.5 MW	Steam Rankine	-	-	-	-	-	-	-	None	-	-	3	Sundrop CSP Project	10/26/2016
4	Atacama-1	7/1/2015	Power tower	Under construction	Chile	Calama	II Región de Antofagasta	-	700 hectares	-	-	Abengoa Solar	6/1/2018	-	-	Abengoa Solar	Abengoa Solar (100%)	Abengoa Solar	1,484,000 m²	10,600	140.0 m²	-	-	243 m	-	-	Receiver Panel Height (for external receiver): 32 m Receiver Diameter (for external receiver): 19 m	Molten Salt	300°C	550°C	250°C	-	110.0 MW	110.0 MW	Steam Rankine	-	-	-	-	-	-	-	2-tank direct	17.5 hours	Molten salt	4	Atacama-1	7/1/2015
5	Copiapó	11/25/2015	Power tower	Under development	Chile	Copiapó	-	-	-	1,800,000 MWh/yr (Expected)	-	Solar Reserve	1/1/2019	-	-	Solar Reserve	-	-	-	-	-	-	-	-	-	-	-	-	-	-	-	260.0 MW (2x130 MW)	260.0 MW (2x130 MW)	Steam Rankine	-	-	-	-	Dry cooling	-	-	2-tank direct	14 hours	Molten salt	5	Copiapó	11/25/2015
6	Dahan Power Plant	2/13/2014	Power tower	Operational	China	Beijing	-	40°22' 55.0" North, 115°56' 15.0" East	13 acres	1,950 MWh/yr	1,290 kWh/m2/yr	Institute of Electrical Engineering of Chinese Academy of Sciences	8/1/2012	32,000,000 CNY	Demonstration and experimental platform	-	-	Institute of Electrical Engineering of Chinese Academy of Sciences	10,000 m²	100	100.0 m²	Himin Solar	64 facets, each facet 1.25x1.25 m2	118 m	-	Cavity Receiver (5x5 m)	-	Water/Steam	104°C	400°C	296°C	-	-	-	-	-	-	-	-	-	-	-	-	-	-	6	Dahan Power Plant	2/13/2014
7	Dunhuang 100 MW Molten Salt CSP Project	9/26/2016	Power tower	Under development	China	Dunhuang	Gansu Province	-	-	-	-	-	-	-	-	SunCan	Beijing Shouhang IHW	-	-	-	-	-	-	-	-	-	-	-	-	-	-	100.0 MW	100.0 MW	-	-	-	-	-	-	-	2-tank indirect	11 hours	Molten salt	7	Dunhuang 100 MW Molten Salt CSP Project	9/26/2016
8	Golden Tower 100MW Molten Salt project	9/26/2016	Power tower	Under development	China	Jinta	Gansu Province	-	-	-	-	-	-	-	-	SunCan	China Three Gorges New Energy Co., Ltd	-	-	-	-	-	-	-	-	-	-	-	-	-	-	100.0 MW	100.0 MW	Steam Rankine	-	-	-	-	-	-	-	2-tank direct	8 hours	Molten Salt	8	Golden Tower 100MW Molten Salt project	9/26/2016
9	Golmud	2/25/2016	Power tower	Under construction	China	Golmud	-	-	25 km2	1,120,000 MWh/yr	-	-	7/1/2018	5,380,000,000 RMB	-	Qinghai CSP Electric Power Group	-	-	-	-	-	-	-	-	-	-	-	Molten salt	-	-	-	-	200.0 MW (2x100)	200.0 MW	-	-	-	-	-	-	-	2-tank direct	15 hours	Molten salt	9	Golmud	2/25/2016
10	Hami 50 MW CSP Project	9/26/2016	Power tower	Under development	China	Hami	Xinjiang Autonomous Region	-	-	-	-	-	-	-	-	Supcon Solar	Northwest Electric Power Design Institute	-	-	-	-	-	-	-	-	-	-	-	-	-	-	50.0 MW	50.0 MW	-	-	-	-	-	-	-	2-tank direct	8 hours	Molten Salt	10	Hami 50 MW CSP Project	9/26/2016
11	Huanghe Qinghai Delingha 135 MW DSG Tower CSP Project	11/10/2016	Power tower	Under development	China	Delingha	Qinghai Province	-	13 km2	628,448 MWh/yr	-	-	1/1/2017	-	-	BrightSource Energy	Huanghe Hydropower Development Corp.	-	-	-	-	-	-	-	-	-	-	-	-	-	-	135.0 MW	135.0 MW	Steam Rankine	-	-	-	Dry cooling	-	-	-	2-tank indirect	3.7 hours	Molten salt	11	Huanghe Qinghai Delingha 135 MW DSG Tower CSP Project	11/10/2016
12	Qinghai Gonghe 50 MW CSP Plant	9/26/2016	Power tower	Under development	China	Gonghe	Qinghai Province	-	-	-	-	-	-	-	-	Supcon Solar	Northwest Engineering Corp.	-	-	-	-	-	-	-	-	-	-	-	-	-	-	50.0 MW	50.0 MW	Steam Rankine	-	-	-	-	-	-	-	2-tank direct	6 hours	Molten Salt	12	Qinghai Gonghe 50 MW CSP Plant	9/26/2016
13	Shangyi 50MW DSG Tower CSP project	9/27/2016	Power tower	Under development	China	Shangyi	Hebei Province	-	-	-	-	-	-	-	-	-	Institute of Electrical Engineering of CAS	Dahua Engineering Management	-	-	-	-	-	-	-	-	-	Water/Steam	-	-	-	-	50.0 MW	50.0 MW	-	-	-	-	-	-	-	2-tank indirect	4 hours	Molten Salt	13	Shangyi 50MW DSG Tower CSP project	9/27/2016
14	Supcon Solar Project	9/26/2016	Power tower	Under construction	China	Delingha	Qinghai	37°21' 59.0" North, 97°17' 34.0" East	330 hectares	120,000 MWh/yr (Expected)	-	-	-	750,000,000 RMB	Commercial	SUPCON Solar	SUPCON Solar (100%)	-	434,880 m²	217,440	2.0 m²	-	-	80 m	-	-	-	Molten salt	-	-	-	-	50.0 MW	50.0 MW	Steam Rankine	-	-	-	-	-	-	-	-	6 hours	Molten Salt	14	Supcon Solar Project	9/26/2016
15	Yumen 100MW Molten Salt Tower CSP project	9/27/2016	Power tower	Under development	China	Yumen	Gansu Province	-	-	-	-	-	-	-	-	SunCan	Beijing Guohua Electric Power Co., Ltd	-	-	-	-	-	-	-	-	-	-	-	-	-	-	100.0 MW	100.0 MW	-	-	-	-	-	-	-	2-tank direct	10 hours	Molten Salt	15	Yumen 100MW Molten Salt Tower CSP project	9/27/2016
16	Yumen 50MW Molten Salt Tower CSP project	9/26/2016	Power tower	Under development	China	Yumen	Gansu Province	-	-	-	-	-	-	-	-	Shanghai Paranel Renewable Energy Company and Jiangsu Xinchen CSP Co., Ltd	Yumen Xinneng Thermal Power Co., Ltd	-	-	-	-	-	-	-	-	-	-	-	-	-	-	50.0 MW	50.0 MW	Steam Rankine	-	-	-	-	-	-	-	2-tank direct	6 hours	Molten Salt	16	Yumen 50MW Molten Salt Tower CSP project	9/26/2016
17	Jülich Solar Tower	2/12/2013	Power tower	Operational	Germany	Jülich	Rhineland	50°54' 54.0" North, 6°23' 16.0" East	17 hectares	-	902 kWh/m2/yr	-	12/1/2008	-	Demonstration	Kraftanlagen München , German Aerospace Center, Solar-Institute Jülich	DLR (100%)	DLR	17,650 m²	2,153	8.2 m²	-	-	60 m	Kraftanlagen München	-	-	Air	-	680°C	-	-	1.5 MW	1.5 MW	-	Siemens	-	-	Dry cooling	-	-	-	Other	1.5 hours	Ceramic heat sink	17	Jülich Solar Tower	2/12/2013
18	ACME Solar Tower	2/13/2014	Power tower	Operational	India	Bikaner	Rajasthan	28°11' 1.2" North, 73°14' 26.0" East	12 acres	-	-	-	4/1/2011	-	-	ACME Group ; eSolar	ACME Group (100%)	ACME Group	16,222 m²	14,280	1.136 m²	eSolar	-	46 m	Victory Energy	-	-	Water/Steam	218°C	440°C	222°C	-	2.5 MW	2.5 MW	Steam Rankine	MaxWatt	-	60.0 bar	Wet cooling	Cooling tower	-	-	None	-	-	18	ACME Solar Tower	2/13/2014
19	Ashalim Plot B	3/22/2016	Power tower	Under construction	Israel	Ashalim	Negev Desert	-	-	-	-	-	1/1/2017	-	Commercial	Megalim Solar Power Ltd	Alstom (25%)	Alstom	1,000,000 m²	50,000	20 m²	-	-	240 m	-	-	-	Water/Steam	-	-	-	-	121.0 MW	121.0 MW	Steam Rankine	-	-	-	-	-	-	-	None	-	-	19	Ashalim Plot B	3/22/2016
20	NOOR III	11/16/2015	Power tower	Under construction	Morocco	Ouarzazate	-	-	-	-	-	-	1/1/2017	-	-	ACWA	-	-	-	-	-	-	-	-	-	-	-	Molten salt	-	-	-	-	150.0 MW	150.0 MW	Steam Rankine	-	-	-	-	-	-	-	2-tank direct	8 hours	Molten salt	20	NOOR III	11/16/2015
21	Khi Solar One	2/8/2016	Power tower	Operational	South Africa	Upington	Northern Cape	28°32' 14.0" South, 21°14' 39.0" East	-	180,000 MWh/yr (Expected)	-	Abengoa Solar	2/5/2016	-	Commercial	Abengoa Solar - IDC	Abengoa Solar (51%)	Abengoa Solar	576,800 m²	4,120	140.0 m²	Abengoa Solar	-	200 m	CMI Solar	-	-	Water/Steam	-	-	-	-	50.0 MW	50.0 MW	Steam Rankine	-	-	-	Dry cooling	-	-	-	Other	2 hours	Saturated steam	21	Khi Solar One	2/8/2016
22	Redstone Solar Thermal Power Plant	9/8/2016	Power tower	Under development	South Africa	Postmasburg	-	-	-	480,000 MWh/yr	-	-	1/1/2018	-	Commercial	ACWA ; Solar Reserve EPC ACCIONA Industrial	ACWA	-	-	-	-	-	-	-	-	-	-	Molten salt	288°C	566°C	278°C	-	100.0 MW	100.0 MW	-	-	-	-	Dry cooling	-	-	-	2-tank direct	12 hours	Molten salt	22	Redstone Solar Thermal Power Plant	9/8/2016
23	Gemasolar Thermosolar Plant	11/28/2016	Power tower	Operational	Spain	Fuentes de Andalucía	Andalucía (Sevilla)	37°33' 44.95" North, 5°19' 49.39" West	195 hectares	80,000 MWh/yr	2,100kWh/m2/yr	Sener	4/1/2011	230,000,000 Euro	-	Torresol Energy EPC UTE C.T. Solar Tres	MASDAR (40%) Sener (60%)	Gemasolar 2006, S.A.	304,750 m²	2650	120.0 m²	Sener	Sheet metal stamped facet	140 m	-	Sener	-	Molten salts (sodium and potassium nitrates)	290°C	563°C	275°C	-	19.9 MW	19.9 MW	-	-	-	-	Wet cooling	-	-	-	2-tank direct	15 hours	One cold-salts tank (290°C) from where salts are pumped to the tower receiver and heated up to 565°C, to be stored in one hot-salts tank (565°C). Annual equivalent hours = 5000.	23	Gemasolar Thermosolar Plant	11/28/2016
24	Planta Solar 10	7/1/2015	Power tower	Operational	Spain	Sevilla	Sanlúcar la Mayor	37°26' 30.97" North, 6°14' 59.98" West	55 hectares	23,400 MWh/yr (Expected/Planned), Gross generation	2,012 kWh/m2/yr	Abengoa Solar	6/25/2007	-	Commercial	Abengoa Solar	Abengoa Solar	Abengoa Solar	75,000 m²	624	120.0 m²	Abengoa (Solucar 120)	Glass-metal	115 m	-	Cavity	-	Water	-	250-300°C	-	-	11.02 MW	11.0 MW	-	-	-	45.0 bar	Wet cooling	Refrigeration towers	Natural gas	-	Other	1 hour	-	24	Planta Solar 10	7/1/2015
25	Planta Solar 20	7/1/2015	Power tower	Operational	Spain	Sevilla	Sanlúcar la Mayor	37°26' 30.97" North, 6°14' 59.98" West	80 hectares	48,000 MWh/yr (Expected/Planned), Gross generation	2,012 kWh/m2/yr	Abengoa Solar	4/22/2009	-	Commercial	Abengoa Solar	Abengoa Solar	Abengoa Solar	150,000 m²	1,255	120.0 m²	Abengoa (Solucar 120)	Glass-metal	165 m	-	Cavity	-	Water	-	250-300°C	-	-	20.0 MW	20.0 MW	-	-	-	45.0 bar	Wet cooling	Refrigeration towers	Natural gas	-	Other	1 hour	-	25	Planta Solar 20	7/1/2015
26	Greenway CSP Mersin Tower Plant	11/24/2014	Power tower	Operational	Turkey	Mersin	Southern Turkey	36°51' 55.0" North, 34°36' 36.0" East	-	-	-	Greenway CSP	1/1/2012	-	Demonstration	Greenway CSP	Greenway CSP (100%)	Greenway CSP	-	-	-	-	-	-	-	-	-	Water	-	-	-	-	1.4 MW	1.0 MW	Steam Rankine	-	-	55.0 bar	-	-	-	-	Other	4 MW/h	Molten salt. Single 3-phase tank, natural circulation, super steam junction design	26	Greenway CSP Mersin Tower Plant	11/24/2014
27	Ivanpah Solar Electric Generating System	11/20/2014	Power tower	Operational	United States	Primm, NV	California, San Bernardino	35°33' 8.5" North, 115°27' 30.97" West	3,500 acres	1,079,232 MWh/yr (Expected/Planned)	2,717 kWh/m2/yr	BrightSource Energy	1/1/2014	2,200,000,000 USD	Commercial	BrightSource Energy	NRG Energy; BrightSource Energy; Google	-	2,600,000 m²	173500	15.0 m²	-	Each heliostat consists of two mirrors	459 ft	Riley Power	Solar receiver steam generator	-	Water	480°F	1050°F	570°F	-	392.0 MW	377.0 MW	Steam Rankine	Siemens SST-900	-	160.0 bar	Dry cooling	-	Natural gas	Annual Solar-to-Electricity Efficiency (Gross): 28.72%	None	-	-	27	Ivanpah Solar Electric Generating System	11/20/2014
28	Palen Solar Electric Generating System	4/4/2013	Power tower	Under development	United States	Desert Center	California, Riverside	33°50' 56.0" North, 115°14' 22.0" West	1,537 hectares	1,430,000 MWh/yr (Expected/Planned)	-	-	1/1/2016	-	-	BrightSource Energy	BrightSource Energy (100%)	Abengoa Solar	-	-	-	-	-	-	-	-	-	-	-	-	-	-	500.0 MW (2x250 MW)	500.0 MW	Steam Rankine	-	-	-	Dry cooling	Air cooled condenser	-	-	None	-	-	28	Palen Solar Electric Generating System	4/4/2013
29	Rice Solar Energy Project	1/30/2013	Power tower	Under development	United States	Rice	California, Riverside, Mojave Desert, near Blythe	34° 4' North, 114°49' West	1,410 acres	450,000 MWh/yr (Expected/Planned)	2,598 kWh/m2/yr	SolarReserve	1/1/2016	-	Commercial	SolarReserve's Rice Solar Energy, LLC	SolarReserve's Rice Solar Energy, LLC (100%)	SolarReserve's Rice Solar Energy, LLC	1,071,361 m²	17170	62.4 m²	Pratt Whitney	-	540 ft	Pratt Whitney Rocketdyne	External - cylindrical	-	Molten salt	550°F	1050°F	500°F	-	150.0 MW	-	Steam Rankine	-	-	115.0 bar	Dry cooling	-	-	-	Other	-	Thermal energy storage achieved by raising salt temperature from 550 to 1050 F. Thermal storage efficiency is 99%	29	Rice Solar Energy Project	1/30/2013
30	Sierra SunTower	2/14/2014	Power tower	Operational	United States	Lancaster	California, Los Angeles	34°43' 53.0" North, 118°9' 19.0" West	-	-	2,629 kWh/m2/yr	eSolar	7/1/2009	-	-	eSolar	eSolar (100%)	eSolar	27,670 m²	24360	1.136 m²	eSolar	-	55 m	External: Babcock & Wilcox Dual- Victory Energy	External, Dual-cavity receiver & tubular external receiver	-	Water	218°C	440°C	222°C	-	5.0 MW	5.0 MW	Steam Rankine	-	-	-	Wet cooling	Cooling tower	-	-	None	-	-	30	Sierra SunTower	2/14/2014
31	Crescent Dunes Solar Energy Project	3/9/2016	Power tower	Operational	United States	Tonopah	Nevada, Nye, Northern Nevada, northwest of Tonopah	38°14' North, 117°22' West	1,600 acres	500,000 MWh/yr (Expected)	2,685 kWh/m2/yr	SolarReserve	9/1/2015	-	Commercial	SolarReserve's Tonopah Solar Energy, LLC	SolarReserve's Tonopah Solar Energy, LLC (100%)	SolarReserve's Tonopah Solar Energy, LLC	1,197,148 m²	10347	115.7 m²	-	-	640 ft	-	External - cylindrical	-	Molten salt	550°F	1050°F	500°F	-	110.0 MW	110.0 MW	Steam Rankine	Ahaton	-	115.0 bar	Hybrid	-	-	-	2-tank direct	10 hours	Thermal energy storage achieved by raising salt temperature from 550 to 1050 F. Thermal storage efficiency is 99%	31	Crescent Dunes Solar Energy Project	3/9/2016
32	Alpine SunTower	10/20/2011	Power tower	Under development	United States	California Lancaster	Antelope Valley	-	-	192,000 MWh/yr	-	-	-	-	-	NRG Energy	-	-	-	-	-	eSolar	-	-	-	-	-	-	-	-	-	92.0 MW	-	-	-	-	-	-	-	-	-	-	-	-	32	Alpine SunTower	10/20/2011
33	BrightSource Coyote Springs 1 (PG&E 3)	1/21/2011	Power tower	Under development	United States	Nevada Coyote Springs	-	-	-	573,000 MWh/yr (Expected/Planned)	-	-	-	-	-	BrightSource Energy	-	-	-	-	-	-	-	-	-	-	-	-	-	-	-	-	200.0 MW	-	Steam Rankine	-	-	-	-	-	-	-	-	-	-	33	BrightSource Coyote Springs 1 (PG&E 3)	1/21/2011
34	BrightSource Coyote Springs 2 (PG&E 4)	1/21/2011	Power tower	Under development	United States	Nevada Coyote Springs	-	-	-	573,000 MWh/yr (Expected/Planned)	-	-	-	-	-	BrightSource Energy	-	-	-	-	-	-	-	-	-	-	-	-	-	-	-	-	200.0 MW	-	Steam Rankine	-	-	-	-	-	-	-	-	-	-	34	BrightSource Coyote Springs 2 (PG&E 4)	1/21/2011
35	Gaskell Sun Tower	1/21/2011	Power tower	Under development	United States	California Kern	Antelope Valley	-	1,100 acres	-	-	NRG Energy, eSolar	-	-	-	eSolar ; NRG Energy	-	-	-	-	-	-	-	-	-	-	-	-	-	-	-	245.0 MW	-	Steam Rankine	-	-	-	-	-	-	-	-	-	-	35	Gaskell Sun Tower	1/21/2011
36	New Mexico SunTower	10/20/2011	Power tower	Under development	United States	New Mexico Santa Teresa	-	31°48' North, 106°39' West	-	-	2,540 kWh/m2/yr	eSolar	-	-	-	NRG Energy	NRG Energy	-	519,107 m²	456,960	1.136 m²	eSolar	-	-	-	-	-	Water	218°C	440°C	220°C	-	92.0 MW	-	-	-	-	-	Wet cooling	Cooling tower	-	-	-	-	-	36	New Mexico SunTower	10/20/2011

3- Plants with linear fresnel reflector CSP technology

S/N	Plant Name	Status Date	Technology	Status	Country	City	Region	Lat/Long Location	Land Area	Electricity Generation	Solar Resource	Company	Start Production	Cost (approx)	Project Type	Developer(s)	Owner(s) (%)	Operator(s)	Solar-Field Aperture Area	# of Lines	Line Length	Mirror Width in Line	# of Mirrors across Line	Collector Manufacturer (Model)	Collector Description	Mirror Manufacturer	Receiver Type	Receiver Length	Receiver Manufacturer	HTF Type	Solar-Field Inlet Temp	Solar-Field Outlet Temp	Solar-Field Temp Difference	HTF Company	Turbine Capacity (Gross)	Turbine Capacity (Net)	Output Type	Turbine Manufacturer	Turbine Efficiency	Power Cycle Pressure	Cooling Method	Cooling Method Description	Fossil Backup Type	General	Storage Type	Storage Capacity	Thermal Storage Description
1	Kogan Creek Solar Boost	3/23/2016	Linear Fresnel reflector	Currently Non-Operational	Australia	Chinchilla	Queensland	26°55' 8.0" South, 150°45' 28.0" East	30 hectares	44,000 MWh/yr	-	CS Energy	1/1/2016	105,000,000 AUD	Commercial	CS Energy	CS Energy (100%)	CS Energy	-	14	500 m	36 m	-	AREVA Solar (CLFR)	Once-through receiver delivering superheated steam	AREVA Solar	-	-	-	Water/Steam	186°C	370°C	184°C	-	44.0 MW	44.0 MW	Steam Rankine	Siemens	-	60.0 bar	Dry cooling	Air cooled condenser	-	-	None	-	-
2	Liddell Power Station	2/5/2013	Linear Fresnel reflector	Operational	Australia	Liddell	New South Wales	32°22' 34.0" South, 150°59' 48.0" East	-	13,550 MWh/yr (thermal)	-	Novatec Solar	10/1/2012	-	Commercial	Novatec Solar	Macquarie Generation (100%)	Macquarie Generation	18,490 m²	4	403 m	-	-	Novatec Solar (Nova-1)	Fresnel	Novatec Solar	-	-	-	Water/Steam	140°C	270°C	130°C	-	9.0 MW	9.0 MW	-	The 9 MWth solar boiler feeds steam into the existing 2000 MW coal-fired power station. 270°C, 55 bar, 9.3 MWth peak thermal output	-	55.0 bar	Dry cooling	Air cooled condenser	-	The 9 MWth solar boiler feeds steam into the existing 2000 MW coal-fired power station. 270°C, 55 bar, 9.3 MWth peak thermal output	None	-	-
3	Dacheng Dunhuang 50MW Molten Salt Fresnel projects	9/29/2016	Linear Fresnel reflector	Under development	China	Dunhuang	Gansu Province	-	-	-	-	-	-	-	-	Lanzhou Dacheng Technology Co., Ltd	Lanzhou Dacheng Technology Co., Ltd	-	-	0	-	-	-	-	-	-	-	-	-	-	-	-	-	-	Molten Salt	-	-	-	-	-	-	-	-	-	2-tank direct	13 hours	Molten salt	-
4	Uzar 50MW Fresnel CSP project	9/29/2016	Linear Fresnel reflector	Under development	China	Uzar Middle Banner	Inner Mongolia	-	-	-	-	-	-	-	-	Huanong North United Power Co., Ltd.	Huanong North United Power Co., Ltd.	-	-	-	-	-	-	-	-	-	-	-	-	-	-	-	-	-	-	-	-	-	-	-	-	-	-	-	-	2-tank indirect	6 hours	Molten Salt
5	Zhanghei 50MW CSG Fresnel CSP project	9/29/2016	Linear Fresnel reflector	Under development	China	Zhanghei	Hebei Province	-	-	-	-	-	-	-	-	Beijing TeraSolar Photothermal Technologies Co., Ltd	Zhanghei Huaqiang Zhaoyang Co., Ltd.	-	-	-	-	-	-	-	-	-	-	-	-	-	-	-	-	-	-	-	-	-	-	-	-	-	-	-	-	other	14 hours	Solid state formulated concrete
6	Zhangjiakou 50MW CSG Fresnel project	9/29/2016	Linear Fresnel reflector	Under development	China	Zhanghei	Hebei Province	-	-	-	-	-	-	-	-	Beijing TeraSolar Photothermal Technologies Co., Ltd	Zhanghei Huaqiang Zhaoyang Co., Ltd.	-	-	-	-	-	-	-	-	-	-	-	-	-	-	-	-	-	-	-	-	-	-	-	-	-	-	-	-	other	14 hours	Solid state formulated concrete
7	Alba Nova 1	8/28/2014	Linear Fresnel reflector	Under construction	France	Ghisonaccia	Corsica Island	42°0' 56.0" North, 9°26' 57.0" East	23 hectares	25,000 MWh/yr (Estimated)	1,800 kWh/m2/yr	Solar Euromed	8/1/2015	-	Demonstration	Solar Euromed	Solar Euromed (100%)	Solar Euromed	140,000 m²	21	750 m	-	12	Solar Euromed (AF1)	Linear Fresnel Reflectors	Solar Euromed (AF1)	Non-evacuated	750 m	-	Water	-	300°C	-	-	12.0 MW	12.0 MW	Steam Rankine	-	-	65.0 bar	Dry cooling	-	-	-	Other	1 hour	Ruths tank
8	Augustin Fresnel 1	5/8/2014	Linear Fresnel reflector	Operational	France	Targassonne	Pyrenoans	42°30' 4.0" North, 1°58' 20.0" East	1 hectares	-	1,800 kWh/m2/yr	Solar Euromed	1/1/2012	-	Prototype	Solar Euromed	Solar Euromed (100%)	Solar Euromed	400 m²	1	40 m	-	12	Solar Euromed (AF1)	Linear Fresnel Reflectors	Solar Euromed (AF1)	Non-evacuated	40 m	-	Water	-	300°C	-	-	0.25 MW	0.25 MW	Steam Rankine	-	-	100.0 bar	Dry cooling	-	-	-	Other	0.25 hours	Ruths tank
9	Lio Solar Thermal Project	11/27/2012	Linear Fresnel reflector	Under contract	France	Lio	Pyrénées Orientales	42°28' 9.0" North, 2°3' 47.0" East	23 hectares	17,000 MWh/yr (Expected)	1,930 kWh/m2/yr	CNIM	1/1/2015	-	Commercial	CNIM	CNIM (100%)	CNIM	120,000 m²	25	340 m	14 m	-	CNIM	-	-	-	-	-	Water	190°C	285°C	95°C	-	9.0 MW	9.0 MW	-	-	-	70.0 bar	Dry cooling	Air cooled condenser	-	-	Other	1 hour	Steam drum
10	Dhursar	11/14/2014	Linear Fresnel reflector	Operational	India	Dhursar	Rajasthan	26°47' 8.5" North, 72°9' 30.0" East	340 hectares	280,000 MWh/yr (Expected)	-	-	11/11/2014	21,000,000,000 Rs Crore	-	Rajasthan Sun Technique Energy	Reliance Power (100%)	Reliance Power	-	-	-	-	-	-	-	-	-	-	-	-	-	-	-	-	125.0 MW	125.0 MW	Steam Rankine	-	-	-	Wet cooling	Cooling tower	-	-	None	-	-
11	Dadri ISCC Plant	11/23/2016	Linear Fresnel reflector	Under construction	India	Dadri	Uttar Pradesh	-	-	14,000 MWh/yr	-	Wehmaster Solar	9/1/2017	-	-	Fresnell EPC Thermax	NTCP	NTCP	33,000 m²	0	-	-	-	-	-	-	-	-	-	-	-	-	-	-	-	14.0 MW	-	Steam Rankine	-	-	-	-	-	-	-	None	-	-
12	Rende-CSP Plant	2/16/2015	Linear Fresnel reflector	Operational	Italy	Rende	Calabria	39°22' 25.0" North, 16°14' 47.0" East	2 hectares	3,000 MWh/yr (Estimated)	1,700 kWh/m2/yr	-	5/30/2014	-	Demonstration	Falck Renewables	Falck Renewables (100%)	Falck Renewables	9,780 m²	-	-	-	-	-	-	-	-	-	-	-	-	-	-	-	-	1.0 MW	1.0 MW	Organic Rankine	-	-	-	-	-	-	-	None	-	-
13	eCare Solar Thermal Project	11/27/2012	Linear Fresnel reflector	Under contract	Morocco	Undefined	-	-	2 hectares	1,600 MWh/yr (Expected)	2,600 kWh/m2/yr	CNIM	1/1/2014	-	Demonstration	CNIM	CNIM (100%)	CNIM	10,000 m²	4	260 m	14 m	-	CNIM	-	-	-	-	-	Water	160°C	280°C	120°C	-	1.0 MW	-	Organic Rankine	-	-	70.0 bar	Dry cooling	Air cooled condenser	-	-	Other	2 hours	Steam drum
14	IRESEN 1 MWe CSP-ORC pilot project	7/26/2016	Linear Fresnel reflector	Under construction	Morocco	Benguerir	-	-	-	1,700 MWh/yr	-	-	9/1/2016	5,560,000 Euro	Demonstration - Research	IRESEN	IRESEN	-	11,400 m²	0	-	-	-	Soltigua	-	-	-	-	-	Mineral oil	180°C	300°C	120°C	-	1.0 MW	-	Organic Rankine	Exergy – Maccaferri Group	-	-	Dry cooling	Direct	-	-	Other	20 minutes	Buffer
15	Puerto Errado 1 Thermosolar Power Plant	9/7/2011	Linear Fresnel reflector	Operational	Spain	Calasparra	Murcia	38°16' 42.28" North, 1°36' 1.01" West	5 hectares	2,000 MWh/yr (Expected/Planned), Following radiation estimation, own electrical consumers and equipment efficiency	2,100 kWh/m2/yr	Novatec Solar GmbH	3/19/2009	-	Prototype	Novatec Solar GmbH	Novatec Solar España S.L. (100%)	Novatec Solar España S.L.	-	2	806 m	16 m	-	Novatec Solar España S.L. (Nova-1)	Fresnel	Novatec Solar España S.L.	-	-	-	Water	140°C	270°C	130°C	Novatec Solar España	1.4 MW	-	-	KKK-Siemens, 270°C, 55 bar	-	55.0 bar	Dry cooling	Air cooled condenser	-	-	Single-tank thermocline	Ruths tank	-
16	Puerto Errado 2 Thermosolar Power Plant	4/26/2013	Linear Fresnel reflector	Operational	Spain	Calasparra	Murcia	38°16' 42.28" North, 1°36' 1.01" West	70 hectares	49,000 MWh/yr (Expected/Planned), Following radiation estimation, own electrical consumers and equipment efficiency	2,095 kWh/m2/yr	Tubo Sol PE 2, S.L.	3/31/2012	-	Commercial	Novatec Biosol AG	Tubo Sol PE 2, S.L. (Elektra Rasellasol) (73%)	-	302,000 m²	28	940 m	16 m	-	Novatec Solar España S.L. (Nova-1)	Fresnel	Novatec Solar España S.L.	-	-	-	Water	140°C	270°C	130°C	Novatec Solar España	30.0 MW	30.0 MW	-	Thermodyn SAS, 270° C, 55 bar	-	55.0 bar	Dry cooling	Air cooled condenser	-	-	Single-tank thermocline	0.5 Hours	Ruths tank
17	Kimberlina Solar Thermal Power Plant	11/8/2016	Linear Fresnel reflector	Operational	United States	Bakersfield	California, Kern	35°34' 0.0" North, 119°11' 39.1" West	12 acres	-	-	Ausra	10/1/2008	-	Demonstration	Ausra	Ausra (100%)	Ausra	25,988 m²	3	385 m	2 m	10	Ausra	Compact Linear Fresnel	Ausra	Non-evacuated	385 m	Ausra	Water	-	300°C	-	-	5.0 MW	5.0 MW	Steam Rankine	-	-	40.0 bar	-	-	-	-	None	-	-

4- Plants with dish engine CSP technology

S/N	Plant Name	Status Date	Technology	Status	Country	City	Region	Lat/Long Location	Land Area	Electricity Generation	Solar Resource	Company	Start Production	Cost (approx)	Project Type	Developer(s)	Owner(s) (%)	Operator(s)	# of Dishes	Dish Aperture Area	Dish Manufacturer (Model)	Dish Description	HTF Type	Solar-Field Inlet Temp	Solar-Field Outlet Temp	Solar-Field Temp Difference	HTF Company	Turbine Capacity (Gross)	Turbine Capacity (Net)	Output Type	Turbine Manufacturer	Turbine Efficiency	Power Cycle Pressure	Cooling Method	Cooling Method Description	Fossil Backup Type	General	Storage Type	Storage Capacity	Thermal Storage Description
1	Maricopa Solar Project	11/21/2013	Dish/Engine	Currently Non-Operational	United States	Peoria	Southwest USA, Arizona, Maricopa	33°33' 31.0" North, 112°13' 7.0" West	15 acres	-	-	-	1/1/2010	-	Demonstration	Tessera Solar	Tessera Solar	Tessera Solar	60	-	Stirling Energy Systems (SES) (SunCatcher™)	Each SunCatcher produces 25 kilowatts of power	-	-	-	-	-	1.5 MW	1.5 MW	Stirling	-	-	-	-	-	Annual Solar-to-Electricity Efficiency (Gross): 26%	None	-	-	1	Maricopa Solar Project	11/21/2013	Dish/Engine	Currently Non-Operational	United States	Peoria	Southwest USA, Arizona, Maricopa
2	Tooele Army Depot	7/27/2016	Dish/Engine	Operational	United States	Tooele	Utah, Tooele County	40° 30' 4.0" North, 112°22' 25.0" West	17 acres	-	-	-	7/1/2013	-	Commercial	Infinia Corp.	Tooele Army Depot (100%)	-	429	35 m²	Infinia Corp (PowerDish™)	Each PowerDish™ produces 3.5 kW of power	Helium	-	-	-	-	1.5 MW	1.5 MW	Stirling	-	-	-	Closed-loop cooling system	-	-	None	-	-	2	Tooele Army Depot	7/27/2016	Dish/Engine	Operational	United States	Tooele	Utah, Tooele County
3	Imperial Valley Solar Project	1/21/2011	Dish/Engine	Under development	United States	California Imperial County	-	-	-	-	-	-	-	-	-	Tessera Solar	-	-	28360	-	Tessera Solar (SunCatcher)	-	-	-	-	-	-	25.0 MW	-	Stirling	-	-	-	Dry-cooling	-	-	None	-	-	3	Imperial Valley Solar Project	1/21/2011	Dish/Engine	Under development	United States	California Imperial County	-

APPENDIX D: AVAILABLE INFORMATION ABOUT THE CRESCENT DUNES SOLAR ENERGY PROJECT

The technical information given below is compiled from SolarPACES and otherwise mentioned.

1- Background

- Technology: Power tower
- Latitude/Longitude Location: 38°14′ North, 117°22′ West
- Land Area: 1,600 acres
- Electricity Generation: More than 500,000 MWh/yr
- Solar Resource: 2,685 kWh/m2/yr

2- Solar Field

- Heliostat Solar-Field Aperture Area: 1,197,148 m²
- Number of Heliostats: 10,347
- Number of horizontal panels: 7
- Number of vertical panels: 5
- Heliostat width: 1.653 m (Measured from an image)
- Heliostat height: 2 m (Measured from an image)
- Heliostat aperture area: 115.7 m2
- Heliostat horizontal gap: 0.04 m (Measured from an image)
- Heliostat vertical gap: 0.04 m (Measured approximately from an image)
- Heliostat structure width: 11.81 m (Measured approximately from an image)
- Heliostat structure height: 10.16 m (Measured approximately from an image)
- Tower height: 195 m
- Receiver type: External – Cylindrical
- Receiver Diameter: 15 m (Measured approximately from an image)
- Receiver height: 17.5 m (Measured approximately from an image)
- Optical tower height: 181.2 m (Measured approximately from an image)

3- Heat transfer fluid

- Heat transfer fluid type: Molten salt (sodium nitrate and potassium nitrate, 50-50 mix) [90]
- Molten salt quantity: 30,000 bags [90]
- Solar field inlet temperature of heat transfer fluid: 287.78 °C

- Solar field outlet temperature of heat transfer fluid: 565.56 °C

4- Power block

- Steam Turbine Capacity: 110 MW
- Power cycle pressure: 115 bar
- Cooling method: Hybrid

5- Thermal storage

- Storage type: 2 tanks of molten salts
- Storage capacity: 10 hours
- Tank dimension: 12.19 m height and 42.67 m diameter [90]
- Tank capacity: 3.6 million gallons [90]